

THESIS

GEOLOGY OF THE TAYLOR SILVER DEPOSIT,  
WHITE PINE COUNTY, NEVADA

Submitted by

Jeffrey M. Edwards

Department of Earth Resources

In partial fulfillment of the requirements  
for the Degree of Master of Science  
Colorado State University  
Fort Collins, Colorado  
Summer, 1988

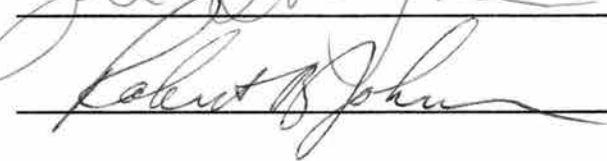
QE138  
.W54  
E38  
1988  
copy 3

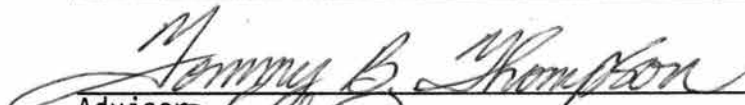
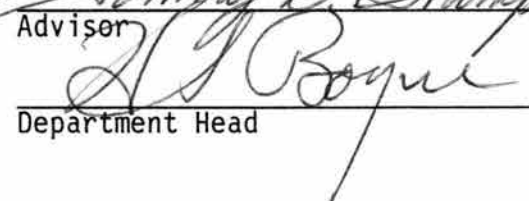
COLORADO STATE UNIVERSITY

Summer, 1988

WE HEREBY RECOMMEND THAT THE THESIS PREPARED UNDER OUR SUPERVISION  
BY JEFFREY M. EDWARDS ENTITLED GEOLOGY OF THE TAYLOR SILVER DEPOSIT,  
WHITE PINE COUNTY, NEVADA BE ACCEPTED AS FULFILLING IN PART  
REQUIREMENTS FOR THE DEGREE OF MASTER OF SCIENCE.

Committee on Graduate Work

  
\_\_\_\_\_  
  
\_\_\_\_\_

\_\_\_\_\_  
  
Adviser  
  
Department Head

COLORADO STATE UNIV. LIBRARIES

## ABSTRACT OF THESIS

### GEOLOGY OF THE TAYLOR SILVER DEPOSIT

#### WHITE PINE COUNTY, NEVADA

The Taylor silver mine is located 15 miles southeast of Ely, Nevada, on the western flank of the Southern Schell Creek Range. The 1200 ton per day open pit mine produces up to 1,200,000 ounces silver and 1000 ounces gold annually. Preproduction reserves totalled 7 million tons @ 3.0 oz Ag/ton and 0.003 oz Au/ton. Soft silver prices since 1982 have forced intermittent shutdowns.

The ore body is an epithermal, high-silica, low-sulfide replacement deposit. Brecciated Devonian Guilmette Formation limestones host silver ores immediately beneath unconformable hydrocarbon-rich Mississippian Pilot Shale siltstone. Intrusion of pre-mineral, lower Oligocene fluorine-rich rhyolite dikes and sills, and post-mineral, lower Miocene latite dikes, bracket ore deposition.

The structural history of the district is complex. Compressive deformation began in Mesozoic time as west to east thrust faults imbricated portions of the section east of a broad north-south fold in the Taylor mine area. Gravity-driven low angle faults, related to Paleocene through Eocene uplift of the neighboring Snake Range, attenuated and severely brecciated portions of the stratigraphic section. Oligocene compressive tectonism reactivated the Taylor fold

and low-angle faults in the district. High-angle reverse faults breached the Taylor anticline, and focussed ore fluids into receptive breccias on and near the fold axis.

Jasperoid outcrop characteristics, paragenesis, and trace metal contents serve to define four hypogene mineral stages: (1) weakly-mineralized stage I jasperoids contain elevated Au, up to 1 ppm, and locally over 1000 ppm As; (2) stage II jasperoids, marked by the presence of stibnite, contain up to 18% Sb, up to 1 ppm Au, locally over 5000 ppm Ba, and up to 2.5 oz Ag/ton; (3) stage III jasperoids represent the main Ag-ore-stage and contain up to 1000 ppm Pb, up to 3000 ppm Zn, and Ag:Au ratios over 1100:1; (4) stage IV open space sulfide-calcite veins and breccia fillings locally contain over 50 oz Ag/ton, with up to 4.5% combined base metals, and up to 3000 ppm Sb. Ore-stages III and IV were structurally confined to the immediate mine area. Stage I and II jasperoids form a distinct Sb-Au-Ba halo from 0.5 to 1 mile around the silver deposit.

Fluid inclusion analyses demonstrate that Taylor was a prograde system. Stage II quartz precipitated from boiling fluids at 200°C. Ore-stage III accessory fluorite was deposited from boiling fluids at about 225°C. Stage IV vein sphalerite precipitated from non-boiling fluids at 306°C. Jasperoid whole rock vapor phase analyses indicate that the vapor phase was dominated by CH<sub>4</sub>, C<sub>2</sub>H<sub>6</sub>, and C<sub>3</sub>H<sub>8</sub> probably derived from the thermal maturation of organic matter, indigenous to the enclosing Guilmette and Pilot sediments.

Exploration drill hole logs define a base of silicification that cross cuts structure and stratigraphy. Lack of evidence for boiling in vein fluorite below this level suggests that the base of silicification

may be coincident with the base of boiling. Banded quartz-sulfide-calcite veins found at depth indicate that episodic boiling reached deeper levels but strength and duration were apparently not adequate to promote wall rock silicification.

Apparent vertical metal zonation grades from Pilot Shale- and Joanna Limestone-hosted Sb-Au-Ba-As-rich jasperoids down into Guilmette Formation limestone-hosted Ag-Zn-Pb-rich jasperoids, and finally into base metal-Ag-Sb-rich veins and breccia fillings below the base of silicification.

District-wide paragenesis, wall rock alteration, and metal zonation thus appears to be related to stratigraphic level, depth, and particularly the boiling of indigenous-organic-derived volatiles.

Both stratigraphic reconstruction and estimates from fluid inclusion data suggest depth of formation in the range of  $3500 \pm 700$  feet (base of the Pilot Shale).

Jeffrey M. Edwards  
Department of Earth Resources  
Colorado State University  
Fort Collins, Colorado 80523  
Summer, 1988.

## ACKNOWLEDGMENTS

I thank Silver King Mines Inc. for permission to work on the Taylor deposit and publish this report. Silver King personnel, especially Antonia Lavin, Carl Pescio, and Stuart Havenstrite, freely gave information, guidance, and support. I am also indebted to John Zunnini who assayed my surface rock samples in Silver King's Ward lab.

Generous grants from Newmont Exploration Ltd., AMSELCO, and Standard Oil of California, helped defray commercial lab costs.

Dr. Tommy B. Thompson deserves special recognition and thanks for initially generating the project, and his subsequent guidance and patience over the years. My other committee members, Dr. Robert Johnson and Dr. John Vauhan, lent valuable time, assistance, and insights to this enterprise.

## TABLE OF CONTENTS

<u>CHAPTER</u>		<u>PAGE</u>
I	INTRODUCTION . . . . .	1
	PHYSIOGRAPHY . . . . .	4
	PREVIOUS INVESTIGATIONS . . . . .	5
	METHODS OF INVESTIGATION . . . . .	7
II	DISTRICT PRODUCTION . . . . .	9
	MINE AND EXPLORATION HISTORY . . . . .	9
	THE OPEN PIT MINE . . . . .	14
	PRODUCTION ECONOMICS . . . . .	21
III	REGIONAL GEOLOGY . . . . .	27
	STRATIGRAPHY . . . . .	27
	INTRUSIVE ROCKS . . . . .	32
	STRUCTURAL SETTING . . . . .	33
	PRE-MIDDLE JURASSIC . . . . .	33
	MIDDLE JURASSIC THROUGH LATE CRETACEOUS . . . . .	35
	LATE CRETACEOUS THROUGH EARLY MIOCENE . . . . .	36
	MIDDLE MIOCENE TO PRESENT . . . . .	38
	METALLOGENY . . . . .	39
IV	DISTRICT GEOLOGY . . . . .	42
	INTRODUCTION . . . . .	42
	LITHOLOGIC UNITS . . . . .	42
	DEVONIAN SIMONSON DOLOMITE . . . . .	42
	DEVONIAN GUILMETTE FORMATION . . . . .	44
	(a) Member a . . . . .	44
	(b) Member b . . . . .	45
	(c) Member c . . . . .	45
	(d) Member d . . . . .	47
	(e) Transition beds . . . . .	47
	DEVONIAN/MISSISSIPPIAN PILOT SHALE . . . . .	49
	MISSISSIPPIAN JOANNA LIMESTONE . . . . .	49
	MISSISSIPPIAN CHAINMAN SHALE . . . . .	51
	PENNSYLVANIAN ELY LIMESTONE . . . . .	51
	PERMIAN THROUGH EOCENE . . . . .	52
	PORPHYRITIC RHYOLITE INTRUSIVES . . . . .	52
	JASPEROIDS . . . . .	55
	(a) Barren jasperoid . . . . .	57

<u>CHAPTER</u>	<u>PAGE</u>
(b) Antimony jasperoid . . . . .	59
(c) Dark grey jasperoid . . . . .	59
(d) Blue grey jasperoid . . . . .	62
OLIGOCENE VOLCANICS . . . . .	62
YOUNGER OLIGOCENE INTRUSIVES . . . . .	63
STRUCTURE . . . . .	63
MESOZOIC IMBRICATE THRUSTS . . . . .	63
EOCENE? STRUCTURES . . . . .	64
OLIGOCENE STRUCTURING . . . . .	66
MIOCENE/PLIOCENE EXTENSION . . . . .	69
MINERALIZATION . . . . .	70
GENERAL DESCRIPTION . . . . .	70
JASPEROID AND ORE PARAGENESIS . . . . .	72
(a) Stage I . . . . .	75
(b) Stage II . . . . .	75
(c) Stage III . . . . .	78
(d) Stage IV . . . . .	86
(e) Supergene mineralogy . . . . .	88
WALL ROCK ALTERATION . . . . .	90
(a) Silicification of sediments . . . . .	90
(b) Alteration of porphyritic rhyolite . . . . .	94
FLUID INCLUSIONS . . . . .	100
(a) Quartz . . . . .	100
(b) Fluorite . . . . .	103
(c) Sphalerite . . . . .	106
DEPTH OF FORMATION . . . . .	106
 V	
GEOCHEMISTRY . . . . .	110
INTRODUCTION AND PROCEDURES . . . . .	110
DRILL HOLE GEOCHEMISTRY . . . . .	114
DISTRIBUTIONS IN DRILL HOLES . . . . .	114
RELATIONSHIP TO SILVER GRADE . . . . .	121
MINOR TRACE ELEMENTS . . . . .	127
VERTICAL ZONATION . . . . .	129
SURFACE ROCK CHIP GEOCHEMISTRY . . . . .	129
LATERAL ZONATION . . . . .	150
TRACE ELEMENTS BY ROCK TYPE . . . . .	150
VOLATILE PHASES . . . . .	158
 VI	
CONCLUSIONS . . . . .	161
SUMMARY OF GEOLOGIC HISTORY . . . . .	161
SUMMARY OF MINERALIZATION . . . . .	164
GENETIC MODEL . . . . .	168
 REFERENCES CITED . . . . .	176
 APPENDICES . . . . .	185
 PLATES . . . . .	back pocket

## LIST OF TABLES

<u>Table</u>	<u>Page</u>
1 Taylor district production . . . . .	10
2 Diamond drill hole / conventional rotary comparisons .	13
3 Taylor mining cost breakdown . . . . .	20
4 Taylor milling cost breakdown . . . . .	20
5 Taylor-type mine cash flow analyses . . . . .	24
6 Economics of hypothetical Taylor-type deposits . . .	26
7 Whole rock data for porphyritic rhyolite and older volcanics . . . . .	54
8 Summary of jasperoid characteristics . . . . .	74
9 Correlation coefficient thresholds at the 95% and 99% confidence levels . . . . .	113
10 Drill data summary statistics . . . . .	115
11 Drill hole correlation coefficients . . . . .	116
12 Low-grade drill data summary statistics . . . . .	122
13 Medium-grade drill data summary statistics . . . . .	123
14 High-grade drill data summary statistics . . . . .	124
15 Drill hole correlation coefficients by silver grade .	125
16 Average metal and metal ratios in drill holes by silver grade . . . . .	126
17 Minor trace elements in drill holes . . . . .	128
18 Surface data summary statistics . . . . .	130
19 Surface rock chip correlation coefficients . . . . .	131

<u>Table</u>		<u>Page</u>
20	Pilot Shale summary statistics . . . . .	151
21	Guilmette Formation summary statistics . . . . .	152
22	Barren (stage I) jasperoid summary statistics . . . . .	153
23	Antimony (stage II) jasperoid summary statistics . . . . .	154
24	Dark grey (stage III) jasperoid summary statistics . . . . .	155
25	Surface rock chip correlation coefficients by rock type . . . . .	156
26	Average metal and metal ratios in surface samples (by rock type) . . . . .	157
27	Volatile phase data . . . . .	159

## LIST OF FIGURES

<u>Figure</u>	<u>Page</u>
1 View, looking north, of the Taylor Silver Mine . . . . .	2
2 Index map of White Pine County, Nevada . . . . .	3
3 Taylor mine production: 1983/1984 . . . . .	15
4 Taylor mine costs: 1983/1984 . . . . .	16
5 Taylor mill production: 1983/1984 . . . . .	17
6 Taylor mill costs: 1983/1984 . . . . .	18
7 Taylor production costs: 1983/1984 . . . . .	19
8 Taylor mill records: January, 1984 . . . . .	22
9 Recovery rates versus grade of mill feed: January, 1984	23
10 General geology of White Pine County . . . . .	28
11 Generalized stratigraphic column: Eastern Nevada . . . . .	29
12 Index of major structural features: Great Basin . . . . .	34
13 Distribution of mineral districts and metallogenic trends: Great Basin . . . . .	40
14 Stratigraphic column, Taylor mine area . . . . .	43
15 Stratigraphic column, upper Guilmette . . . . .	46
16 Sedimentary breccia textures in upper Guilmette member c	48
17 Possible collapse breccias in Joanna Limestone . . . . .	50
18 Silver-bearing jasperoid fragments in rhyolite fault breccia . . . . .	55
19 Guilmette transition beds faulted into rhyolite near the Southwest Pit reverse fault . . . . .	56
20 Partially silicified breccia with limestone cores and post-silica calcite veining . . . . .	58

<u>Figure</u>	<u>Page</u>
21 Barren jasperoid (stage I) outcrop . . . . .	58
22 Antimony jasperoid (stage II) with barren jasperoid (stage I) fragments . . . . .	60
23 Dark grey jasperoid (stage III) outcrops . . . . .	61
24 Summary paragenetic diagram . . . . .	73
25 Stage I jasperoid. Jigsaw to granular textured silica preserving bioclastic textures in Joanna Limestone	76
26 Stage I jasperoid. Fine- to coarse-grained granular quartz . . . . .	76
27 Stage II jasperoid. Early coarse-grained vug quartz surrounded and replaced by later fine-grained reticulate quartz . . . . .	77
28 Typical stage II reticulate quartz . . . . .	77
29 Stage II jasperoid. (a) Coarse idiomorphic quartz. (b) Vug-filling stibnite . . . . .	79
30 Stage II jasperoid. Spherulitic textures . . . . .	80
31 Stage I jasperoid fragments in stage II reticulate matrix	80
32 Fragment of stage II reticulate textured jasperoid in stage III matrix, followed by stage IV open space sulfide and calcite . . . . .	81
33a Stage III incipient granular silicification . . . . .	81
33b Partial stage III reticulate quartz replacement following limestone recrystallization . . . . .	82
33c Partial stage III silicification with limestone recrystallization . . . . .	82
34 Typical stage III hypidiomorphic-textured jasperoids . . . . .	83
35 Stage III jasperoid. Late jigsaw silica with high sulfide content and this case, fluorite . . . . .	85
36 Stage III jasperoid, showing disseminated sulfides under reflected light . . . . .	85
37 Stage IV jigsaw silica, open space sulfides (oxidized here) and calcite on jasperoid fragments; cut by late calcite . . . . .	87

<u>Figure</u>	<u>Page</u>
38	Stage IV unnamed Ag-Pb-Sb-S mineral (M) replaces galena (Gn) and tetrahedrite (T) adjacent to calcite (cc) . . . . . 87
39	Post mineral shearing locally induced recrystallization on unnamed mineral (M) perpendicular to shear surfaces . . . . . 88
40	Banded calcite-sulfide-quartz veins on the Argus fault, Taylor -350 level . . . . . 89
41	Plumose calcite-sulfide-quartz veins on the Argus fault, Taylor -350 level . . . . . 89
42	Banded calcite (cc)-sulfide (opaques)-quartz (Q) vein in transmitted, plane light . . . . . 90
43	Silicified Pilot Shale in Argus Pit . . . . . 92
44	Silicified Pilot Shale in transmitted light . . . . . 92
45	Brecciated and strongly silicified Guilmette transition beds adjacent to the Argus fault . . . . . 93
46	Heterolithic tectonic breccia in Guilmette member a limestone . . . . . 95
47	Partial silicification of Guilmette member a limestone breccias . . . . . 95
48	Kaolinite-montmorillonite alteration in porphyritic rhyolite . . . . . 96
49	Silica flooding in porphyritic rhyolite . . . . . 96
50	Montmorillonite-kaolinite alteration of porphyritic rhyolite . . . . . 98
51	Intense montmorillonite alteration of porphyritic rhyolite . . . . . 98
52	Major oxide trends across argillized dike . . . . . 99
53	Pyrite-siderite-calcite alteration in porphyritic rhyolite . . . . . 101
54	Carbonatized rhyolite fault breccia with jasperoid fragments . . . . . 101
55	Fluid inclusion homogenization temperatures . . . . . 102

<u>Figure</u>	<u>Page</u>
56 Fluid inclusions in stage II quartz display a wide range of fluid : vapor ratios . . . . .	104
57 Fluid inclusions in stage III fluorite with wide range in fluid : vapor ratios . . . . .	104
58 Stage IV sphalerite-tetrahedrite-galena-unnamed Ag-Pb-Sb sulfosalt-calcite vein in Argus Pit . . .	107
59 Secondary inclusions in sphalerite (with double meniscus)	107
60 Primary fluid inclusions in sphalerite with double meniscus . . . . .	108
61 Drill hole D-1 histogram . . . . .	117
62 Drill hole D-9 histogram . . . . .	118
63 Drill hole D-10 histogram . . . . .	119
64 Drill holes D-7, D-14, and SKT-304 histograms . . .	120
65 Silver distribution in silicified surface rocks . . .	133
66 Gold distribution in silicified surface rocks . . .	135
67 Antimony distribution in silicified surface rocks . . .	137
68 Arsenic distribution in silicified surface rocks . . .	139
69 Copper distribution in silicified surface rocks . . .	141
70 Lead distribution in silicified surface rocks . . .	143
71 Zinc distribution in silicified surface rocks . . .	145
72 South rock chip traverse histogram . . . . .	147
73 North rock chip traverse histogram . . . . .	149
74 Schematic cross section illustrating the Taylor silver system . . . . .	171

## LIST OF APPENDICES

<u>Appendix</u>	<u>Page</u>
I Whole Rock Data . . . . .	185
II Fluid Inclusion Data . . . . .	186
III Bondar-Clegg Analytic Procedures . . . . .	190
IV Drill Hole Geochem Data . . . . .	191
V Surface Rock Chip Geochem Data . . . . .	198

LIST OF PLATES

<u>Plate</u>		<u>Page</u>
1	1 : 2400 geologic map of Taylor Mine area .	back pocket
2	1 : 2400 geologic cross sections . . .	back pocket
3	1 : 2400 sample location overlay . . .	back pocket
4	Drill section 99,100 North . . . .	back pocket

## CHAPTER I

### INTRODUCTION

The Taylor Silver Mine (Fig. 1) is located 15 miles southeast of Ely, Nevada, on the western flank of the Southern Schell Creek Range (Fig. 2). A maintained gravel road accesses the mine from U.S. 6-50-93 approximately 13.5 miles south of Ely.

Silver King Mines (SKM) operates the 1200 ton per day open pit mine in a 50/50 joint venture with NERCO. Preproduction reserves of 7,000,000 tons @ 3 oz Ag/ton included 5,000,000 tons @ 3.3 oz Ag/ton and 2,000,000 tons @ 2.25 oz Ag/ton (this being stockpiled). A break-even silver price of \$6.20 and a shut-down price of \$5.40 has resulted in intermittent production due to soft silver prices since 1982. Since opening in April, 1981, until its most recent closing in October, 1984, the mine produced a total of 3,766,348 ounces Ag and about 3000 ounces Au (Pescio, 1988, personal commun).

The ore body is a bulk tonnage stratabound siliceous replacement deposit, hosted in Devonian limestones. Ore is characterized by its high silica and low sulfide contents, its associated Sb deposits, and locally high Hg, As, and Au concentrations. For these reasons, previous workers have classified the deposit as epithermal (Bagby and Berger, 1985).



Fig. 1. View, looking north, of the Taylor Silver Mine (1982). Southwest Pit in foreground. Bishop Pit right of crushers. Tailings dam above and left of the mill/concentrator buildings.

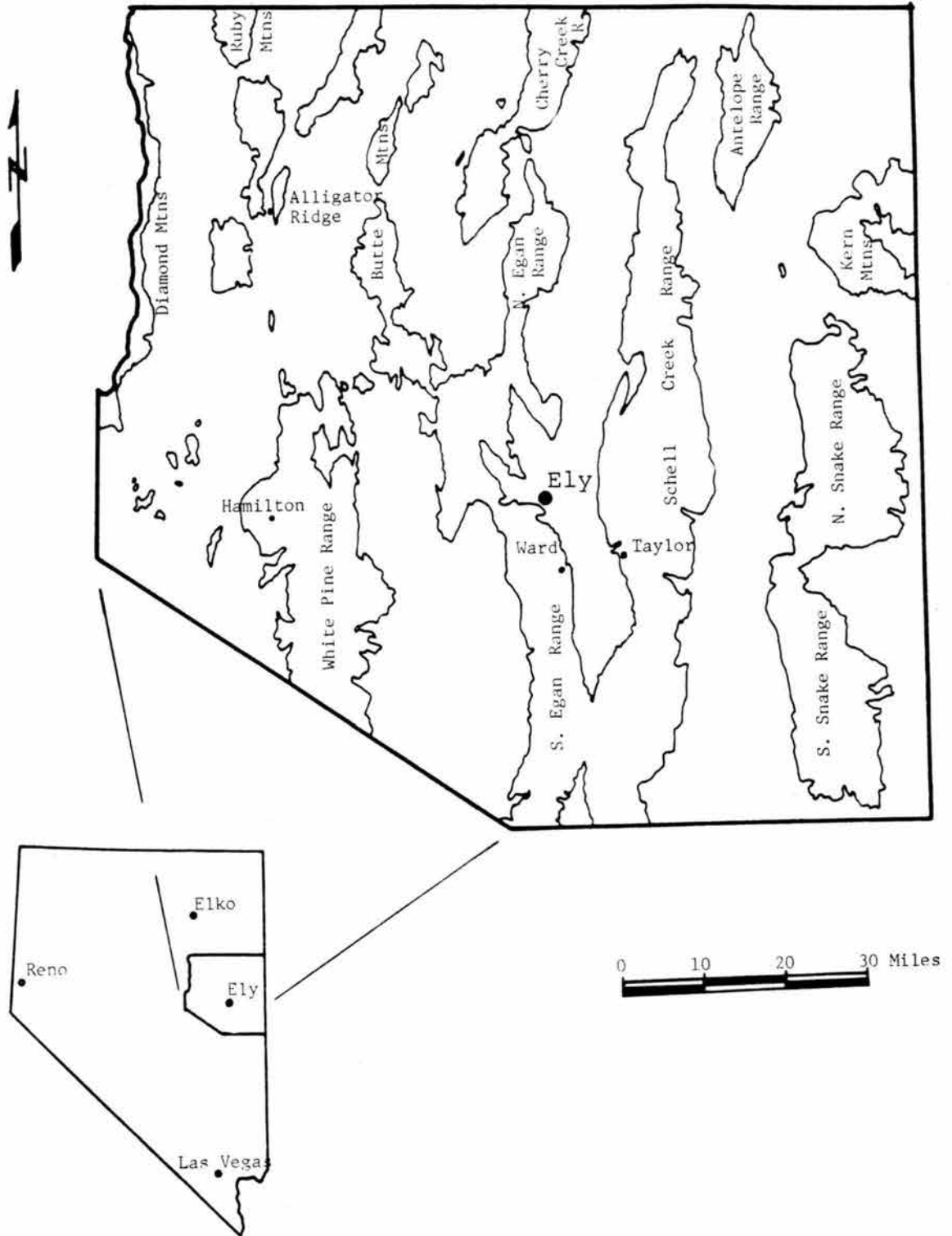


Fig. 2. Index map of White Pine County, Nevada.

The Taylor deposit is the only carbonate-hosted disseminated silver deposit currently mined in the United States. It is characteristic of a class of Ag deposits whose high grade ores were exploited in the late 1800's and early 1900's (most notably the Hamilton district, White Pine County, Nevada), but which have received little attention in the recent literature.

The purpose of this study is to describe the lithologic and structural controls of ore deposition, hypogene ore and jasperoid paragenesis, trace element content and zonation, and develop evidence that helps explain deposit genesis. The deposit is evaluated from an exploration viewpoint.

#### PHYSIOGRAPHY

Eastern Nevada, including the Southern Schell Creek Range, epitomizes Basin and Range physiography. Long linear north-south-oriented mountain ranges are bounded on one or both sides by steeply dipping normal faults. Ranges climb sharply from the depths of equally long, flat-bottomed valleys, many containing closed drainage systems. Elevations range from valley lows below 6000 feet to mountain highs above 10,000 feet.

Extreme relief accounts for the resultant gains in precipitation with increasing elevation. While precipitation averages less than 8 inches annually below 6000 feet, each elevation gain of 1000 feet may account for a 2 to 4 inch increase in precipitation so that mountain slopes above 9000 feet may receive over 20 inches per year (Hose and Blake, 1976, p.2).

Vegetation zonation, related to precipitation and temperature variation, is equally striking. At lower elevations shrubs such as sage brush, shadscale, winter fat, kochia, greasewood, various grasses, and Russian thistle comprise the dominant vegetation. Juniper and pinon pines prevail between 7000 and 8500 feet. Above 8500 feet, limber pine, bristlecone pine, and white fir dominate (Hose and Blake, 1976, p.2).

Ely, at an elevation of 6400 feet, has a mean annual temperature of 44°F. Summers can be miserably hot. Winters can be miserably cold and windy. Normally, though, it's not half bad.

The Taylor Silver District is located between elevations of 7300 and 8800 feet. Slopes in the mine area are gentle to moderate. Massive cliff-forming limestone units of the Joanna and Guilmette Formations form a rugged terrain east of the mine.

#### PREVIOUS INVESTIGATIONS

Several early reports describe, or refer to, the Taylor silver district (Hill, 1916; Spencer, 1917; Lincoln, 1923; Roberts, 1942; and Couch and Carpenter, 1943). Drewes' (1962) report on the district was the first synthesis of lithologic and structural controls on mineralization. Drewes' Professional Paper 557 (1967) on the Conners Pass Quadrangle remains the most detailed and comprehensive geologic account of the Southern Schell Creek Range.

Lawrence (1963) described the Sb deposits in the Taylor district. Lovering (1972) studied the mineralogy and chemistry of seven jasperoid hand samples from the Taylor district. In 1974, Lovering and Heyl

reported a more detailed study of jasperoids from the district. Mineralogic and semi-quantitative emission spec examination of 95 jasperoid hand samples from 23 localities formed the basis of their study. Smith (1976) discussed the history and mineral resources of the Taylor district. Hill et al. (1986) report geochemical data on several Taylor samples.

Papers by Watson (1980) and Graybeal (1981) which summarize bulk tonnage silver deposits in the western U.S. include descriptions of the Taylor silver deposit. Bagby and Berger (1985) summarized general deposit characteristics and compared the Taylor deposit to their disseminated gold model.

Havenstrite (1983) provided details of the mine and concentrator, and discussed the 20 years of exploration and development work performed by Silver King and Phillips Petroleum in the district, with a summary of genetic concepts developed by Silver King geologists.

Silver King Mines and Phillips Petroleum personnel performed the vast majority of detailed work on the Taylor deposit prior to 1982. Except for Havenstrite's (1983) summary, this work is unpublished. Silver King has graciously permitted the incorporation of all pertinent company data into this report.

Several studies elsewhere in the Schell Creek Range and neighboring ranges helped place the Taylor district into a regional context. Young (1960) mapped and described the structure and stratigraphy in the Northern Schell Creeks. Conway (1965) did the same in the Southern Schell Creeks, south of the Connors Pass Quad. Kellogg (1959, 1963, 1964) studied the structure and stratigraphy of the Southern Egan Range, southwest of Taylor.

Studies of other carbonate-hosted disseminated silver deposits are rare in the literature. The Hamilton district, located 44 miles west-northwest of Taylor, is described in detail by Humphrey (1960), and briefly by Smith (1970, 1976).

#### METHODS OF INVESTIGATION

Field work was completed during the summer of 1982. Geology of the mine and surrounding area totalling 1.5 square miles (approximately half the district) was mapped on 1:2400 scale topography with 10 foot contours furnished by Silver King. Pit boundaries and other survey points provided good ground control in the immediate mine area. Outside the mine area, aerial photos facilitated orientation if all else failed. One hundred-eighty-nine rock chip samples were collected for trace element analysis, with 126 hand samples for thin sections, polished sections, fluid inclusion plates, and vapor phase analyses. Over 1300 feet of diamond drill core were logged and sampled to provide materials for thin sections and polished sections. One hundred-eleven assay pulps were selected from six drill holes for trace element analysis.

Lab work began in September, 1982, and was completed in March, 1984. Bondar-Clegg, Lakewood, Colorado, completed trace element analyses on rock and drill samples. Exploration Research Laboratories, Salt Lake City, Utah, analyzed 23 hand samples for contained vapor phases. Technical Service Laboratories, Mississauga, Ontario, analyzed whole rock major elements of seven altered rhyolite samples. Chapter 5 contains details of all prep and analytic procedures. Petrographic

study of 81 thin sections and 25 polished sections defined ore and jasperoid paragenesis, as well as alteration in the limestones and porphyritic rhyolite bodies. Powder x-ray diffraction studies helped identify low temperature alteration mineral species. Fluid inclusion analyses in quartz, fluorite, and sphalerite, defined the minimum temperatures of formation of these minerals and yielded evidence concerning the nature of the hydrothermal fluids. A scanning electron microscope with Kevex attachment helped identify an unknown Ag sulfosalt. The GEOCHEM software package by Geomicro Systems Services Ltd. facilitated statistical analysis of trace element data.

## CHAPTER II

### DISTRICT PRODUCTION MINE AND EXPLORATION HISTORY

B. Taylor and John Platt discovered silver-lead-copper ores at Taylor in July, 1872 (Whitehill, 1875; Hill, 1916; Erickson, 1964; and Drewes, 1967). Continuous mine production from 1875 to 1892, when a decline in silver prices to \$0.87 per ounce forced closure, yielded some 2,000,000 ounces silver. Ores mined in the early days reportedly contained 50 ounces Ag and 0.04 ounces Au per ton (Smith, 1976).

After the turn of the century the district saw several renewed efforts, most importantly during 1934 to 1942, but the "flush times" didn't return until the 1979 surge in silver prices. Smith's (1976) compilation of production records for the district through 1961 is included in Table 1, with Silver King's production since 1961.

K.L. Stoker acquired the Taylor Mine area in 1960, and in 1961 formed Silver King Mines Inc.(SKM) (Havenstrite, 1983). SKM began exploration of the district in 1962, initially seeking high grade ore at depth along high angle feeder structures. A small ore body was found adjacent to the Argus fault, and in 1964 SKM sank the Taylor shaft 400 feet to exploit the deposit. In 1966 the mine produced 4000 tons of ore averaging 30 oz Ag/ton (Havenstrite, 1983). Underground exploration drifting and longholing continued through the late 1960's

Table 1: Taylor District Production

Years*	Tons treated	sales U.S. \$	oz Au	oz Ag	lbs Cu	lbs Pb	lbs Zn	st Sb**
1875-1892	?	1,000,000	?	800,000	0	0	0	0
1883-1892	39,946	1,214,648	?	1,143,000	0	0	0	0
1909-1911	162	1515	0	2854	0	0	0	0
1917	3580	71,019	0	12,455	1770	700,775	0	0
1920-1921	> 326	> 2239	1	> 2029	903	1683	0	0
1924,1926	1162	18,039	7	2717	2701	197,435	0	0
1934-1942	93,373	585,955	2236	696,867	0	0	0	10.4
1946-1954	> 7258	47,044	127	41,334	1800	27,700	7200	?
1958-1961	> 1063	?	8	> 1299	218	?	?	12.6
1966-1967	4000	?	?	120,000	?	?	?	?
1981				841,473	0	0	0	0
1982				790,961	0	0	0	0
1983				1,282,000	0	0	0	0
1984				851,914	0	0	0	0
1985-1987	0	0	0	0	0	0	0	0
TOTALS				> 6,581,903	7392	927,593	7200	23.0

\* Years 1875-1961 from Smith (1976, p 78).

Years 1961-1986 from Pescio (1988, personal commun).

\*\* Antimony [mine] production from Lawrence (1967).

(Banghart, 1966; Wise and Banghart, 1970), but failed to define significant new reserves. The mine closed in the mid 1970's.

In addition to silver, by 1960 the district had produced some 46,000 lbs antimony from Joanna-hosted stibnite-rich jasperoids (Lawrence, 1963). SKM drilled one antimony prospect, located about a half mile east of the silver mine, in the mid-1960's. They defined a small body that averaged about 3% Sb and 0.4 oz Ag/ton, reaching highs of 18% Sb and 2.6 oz Ag/ton (based on SKM drill logs). The holes were not assayed for Au. Seetone Antimony and Milling Company leased the prospect from SKM in the mid-1960's (Wise and Banghart, 1970), but production was not significant.

In April, 1966, Phillips Petroleum and Silver King signed a joint venture agreement whereby Phillips would explore Silver King's properties in White Pine County (Havenstrite et al., 1966). Phillips explored the Taylor district through the early 1970's when the joint venture was terminated. Havenstrite (1983), gives the following account of exploration and development activities which took place prior to the open pit mine opening:

Many of the percussion holes drilled in the early 1960's penetrated substantial thicknesses of low grade silver mineralization at or near the surface. The mineralization was too low grade to constitute ore at prevailing silver prices; however, when silver prices began to escalate in 1973, Silver King resumed its exploration and development drilling program. Several core holes were drilled 10 to 20 feet from existing hammer-drill holes, to check the validity of the chip samples. The core data confirmed the chip data (core samples assayed, on average, 5% higher than comparable chip samples). This check drilling also demonstrated the unique uniformity of the Taylor ore deposit; mineralization within the exterior ore boundaries is ubiquitous, and there exist few barren or high grade areas.

The percussion drilling program resumed in 1974, and has continued intermittently to the present. In all, about 450

holes have been drilled in the district since 1962, of which 22 are core holes. The drilling has outlined an area of about 40 acres underlain by ore grade mineralization, which is defined as at least a 30 foot thickness containing at least two ounces silver per ton. Using this cutoff, the ore averages 50 feet in thickness (up to 200 feet thick in a few places), with average overburden of 50 feet (waste to ore ratio is 2.0 to 1).

Measured diluted reserves using the two ounce cutoff are presently five million tons averaging 3.3 ounces silver per ton. Much of the overburden is low grade mineralized rock; if all overburden which exceeds one ounce silver per ton is "stripped to the mill", diluted reserves become seven million tons averaging 3.0 ounces silver per ton. Inferred reserves based on reasonable geologic projection will add at least three million tons of ore to the reserve.

Financing to develop the project was secured in 1979; open pit development, and construction of a 1200 ton-per-day counter-current decantation cyanide leach plant began immediately, and was completed in early 1981. Total expenditure in the district, including drilling, mine development, and mill construction, was about \$10 million.

As stated above, SKM drilled a total of 22 core holes, primarily to obtain metallurgical samples. Most holes twinned conventional rotary percussion holes. Table 2 shows comparison data for the twinned holes. Diamond holes cut 1088 feet of ore-grade rock, 3.5% less than rotary holes. Weighted average silver content of diamond hole intercepts is 5.1 oz/ton, representing a 25% increase over rotary holes which average 4.1 oz/ton. Grade-tonnage factors are 19% higher in the diamond holes. SKM did not perform size fraction analyses on drill cuttings; the discrepancy is assumed to be due to dilution of cuttings by up-hole contamination. These results suggest that the ore body is slightly smaller, but significantly higher grade than reserve estimates based on conventional rotary drill holes. Production figures, discussed below, generally confirm the conclusion that conventional rotary drilling down graded the deposit.

Table 2. Diamond drill hole / conventional rotary comparisons.

Rotary hole #	Interval	thickness (ft)	Ag (oz/t)	Grade X thickness	Core hole #	Interval	Thickness (ft)	Ag (oz/t)	Grade X thickness	Distance offset	
PT-1	32-80	48	2.9	139	SKT-100	24-72	48	3.4	163	17	
PT-2	8-40	32	7.5	240	SKT-101	8-40	32	10.7	342	12	
TA-26	40-172	132	2.8	370	SKT-102	33-172	139	3.3	459	21	
PT-5	40-92	52	4.3	224	SKT-103	44-84	40	3.4	136	12	
PT-41	10-44	34	3.4	116	SKT-104	10-36	26	3.0	78	18	
PT-8; TB-2	12-76	64	3.0	192	SKT-105	12-76	64	3.4	218	8	
SKT-272	5-80	75	2.7	202	D-1	10-85	75	5.0	375		
TA-9	10-84	74	4.6	340	D-2	10-85	75	6.5	488		
	84-160	76	2.1	160		85-175	90	2.0	178		
SKT-224		28	4.5	126	D-5	3-30	27	10.1	273	20	
TT-45		15	5.1	76	D-6	4-15	11	5.4	59	20	
		23	5.9	136		45-65	20	2.9	58		
SKT-346		11	4.6	51	D-7	40-50	10	5.9	59	15	
SKT-313		110	6.5	715	D-9	20-90	70	6.1	427	30	
SKT-261	30-250	220	3.2	704	D-10	30-250	220	6.3	1386	28	
SKT-215		62	4.5	279	D-12	8-70	62	3.6	223	24	
SKT-208		12	1.8	22	D-13	10-15	5	1.3	6	20	
PT-18	40-64	24	18.5	444	D-14	35-68	33	13.4	442	13	
SKT-239	25-60	35	3.1	108	D-17	4-45	41	3.8	157	25	
		x=59.3	x=4.1	tot=4644			x=57.3	x=5.1	tot=5527		

## THE OPEN PIT MINE

Development of the open pit mine began in 1979. Production commenced in April, 1981. Havenstrite (1983) gives the following description of the mine and plant:

The open pit mine was developed and is being mined using an Ingersoll-Rand DM 25 hammerdrill; an Ingersoll-Rand crawlair drill powered by a 850 cfm diesel compressor; a Komatsu D155A dozer; two Clark-Michigan 7 yard loaders; three Wabco 35 ton haulpack dump trucks. The mine is presently producing 35,000 tons of ore and 75,000 tons of waste per month, at a cost of \$1.30 per ton rock.

The crushing plant consists of a 30" x 42" jaw crusher; 4.25 foot standard cone crusher; 4.25 foot shorthead cone crusher in closed circuit with a 6'x 20' double-deck vibrating screen (slotted, 3/8" x 1.5"); and an open-air live storage area.

The grinding section consists of four primary and four secondary 8 foot x 72 inch Hardinge ball mills. Two stage classification using Krebs cyclones allows a grind which consistently exceeds 90% passing a 325 mesh screen.

Sodium cyanide, concentration four pounds per ton, is introduced in the ball mills. Leaching begins here and is completed in three agitation tanks arranged in series; extraction ranges from 70 to 85 % depending on which area of the ore deposit is being mined.

The pulp is washed in four stages using Enviroclear high-rate thickeners, before reporting to the tailings pond. Pregnant solution, averaging 1.5 ounces silver per ton, is clarified in two U.S. drum-type filters; de-aerated; precipitated by zinc (Merrill-Crowe process); and the metallic silver separated from the now barren solution in three filter presses. The silver precipitate, averaging 80% silver, is dried and shipped for refining.

Taylor operated continuously from March, 1983 through March, 1984. Production and cost records for that period are summarized by Figures 3 through 7, and Tables 3 and 4.

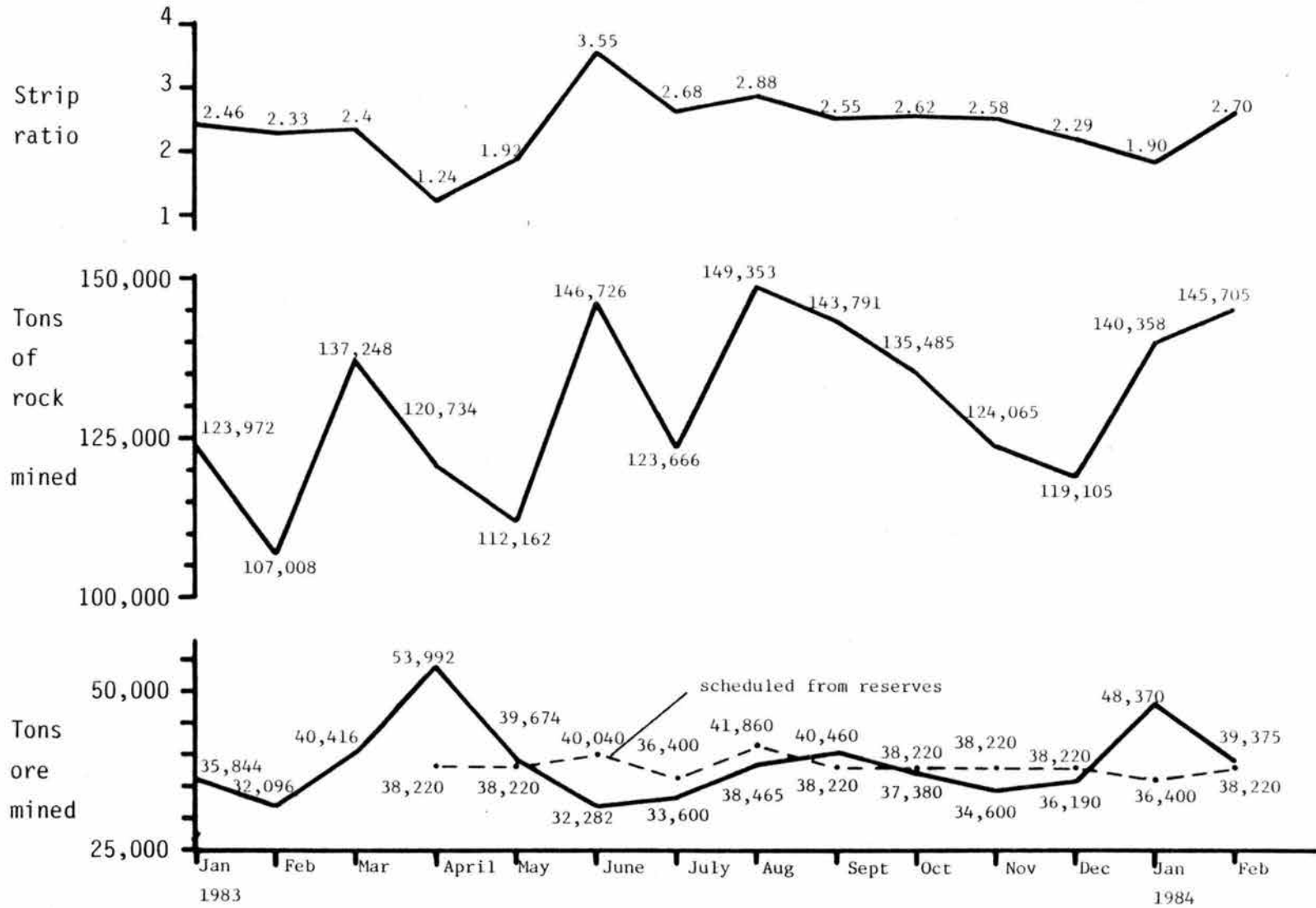


Fig. 3. Taylor mine production: 1983/1984.

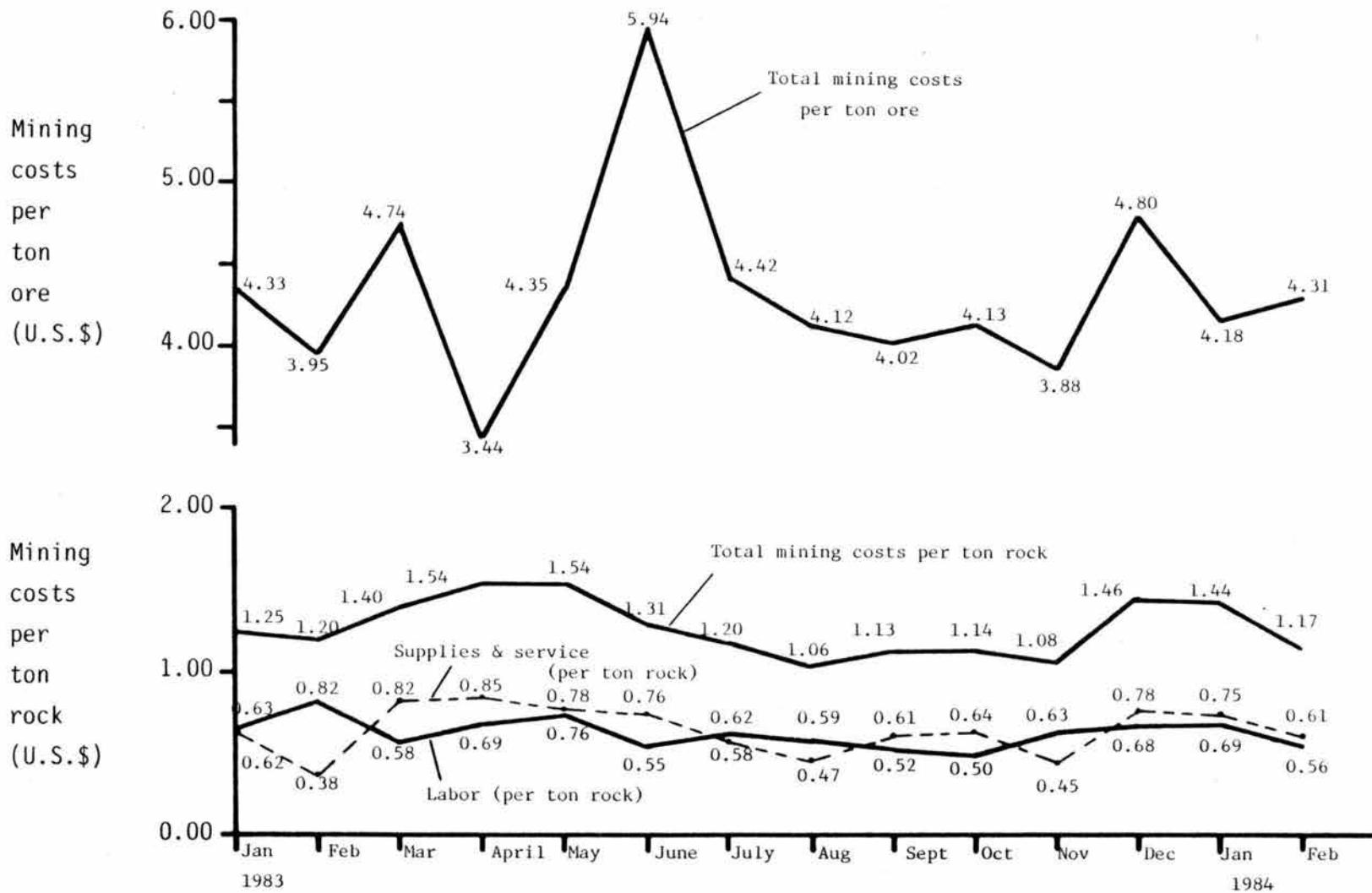


Fig. 4. Taylor mine costs: 1983/1984.

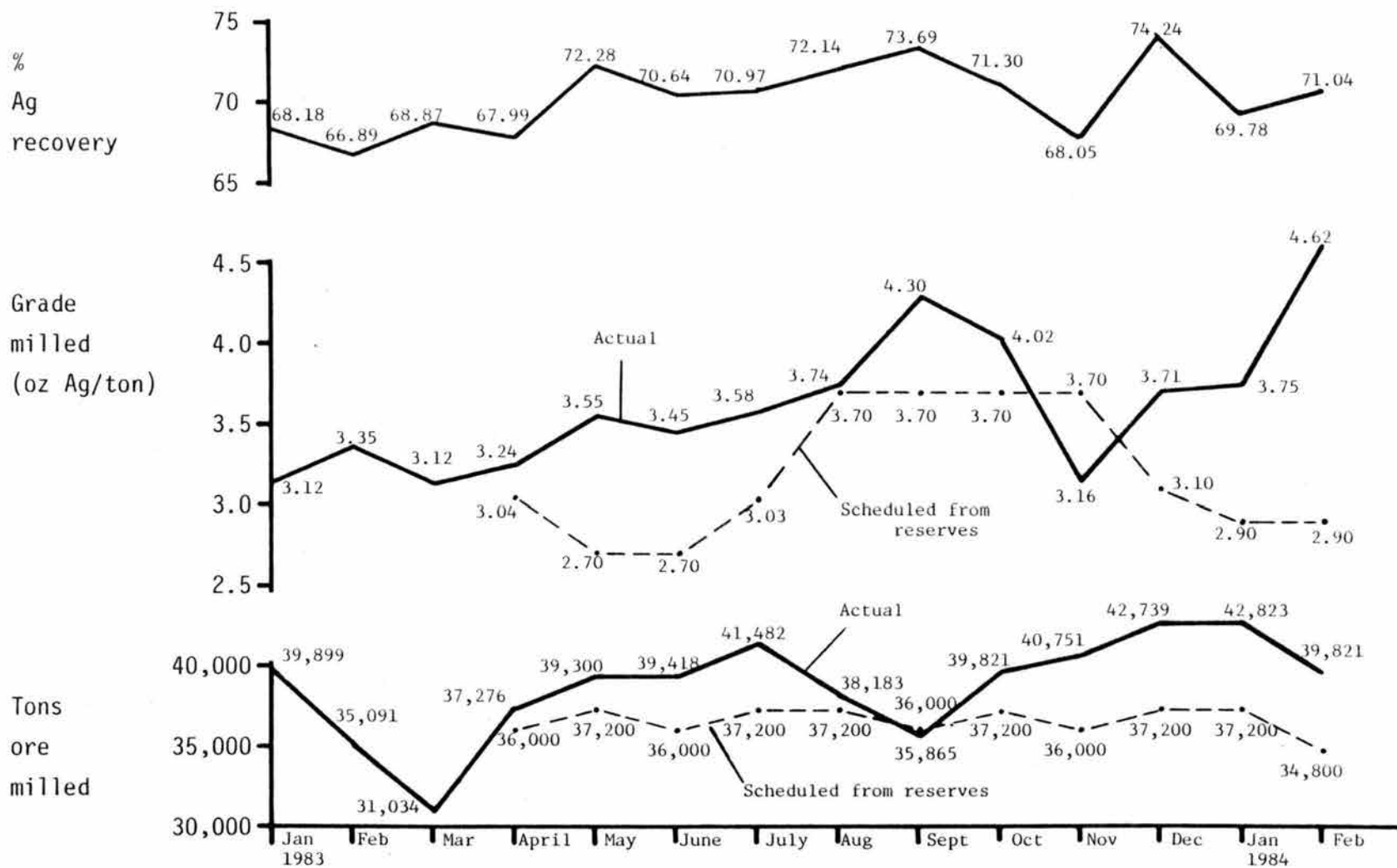


Fig. 5. Taylor mill production: 1983/1984.

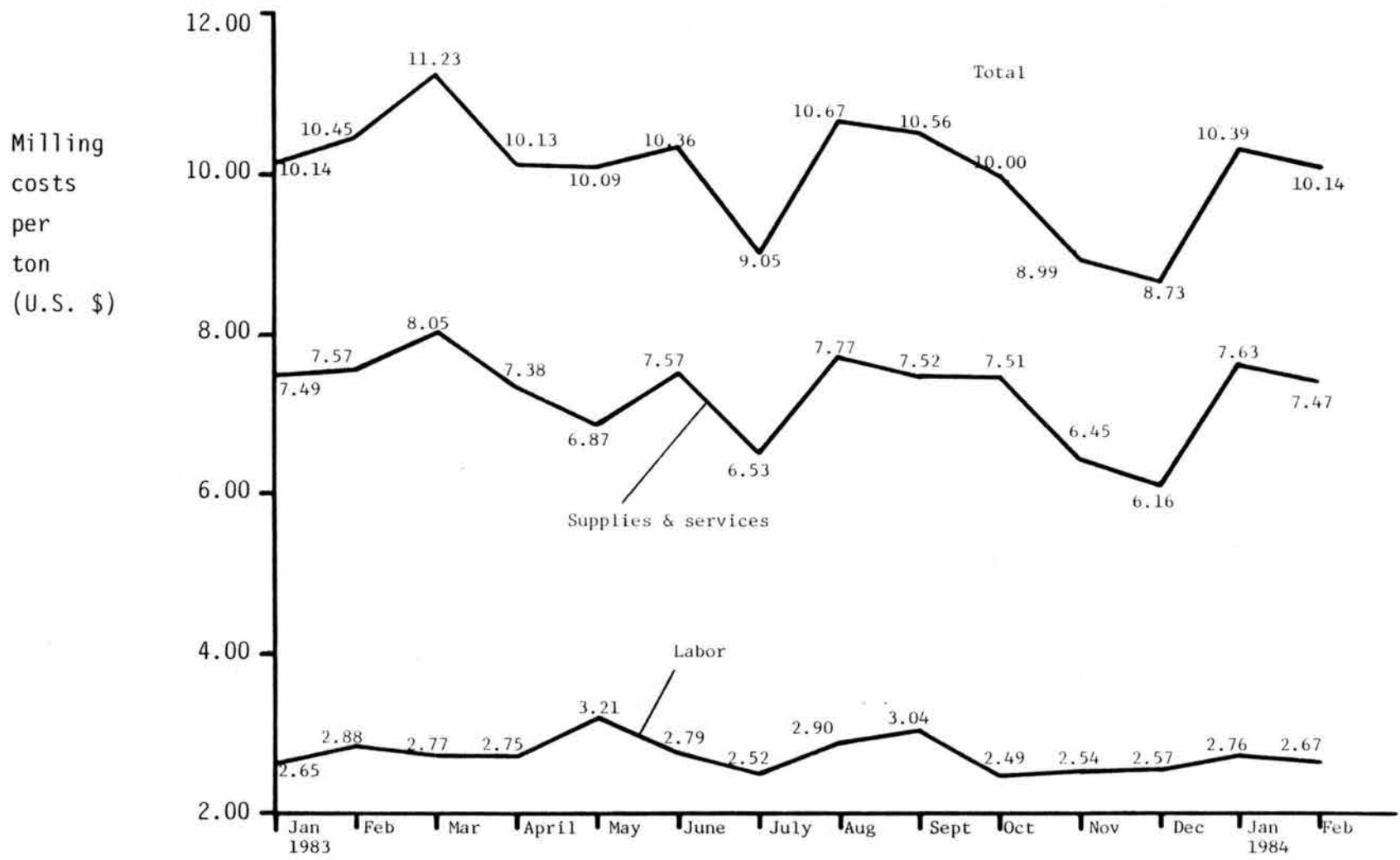


Fig. 6. Taylor mill costs: 1983/1984.

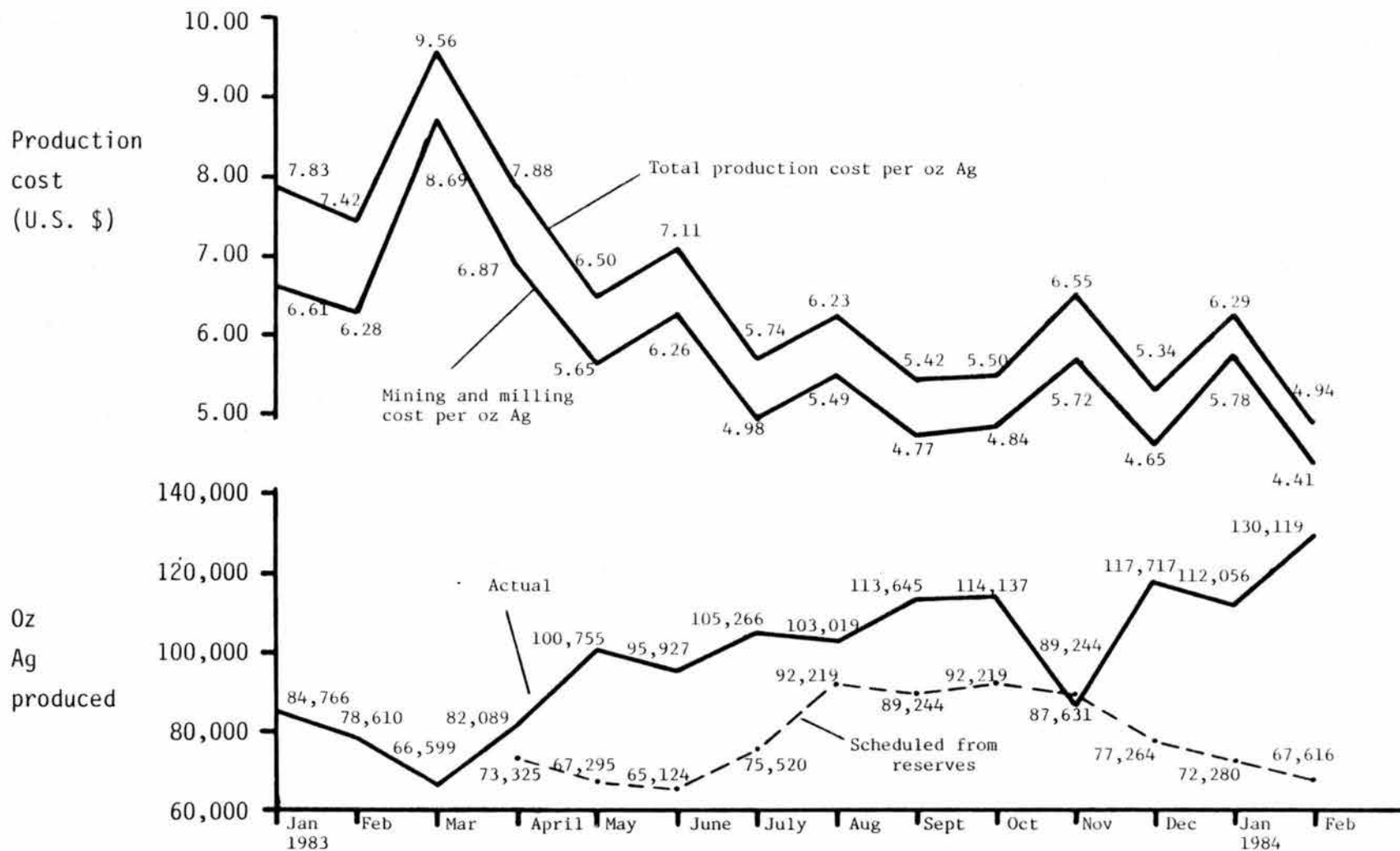


Fig. 7. Taylor production costs: 1983/1984.

Table 3: Taylor mining cost breakdown. Fiscal year 1983-1984.

	1st quarter	2nd quarter	3rd quarter	total
Rock tons	379,622	416,810	378,655	1,175,087
Blast hole drilling	\$0.31	\$0.21	\$0.23	\$0.25
Blasting	0.20	0.14	0.14	0.16
Exploration drilling	0.04	-	-	0.01
Eng. and geology	0.06	0.05	0.07	0.06
Assaying	0.10	0.08	0.08	0.09
Load-haul-stockpile	0.40	0.35	0.39	0.38
Mine main. shop	0.01	0.01	0.02	0.01
Mine mobile equip.	0.06	0.08	0.02	0.05
Mine power and air	-	-	-	-
Fuel and lube	0.17	0.13	0.19	0.16
Mine overhead	0.03	0.02	0.02	0.03
Mine cost per ton rock	\$1.45	\$1.13	\$1.22	\$1.26

Table 4: Taylor milling cost breakdown. Fiscal year 1983-1984.

	1st quarter	2nd quarter	3rd quarter	Total
Tons milled	115,994	115,530	123,311	354,835
Power	\$1.85	\$1.42	\$1.57	\$1.61
Crushing	0.91	1.04	0.76	0.90
Grinding	2.91	2.78	2.58	2.75
Leaching and filtering	3.29	3.54	3.11	3.31
Assaying	0.21	0.20	0.15	0.19
Warehouse	0.12	0.13	0.15	0.13
Mobile equip.	0.07	0.06	0.04	0.06
Tools and shop	0.03	0.03	0.02	0.03
Fuel and lube	0.03	0.05	0.06	0.05
Tails pond	0.11	0.19	0.19	0.16
Overhead	0.54	0.53	0.49	0.52
Other	0.13	0.09	0.11	0.11
Mill cost per ton rock	\$10.20	\$10.06	\$9.23	\$9.82

Total ore and waste mined during the first three quarters was 1,575,531 tons. This included 466,424 tons @ 3.64 oz Ag/ton to the mill, 204,920 tons @ 1.45 oz Ag/ton to low grade stock piles, and 904,187 tons to dumps. The strip ratio averaged 2.39 : 1. Mining costs averaged \$1.26 per ton rock, or \$4.28 per ton ore.

Mill feed averaged 3.64 oz Ag/ton through the period, with about 0.003 oz Au/ton. These grades were 12% higher than estimated reserves of 3.26 oz Ag/ton (reserves were estimated by the polygonal method on a somewhat irregular, 100 foot  $\pm$ , conventional rotary drill grid). Milling costs averaged \$9.82 per ton. Recovery averaged 71.26%.

Mining and milling costs averaged \$5.40 per ounce. Additional management costs ran about \$0.80 per ounce for a total production cost of \$6.20 per ounce. Depreciation was estimated at \$1.20 per ounce.

Figure 8 shows production figures for the month of January, 1984. Daily mill feed grades ranged from 2.71 to 5.52 oz Ag/ton, while tails were more constant, ranging between 0.96 and 1.36 oz Ag/ton. Percent recovery is plotted verses mill feed grade in Figure 9. The regression line and a correlation coefficient of 0.863 indicate that recovery rates increase markedly with grade. Higher grade rock contains increasing proportions of relatively coarser grained silver-bearing minerals (discussed in chapter IV) which are more accessible to cyanide solution.

#### PRODUCTION ECONOMICS

Table 5 shows pro forma cash flow and net present value analyses that follow the general format described by Peters (1978, p265-278).

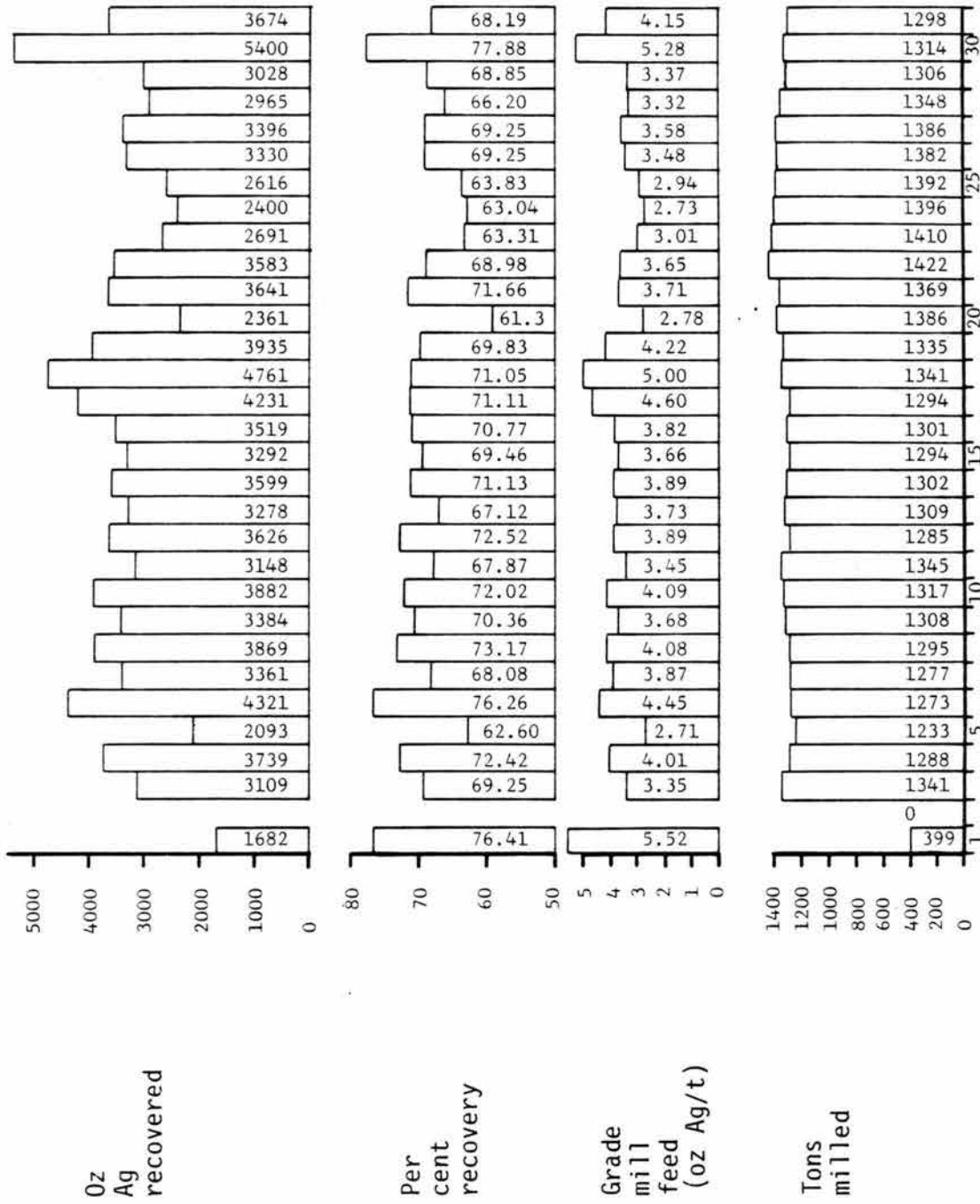


Fig. 8. Taylor mill records: January, 1984.

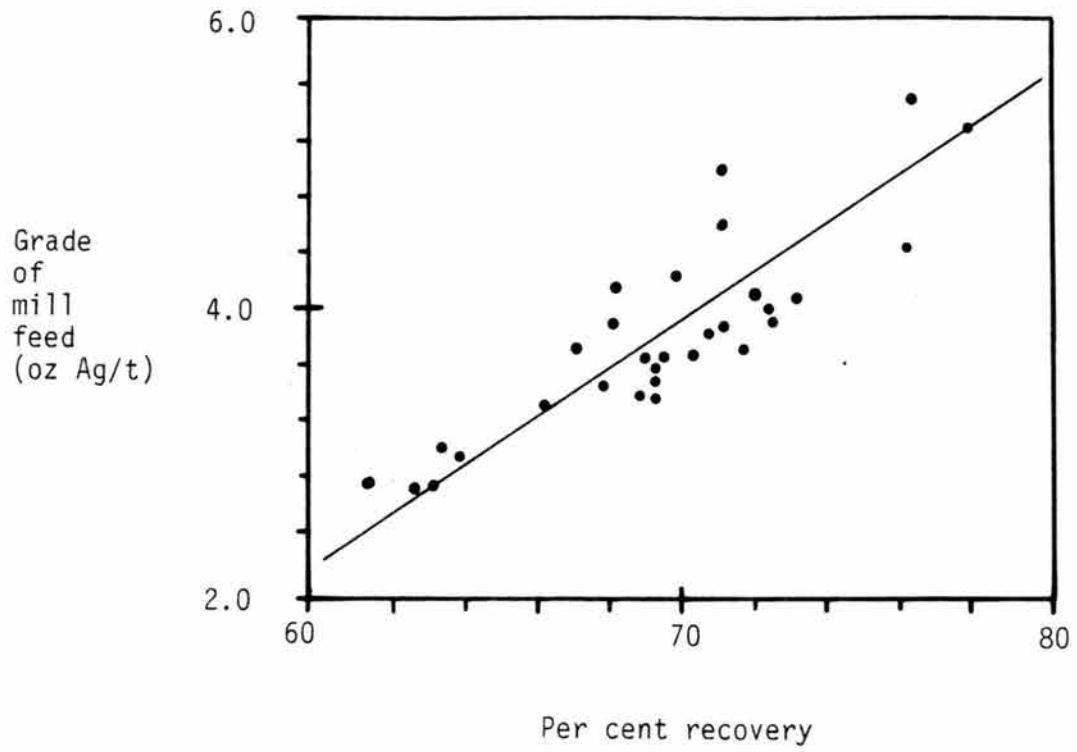


Fig. 9. Recovery rates versus grade of mill feed: January, 1984. (n = 30; regression coefficient = 0.863).

Table 5: Taylor-Type mine cash flow analysis.

## Parameters used:

5,000,000 tons reserves @  
 3.5 oz Ag/t  
 0.003 oz Au/t  
 1300 tons/day milling: 350 days/year  
 \$10,000,000 capitol costs  
 2.4 : 1 strip ratio  
 \$10 /t milling costs  
 \$1.25 /rock ton mining costs  
 \$0.80 /t management costs  
 5% royalty  
 71% recovery rate  
 \$400 /oz Au price  
 annual Ag prod.: 1,130,675 oz  
 annual Au prod.: 969 oz  
 mine life: 11 yr

Ag price:	\$12	\$10	\$8	\$6
ANNUAL:	(thousands \$ except payback and prod. cost)			
Revenues	13,956	11,694	9,433	7,172
management costs	(364)	(364)	(364)	(364)
royalties	(680)	(567)	(453)	(340)
net sales	12,912	10,764	8,616	6,467
mining costs	(1,934)	(1,934)	(1,934)	(1,934)
milling costs	(4,550)	(4,550)	(4,550)	(4,550)
operating income	6,428	4,280	2,132	(16)
depreciation	(1,000)	(1,000)	(1,000)	(1,000)
net before depl.	5,428	3,280	1,132	(1,016)
depletion	(1,937)	(1,615)	(566)	0
taxable income	3,492	1,666	566	(1,016)
tax (50%)	(1,746)	(833)	(283)	0
net income	1,746	833	283	(1,016)
plus depreciation	1,000	1,000	1,000	1,000
plus depletion	1,937	1,615	566	0
annual cash flow	4,683	3,447	1,849	(16)
payback period	2.1	2.9	5.4	NEVER
cash cost of prod.	\$5.39	\$5.39	\$5.39	\$5.39
net present value (15% discount rate)	11,302	5,924	(1,037)	(9,159)

These back-of-the-envelope analyses do not represent precise cash flows achieved by SKM at Taylor. Specific finance and accounting methods utilized by SKM are not considered. Rather, the deposit is evaluated from a grass-roots exploration viewpoint, to determine whether the deposit type warrants expenditure of resources. Parameters used to construct Table 5 are: total reserves of 5,000,000 tons @ 3.5 oz Ag/ton and 0.003 oz Au/ton; 455,000 tons milled per year at a rate of 1300 tons per day; 71% average Ag recovery; mining costs of \$1.25 per ton rock; strip ratio of 2.4:1; milling costs of \$10.00 per ton; total preproduction capital of \$10,000,000; and a 5% royalty. Straight line 10% annual depreciation was used with a 15% depletion rate. Net present value calculations were simplified by assuming constant cash flow over a 10 year mine life and a 15% discount rate.

The Taylor mine is highly profitable at \$12 Ag and \$400 Au (the prices which prevailed at the time it opened). It is marginal below \$8 Ag, and sub-economic below \$6.20 Ag.

Another analysis, presented in Table 6a, indicates the minimum price of Ag at which a Taylor-type deposit could be developed today. Additional assumptions include a more reasonable \$20,000,000 capital outlay. The deposit requires nearly \$11 Ag and \$400 Au to be viable.

Table 6b indicates that a ten million ton [Taylor-type] deposit containing 5 oz Ag/ton and 0.004 oz Au/ton might be viable at \$6.50 Ag. A capital outlay of \$45,000,000 for a 3000 ton per day mill was assumed, with mining and milling costs of \$3.40 per ton ore and \$10.00 per ton respectively, and a 78% recovery factor (scaled from Fig. 9).

Table 6: Economics of hypothetical Taylor-Type deposits

(a) Minimum prices required to develop the Taylor deposit in 1987.      (b) Minimum size and grade required to develop a deposit at \$6.50 Ag

## Parameters:

5,000,000 tons @  
3.5 oz Ag/ton  
0.003 oz Au/ton  
1300 tons/day mill  
350 days/year  
\$20,000,000 capital  
2.4 : 1 strip ratio  
\$1.25/ton mining costs  
\$10.00/ton milling  
\$0.80/ton management  
5% royalty  
71% recovery  
11 year mine life  
1,130,675 oz Ag/yr  
969 oz Au/yr  
\$400 Au  
\$11 Ag

## Parameters:

10,000,000 tons @  
5.0 oz Ag/ton  
0.004 oz Au/ton  
3000 ton/day mill  
350 days/year  
\$45,000,000 capital  
2.4 : 1 strip ratio  
\$1.00/ton mining costs  
\$10.00/ton milling  
\$0.80/ton management  
5% royalty  
78% recovery  
10 year mine life  
4,095,000 oz Ag/yr  
3,276 oz Au/yr  
\$400 Au  
\$6.50 Ag

## ANNUAL:

revenues	12,825	27,928
management costs	(364)	(840)
royalties	(623)	(1,354)
net sales	11,838	25,734
mining costs	(1,934)	(3,570)
milling costs	(4,550)	(10,500)
operating income	5,354	11,664
depreciation	(2,000)	(4,500)
net before depl.	3,354	7,164
depletion	(1,677)	(3,582)
taxable income	1,677	3,582
tax (50%)	(839)	(1,791)
net income	839	1,791
plus depreciation	2,000	4,500
plus depletion	1,677	3,582
annual cash flow	4,516	9,873
payback	4.4 yrs	4.6 yrs
cash cost of prod	\$5.39/oz Ag	\$3.12/oz Ag
Net present value (15% discount rate)	1,488	2,096

## CHAPTER III

### REGIONAL GEOLOGY

#### STRATIGRAPHY

Eastern Nevada is underlain by a thick sequence of Upper Precambrian and Paleozoic platform carbonates interbedded with lesser shales, siltstones, and quartzites (Fig. 10). Only minor disruptions in sedimentation occurred from Late Precambrian through Early Triassic. Over 40,000 feet of sediments accumulated in much of eastern Nevada (Stewart, 1980). The sedimentary prism thins eastward, pinching out in the Wasatch Range of Utah, while thickening westward. Sediments indicative of shallow water continental shelf deposition in western Utah and eastern Nevada grade westward into deep water pelagic rocks in central Nevada.

The sedimentary prism in eastern Nevada can be broken into 4 major episodes based on the clastic component (Fig. 11). A thick clastic wedge dominates the base of the section. Through Late Precambrian and Cambrian time, erosion on the craton shed clastics westward onto an initially rapidly subsiding shelf. This clastic wedge, comprised of Upper Precambrian metasediments, the Prospect Mountain Quartzite and the Pioche Shale, is over 5000 feet thick in the Southern Schell Creeks (Drewes, 1967), with at least another 10,000 feet of Upper Precambrian sediments at depth. Twelve thousand feet of open marine shelf to

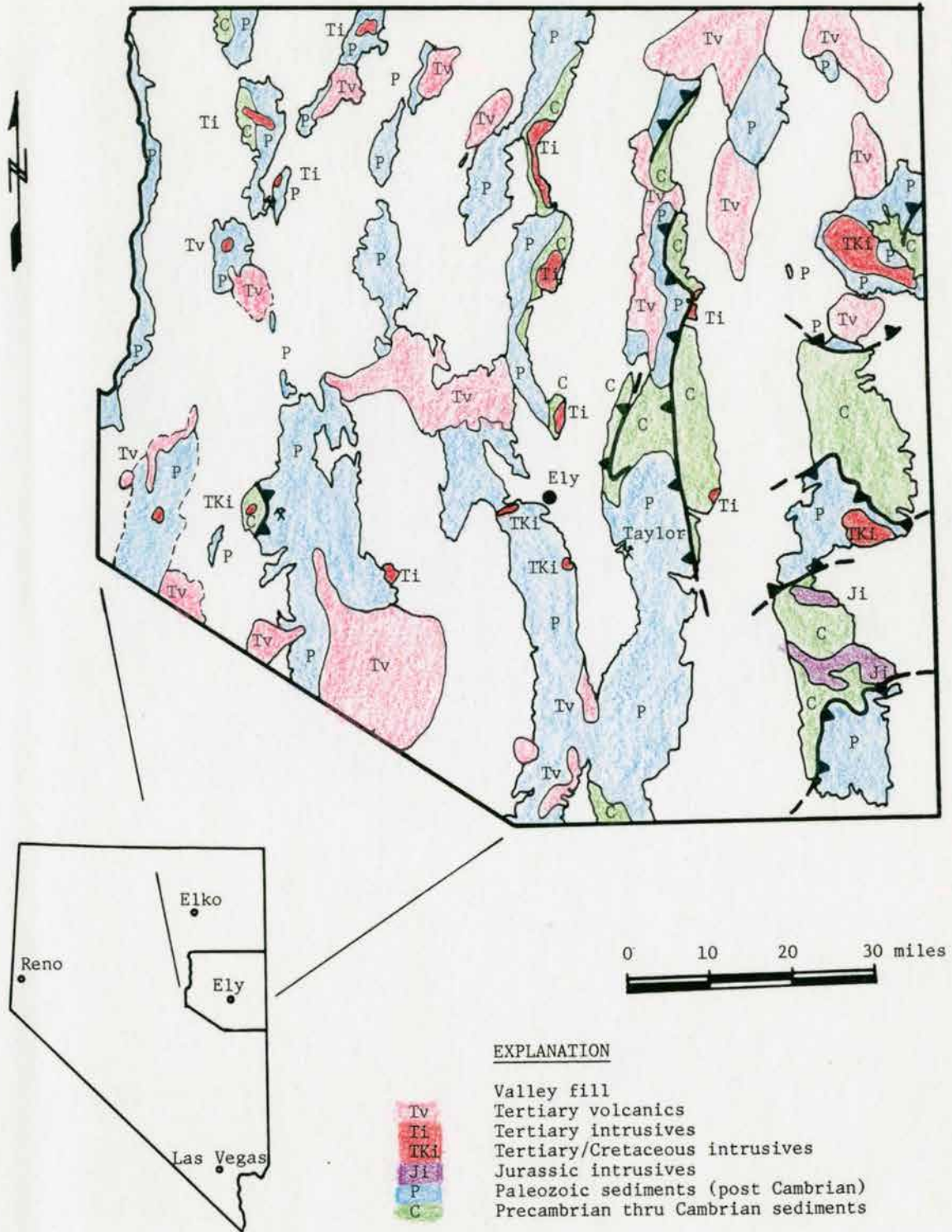


Fig. 10. General geology of White Pine County.  
(generalized from Hose and Blake, 1976, Plate 1).

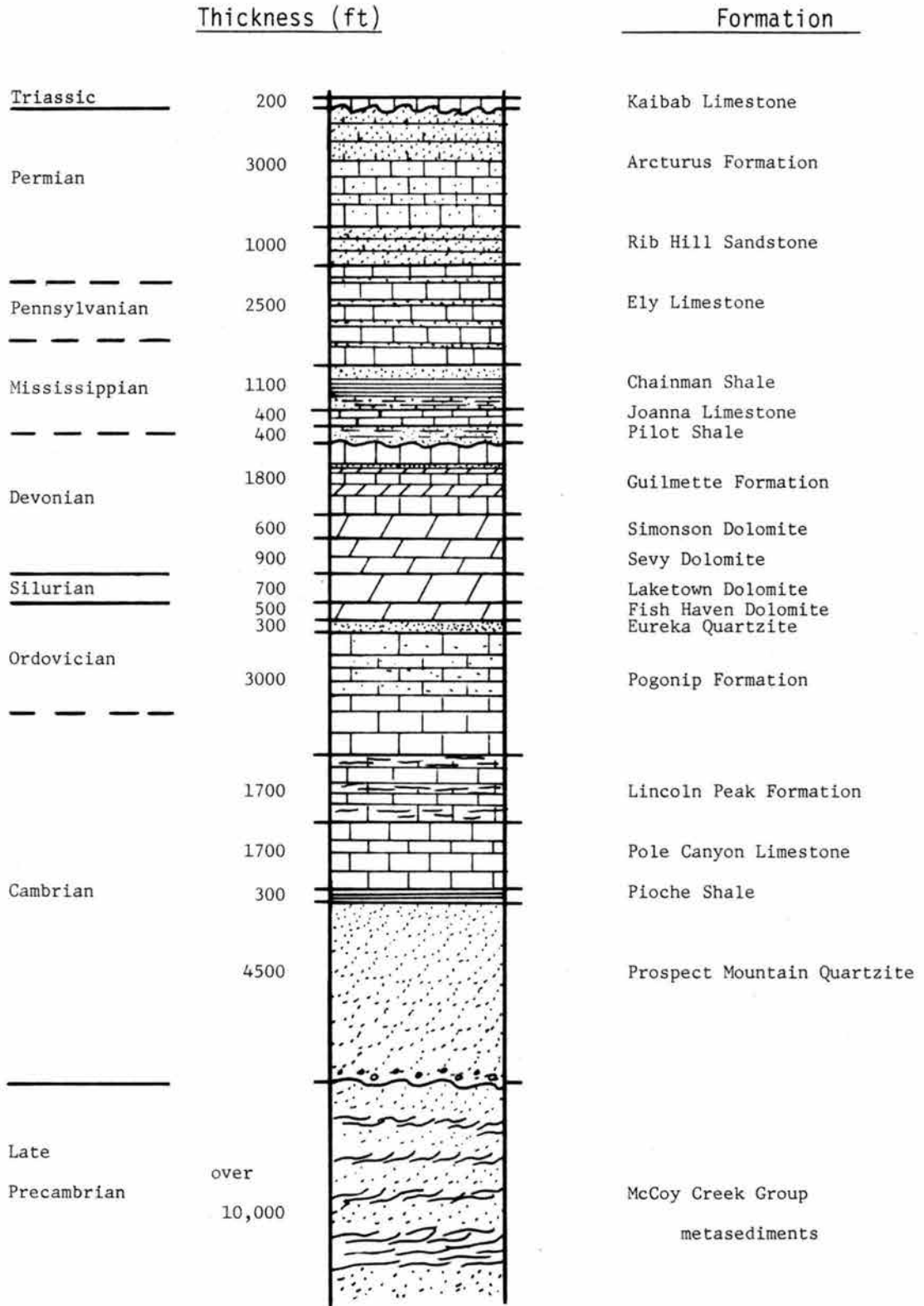


Fig. 11. Generalized stratigraphic column: Eastern Nevada. Vertical scale 1 in. = 4000 ft. Compiled from Drewes (1967) and Hose and Blake (1976).

platform carbonates (Matti, 1978) accumulated during Late Cambrian through Middle Devonian epochs in the Southern Schell Creeks (Drewes, 1967). The Pole Canyon Limestone, Lincoln Peak, Pogonip, Eureka Quartzite, Fish Haven Dolomite, Laketown Dolomite, Sevy Dolomite, Simonson Dolomite, and Guilmette Formations comprise this thick carbonate section. In Late Devonian time, a major change occurred in sedimentation of eastern Nevada. The Antler orogeny shoved allochthonous western facies rocks over the transitional rocks of central Nevada, creating a highland which shed clastics eastward onto the platform. Clastic sediments dominate the Upper Devonian through Mississippian section. The Pilot Shale, Joanna Limestone, and Chainman Shales, totalling 2000 feet in the Schell Creeks, comprise this interval. Re-emergence of shallow water carbonate sedimentation in eastern Nevada marks the Pennsylvanian through Triassic periods. The clastic component in these rocks increases westward toward the Antler highlands in central Nevada. The Ely Limestone, Rib Hill Sandstone, and Arcturus Formations represent this 6000 foot section in the Southern Schell Creeks, where more than 1100 feet of Upper Permian and Lower Triassic rocks are not preserved (Drewes, 1967; Hose and Blake, 1976).

Upper Triassic and Lower Jurassic fluvial and lacustrine sediments totalling over 2500 feet are locally preserved in Elko and White Pine Counties (Stewart, 1980). Lack of sedimentation from Middle Jurassic to Late Cretaceous suggests that the region was a highland throughout this time.

In Late Cretaceous (?) and Paleocene time, the Sheep Pass Formation was deposited over the Southern Egan Range and into Railroad

Valley (Kellogg, 1959, 1964; Fooch, 1977). Up to 3300 feet of these heterolithic conglomerates and lacustrine sediments overlie the upper Chainman Shale and lower Ely Limestone (Miss. /Penn.) with slight angular unconformity (Kellogg, 1959; 1964).

Eocene Stinking Spring Conglomerates unconformably overlie the Sheep Pass Formation in the Southern Egan Range (Fooch, 1977). The Stinking Spring Conglomerate was deposited onto the Permian Arcturus Formation in the central and northern Egan Range (Brokaw and Shawe, 1965; Brakaw, 1967; Fooch, 1977), and onto lower Ely Limestone and Arcturus Formation in the Schell Creeks, implying significant pre-Eocene structural offsets (Young, 1960; Drewes, 1967; Hose and Blake, 1976). Sub-angular to sub-rounded clasts derived primarily from the Ely, Arcturus, and Rib Hill Sandstone formations comprise the conglomerates in the Southern Schell Creeks (Drewes, 1967). Drewes (1967) suggested that the Snake Range uplift was the most likely source. The upper portion of the Stinking Spring Conglomerate contains a significant tuffaceous component. Widespread volcanism broke out across northeastern Nevada at 43 Ma and spread south through 34 Ma (Stewart, 1980). A 300 foot thick rhyolite flow, possibly correlative with Young's (1960) Oligocene Kalamazoo volcanics, overlies the Stinking Spring Conglomerates in the Southern Schell Creeks (Drewes, 1967). Welded ash flow tuffs which Hose and Blake (1976) correlate with the 32 to 34 Ma Stone Cabin Formation in turn overlay this unit. Several younger volcanic episodes are recorded elsewhere in Eastern Nevada, with dates of 29 to 32 Ma, 22 to 24 Ma, and 20 to 21 Ma (Hose and Blake, 1976). Olivine basalt flows first appeared in the region at 17 Ma, marking the onset of Basin and Range extension (Stewart, 1980).

## INTRUSIVE ROCKS

Hose and Blake (1976) recognize three general groups of intrusive rocks in White Pine County. The oldest comprise a north-south belt of muscovite-bearing granites found in the Snake, Pilot, Kern, and Ruby Ranges, dated between 149 and 161 Ma (Lee et al., 1970; Miller and Bradfish, 1980; Jordan et al., 1983; Snoke et al., 1984). This belt is part of a broader zone of peraluminous magmatism described by Miller and Bradfish (1980), which extends the length of the cordillera from Canada into northern Mexico. The western edge of the belt defines the inferred edge of the Precambrian sialic crust. An apparent bimodal distribution of age dates (149 to 161 Ma and 43 to 73 Ma) suggests that renewed peraluminous magmatism occurred during Paleocene to Eocene time along the belt (Lee et al., 1970; Miller and Bradfish, 1980; Hose and Whitebread, 1983; Gans et al., 1986).

A second group of plutons recognized by Hose and Blake (1976) define an east-west trend from Eureka through Ely. These calc-alkaline stocks intruded the region between 70 and 110 Ma (Miller et al., 1986). Monzonite porphyries of this group are the source of copper ores in the Robinson district, near Ely (McDowell and Kulp, 1967).

The third group of intrusives is also the most widespread, and relate both in age and composition to Oligocene volcanism described above (Hose and Blake, 1976; Stewart, 1980). Rhyolite porphyries of this group are dated at 35 Ma in the Robinson and Ward districts, near Ely (McDowell and Kulp, 1967; Havenstrite, written communication, 1983). Dates reported by Hose and Blake (1976) range from 33 to 37 Ma through eastern White Pine County.

Younger latite vitrophyre dikes cut Oligocene volcanics in the Southern Schell Creeks (Drewes, 1967) and are probably related to early Miocene volcanism.

### STRUCTURAL SETTING

Eastern Nevada is structurally complex. Piecemeal evidence across eastern Nevada and western Utah indicates that a polyphase deformational history began in Middle Jurassic time and produced recurrent movements of diverse origin on many fault surfaces. The general lack of Mesozoic sedimentary rocks complicates structural interpretation. Accordingly, a large number of conflicting interpretations have evolved in the literature. The following summary of documented and inferred structural events is consistent with the geology of the Southern Schell Creek Range as mapped by Drewes (1967). Figure 12 shows the principal pre-Basin and Range structural features of Nevada.

#### PRE-MIDDLE JURASSIC

Major pre-Middle Jurassic structural events, including the Antler (Mississippian), Sonoma (Early Triassic), and Nevadan (Early Jurassic), deformed large areas of western and central Nevada (Stewart, 1980). Only the Antler significantly affected eastern Nevada by producing a north-south-oriented trough at the toe of the Roberts Mountain allochthon and, further to the east, an up-arched area in response to down loading to the west (Speed and Sleep, 1982).

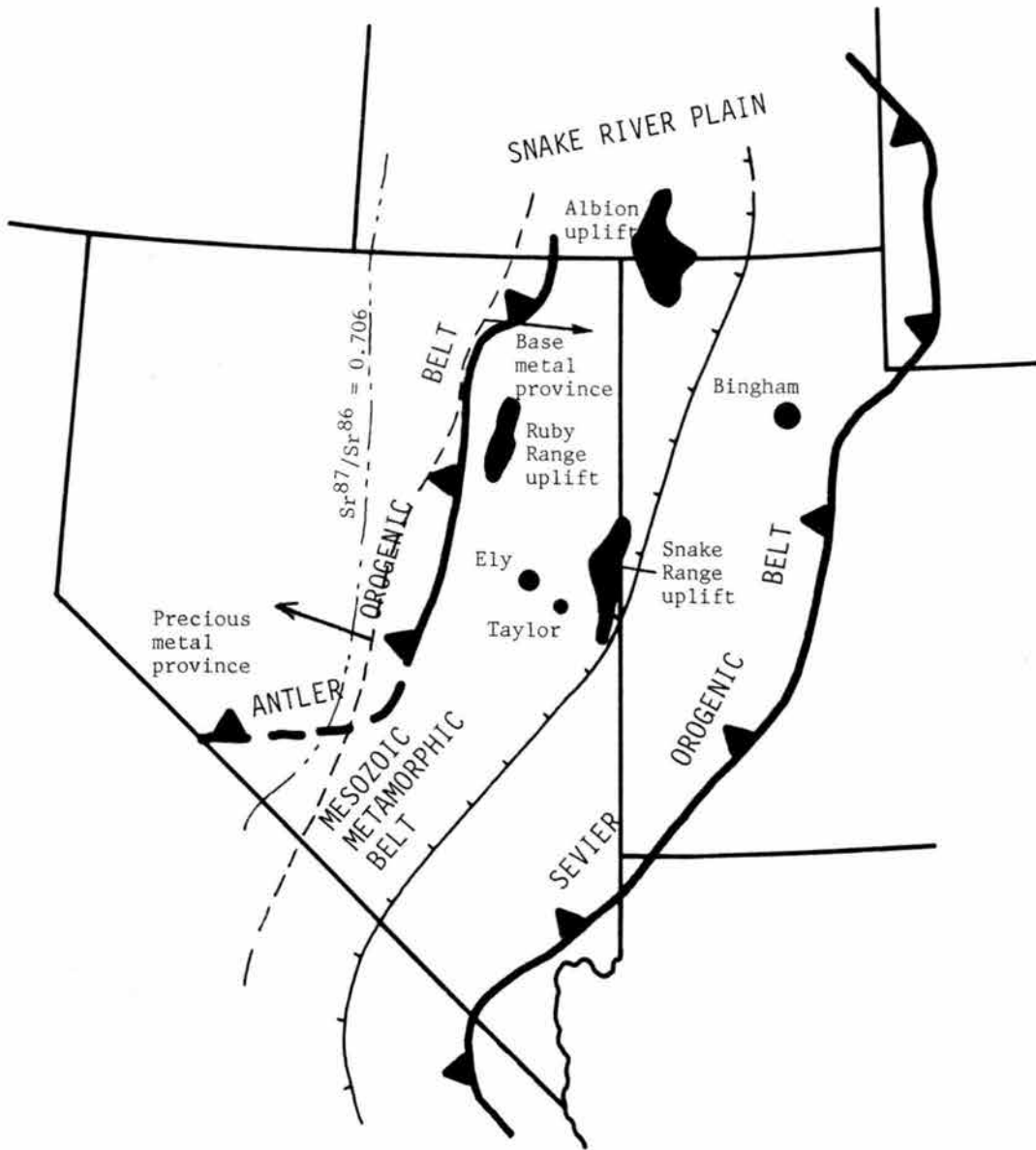


Fig. 12. Index of major structural features: Great Basin (compiled from Stewart et al. 1977; Shawe et al. 1978; Coney, 1980; Stewart, 1980; Dickinson, 1981; Wilkins, 1984).

## MIDDLE JURASSIC TO LATE CRETACEOUS

Deformation in the Sevier overthrust belt of central-western Utah began at approximately 150 Ma (Late Jurassic), and continued without break until about 75 Ma (Late Cretaceous)(Armstrong, 1974). Estimates of total west-to-east shortening across the overthrust belt range from 40 to 60 miles (Armstrong, 1968). Evidence reported from ranges throughout the hinterland of western Utah and eastern Nevada indicate that polyphase deformation began there by Late Jurassic and continued until Late Cretaceous, as thrusting in the Sevier belt progressed eastward.

Many workers, including Misch (1960, 1983), McDowell and Kulp (1967), Roberts and Crittenden (1973), Hose and Blake (1976), Stewart (1980), Jordan et al. (1983), Miller (1983), Rodgers (1983, 1986), Snoke (1983), Fryxell (1984), Heck et al. (1984), Snoke et al. (1984), Gans et al. (1986), Lund and Beard (1986), and Miller et al. (1986) describe Jurassic and Cretaceous metamorphic, intrusive, and structural relationships in the hinterland. The important aspects can be summarized as follows: Early deformation in the hinterland of eastern Nevada was associated with the emplacement of 149 to 161 Ma muscovite-bearing plutons (Hose and Blake's first group) to levels as high as the Ely Limestone. These plutons locally cut thrust faults. They were accompanied by migmatization and produced broad contact metamorphic aureoles. Some thrust faults which both predate and accompany regional metamorphism produced up to 5 kilometers of stratigraphic duplication. Greenschist- to staurolite-grade regional penetrative metamorphism postdates small to large scale east vergent recumbent folding and

formed east-dipping cleavage. Degree of metamorphism increases with depth below the brittle/ductile transition, at >6km. Seventy to one hundred-ten Ma calc-alkaline plutons (Hose and Blake's second group) subsequently intruded the region; their contact aureoles overprinted older metamorphic textures. Regional metamorphism continued at depth until Late Cretaceous, and imposed west-dipping cleavage on older fabrics. Cretaceous plutons crosscut thrust faults in the overlying supracrustal rocks.

#### LATE CRETACEOUS THROUGH EARLY MIOCENE

Compressive deformation and related calc-alkaline magmatism propagated eastward into the Laramide belts of Colorado and Wyoming around 75 Ma (Armstrong, 1974; Dickinson, 1981). Between the end of the Sevier Orogeny and the onset of Basin and Range normal faulting at 17 Ma the hinterland of eastern Nevada and western Utah was subjected to apparent extension (Armstrong, 1972; Coney, 1974). This resulted in tectonic denudation of up to 15,000 feet of supracrustal rocks across a complex series of low angle younger on older faults (Whitebread, 1966; Armstrong, 1972). Degree of denudation appears to decrease both eastward and westward away from core complexes exposed in the Snake and Ruby/Humboldt ranges (Coney, 1974, 1980; Coney and Harms, 1984). Post-Cretaceous low-angle denudational fault movement along the brittle/ductile transition imparted a mylonitic fabric to underlying metamorphics of the infrastructure. The core complexes shed rocks of the suprastructure both east and west (Coney, 1974). Many workers propose a single or two-stage post early Oligocene uplift and

denudational event based on reset age dates from rocks of the infrastructure and the fact that Oligocene volcanics were offset (Coney, 1974, 1980; Coney and Harms, 1984; Gans, 1982; Miller et al., 1982; Miller et al., 1983; Bartley and Wernicke, 1984; Bartley et al., 1984; Blackwell et al., 1984; Gans et al., 1985; Rehrig, 1986).

The distribution of Paleocene and Eocene conglomerates and Oligocene igneous rocks, however, indicate a more complex history. Hose and Whitebread (1983) propose three-stage extensional denudation of the Northern Snake Range. Stage 1 arched the region during Late Cretaceous and Paleocene time (Hose and Danes, 1973; Hose and Blake, 1976). This highland may have been the source for the Sheep Pass Formation conglomerates. Kellogg (1964) states that "large scale gravity sliding" emplaced blocks into the Sheep Pass basin prior to deposition of the conglomerates. Newman (1978) shows that contemporaneous high angle fault movement controlled deposition of the Sheep Pass Fm. In the Northern Snake Range, inferred 56 Ma granites cut a mylonitized fault contact.

Stage two occurred after 56 Ma but prior to Oligocene volcanism. Hose and Whitebread (1983) suggest that the major uplift and denudation of the Snake Range took place during this time. Renewed peraluminous magmatism may have triggered Cretaceous and Eocene uplifts as suggested by dates reported by Miller and Bradfish (1980) and Gans et al. (1986). This Eocene highland could be the source area for the Stinking Spring Conglomerates, shed westward onto the Schell Creek and Egan Ranges. Oligocene volcanics depositionally overlap the younger on older low angle fault complex in the Snake Range (Hose and Whitebread, 1983), and in the Northern Schell Creek Range (Young, 1960).

The events of stage 3 deformed Oligocene volcanics, which are faulted onto Precambrian quartzite in the Snake Range (Hose and Whitebread, 1983). Existing low angle faults were reactivated. Dates of mylonitic fabrics on the decollement were reset (Lee et al., 1970). Humphrey (1960), Young (1960), Drewes (1964, 1967), Moores et al. (1968) and Anderson (1983), describe folded Oligocene volcanics above low angle faults in eastern Nevada and western Utah. Moores et al. (1968) propose that post early Oligocene folding and faulting was generated in a compressive tectonic environment related to crustal shortening.

#### MIDDLE MIOCENE TO PRESENT

Bimodal basaltic volcanism swept Nevada after 17 Ma (Stewart, 1980) and marked the onset of Basin and Range extension. Principal uplift and extension probably occurred later. Glazner and Bartley (1984) show that Basin and Range uplift began in southern Arizona about 25 Ma, propagated north, and reached the Las Vegas area at about 15 Ma. Kellogg (1959) suggests that maximum uplift and rotation of the Southern Egan Range occurred during Pliocene time.

Numerous models of Basin and Range extensional faulting are available in the literature. A short list includes: Proffett (1977), Stewart (1978, 1980a, 1980b), and Okaya and Thompson (1985). Bartley and Wernicke (1984) propose a model which suggests that, as of early Oligocene, the Taylor district could have been attached to the Egan district, now 10 miles west across the Steptoe Valley.

An east-dipping normal fault bounds the east side of the Schell Creeks, tilting the range to the west (Stewart, 1980b). Young's (1960) North Creek Formation of late Tertiary age (Miocene?) is tilted an average of 15° west.

Widespread gravity slides accompanied Basin and Range uplift. Compton and Todd (1983), Miller and Hoggatt-Hillhouse (1983), Snoke et al. (1983), and Walker et al. (1984), describe "mega-landslides" which commonly involve rocks younger than the Pilot Shale (Walker et al., 1984). The Pilot and Chainman Shale units acted as an incompetent base during uplift and rotation since 15 Ma. Slide blocks of Ely Limestone and younger rocks are common in the Southern Schell Creeks (Drewes, 1967).

### Metallogeny

Stewart et al. (1977) relate regional metallogeny to east-west-trending belts of Tertiary magmatism (Fig. 13). They also draw a NNE line through central Nevada between dominantly base metal-related deposits on the east and precious metal deposits without base metals to the west. Local structural trends, such as the Battle Mountain-Eureka, and Carlin trends are important in localizing ore bodies (Shawe et al., 1978).

The largest silver producer in eastern Nevada is the White Pine (Hamilton) district, located 44 miles west of Taylor. Over 21,000,000 ounces of silver were won, primarily from the upper 200 feet of the Guilmette Limestone. The Hamilton district is zoned eastward away from the Tertiary quartz monzonite Monte Cristo stock (Smith, 1976). The

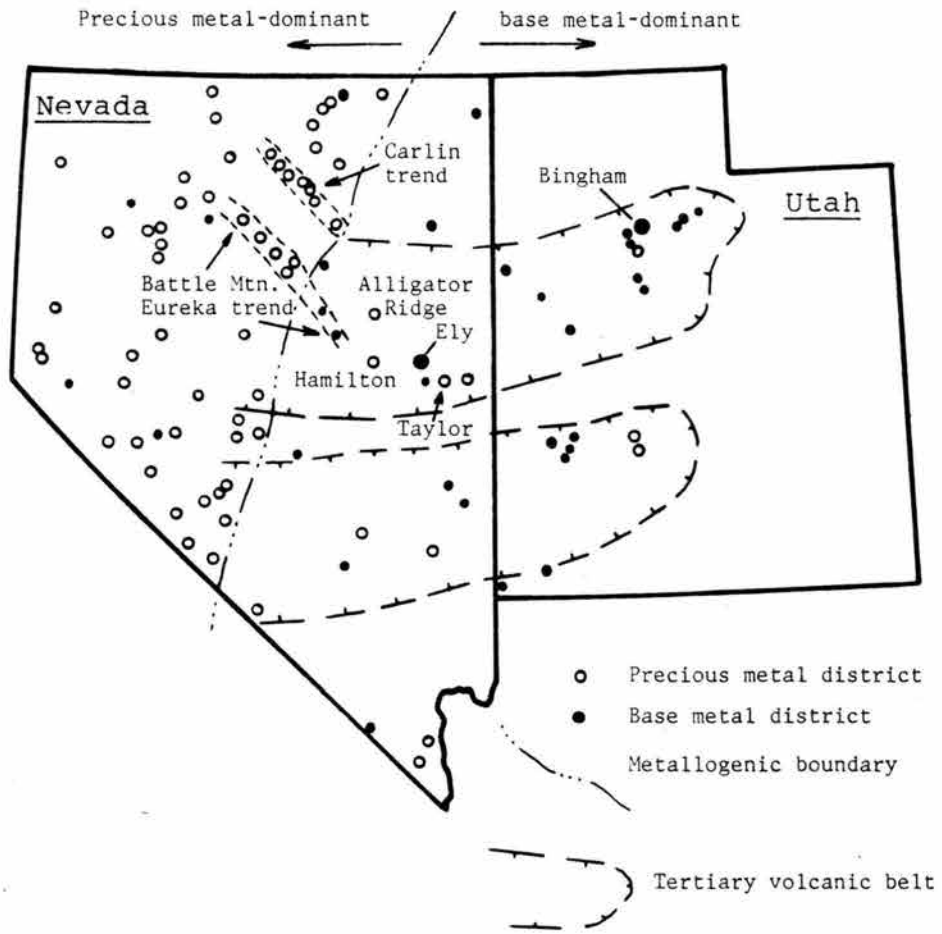


Fig. 13. Distribution of mineral districts and metallogenic trends: Great Basin (modified from Stewart et al. 1977).

stock itself contains disseminated chalcopyrite and quartz-chalcopyrite-(molybdenite) veins. East of the stock, massive Pb-Ag-(Cu-Zn) replacements in the Hanson Creek, Lone Mountain, and Nevada (Guilmette) Formations, occur adjacent to high-angle feeders and low-angle bedding plane faults (Smith, 1976). Further east, the famous cerargyrite bonanzas underlay Treasure Hill where high-angle reverse faults focused hydrothermal fluids into an anticline (Humphrey, 1960). Ore occurred with banded black and manganiferous calcite in tectonic bedding plane breccias at the top of the Guilmette (Smith, 1970), and in some cases in "openings and chambers, filled with ore, exposed, without any visible connection with each other at the surface" (Smith, 1976; after Hague, 1870, p420).

The Ely Limestone and Guilmette Formations host massive sulfide Pb-Zn-Ag replacements in the Ward district, 10 miles west of Taylor. Ore bodies are associated with porphyritic rhyolite intrusives dated at 35 Ma by Silver King (Havenstrite, written commun., 1983).

Taylor is the only active (shutdown from October, 1984 to present (May, 1988)) primary silver producing mine in eastern Nevada. Recent exploration in the area has emphasized gold.

## CHAPTER IV

### DISTRICT GEOLOGY

#### INTRODUCTION

The Taylor district is a north south oriented, elliptical-shaped area of three square miles. A distinct concentration of jasperoids, partially silicified Devonian and Mississippian limestone breccia, and argillized porphyritic rhyolite dikes and sills define the district.

The following discussion is based on the study of approximately 1.5 square miles (half) of the district, centered on the Taylor Silver Mine. Please refer to Plates 1 through 4 for a map, sample location overlay, and cross sections. See Figure 14 for a summary stratigraphic column.

#### LITHOLOGIC UNITS

##### DEVONIAN SIMONSON DOLOMITE

Simonson Dolomite is the oldest rock exposed in the study area. It forms moderate, blocky-weathering slopes beneath the basal cliff-forming Guilmette Limestones. Drewes (1967, after Osmond, 1954), separates four informal members including a 200 foot basal buff member, a 150 foot lower alternating member, a 100 foot brown cliff-forming member, and a 150 foot upper alternating member. The entire 600 to 700

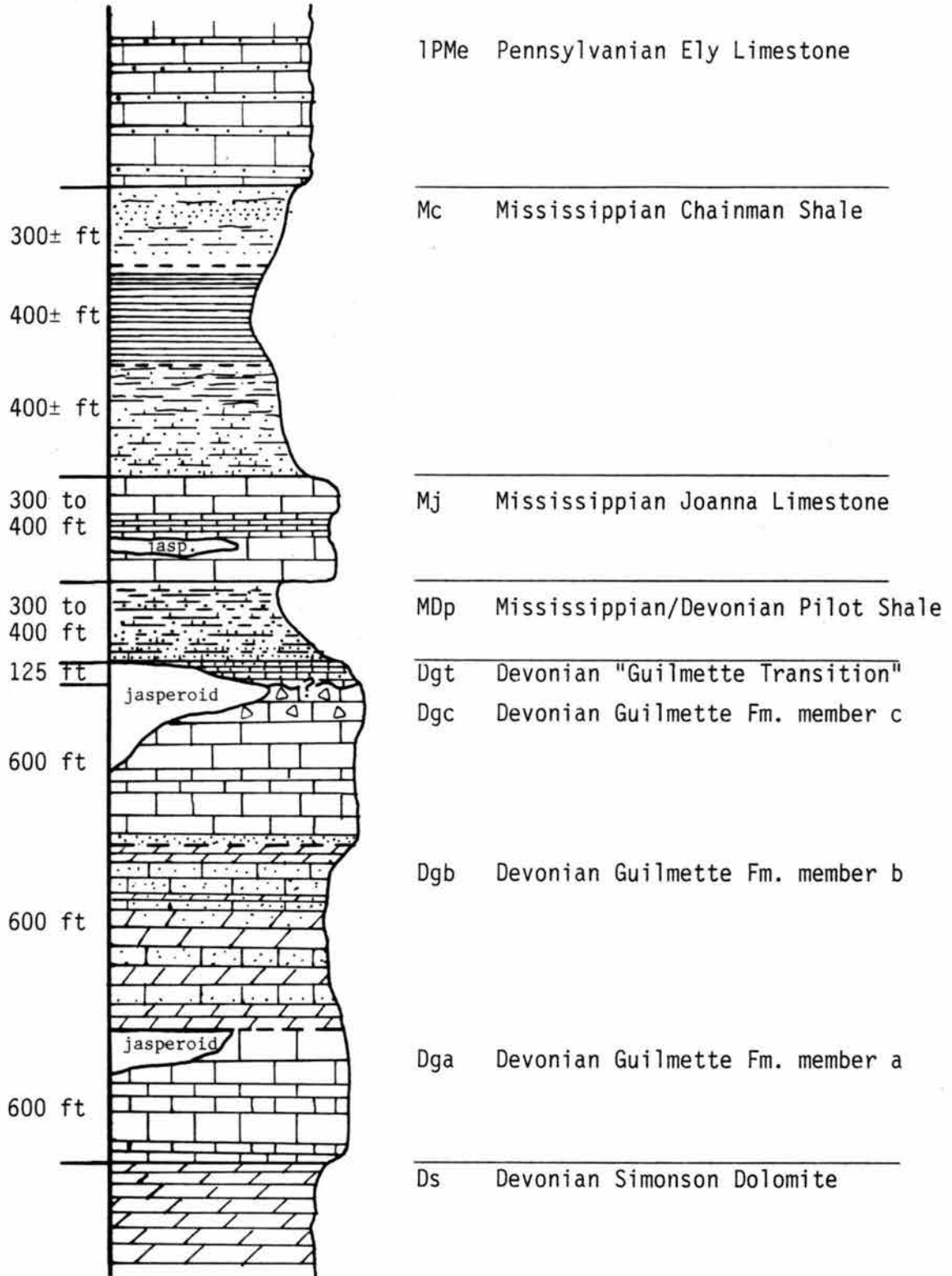


Fig. 14. Stratigraphic column, Taylor mine area.  
Vertical scale 1 in. = 600 ft.

foot Simonson is well exposed just north of Plate 1, however only the upper alternating member appears in the extreme north west corner of Plate 1.

The upper member is comprised of brown to brownish-grey coarse-grained, distinctly laminated limy dolomite beds several feet to tens of feet thick which alternate with medium-grey finer-grained, weakly laminated dolomitic-lime beds. The unit contains dark-grey chert nodules and lenses one to two inches thick.

An east-dipping normal fault separates the Simonson from the overlying Guilmette. The fault is bleached and weakly mineralized (up to 2 ounces Ag/ton), however brecciation and mineralization persist only a few feet into the Simonson footwall. North of the area of plate 1, Drewes (1967) reports that where the overlying lower Guilmette is strongly brecciated, the Simonson remained coherent, suggesting that it is resistant to brecciation. The Simonson has not been tested in the mine area as a potential host for replacement ores.

#### DEVONIAN GUILMETTE FORMATION

The 2000 foot thick Guilmette Formation hosts all of the known silver ores in the Taylor District. Drewes (1967) separated the Guilmette into four informal members, and Silver King geologists subsequently distinguished an additional member at the top of Drewes's c member.

##### (a) Member a

The 500 to 600 foot lower member, a, is dominantly a thick-bedded to massive, light-medium-grey to blue-grey cliff-forming limestone.

Minor silt, sandstone and conglomerate beds appear in associated float. It conformably overlies the Simonson. North of Plate 1 the basal transition is a distinct blue-grey platy limestone cut by strong calcite veining. It is unclear whether these veins resulted from tectonic preparation or simply hydraulic solution and healing. Thick intervals of the lower Guilmette are tectonically brecciated, both within and north of Plate 1 (Drewes, 1967). The base of the member a is not exposed within the area of Plate 1, thus it is unknown if the member suffered tectonic thinning during brecciation.

(b) Member b

Drewes (1967) reports a regional thickness of member b, between 300 and 700 feet. The lower half of member b consists of alternating thin-bedded dark-brown coarse-grained dolomite, platy limestone, shaly limestone and calcareous siltstone. The upper half contains thin- to medium-bedded grey and tan silty limestones and calcareous siltstones. Limestone content increases up section. A ten to thirty foot quartzite bed marks the top of member b.

Much of member b is faulted out of the Taylor Mine area. A heterolithic breccia in the top of member a contains clasts of brown dolomite, probably derived from the bottom of the b member as it was ground up along low-angle denudational faults.

(c) Member c

Guilmette member c ranges from 400 to 600 feet in the region (Drewes, 1967). Thickness in the mine area is about 400 feet. Tectonic breccia in the upper 100 to 200 feet of the c member host most of the district's silver ores. The unit is fine-grained, light-grey to blue-grey, thick-bedded to massive cliff-forming limestone. Figure 15,

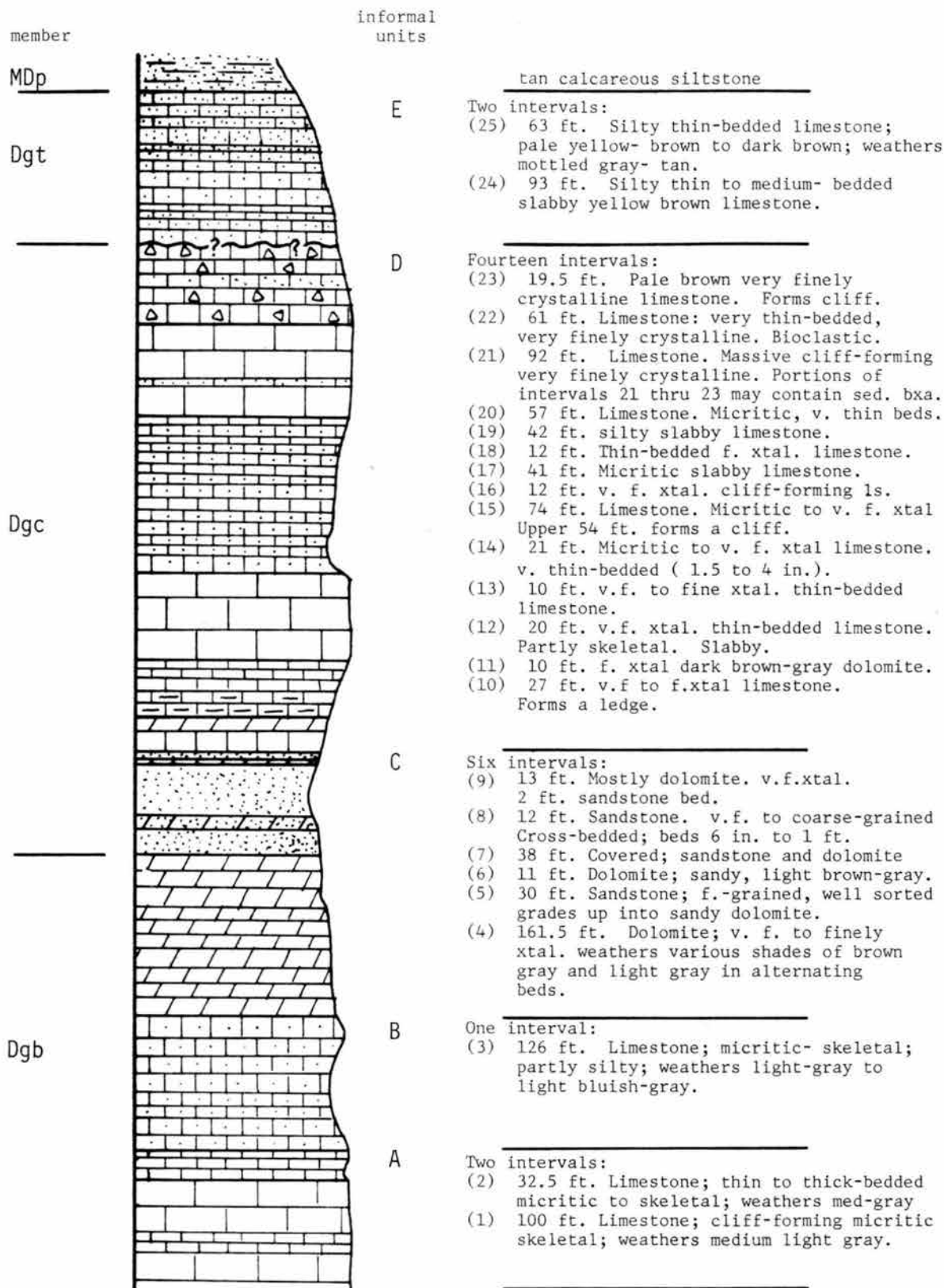


Fig. 15. Stratigraphic column, upper Guilmette. Vertical scale 1 in. = 150 ft. Simplified from Young (1966).

modified from Young (1966), shows some of the details of the c member. The upper 80± feet of the massive unit hosts lenses of sedimentary rip up breccia which alternate with biostromes and lenses of coral- and brachiopod-rich limestone. Several exposures 300 feet SSW of the Argus Pit demonstrate their presence (Fig. 16). Sedimentary breccias made the top of the Guilmette particularly susceptible to subsequent tectonic brecciation.

(d) Member d

Drewes (1967) identified the Guilmette member d in a single area two miles north of the mine, where the unit is preserved as an erosional remnant surrounded by Pilot Shale. The 600 foot member d is composed of limestone, shale, sandstone, conglomerate, sedimentary breccia and shaly limestone, with reef limestone at the top.

(e) Transition beds

Silver King geologists separated a 100 to 125 foot thick section above the massive c member comprised of medium-grey thin- to medium-bedded silty limestones to which they applied the field term Guilmette transition beds. These beds locally possess a breccia texture with a silty matrix. Silt content increases upward to the Pilot Shale contact, which is placed at the uppermost medium-bedded limestone. The transition beds unconformably overlie the massive Guilmette member c. They may be correlative with some portion of Kellogg's (1963) West Range Formation, which thickens southward through the southern Egan Range, or perhaps part of Drewes's (1967) Guilmette member d. The transition beds are partially silicified within 100 to 200 feet of feeder structures, and host ore grade jasperoids 500 feet north of the Argus Pit.



Fig. 16. Sedimentary breccia textures in upper Guilmette member c.

## DEVONIAN/MISSISSIPPIAN PILOT SHALE

The Pilot Shale ranges up to 480 feet in the Southern Schell Creeks (Drewes, 1967), however no unfaulted sections occur in the mine area where it ranges from 200 to 500 feet thick (scaled from Plate 2). The unit is primarily a thinly to thickly laminated, carbonaceous, calcareous, pyritic siltstone and silty shalestone, in subequal amounts. The Pilot forms subdued tan-weathering slopes covered with characteristic tan siltstone plates 0.25 to several inches thick. Clay content increases near the top where it weathers to paper thin fissile maroon plates. The Pilot contains 1.5 wt % average total organic carbon at Alligator Ridge (Ilchik et al., 1986).

The base of the Pilot contains a few thin limestone beds, and appears to be conformable above the Guilmette transition beds. The upper contact with the Joanna is sharp, and faulted in the mine area.

## MISSISSIPPIAN JOANNA LIMESTONE

The Joanna Limestone, where unfaulted, is about 480 feet thick. Drewes (1967) divided the formation into five informal members. These include a basal 15 to 20 foot unit of thin- to medium-bedded platy limestone, a lower 200 foot thick light- to medium-grey massive bioclastic cliff-forming member, a middle 30 to 50 foot, thin-bedded bioclastic silty platy limestone, an upper 150 foot, thick-bedded to massive limestone unit, and an upper thin-bedded platy limestone unit 60 feet thick. The upper two members appear to be faulted out of the mine area. The Joanna is distinctly fetid and yields a petroliferous

odor when broken. Limestones of the lower massive member host possible sedimentary collapse breccias (Fig. 17). This horizon suffered subsequent tectonic brecciation at its upper fault contact with the Chainman Shale. Brecciation, however, persists only several feet to several tens of feet into the footwall Joanna Limestone.



Fig. 17. Possible collapse breccias in Joanna Limestone.

## MISSISSIPPIAN CHAINMAN SHALE

The 1100 foot Chainman Shale consists of three units, which are generally not mappable, due to poor exposure. Laminated to thin-bedded calcareous siltstone, silty limestone, silty claystone and mudstone comprise the lower third of the Chainman. The unit weathers to somewhat more reddish and maroon colors, and contains more clay than the Pilot but, in areas of poor exposure, the lower Chainman could easily be confused with the Pilot. The middle third of the Chainman is dominantly black fissile shale. Near the middle, it contains a 50 foot medium- to thick-bedded quartzite marker unit which forms short blocky orange-weathering cliffs above the underlying black shales. The upper third contains numerous medium-bedded brownish- to olive-grey-weathering quartzite beds interbedded with shale, argillite, and local conglomerate and limestone.

The Chainman forms a broad bench between the cliff forming Joanna and Ely Limestone Formations. The upper 40 to 60 feet contain brownish-grey sandy bioclastic limestone beds which grade upward into the Ely Limestone (Drewes, 1967). The top of the Chainman is not present in the mine area.

## PENNSYLVANIAN ELY LIMESTONE

The 2500 foot Ely Limestone conformably overlies the Chainman Shale, although the contact is rarely unfaulted. The Ely forms distinctive ledges in outcrop, comprised of alternating medium-bedded

light- to medium-grey bioclastic limestone, and platy medium-grey silty limestone.

Ely Limestone occurs as thin slide blocks west of the mine within Plate 1. Drewes (1967), notes that the Ely is faulted throughout the quadrangle.

#### PERMIAN THROUGH EOCENE

The Permian Arcturus Formation and the Eocene Stinking Spring Conglomerates are exposed several miles east of the mine, however they do not crop out in Plate 1. Please see chapter 3 for a general description of these units.

#### PORPHYRITIC RHYOLITE INTRUSIVES

As many as 45 porphyritic rhyolite dikes and sills intrude the mine area. They range in size from 20 to 800 feet long by 4 to 180 feet wide. Dikes intruded high-angle NE-trending faults and fractures, while sills intrude imbricate bedding plane faults within the Pilot and Chainman Shales, low-angle denudational faults in the Guilmette, and along contacts (often faulted), particularly at the top and bottom of the Joanna Limestone. The largest and most extensive dikes intruded the Taylor Fault, a shallow west-dipping normal fault.

Porphyritic rhyolite is light grey on fresh surfaces, while weathered surfaces are weakly iron stained tan to orange. The rock consists of 5 to 10% quartz phenocrysts 1 to 3.5mm, 12 to 16% sanidine phenocrysts 2 to 5.5mm, 5 to 10% albite phenocrysts up to 2 mm, and

trace to 2% biotite phenocrysts up to 1.5mm in a fine-grained, granular groundmass less than 0.1mm, comprised principally of quartz and potassium feldspar. Grain size commonly decreases at dike margins. Total phenocryst content ranges from 15 to 30%. Dikes contain accessory apatite, zircon, and fluorite.

Table 7 shows whole rock data for four porphyritic rhyolite samples from the Taylor district, and for comparison, data on the older rhyolite flow (described below), five miles north of the mine, and data on porphyritic rhyolite dikes in the Egan district, 10 miles west of Taylor. All these rocks contain high  $\text{SiO}_2$  and  $\text{K}_2\text{O}$ . The intrusives are, in all cases, at least weakly argillized which probably accounts for the low  $\text{CaO}$  contents relative to the volcanics. Drewes' (1967) intrusive sample # H3186 contains abnormally high  $\text{CaO}$  and  $\text{CO}_2$ , undoubtedly the result of late stage carbonatization (described in more detail below).

Some of the larger dikes marbleized several feet of adjacent limestone. Otherwise, the dikes have no associated contact metamorphic halos.

Havenstrite (1983) concluded that rhyolite intrusion postdates jasperoid, based on the apparent inclusion of jasperoid fragments in several rhyolite dike exposures (Fig. 18). Several jasperoid fragments assayed up to 2 oz Ag/ton (Havenstrite, personal comm., 1983). These relationships are ambiguous, however, since exposures were sheared and brecciated after dike intrusion and jasperoid deposition.

Structural relationships, discussed below, show that the Taylor fault is older than the high-angle NS-trending reverse faults which acted as principal ore feeders. The NS-trending reverse fault set is

Table 7. Whole rock data for porphyritic rhyolite and older volcanics.

Sample #	Intrusive rhyolite, Hard district (from Shaue, 1961) [Dated by SKM: 35 Ma]				Older volcanics, Southern Schell Creeks. (from Dreues, 1967) [Kalanazoo volcanic equivalents ?]					Intrusive rhyolite, S. Schell Creeks (from Dreues, 1967)		Intrusive rhyolite Taylor District (present study)	
	DRS-45	DRS-22	DRS-21	DRS-52	H3179	H3180	H3181	H3182	H3188	H3186	H3187	13	19
SiO <sub>2</sub>	75.36	73.09	72.92	72.49	72.13	70.60	71.85	70.64	71.97	65.54	76.26	74.37	74.62
Al <sub>2</sub> O <sub>3</sub>	13.55	13.59	13.63	13.45	13.36	14.26	13.71	13.99	13.88	11.73	12.61	13.06	12.71
Fe <sub>2</sub> O <sub>3</sub>	0.31	0.44	0.51	0.55	1.06	1.26	1.22	1.11	0.77	0.40	0.25	0.29	0.10
FeO	0.43	0.34	0.27	0.25	1.06	1.06	0.99	1.13	1.06	0.59	0.44	0.48	0.48
MgO	0.07	0.07	0.14	0.08	0.66	0.70	0.72	0.70	0.66	0.43	0.22	0.52	0.20
CaO	0.84	0.90	0.97	0.88	2.40	2.39	2.56	2.59	2.50	6.83	0.71	1.19	0.44
Na <sub>2</sub> O	3.8	3.42	3.48	3.30	2.78	2.33	2.81	2.71	2.83	2.47	3.03	1.87	1.19
K <sub>2</sub> O	4.61	5.11	4.83	5.00	4.01	4.82	4.05	4.39	4.17	4.19	4.79	4.83	5.79
H <sub>2</sub> O <sup>+</sup>	0.35	2.46	2.66	3.33	0.79	1.00	0.61	0.77	0.45	0.85	0.52		
H <sub>2</sub> O <sup>-</sup>	0.19	0.12	0.29	0.23	0.62	0.70	0.59	0.64	0.79	1.37	0.68	[LOI] 1.49	1.14
TiO <sub>2</sub>	0.05	0.05	0.05	0.05	0.37	0.41	0.39	0.41	0.38	0.05	0.05	0.07	0.05
P <sub>2</sub> O <sub>5</sub>	0.09	0.01	0.01	0.00	0.20	0.01	0.09	0.11	0.09	0.01	0.01	0.01	0.01
MnO	0.07	0.08	0.07	0.08	0.09	0.06	0.04	0.04	0.04	0.19	0.05	0.06	0.05
F	0.11	0.14	0.11	0.13	0.08	0.08	0.07	0.08	0.07	0.12	0.10		
-----													
A/NCK	1.06	1.06	1.07	1.08	1.00	1.06	1.00	1.00	1.01	0.56	1.10	1.25	1.41



Fig. 18. Silver-bearing jasperoid fragments in rhyolite fault breccia.

the only fault set in the district which does not host rhyolite dikes. The Southwest Pit reverse fault truncates one rhyolite sill. High-angle shears in the pit faulted slices of Guilmette transition beds into the dike (Fig. 19). This evidence, in addition to alteration patterns in the rhyolite [discussed below] strongly indicates that rhyolite intrusion predates jasperoid deposition.

#### JASPEROIDS

Lovering (1972) defines jasperoid as "a rock composed dominantly of silica, most commonly quartz, that has formed largely by epigenetic replacement." Accordingly, as a field term, any mappable body of rock (units over fifty square feet), comprised of greater than 50% epigenetic replacement silica, is shown as jasperoid on Plate 1.

Fig. 19. Guilmette transition beds faulted into rhyolite near the Southwest Pit reverse fault.



Jasperoid is a discreet rock type, not to be confused with partially silicified sediments, which will be discussed in the section on wall rock alteration.

Four stratigraphic horizons host jasperoids in the Taylor mine area including the upper 100 feet of the massive Guilmette member a, all of the massive Guilmette member c, the Guilmette transition beds, and the upper 50 feet of the lower massive member of the Joanna Limestone. Jasperoids are confined to previously brecciated or shattered zones within these strata. Breccia fragments or fractured limestone blocks greater than four inches in dimension commonly retain

a limestone core, surrounded by a silica replacement front (Fig. 20). Where breccia grades into shattered rock, then into fractured rock, jasperoid grades into strongly silicified limestone, then into weakly silicified limestone. The distribution of jasperoid is controlled entirely by the extent of tectonic ground preparation, and proximity to high-angle feeder structures.

Four types of jasperoid were distinguished, using the field terms barren jasperoid, antimony jasperoid, dark grey jasperoid, and blue grey jasperoid. Field work was completed prior to examination of thin sections or trace element chemistry, so field units reflect only outcrop characteristics.

(a) Barren Jasperoid

Barren jasperoid (bar-jasp) is light grey on fresh surfaces and weathers light- to medium-grey, commonly with orange and maroon hematitic stain on fractures (Fig. 21). Some weathered exposures develop Liesegang banding. The jasperoid is phaneritic, even textured, and contains no vugs or recognizable accessory minerals other than weak to moderate iron oxide. The outcrops are unbroken and quite tenacious. There is no suggestion of multiple stage brecciation/ silicification.

Bar-jasp was mapped in the Guilmette member c, Guilmette transition, and Joanna Limestone units. Joanna-hosted antimony-jasperoid contains fragments of bar-jasp. Younger dark grey jasperoid cross cuts bar-jasp along fractures. Bar-jasp therefore appears to represent an early stage of silicification. No field relationships were noted between bar-jasp and blue-grey jasperoid.



Fig. 20. Partially silicified breccia with limestone cores and post-silica calcite veining. Photo by T.B. Thompson.

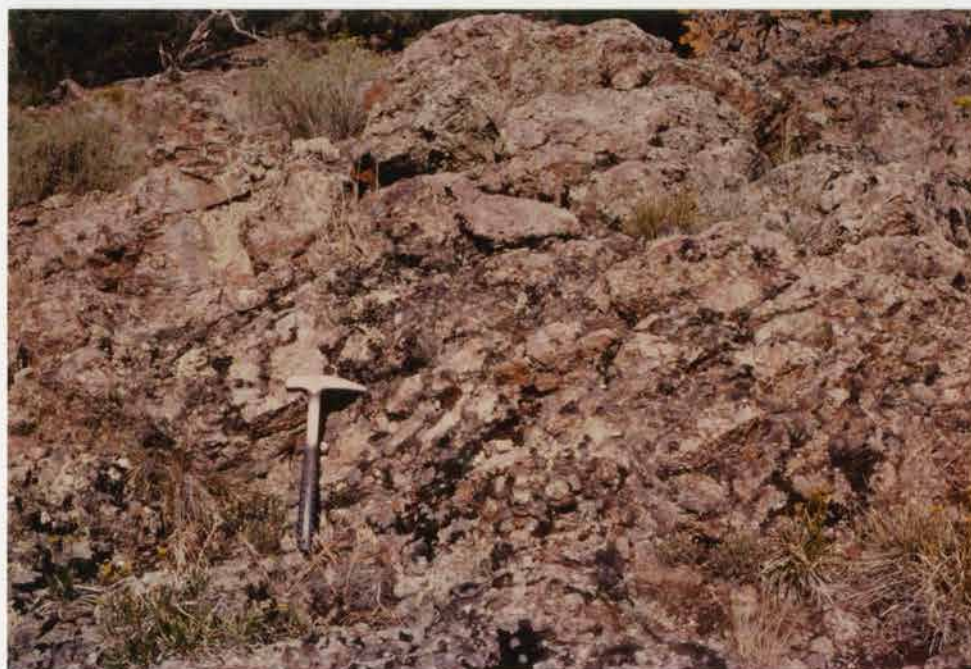


Fig. 21. Barren jasperoid (stage I) outcrop. Sample #162: 3.7 oz Ag/ton; 30 ppb Au; 1400 ppm Sb; 15 ppm As.

(b) Antimony Jasperoid

Antimony jasperoid (Sb-jasp) is distinguished by the presence of stibnite blades up to 2 inches long, its oxidation products, or at least bladed casts after stibnite. Sb-jasp is dark grey on fresh surfaces and weathers to medium- to dull-mottled-brown, locally with yellow- to greenish-yellow Sb oxides on fractures. Stibnite blades are commonly oxidized to white, brown, or yellow oxides within several inches to several feet of the surface. Erickson (1964) notes the oxidation products kermesite, stibiconite, valentinite, senarmotite, and bindheimite. The jasperoid is phaneritic, vuggy, and locally contains clots, 1 to 2 cm in diameter, of coarse-grained idiomorphic quartz crystals. Accessory barite fills some vugs. Rare, native antimony occurs in zones with high stibnite content. Sb-jasp commonly contains breccia fragments of bar-jasp (Fig. 22), however, no field relationships were observed between Sb-jasp and dark grey jasperoid, or blue-grey jasperoid. Sb-jasp was mapped only within Joanna Limestone [Drewes (1967) noted the presence of stibnite-bearing jasperoid in the mine area, however mining removed these exposures. Fragments of Sb-jasp were seen in thin section in Guilmette-hosted jasperoid].

(c) Dark Grey Jasperoid

Dark grey jasperoid (dk-jasp) is dark grey to near black on fresh surfaces and weathers mottled-brown (Fig. 23). The jasperoid is phaneritic with minor vugs. White calcite fills post-jasperoid fractures and breccias. Complete oxidation persists only inches to several feet to depth, except where controlled by high-angle structures. Rare malachite and azurite, along with goethitic iron oxides coat fractures. Casts after stibnite are rare (seen only in



Fig. 22. Antimony jasperoid (stage II) with barren jasperoid (stage I) fragments. Sample #144: 0.5 oz Ag/ton; 700 ppb Au; > 1% Sb; 90 ppm As.

Fig. 23. Dark  
grey jasperoid  
(stage III)  
outcrops.

Sample #201:  
4.04 oz Ag/ton;  
60 ppb Au;  
285 ppm Sb;  
25 ppm As.



Sample #222: 3.18 oz Ag/ton; 80 ppb Au; 141 ppm Sb; 15 ppm As.

thin section), and may represent fragments of Sb-jasp. Accessory fluorite and casts after fluorite occur locally along fractures and in masses replacing jasperoid silica. Outcrops of dk-jasp are highly fractured, if not brecciated, and are relatively incompetent. Dk-jasp was mapped exclusively in the Guilmette Formation.

(d) Blue Grey Jasperoid

Two outcrops of distinct blue-grey weathering (when-the-sun-hits-it-right) jasperoid were mapped in the mine area, along high-angle faults. The jasperoid is medium-grey on fresh surfaces, with yellow jarosite coatings on fractures. It contains no other visible accessory minerals. No crosscutting relationships were noted between blue-grey jasperoid and other jasperoid types.

#### OLIGOCENE VOLCANICS

Slices of weakly to moderately welded ash flow tuffs overlay slide blocks of Ely Limestone west of the mine. Hose and Blake (1976) correlate these tuffs with the Stone Cabin Formation, dated at 32 to 34 Ma. The welded ash flow sequence attains thicknesses of 900 feet where it is unfaulted four miles east of the mine.

Five miles north of the mine, these ash flows are underlain by a 300 foot rhyolite flow which may be correlative with Young's (1960) Kalamazoo volcanics, dated between 38 and 34 Ma, with greatest activity at 35 Ma (Hose and Blake, 1976). Table 7 includes whole rock data for the rhyolite flow which unconformably overlies Eocene conglomerates.

## YOUNGER OLIGOCENE INTRUSIVES

Two small quartz latite vitrophyre dikes intruded the mine area, one 300 feet north of the Argus Pit, and the other 500 feet NNW of the Argus Pit. The rock consists of about 35% phenocrysts, with plagioclase, sanidine, quartz, and biotite, all less than 2mm, in a glassy green to black groundmass. The dikes intrude major faults and are found adjacent to jasperoid and strongly argillized porphyritic rhyolite, yet they are only partially devitrified. Intrusion of latite dikes clearly post-dates hydrothermal activity in the district. Drewes (1967) reports similar rocks cutting the younger welded tuffs east of Plate 1.

## STRUCTURE

### MESOZOIC IMBRICATE THRUSTS

The oldest structures identified in the mine area are low-angle imbricate bedding plane faults which repeat the base of the Joanna and uppermost Pilot up to five times. Individual slices are lens or wedge shaped. Lenses of Joanna up to 100 feet thick pinch out over a lateral distance as little as several hundred feet, indicating that overall displacement on the fault system may total only several thousand feet. Limestone slices are not brecciated, and only the top of the upper Joanna slice (where subjected to much younger low-angle faulting), hosts jasperoid. Drewes (1967) reports repetitions of the base of the Ely Limestone two miles east of the mine, and similar repetitions near the Cambrian Lincoln Peak Formation/ Ordovician Pogonip(?) Formation

contact, four miles east of the mine. The direct east-west alignment of these structures suggests that concomitant folding may have forced local ramping of thrusts. Conway (1965) also describes imbrication of the lower Joanna and upper Pilot south of Conners Pass.

The age of thrusting at Taylor is ambiguous due to lack of Mesozoic rocks; the faults cut Pennsylvanian rocks but are intruded by Oligocene dikes. Based on the older over younger style, lack of brecciation, and the presence of pre- 110 Ma thrust faults in the region (McDowell and Kulp, 1967), these faults are considered to be Cretaceous.

#### EOCENE(?) STRUCTURES

A set of low-angle bedding plane denudational faults brecciated portions of the Joanna Limestone, the Guilmette member c, the Guilmette member a, and cut out substantial portions of the section. The upper half of the Joanna is missing, along with most of the Guilmette member b. Greater thicknesses of section are missing and brecciation is more intense in the mine area than in immediately adjacent regions. An existing gentle open fold in the mine area could have produced this effect by locally forcing faults down section into massive limestone beds (ie. the faults sliced off the axial portion of the fold).

Two principal denudational faults of this type are shown on Plate 1. The deepest fault cuts the top of the Guilmette member b. The fault, as it approaches the mine from the north, sinks deeper into the section, and cuts out most of the Guilmette member b. The upper fault appears to follow the contact between the Guilmette member c, and the

Guilmette transition beds. As it approaches the mine from the north, the fault cuts down section, and brecciates and shatters the upper 100+ feet of member c. At least two other low-angle faults cut out portions of the section, although exposures are not adequate to map the structures. The Joanna is thinner in the mine area than to the north or south. Low-angle denudational faulting apparently cut out the top two or three members and brecciated the top of the lower massive member through most of the mine area. A west-vergent recumbent fold at the base of a Joanna slice evidences local reactivation of Mesozoic imbricate faults. Fault movement on the contact between the Guilmette a and b members brecciated the top of the massive Guilmette member a.

Movement on denudational faults postdates initial movement on high-angle N40E- to N50E-trending NW-dipping faults which locally display either reverse or normal ( $\pm$  right lateral) separation, in part due to recurrent movements. Low-angle denudational faults cut the NE-trending fault 800 feet north of the mill. NE- structures may have acted, in part, as tear faults during denudation.

The Taylor fault is a west-dipping fault displaying normal separation. Due to recurrent shearing and brecciation on the fault, it is poorly exposed, and could not be measured directly. Three point solutions indicate current dips of  $14^{\circ}$  to  $32^{\circ}$  west. Drill intercepts (Plate 4) suggest steeper dips of about  $50^{\circ}$  west. Prior to Basin and Range tilt of  $15^{\circ}$  west, the Taylor fault probably dipped between  $30^{\circ}$  and  $40^{\circ}$  west.

The Taylor fault offsets, and must postdate, low-angle denudational faults. Reactivation of the high-angle NE-trending fault just southeast of the Southwest Pit accompanied movement on the Taylor

fault. This structural block downdropped Pilot Shale against the middle of the Guilmette member c, and indicates a minimum 400 foot separation across the Taylor fault. Lack of significant northeast displacement across the Southwest Pit reverse fault therefore shows that principal movement on the Southwest Pit reverse fault occurred after movement on the Taylor fault.

High-angle NE-trending faults, low-angle west-vergent denudational faults, and the low-angle west-dipping Taylor normal fault all host lower Oligocene porphyritic rhyolite dikes and sills. Regional evidence, discussed in Chapter III, indicates that low-angle denudational faulting postdates intrusion of Upper Cretaceous granitoids. An inferred Eocene age of this structuring is compatible with Hose and Whitebread's (1983) analysis of the Northern Snake Range [discussed in Chapter III].

#### OLIGOCENE STRUCTURING

A complete structural analysis of the Taylor district requires the following assumptions:

Based on ages of similar rock types throughout the region, and the similarity in whole rock chemistry between the porphyritic rhyolite dikes and the older rhyolite flow (Table 7), these two rock types are assumed to be more or less comagmatic and both approximately 35 Ma. Furthermore, lack of cross cutting relationships or any significant mineralogic or textural differences between rhyolite bodies permits the assumption that porphyry intrusion took place in a single short-lived event. Basin and Range tilt is assumed to be approximately 15° west.

This assumption is consistent with the tilt imposed on Miocene/Pliocene sediments in the Northern Schell Creeks (Young, 1960). There are no sediments of similar age mapped in the Southern Schell Creeks.

These assumptions permit the following conclusions: Post early Oligocene structuring began with reactivation of a south-plunging open fold in the mine area. Wavelength is about two miles. Both flanks dip less than  $50^\circ$ . Folding brecciated the axial region (or rebrecciated existing structures). The fold is probably a reactivated Cretaceous structure, suggested by the fact that low-angle denudational faults cut down section into massive limestone units in the mine area, and that older imbricate thrusts were focused in the same region. The fold is most acute in the immediate mine area. Limbs appear to shallow some  $10^\circ$ , both north and south of the mine.

Three N- to NNW-trending high-angle reverse fault systems breached the fold. These include the Southwest Pit fault, the Argus fault, and the Antimony Pit fault systems. Observed separation on these faults ranges up to 400 feet. Renewed movement on N40E to N50E high-angle faults accompanied movement on NNW-trending reverse faults.

The Southwest Pit reverse fault dragged footwall sediments into overturned-to-the-west attitudes, suggesting west-vergence or back-thrusting. The fault and drag fold intensely brecciated footwall rocks in the process.

This compressive structural environment controlled deposition of Ag-(Pb-Zn-Cu-Sb) ores in the Taylor district. NNW-trending reverse faults, primarily the Argus and Southwest Pit faults, localized high grade silver ores; intersections with NE-trending fault zones localized the major ore chutes. Ore fluids bled out along low-angle breccia

zones, updip from NNW-trending feeders to produce bulk tonnage low-grade silver ores. Brecciated Guilmette transition beds, dug up in the footwall of the Southwest Pit reverse fault, also host ore. Repeated episodes of brecciation and healing indicate that all faults were active during ore deposition.

Four miles east of Taylor, Eocene conglomerates and mildly unconformable Oligocene volcanics were rotated 30° east and faulted above the reactivated Schell Creek Range Thrust Fault (Drewes, 1964, 1967). Drewes (1967) proposes that a series of north south oriented arches (or antiforms) developed in the Snake, Schell Creek, and Egan Ranges with 15 to 20 km wavelength. Although Drewes (1964, 1967) attributes this arching to Cretaceous structuring, Cameron and Frost (1981) and Cameron et al. (1981) report that antiforms of this type and wavelength developed beneath regional Oligocene/Miocene detachments in southern Nevada, Arizona, and California. A similar model may be applicable to Taylor, although the nature of the post early Oligocene stress field remains controversial. Post early Oligocene arching of the Southern Schell Creeks activated low-angle faults which may merge downward into the Schell Creek Range Thrust, or a deeper decollement (the original Jurassic-Cretaceous brittle-ductile transition), and rotated overlying units to the east. The pre-existing Taylor anticline probably helped focus Oligocene compression in the Taylor Mine area.

#### MIOCENE/PLIOCENE EXTENSION

Basin and Range block faulting truncated the low-angle fault system at about 15 Ma. An east-dipping normal block fault bounds the

east flank of the Southern Schell Creek Range (Stewart, 1980 a and b; Young, 1960; Drewes, 1967), which tilted the range about 15° west. Offset on the range front fault was many thousands of feet, although workers have not published precise estimates.

A west-dipping normal fault (cuts the extreme northeast corner of Plate 1) downdropped the Taylor Mine area nearly 3000 feet to the west. The Taylor fault, and several of the high-angle faults were probably reactivated at this time, although offsets appear not to exceed several tens of feet. Lineations on the reactivated Argus fault suggest a horizontal shear component.

Basin and Range faulting produced unnaturally steep and unstable slopes. Rocks overlying Upper Devonian and Mississippian shales were particularly susceptible to sliding during the Pliocene. Several slide blocks, including slices of Joanna Limestone, Chainman Shale, Ely Limestone, Eocene conglomerates, and Oligocene volcanics came to rest along the west flank of the range, and underlie the Taylor mill and mine offices. One slice of Guilmette member b, slid down just southwest of the Southwest Pit and is overlain by slides of younger rocks. The Guilmette slide is strongly shattered, although beds remain recognizable. A rubblized breccia zone marks the base of the slide.

Miocene/Pliocene slide blocks in the Southern Schell Creek Range involve coherent slabs up to several square miles in area (Drewes, 1967, Plate 1).

## MINERALIZATION

## GENERAL DESCRIPTION

The Taylor silver deposit is a bulk tonnage siliceous replacement deposit hosted by brecciated and shattered Guilmette Limestone. Mill feed through the first year of production, however, contained less than 50% silica. Siliceous ores average 80% silica (Pescio, personal comm., 1988). The ore body is more or less centered on jasperoids but ore grade values persist from tens to hundreds of feet outward into partially silicified, shattered limestone. Low-angle fault breccia zones host ore up dip from high-angle feeders.

When cross sections are restored to pre-Basin and Range attitudes (minus 15° westward tilt), there appears to be a base to silica replacement above 7350 feet current elevation. This elevation line crosses stratigraphic and structural levels. Ores found below this level do not replace host rock, but consist entirely of open space sulfide-calcite-(silica) veins and breccia fillings. Thus, there appears to be a fundamental depth, above which, P-T-X conditions favored the dissolution of limestone, and deposition of silica.

Siliceous ore averages low total microscopic to sub-microscopic sulfide (probably under 2%, but this has not been quantified). The carbonaceous component, which is substantial in the Guilmette transition beds (but by visual estimate, less than the overlying Pilot Shale), does not pose a metallurgical problem. Oxidized, partially oxidized, and sulfide ores are milled together without chlorination.

The bulk of the ore body is partially oxidized. Strong oxidation persists to depths of over 200 feet down the principal high-angle

faults and fracture systems, which control the downward migration of ground water. Active karstification is apparent down the Argus fault, evidenced by open caves and karst infillings (some host silver values up to 33 oz/t. See hole D-14 in Appendix 3). Strong oxidation extends only inches up to several feet into unfractured rock. Goethitic to hematitic iron oxides, indicative of partial oxidation, are common in fractures down to 200 feet.

Havenstrite (1983) suggests that oxidation, leaching and supergene enrichment may have upgraded the Taylor deposit and produced a blanket-like deposit which nearly parallels the current topographic surface, but crosscuts bedding at a small angle. However, the fact that ore-controlling low-angle faults cut down section in the mine area adequately explains this relationship (plate 4). The general lack of thorough oxidation at the surface, the dominance of goethitic oxides (rather than lower pH "live limonites" and jarosite) on fractures, surface trace element geochemistry (discussed in Chapter V), and simply the low sulfide content of the system, all argue that supergene leaching and enrichment was not an important factor. Most supergene ground water was focussed down a few principal high-angle structures. Supergene enrichment down these structures undoubtedly added substantial silver in the form of ceragyrite to the high-grade pods and lenses developed in the late 1800's.

Silver King geologists found they could predict the tenor of drill samples with surprising accuracy based on visual inspection of drill cuttings. Higher-grade intervals contain a greater percentage of silica. The blacker the silica, the higher is the grade. Darker colors reflect greater disseminated microscopic sulfide contents.

Pyrite and sphalerite grains up to 0.01 mm, were identified under the microscope. Other minerals, probably including galena, tetrahedrite, and acanthite, show up only as shiny specks at 500X. Fluorite, although not common, is erratically distributed within and near feeder structures in some of the higher-grade dark-grey to black jasperoids. Brecciated jasperoid healed by white calcite typically contains the highest grades, over five oz Ag/ton. The gaudiest breccias contain visible open space sulfides. Sphalerite, galena, tetrahedrite, a Pb-Ag-Sb sulfosalt, and trace pyrite have been identified in hand sample. Where oxidized, azurite and lesser malachite are common accessories in high-grade ores.

Taylor silver ore is anything but flashy. By the time the ore is shot, hauled, crushed, and arrives at the mill, it is fairly homogeneous medium-grey partially silicified limestone, with associated white calcite and brown to orange-brown goethitic iron oxide.

#### JASPEROID AND ORE PARAGENESIS

Figure 24 is a summary paragenetic diagram. Deposition of late stage open space sulfide-calcite veins follows three principal jasperoid stages, corresponding to the field units barren jasperoid, antimony jasperoid, and dark grey jasperoid. Episodes of brecciation along principal high-angle feeder structures separates major paragenetic stages. Later stage jasperoid commonly cross cuts and inundates previous stages.

Table 8 summarizes jasperoid characteristics and shows all textural types in order of apparent deposition. Due to complex cross

HYPOGENE PARAGENESIS				
Mineral	Stage I	Stage II	Stage III	Stage IV
quartz				---
stibnite		---	---	
barite		---		
pyrite		---	---	---
sphalerite		---	---	---
native Sb		---		
chalcopyrite			---	
galena			---	---
tetrahedrite			---	---
fluorite			---	
Ag-Pb-Cu-Sb-sulf.				---
calcite				---
kaolinite				
sericite	---	---	---	
montmorillonite				---
		breccia	breccia	breccia

Fig. 24. Summary paragenetic diagram.

Table 8. Summary of jasperoid characteristics.

Stage	Texture	quartz grain size range (mm)	accessory minerals comments	Representative samples
I	jigsaw	< 0.005 to 0.014		64b
	fine-gr. granular/reticulate	0.023 to 0.15		87, 130, 150
	coarse-gr gran./reticulate	0.023 to 0.82		87, 150, 162
	brecciation			
II	coarse idiomorphic quartz	1 to 20	flat extinction	69, 154
	fine-gr. reticulate to jigsaw	< 0.01 to 0.04		64a, 144, 154
	monomorphic gran. to reticulate	< 0.01 to 0.4		31, 36, 64a, 76, 144, 154
	brecciation			
	fine-gr. monomorphic gran./retic. brecciation	< 0.01 to 0.12	trace to 1% pyrite	31, 36, 64a, 69, 76
	coarse-gr. comb and gran. quartz sulfide deposition local spherulitic recrystallization	0.046 to 1.6	locally preserves sed. text. stibnite-(sl-py-barite)	64a, 69, 76, 144 64a, 69, 76, 144, 154 76
	brecciation			
III	coarse gran./reticulate brecciation	up to 0.46		46e, 170h
	fine-gr. gran./reticulate	0.01 to 0.34	possible confusion w/ stage II fragments	29b, 43, 44, 46a,b,c,e 57a, 170k
	brecciation			
	coarse reticulate	0.01 to 0.44	minor stibnite	29b, 43, 46a,d, 52d, 57a, 164, 170h, k, f, o 29b,43,44,52d,170f,h,k,o
	open-space comb quartz brecciation	up to 0.6		
	very fine-gr. gran./reticulate	< 0.01 to 0.035	microscopic disseminated sulfides, fluorite	43,44,46a,d,52d,57a, 170h,k,o 29b, 57a
	local spherulitic recrystallization			
	brecciation			
IV	open-space sulfide-calcite-(quartz)			

cutting relationships, and the fact that small scale sedimentary features affected jasperoid textures on a local basis, individual thin sections never exhibit all textural types.

(a) Stage I

Stage I jasperoid corresponds to the field unit barren jasperoid. It occurs as replacements in the Guilmette member c, Guilmette transition, and Joanna Limestones. The general progression of stage I silica textures includes initial deposition of very fine-grained jigsaw texture silica locally preserving sedimentary textures (Fig. 25). Jigsaw textures locally grade outward into fine-grained granular to coarse-grained granular quartz (Fig. 26). Opaque minerals, including minor stibnite, are concentrated near the later coarse-grained granular quartz.

Stage I jasperoids are noticeably more equigranular than subsequent jasperoid stages. In general, brecciation and multiple episodes of silicification are not apparent in stage I jasperoid, except where crosscut or inundated by stages II or III jasperoids.

(b) Stage II

Stage II jasperoid was mapped only in the Joanna Limestone. Replacement of Joanna Limestone began with deposition of coarse-grained idiomorphic quartz in vugs up to two centimeters in diameter. Vug-filling quartz occurs in partially silicified rock and was replaced in part by subsequent fine-grained reticulate to jigsaw silica (Fig. 27). Coarser-grained xenomorphic quartz follows fine-grained reticulate quartz. Younger, fine-grained xenomorphic granular to reticulate quartz (Fig. 28), with trace to 1% pyrite, rims and veins coarse granular fragments. Stibnite, with barite and minor sphalerite, filled

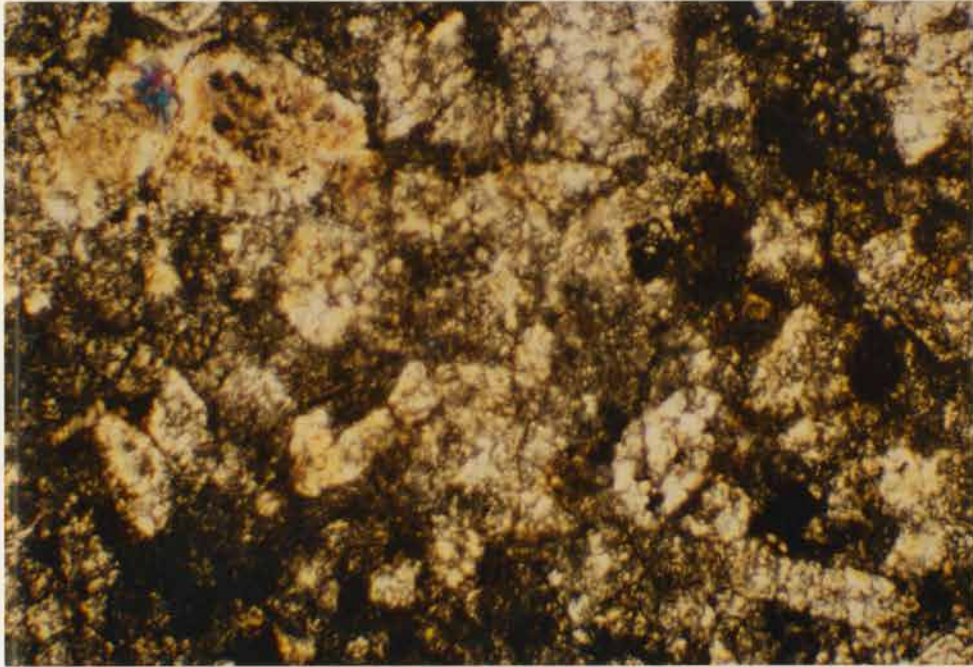


Fig. 25. Stage I jasperoid. Jigsaw to granular texture silica preserving bioclastic textures in Joanna Limestone. Field of view 1.1 X 1.6 mm. Sample #64b: 0.1 oz Ag/ton; 90 ppb Au; 4000 ppm Sb; 88 ppm As.

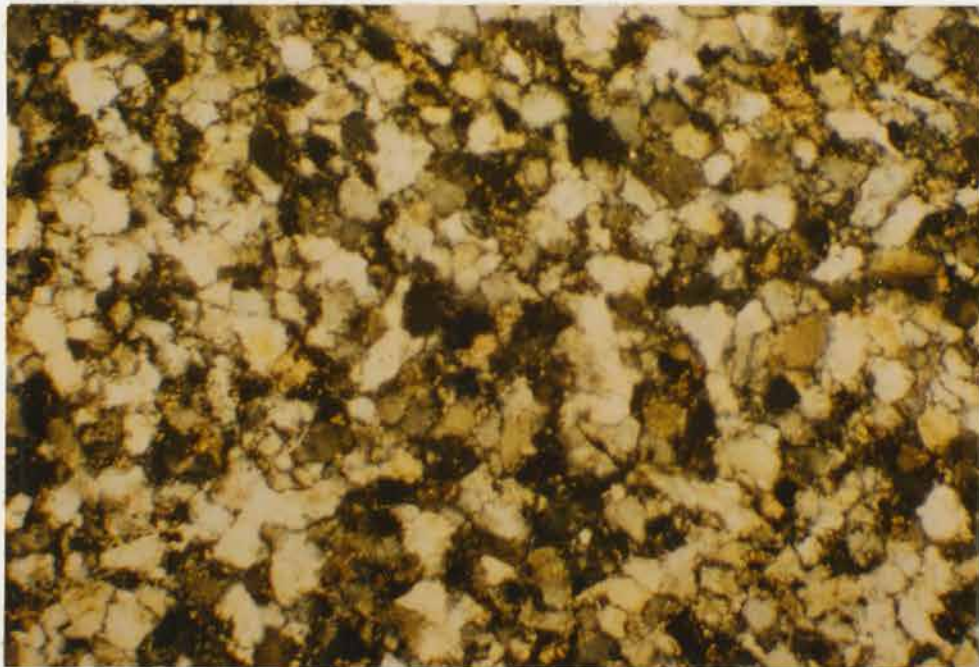


Fig. 26. Stage I jasperoid. Fine to coarse grained granular quartz. Field of view 1.1 X 1.6 mm. Sample #130: 0.03 oz Ag/ton; 10 ppb Au; 8 ppm Sb; 135 ppm As.

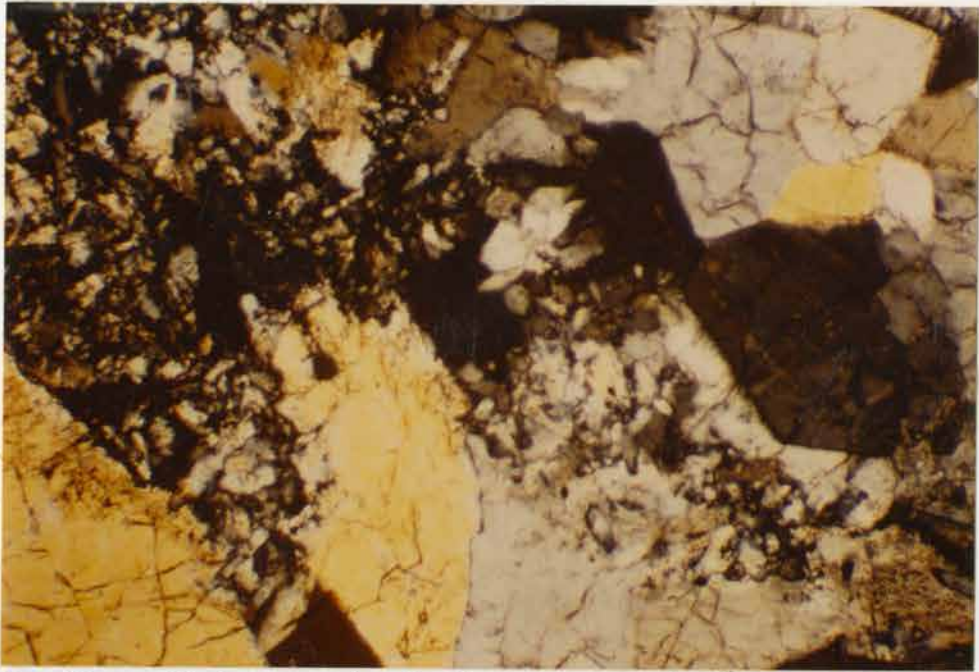


Fig. 27. Stage II jasperoid. Early coarse-grained vug quartz surrounded and replaced by later fine-grained reticulate quartz. Field of view 1.1 X 1.6 mm. Sample #76: 0.19 oz Ag/ton; 300 ppb Au; 92 ppm Sb; 40 ppm As.

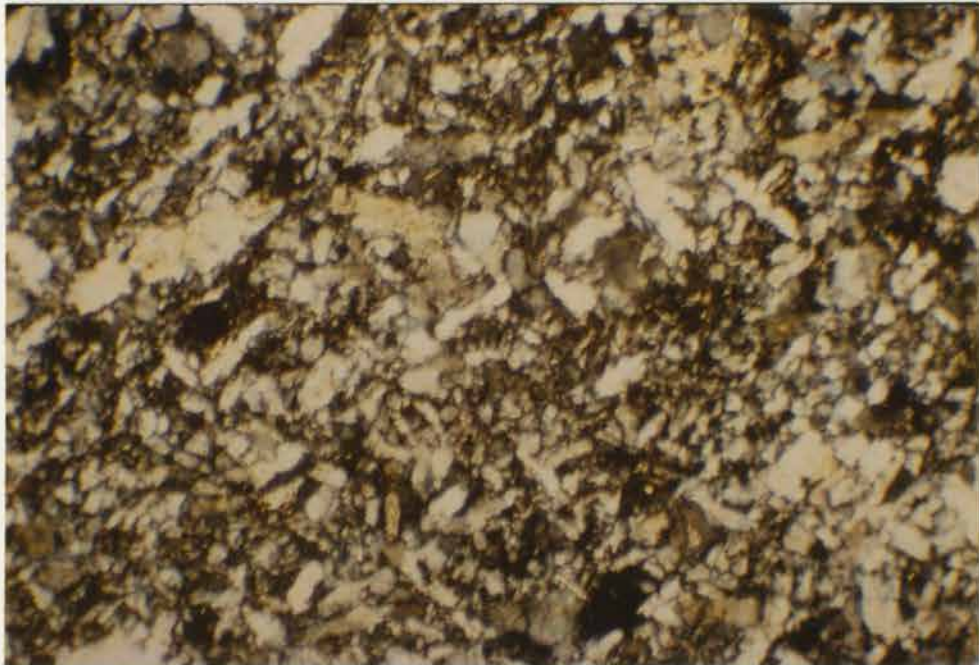


Fig. 28. Typical stage II reticulate quartz. Field of view 1.1 X 1.6 mm. Sample #76: 0.19 oz Ag/ton; 300 ppb Au; 92 ppm Sb; 40 ppm As.

vugs following late coarse-grained, comb-textured quartz (Fig. 29). Stibnite concentrations reach 40% in pods that [rarely] contain native antimony. Coarse-grained quartz locally preserves fossil fragment textures. Local recrystallization generated fibrous colloform bands of chalcedony and spherulitic textures (Fig. 30). Associated iron oxides include goethite with lesser hematite. Jarosite is not common, but occurs in the oxidized portions of some of the most stibnite-rich outcrops with antimony sulfates.

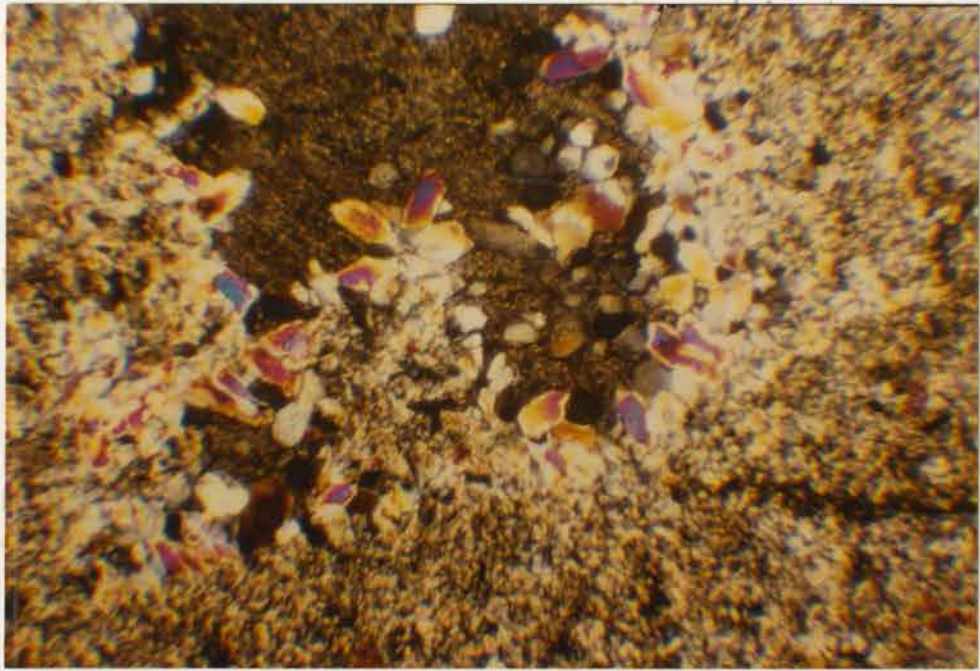
Reticulate, coarse-granular, and comb-quartz textures dominate stage II jasperoid. Stage II is much more complex than stage I, and displays several episodes of brecciation. Stage II jasperoid outcrops commonly contain fragments of stage I jasperoid (Fig. 31). No stage II jasperoid outcrops were mapped in the Guilmette, however, stage III jasperoid contains stage II jasperoid fragments (drill core) (Fig. 32).

### (c) Stage III

Deposition of main silver ore stage III jasperoid, began with granular grain for grain replacement of up to 20% of the host limestone (Fig. 33 a,b,c). Deposition of reticulate-textured quartz then followed recrystallization of remnant limestone which increased calcite grain size from less than 0.2 mm to 3mm ( $\pm$ ). Resultant jasperoid textures are invariably hypidiomorphic (Fig. 34 a,b).

Early quartz grain sizes typically ranged from 0.02 to 0.2 mm. Quartz grain size increased to 0.04 to 0.4 mm after limestone recrystallization. Deposition of finer granular to reticulate quartz followed a brecciation event. Further brecciation was followed by precipitation of coarse-grained reticulate to idiomorphic comb textured quartz in open space, rarely with stibnite. Visible opaque minerals

(a)



(b)

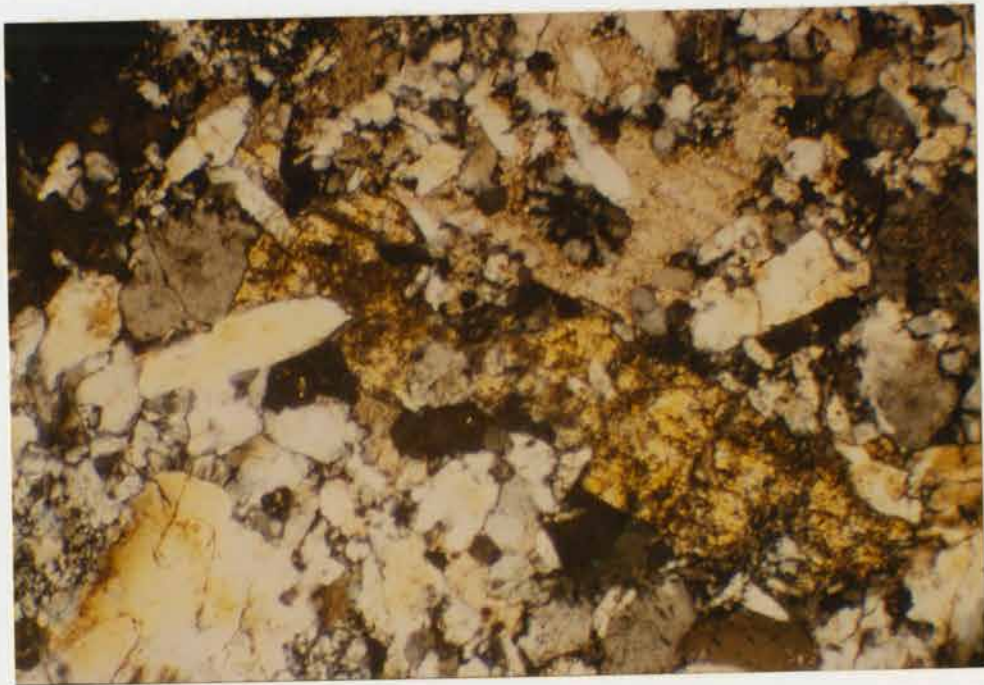


Fig. 29. Stage II jasperoid. (a) Coarse idiomorphic quartz. Sample #36. Field of view 1.9 X 2.85 mm. (b) Vug-filling stibnite. Sample #76. Field of view 1.1 X 1.6 mm.

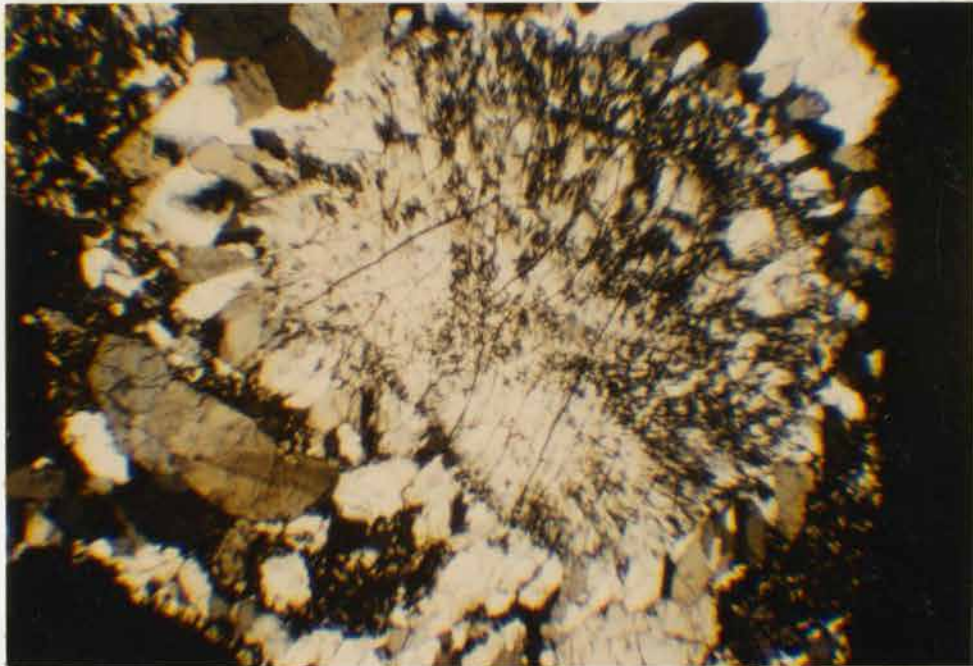


Fig. 30. Stage II jasperoid. Spherulitic textures. Field of view 1.9 X 2.85 mm. Sample #69: 0.1 oz Ag/ton; 245 ppb Au; Over 1% Sb; 63 ppm As.

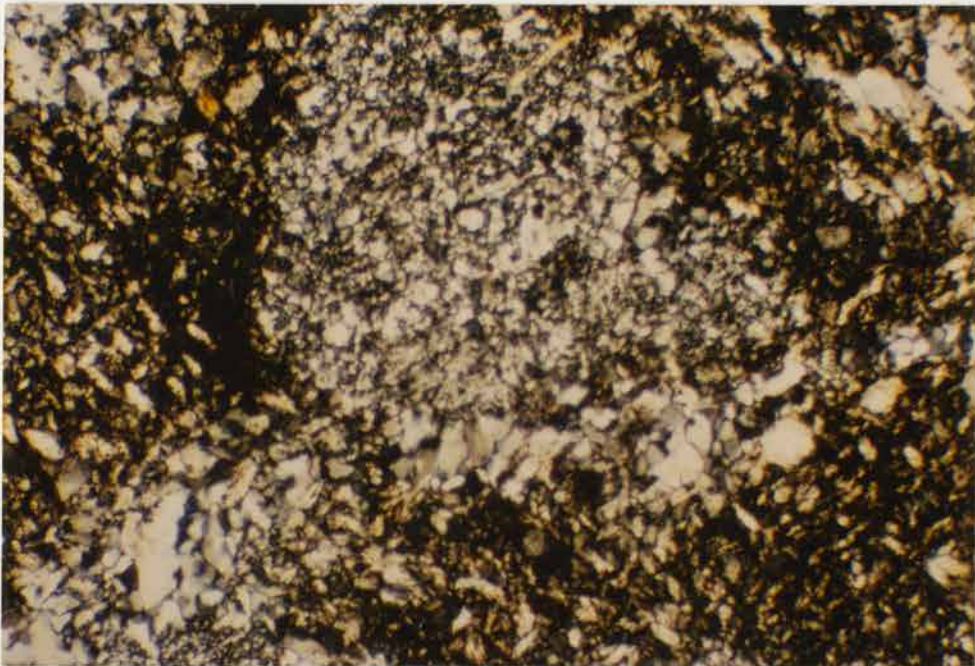


Fig. 31. Stage I jasperoid fragments in stage II reticulate matrix. Field of view 1.1 X 1.6 mm. Sample #69: 0.1 oz Ag/ton; 245 ppb Au; over 1% Sb; 63 ppm As.

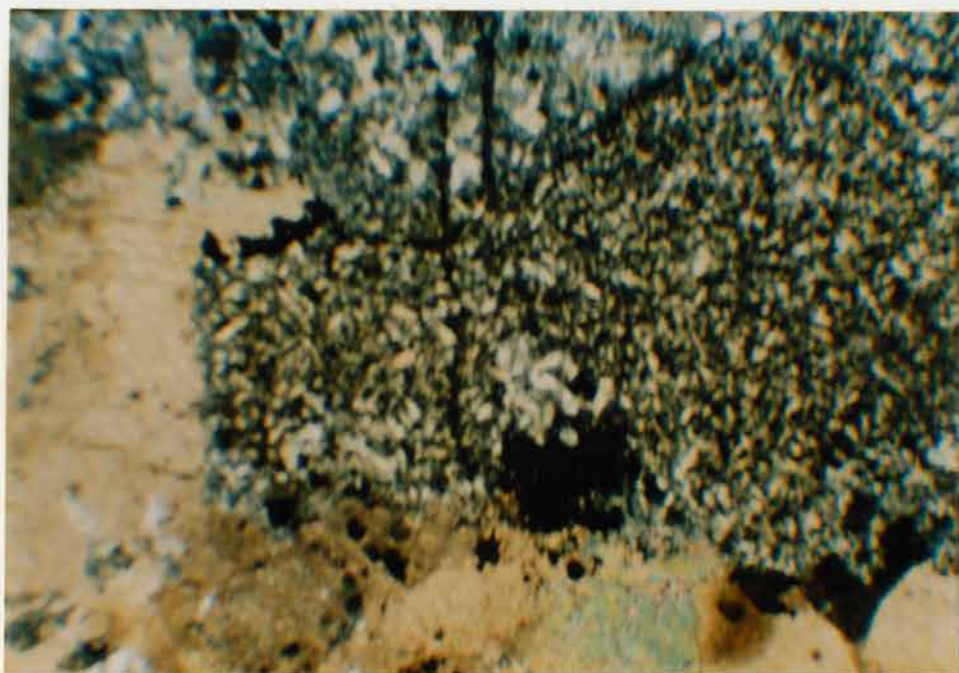


Fig. 32. Fragment of stage II reticulate textured jasperoid in stage III matrix, followed by stage IV open space sulfide and calcite. Field of view 4.1 X 6.25 mm. Sample from drill hole D-9, 60-65: 10.24 oz Ag/ton; 155 ppb Au; 2200 ppm Sb; 47 ppm As.

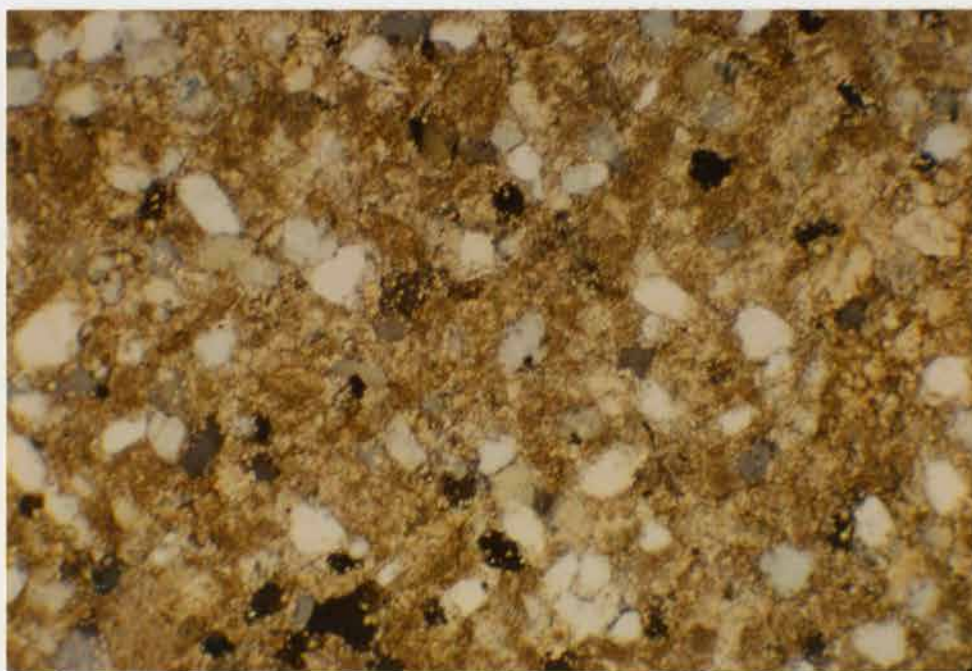


Fig. 33a. Stage III incipient granular silicification. Field of view 1.1 X 1.6 mm. Sample from drill hole D-1 90-95: 1.0 oz Ag/ton; 60 ppb Au; 11 ppm Sb; 5 ppm As.

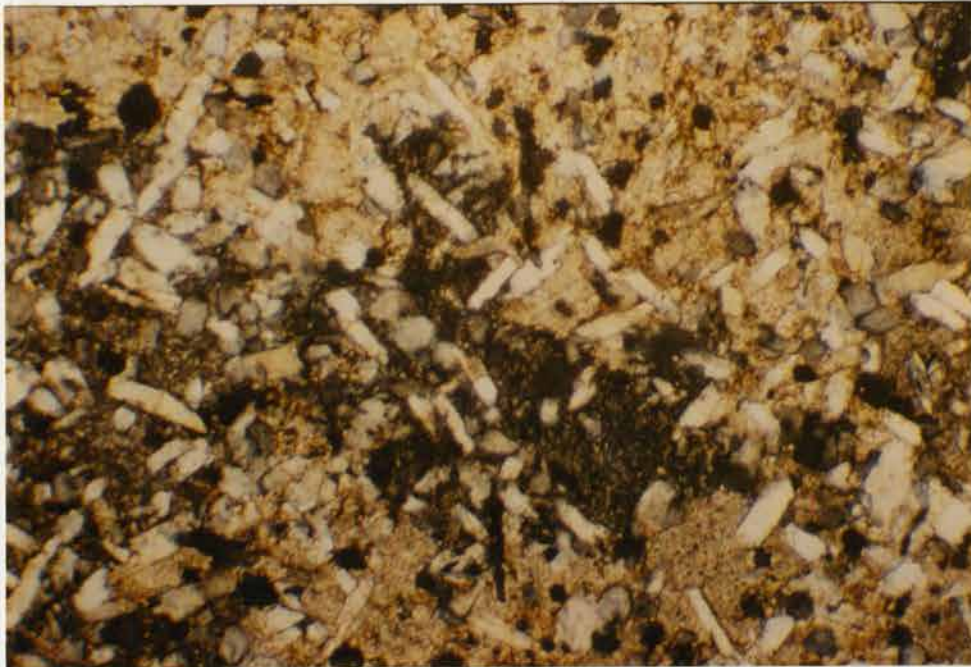


Fig. 33b. Partial stage III reticulate quartz replacement following limestone recrystallization. Field of view 1.1 X 1.6 mm. Sample #129: 0.04 oz Ag/ton; 15 ppb Au; 10 ppm Sb; 38 ppm As.

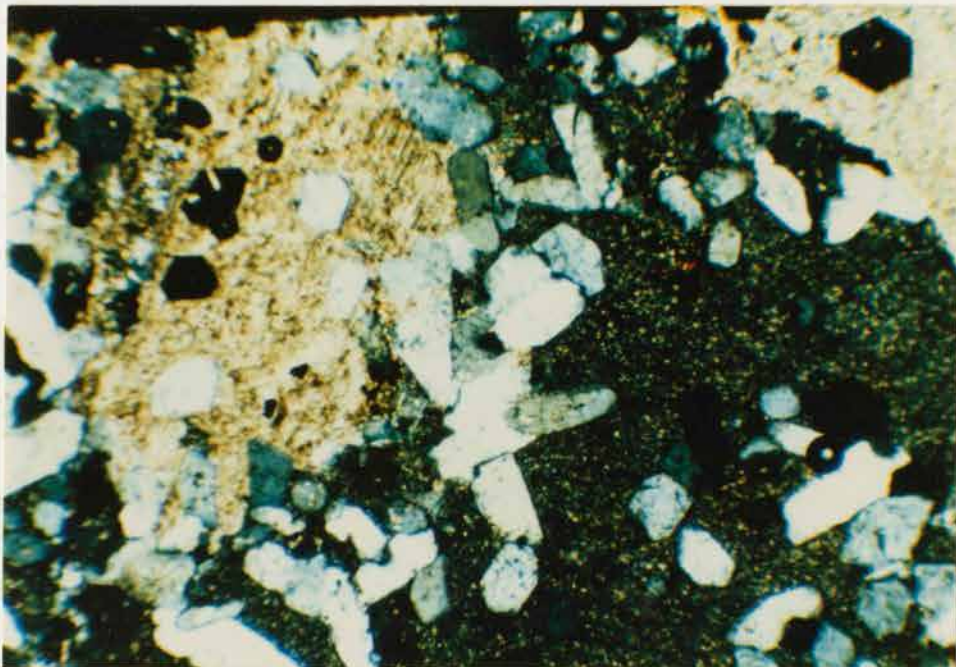
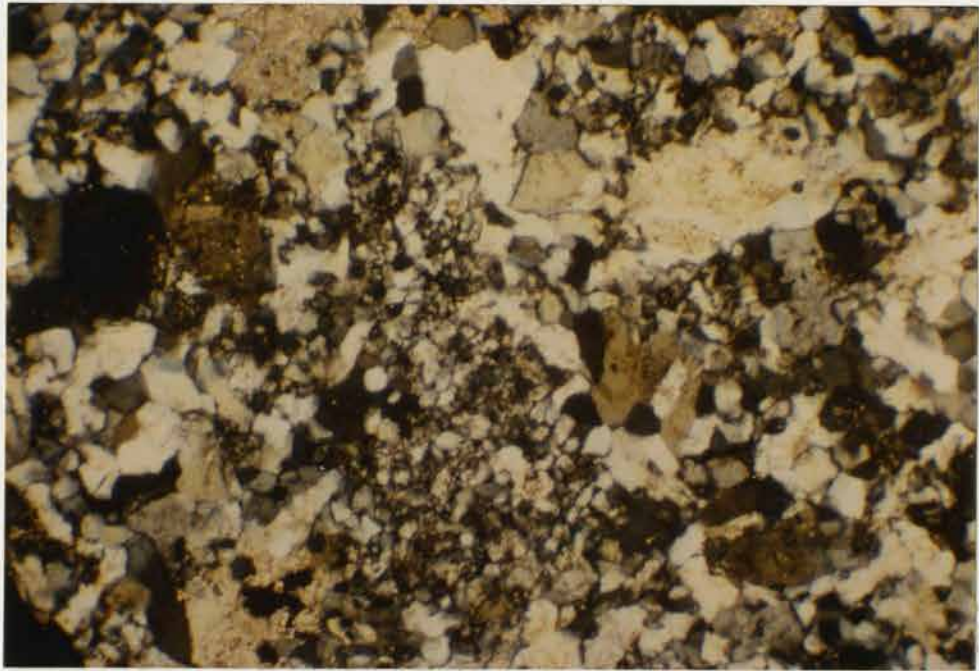


Fig. 33c. Partial stage III silicification with limestone recrystallization. Field of view 1.1 X 1.6 mm. Sample #29a: 0.1 oz Ag/ton; 35 ppb Au; 54 ppm Sb; 17 ppm As.

(a)



(b)

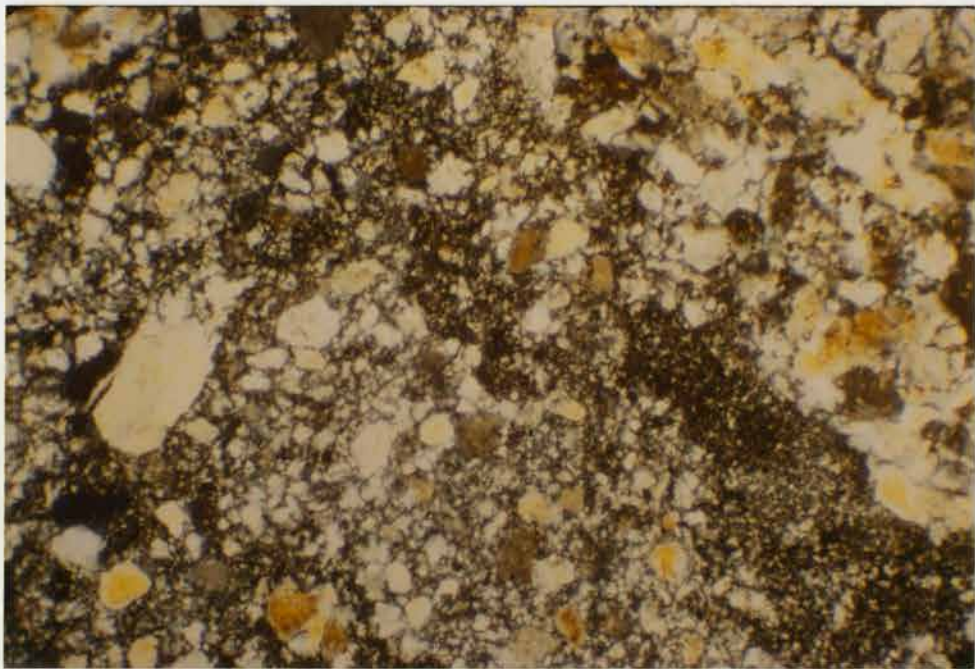


Fig. 34. Typical stage III hypidiomorphic textured jasperoids. Field of view (both a and b) 1.1 X 1.6 mm. (a) Sample from drill hole D-1, 130-135: 8.84 oz Ag/ton; 155 ppb Au; 101 ppm Sb; 40 ppm As. (b) Sample #222: 3.18 oz Ag/ton; 80 ppb Au; 141 ppm Sb; 15 ppm As.

occur only in trace amounts. Deposition of very fine-grained granular to jigsaw texture silica in fractures, open space, and possibly vugs, with large concentrations of sulfides and rare fluorite followed a third brecciation event (Fig. 35). Higher-grade rock invariably contains late jigsaw silica. Jigsaw silica hosts noticeably high concentrations of disseminated opaques including pyrite and sphalerite. Other minerals, probably including galena and tetrahedrite (based on trace element contents) appear only as bright specks at 500X (Fig. 36). Remaining open space is filled by stage IV open space white calcite-(sulfide) veins. Calcite often cuts jasperoid and more rarely replaces the margins of jasperoid fragments. Spherulitic textures are rare, but suggest local recrystallization of very fine-grained silica. Goethite and hematite are the dominant iron oxides contained in oxidized stage III jasperoid. Lovering and Heyl (1974) identified accessory tourmaline, monazite, and apatite from jasperoids in the district.

Stage III contains the most diverse silica textural varieties. It was clearly deposited in the most tectonically active and structurally complex portion of Plate 1. Diverse fragment types evidence multiple brecciation events. Overall jasperoid texture is invariably hypidiomorphic. As discussed above, stage III jasperoid contains fragments of stage I and stage II jasperoid with stibnite.

Based on thin section examination and trace element geochemistry, blue-grey jasperoid is believed to be strongly leached stage III jasperoid. One of the distinguishing features of blue-grey jasperoid is the presence of strong fracture-controlled jarosite. That blue-grey jasperoid was identified in only two narrow exposures near high-angle faults, suggests that acid supergene leaching was not widespread.

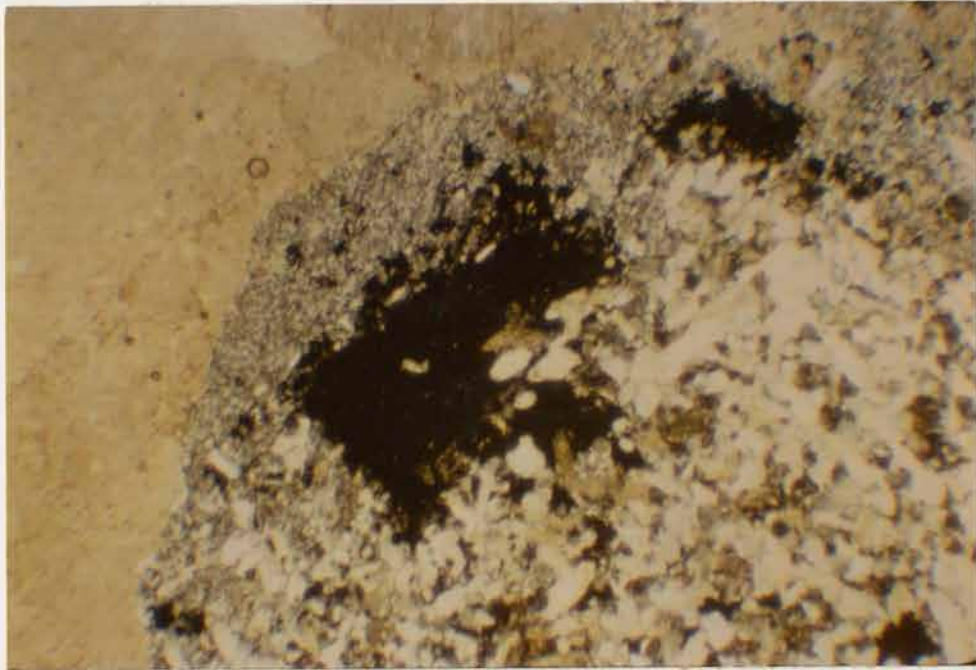


Fig. 35. Stage III jasperoid: late jigsaw silica with high sulfide content and in this case, fluorite. Field of view 4.1 X 6.25 mm. Sample from drill hole D-9, 65-70: 10.24 oz Ag/ton; 155 ppb Au; 2200 ppm Sb; 47 ppm As.

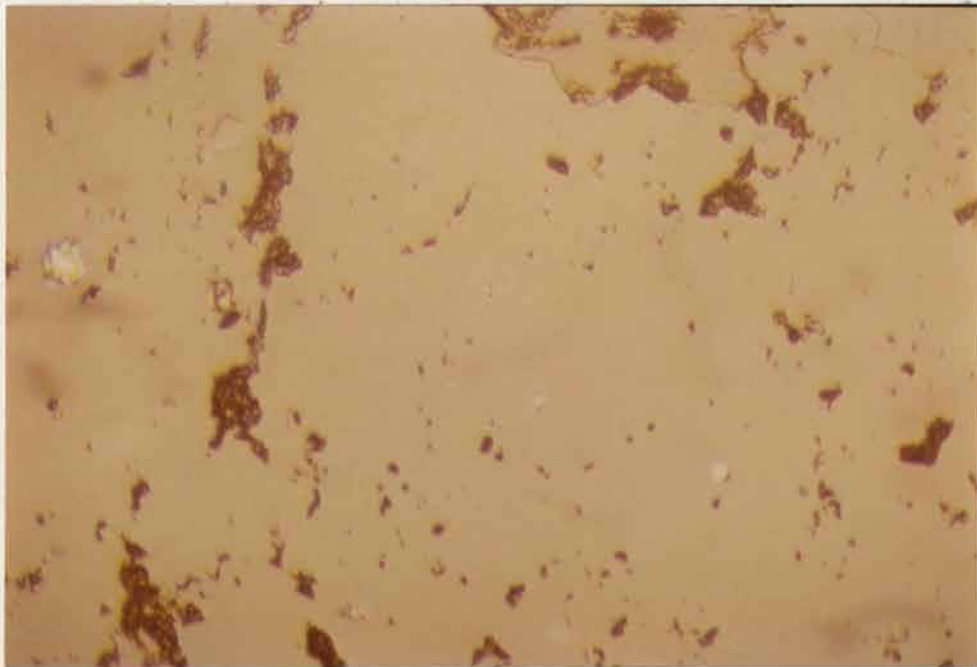


Fig. 36. Stage III jasperoid, showing disseminated sulfides under reflected light. Field of view 0.17 X 0.27 mm. Sample from drill hole D-1, 130-135: 8.84 oz Ag/ton; 155 ppb Au; 101 ppm Sb; 40 ppm As.

## (d) Stage IV

Deposition of stage IV open space coarse-grained sulfide-calcite-(silica) followed brecciation along the principal Southwest Pit and Argus high-angle feeder structures. Deposition of very fine-grained granular- to jigsaw-texture silica continued into stage IV, where it rims jasperoid fragments, followed by coarse open space sulfides (Fig. 37). Pyrite, sphalerite, and galena precipitated directly on jasperoid fragments or on fine-grained jigsaw silica. Sphalerite contains very little iron, and up to 2.4 wt % Cd (Semi-quantitative Kevex analyses). Tetrahedrite veinlets cut both sphalerite and galena. Whole rock trace element chemistry suggests the tetrahedrite is Sb-rich. An unknown sulfosalt comprised of Ag, Pb, Sb, and S subsequently replaced most of the galena (Fig. 38). The mineral dominated all samples of high-grade ores collected along the Southwest Pit and Argus faults, and may be the most abundant ore mineral in the Taylor district. It displays very weak reflective pleochroism, is olive-grey to grey against galena, and is distinctly anisotropic black to dark-blue, although less prominent than in stibnite. The mineral is harder than galena and softer than sphalerite (based on false becke lines). Distinct twinning was not recognized. Semi-quantitative Kevex analyses indicate a composition approaching  $Pb_9Ag_2Sb_4S_{10}$  (noting severe overlap between Pb and S).

Erickson (1964) reported the occurrence of bournonite, famatinite, stephanite, and miargyrite in high-grade ores at depth. Lovering and Heyl (1974) also identified pyrargyrite. Shearing followed sulfide deposition. Broken pyrite grains were dragged along micro shears (Fig. 39). The Ag-Pb-Sb sulfosalt recrystallized, with crystal

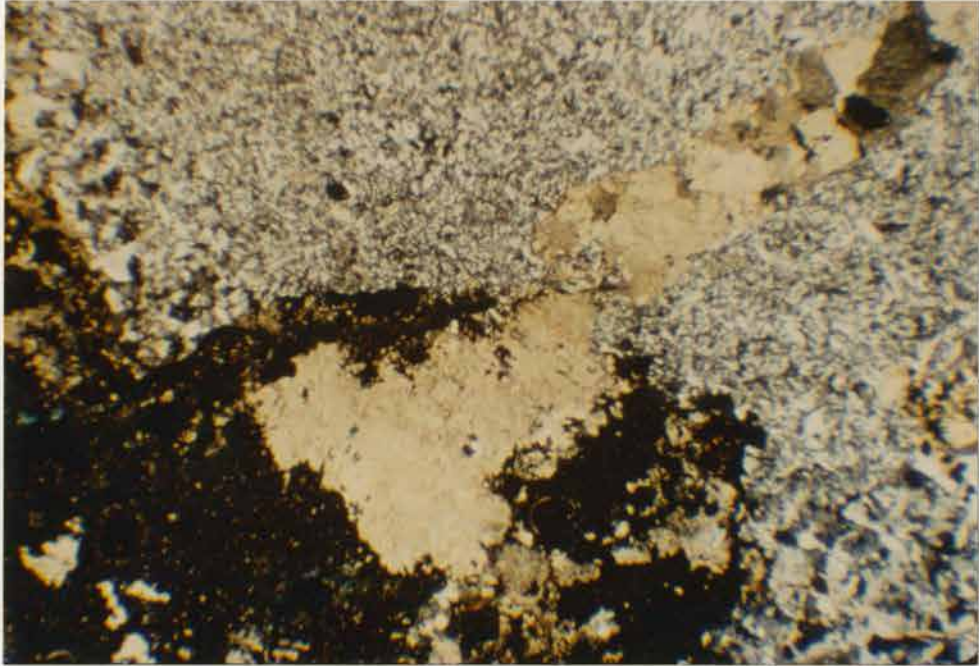


Fig. 37. Stage IV jigsaw silica, open space sulfides (oxidized here), and calcite on jasperoid fragments; cut by late calcite. Field of view 4.1 X 6.25 mm. Sample from drill hole D-14, 40-45: 33 oz Ag/ton; 120 ppb Au; 1750 ppm Sb; 60 ppm As.

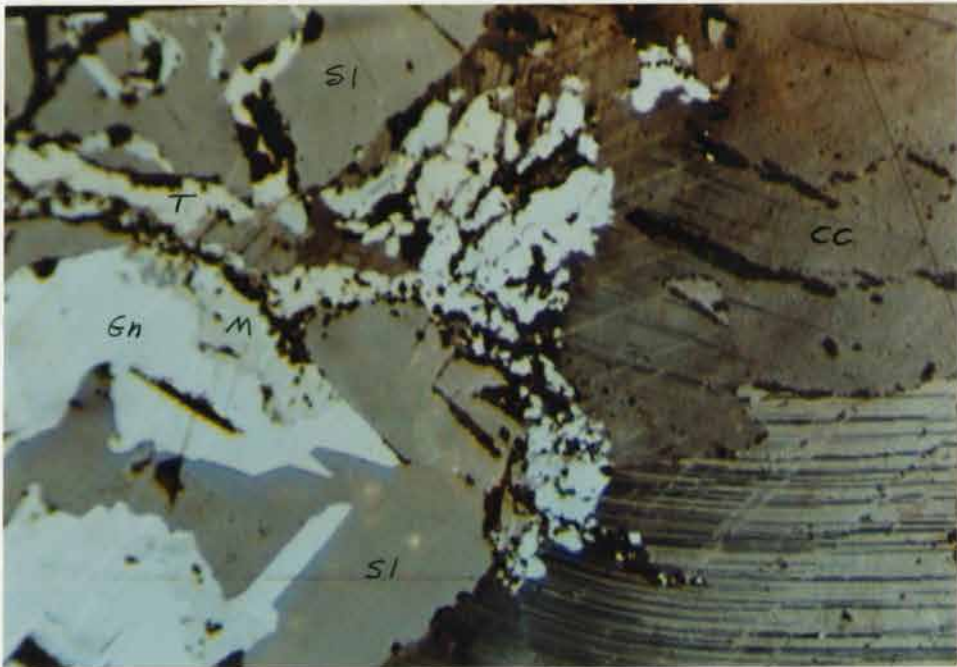


Fig. 38. Stage IV unnamed Ag-Pb-Sb-S mineral (M) replaces galena (Gn) and tetrahedrite (T) adjacent to calcite (cc). Field of view 0.42 X 0.63 mm. Sample #26.

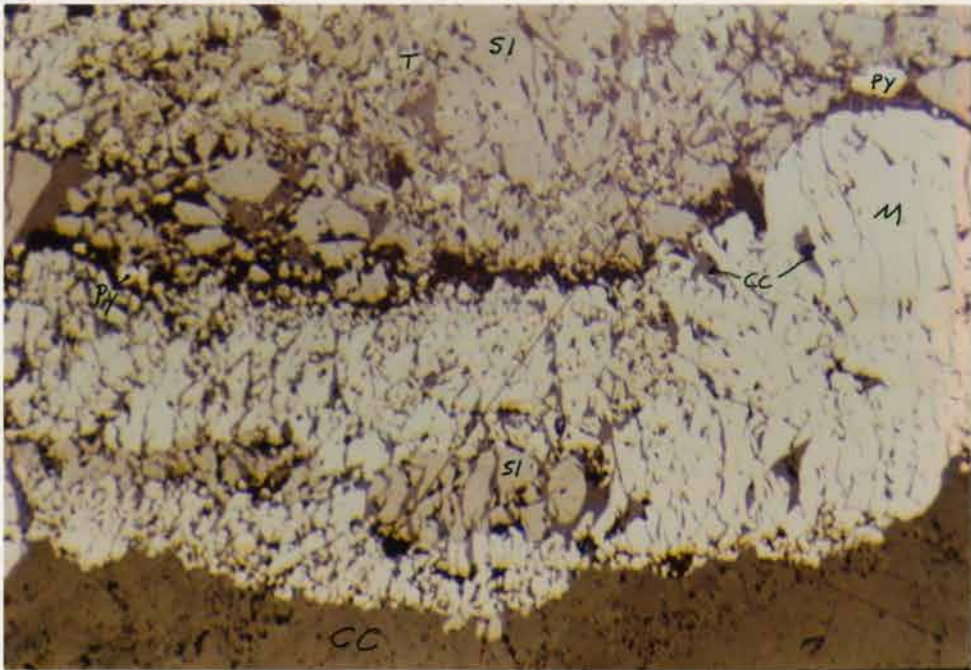


Fig. 39. Post-mineral shearing locally induced recrystallization of unnamed mineral (M) perpendicular to shear surfaces. Pyrite grains are broken along shears. Brittle fractures are filled with late calcite (cc). Sample #26.

orientation perpendicular to shear surfaces. Late calcite fills remaining open space.

The Taylor -350 drift cuts banded black/white calcite veins hosted on the Argus fault (Figs. 40, 41). In detail, the dark layers are actually quartz-sulfide bands within white calcite (Fig. 42). The banded nature of the mineralogy indicates that fluid chemistry oscillated between calcite soluble and quartz soluble conditions. Sulfide bands precipitated onto open space quartz layers, followed by white calcite.

(e) supergene mineralogy

Lovering and Heyl (1974) reviewed supergene mineralogy. They state that strong oxidation is important only within a few feet of the surface and down faults. Lovering and Heyl (1974) identified hematite,



Fig. 40. Banded calcite-sulfide-quartz veins on the Argus fault, Taylor -350 level. Grab sample #134: 16.5 oz Ag/ton.



Fig. 41. Plumose calcite-sulfide-quartz veins on the Argus fault, Taylor -350 level. No sample collected.

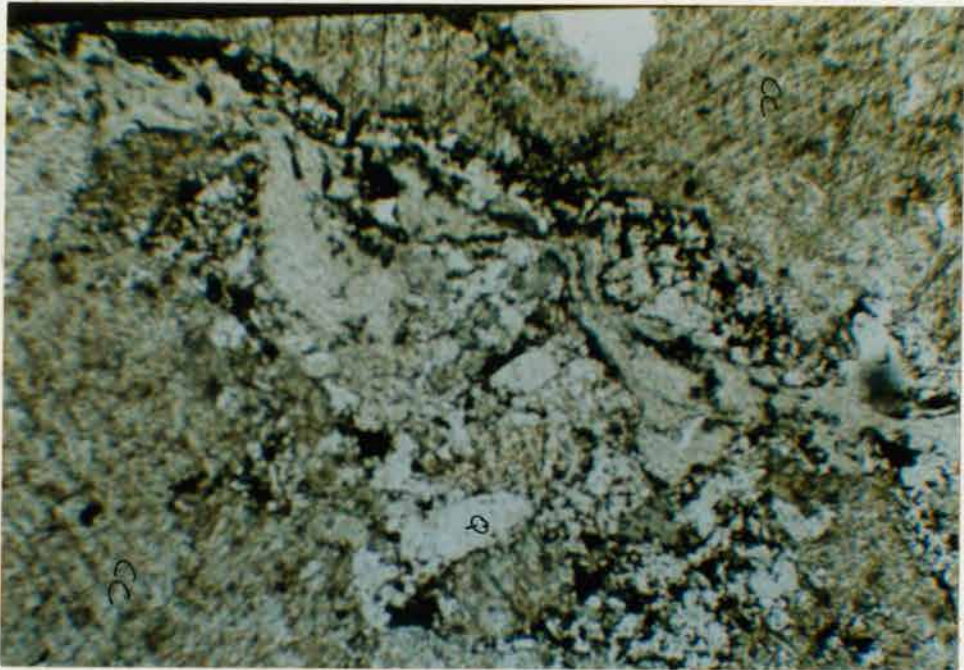


Fig. 42. Banded calcite (cc) - sulfide (opaques) - quartz (Q) vein in transmitted, plane light. Field of view 1.1 X 1.6 mm. Grab sample #134: 16.5 oz Ag/ton.

limonite, pyrolusite, bindheimite, cervantite, smithsonite, cerussite, cerargyrite, azurite, malachite, jarosite, hemimorphite, conichalcite, anglesite, wulfenite, willemite, tenorite, chrysocolla, "antimony ocher", kaolinite, and leucoxene, in the oxidized surface environment.

#### WALL ROCK ALTERATION

##### (a) Silicification of sediments:

Partial silicification of the Guilmette Formation, Pilot Shale, and to a lesser extent the Joanna Limestone, is common adjacent to jasperoid and feeder structures (Plate 1). In thin section, jasperoid grades into silicified limestone, comprised of idiomorphic or granular texture quartz grains isolated in limestone or recrystallized limestone matrix (Figs. 33 a,b,c). Recrystallization of remnant limestone is

erratic and not correlative with any specific jasperoid stage. Secondary quartz is the only alteration product recognized. XRD studies of nine partially silicified Guilmette and Joanna limestone samples indicated the presence of dolomite in only one Dgt sample. This dolomite may have been indigenous. Otherwise, only calcite was detected in these samples.

Joanna Limestone was not subject to widespread silicification away from jasperoid. Contacts with jasperoid are often sharp. Typical alteration persists only several feet into adjacent Joanna Limestone.

The underlying Pilot Shale is partially decalcified and silicified in the Argus Pit near the intersection of a principal NE-trending feeder with the Argus Fault. Strong silicification extends several tens of feet away from the intersection (Fig. 43). Fine-grained jigsaw silica floods the rock both parallel and perpendicular to laminations (Fig. 44). Well silicified Pilot rings under the hammer and breaks along conchoidal fractures. One small outcrop of silicified Pilot, identified 600 feet north of the Antimony Pit, displayed weak hematitic liesegang banding on weathered surfaces.

Guilmette transition silty limestone beds suffered widespread silicification around the ore body (Plate 1). The halo extends as much as 75 feet up-section east of the Argus fault, and as much as 300 feet on strike from the nearest mapped jasperoid body. Intensity of alteration ranges from weak to strong, reflecting increases in epigenetic silica content from negligible to 50%. In outcrop, strongly silicified, brecciated, Dgt beds consist of limestone fragments in a medium brown-weathering siliceous matrix (Fig. 45). Both detrital and epigenetic quartz grains comprise the matrix. A dusting of relict



Fig. 43. Silicified Pilot Shale in Argus Pit. Sample #230: 0.18 oz Ag/ton; 5 ppb Au; < 2 ppm Sb; 40 ppm As.

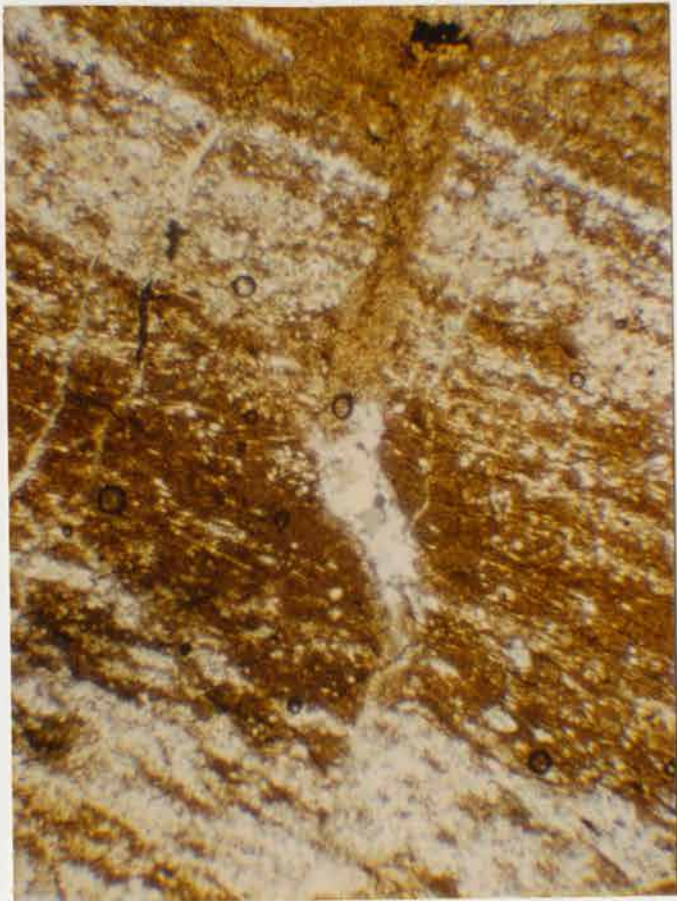


Fig. 44. Silicified Pilot Shale in transmitted light. Field of view 4.1 X 6.25 mm. Sample #71: 0.06 oz Ag/ton; 5 ppb Au; 182 ppm Sb; 32 ppm As.



Fig. 45. Brecciated and strongly silicified Guilmette transition beds adjacent to the Argus fault. Photo by T.B. Thompson. Near sample #102: 0.82 oz Ag/ton; 10 ppb Au; 3 ppm Sb; < 2 ppm As.

calcite inclusions distinguishes the replacement silica.

A light-tan- or buff-weathering silty matrix surrounding grey unaltered limestone fragments or clasts produces a mottled appearance in weathered moderately silicified Dgt beds. Breccia textures may reflect primary sedimentary texture. The buff to light-tan weathered surfaces result presumably from trace iron addition; fresh surfaces do not show the effects of moderate silicification. Weak alteration, as mapped, might be unrecognizable out of context. Very light-tan mottled weathered surfaces persist beyond stronger alteration zones, but are not seen isolated in Dgt beds far removed from mineralization.

As described above, the upper Dgc limestones are extensively silicified within and adjacent to the ore body.

Dgb silty limestones are bleached and weakly silicified above jasperoids hosted in the underlying Dga, north of the mill. Tan to light-brown mottled float looks much like silicified Dgt beds.

Jasperoid is found in fairly sharp contact with fresh Dga limestone in the Northwest Pit area. Silica extends less than 30 feet away from jasperoids into adjacent heterolithic breccia (Fig. 46), where it stands out as brown-weathering ribs surrounding breccia fragments (Fig. 47).

(b) Alteration of porphyritic rhyolite

Porphyritic rhyolite dikes and sills display wide ranges in intensity and type of alteration across the district. Rhyolite outside the immediate mine area suffered weak kaolinite-sericite argillic alteration (Fig. 48). Kaolinite and silica partially replace plagioclase phenocrysts. The ground mass contains trace sericite. One dike, located at 94,000 north, 98,300 east, about 2300 feet southeast of the mine, is silicified (Fig. 49). Fine-grained jigsaw texture silica flooded the ground mass with trace montmorillonite.

Rhyolite bodies in the immediate mine area suffered moderate to intense montmorillonite argillization. Biotite often remained stable, even in some of the most intensely altered sills. Several dikes contain trace to 15% disseminated pyrite with montmorillonite.

A five foot thick argillized sill intercepted in diamond drill hole D-16 was studied in detail. Argillization becomes visibly more intense at the margins, which contain trace fresh pyrite, demonstrating the hypogene origin of alteration fluids. Both footwall and hangingwall rocks contain 1 to 2 ounces Ag per ton. Five samples were collected across the sill, one at the center, one at each margin, and



Fig. 46. Heterolithic tectonic breccia in Guilmette member a limestone. Not assayed.

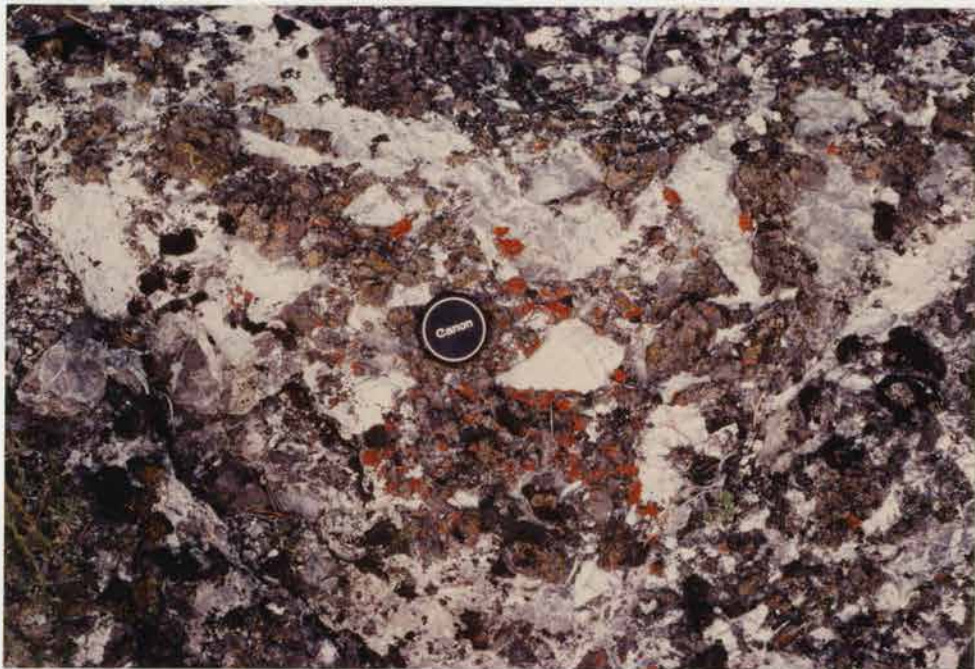


Fig. 47. Partial silicification of Guilmette member a, limestone breccias. Not assayed.

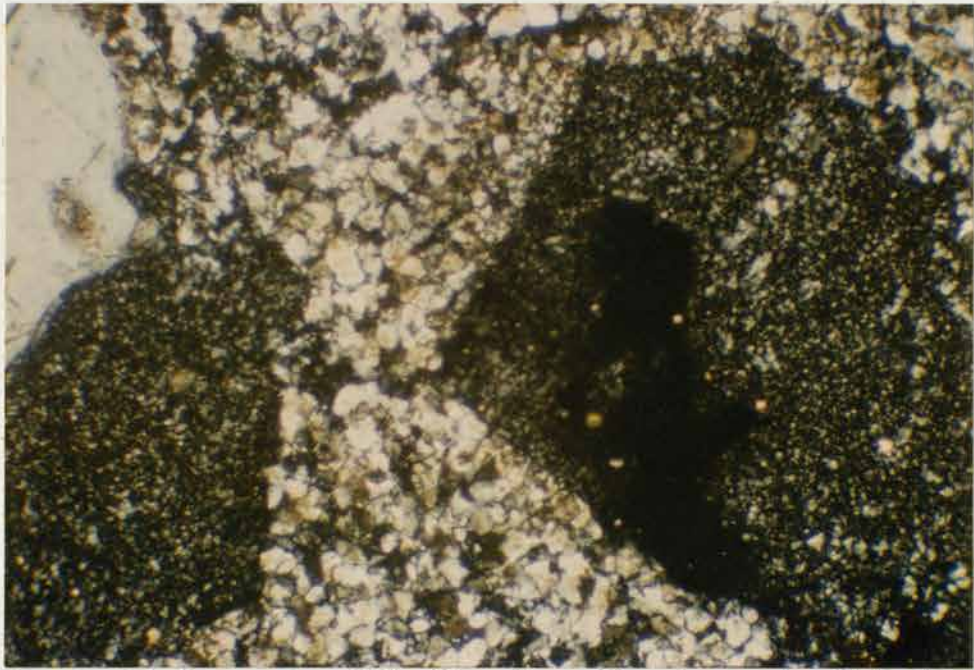


Fig. 48. Kaolinite-montmorillonite alteration in porphyritic rhyolite. Field of view 0.66 X 1.0 mm. Sample #172c.

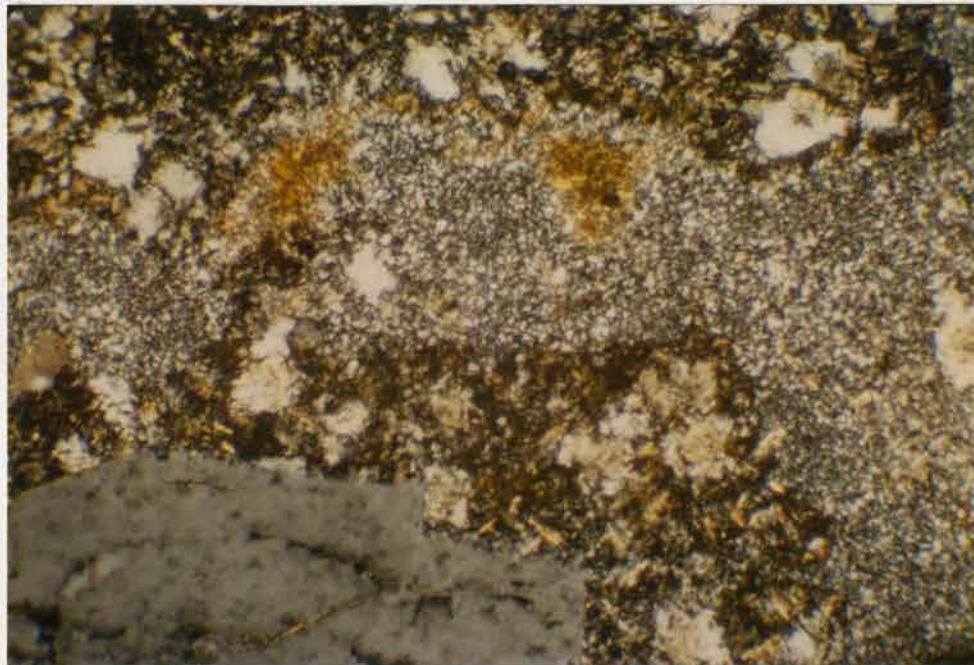


Fig. 49. Silica flooding in porphyritic rhyolite. Field of view 0.66 X 1.0 mm. Sample #79.

two from intermediate positions. Samples collected from a surface exposure of argillized rhyolite near the collar of hole D-16 helped evaluate the effects of supergene overprinting. Thin sections were prepared for each sample. XRD studies facilitated clay mineral identifications, and whole rock analyses defined major oxide gains and losses. Two samples of weakly kaolinized rhyolite were analyzed for comparison.

In thin section, kaolinite is seen near the center of the sill after plagioclase (Fig. 50). Sanidine is stable, while the ground mass is strongly altered to montmorillonite and minor sericite. Moving toward sill margins, kaolinite is gradually inundated by montmorillonite and sanidine phenocrysts are partially altered. All that remains at the sill margins are quartz and montmorillonite (Fig. 51). Petrographic evidence clearly indicates that kaolinite and sericite were deposited during early stages of alteration, and were systematically inundated by late stage montmorillonite in regions of most intense alteration.

XRD patterns likewise show that kaolinite and sericite, which are most abundant in the center of the sill, are progressively replaced by montmorillonite toward the borders. X-ray patterns from surface samples are identical to those at depth, suggesting that supergene fluids are not sufficiently acidic to induce retrograde alteration to lower pH clay mineral phases.

Figure 52 shows density corrected whole rock data, in grams per cc (raw data included in Appendix I). Densities of samples were calculated by simply weighing chips, submerging them in a graduated cylinder, and reading the volume of displaced water off the cylinder.

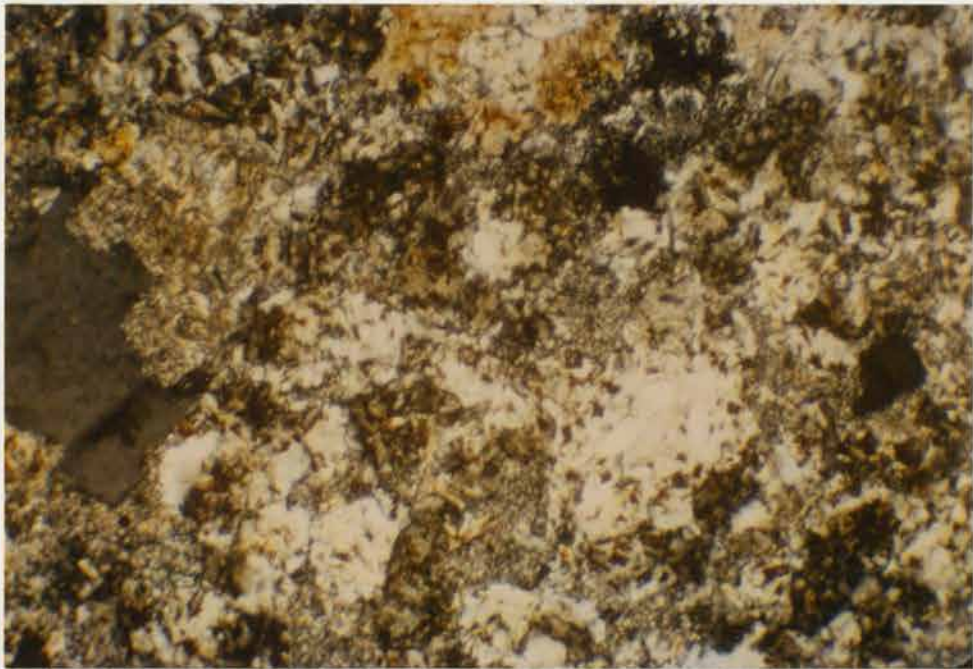


Fig. 50. Montmorillonite-kaolinite alteration of porphyritic rhyolite. Field of view 1.1 X 1.6 mm. Sample #172c.

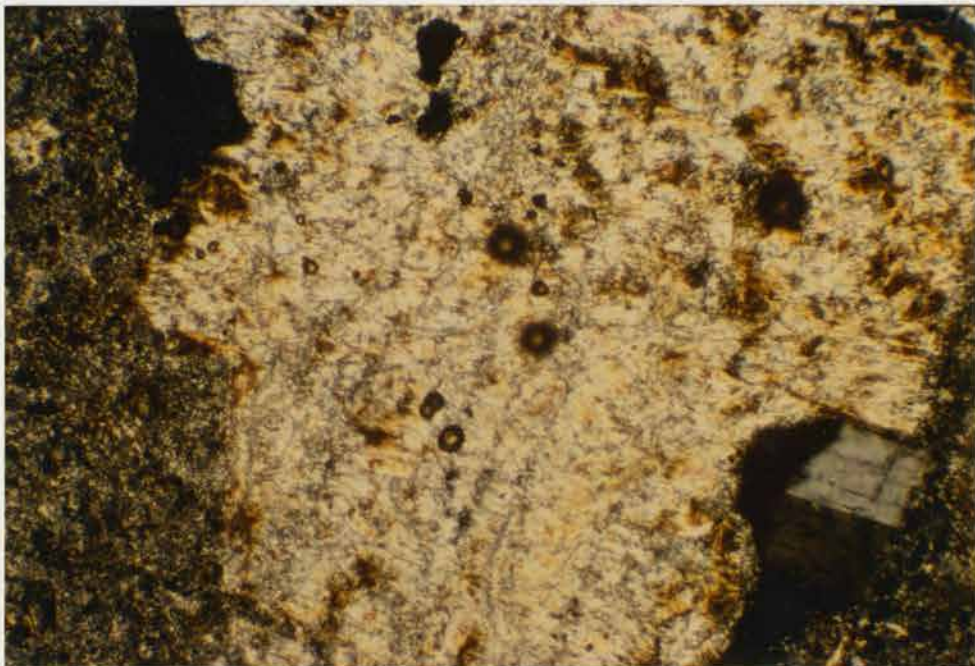


Fig. 51. Intense montmorillonite alteration of porphyritic rhyolite. Field of view 1.1 X 1.6 mm. Sample #172e.

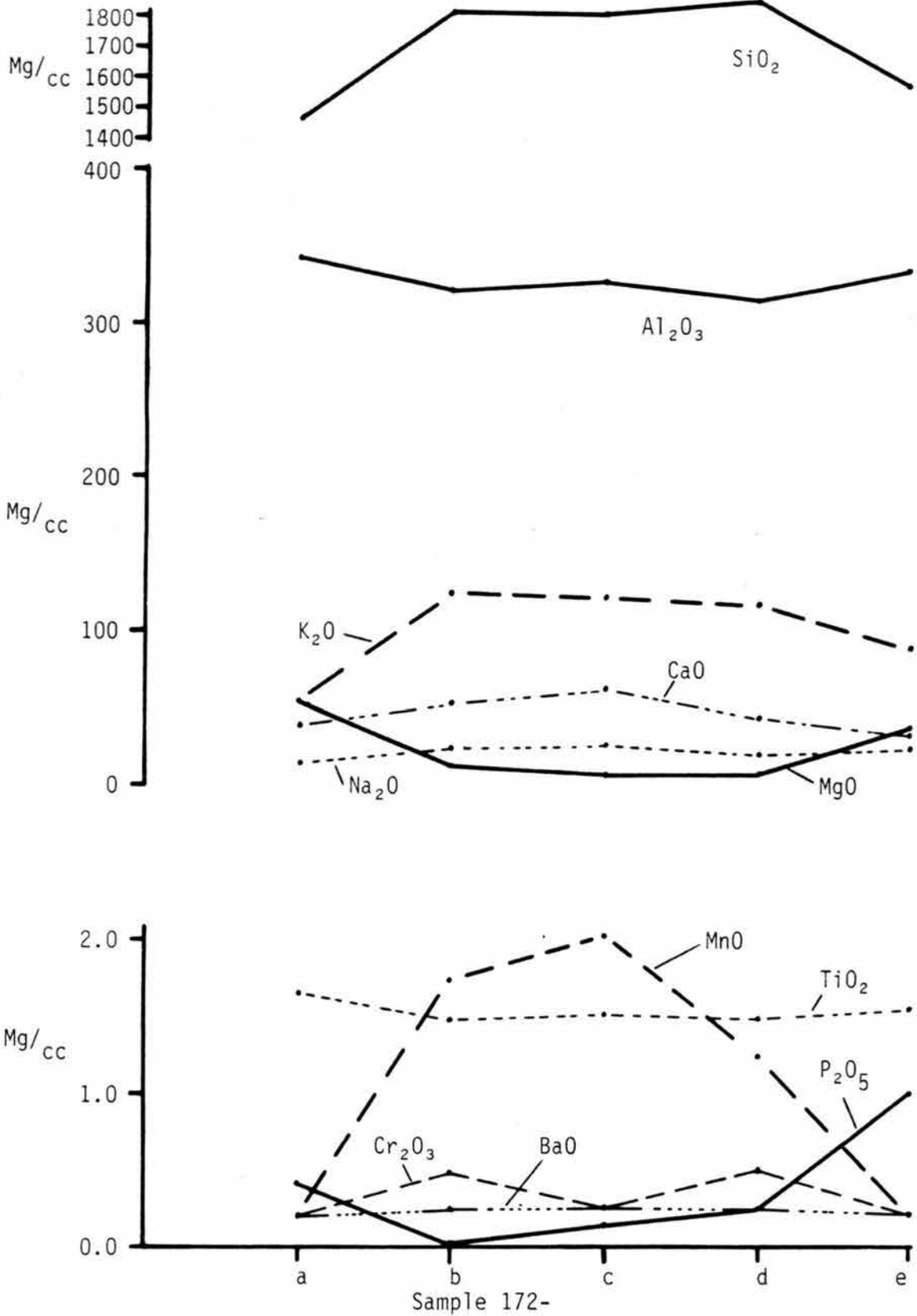


Fig. 52. Major oxide trends across argillized dike.

Three to five replications using different chips were averaged to arrive at sample density.

MgO, Al<sub>2</sub>O<sub>3</sub>, and P<sub>2</sub>O<sub>5</sub> increase outward to the sill margins, while MnO, K<sub>2</sub>O, CaO, and SiO<sub>2</sub> decrease. Deposition of montmorillonite during late stage alteration, therefore, resulted primarily from increased  $a_{Mg^{+}}/a_{H^{+}}$  and higher pH, effecting Mg metasomatism.

One other style of alteration occurs only in the mine area in dikes cut by the Argus and Southwest Pit faults. Portions of these dikes were brecciated along the faults. Late calcite healed the fault zones. Calcite inundated portions of adjacent rhyolite dikes and rhyolite breccia fragments, while preserving primary igneous textures (Fig. 53). Locally, carbonatized fault breccias of this type contain jasperoid fragments (Fig. 54).

#### FLUID INCLUSIONS

Fluid inclusions were examined in three mineral phases including quartz from stage II jasperoid, fluorite from stage III jasperoid, and sphalerite from stage IV sulfide veins. Figure 55 shows results. Appendix II contains raw data. No freezing data were generated due to the small size of inclusions in quartz and fluorite and severe internal reflection problems in sphalerite.

##### (a) Quartz

The quartz sample is coarse-grained, idiomorphic, vug-filling quartz, that precipitated early during stage II jasperoid formation. Younger fine-grained reticulate quartz surrounded and locally replaced the vug quartz (Fig. 27). The sample was collected from the Antimony

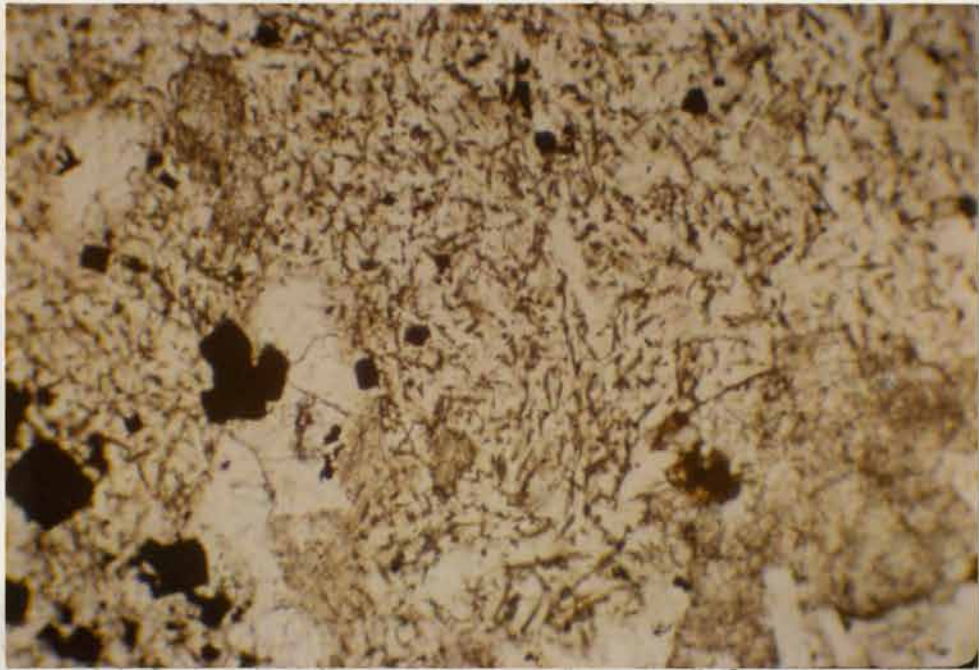


Fig. 53. Pyrite-siderite-calcite alteration in porphyritic rhyolite. Field of view 0.66 X 1.0 mm.

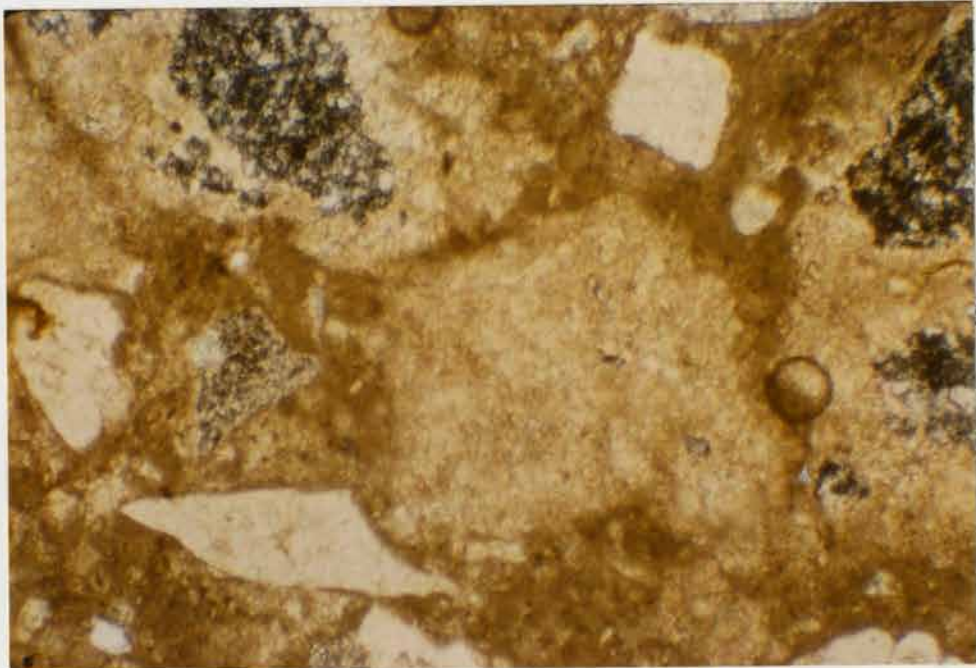


Fig. 54. Carbonatized rhyolite fault breccia with jasperoid fragments (see Fig. 18). Field of view 1.1 X 1.6 mm.

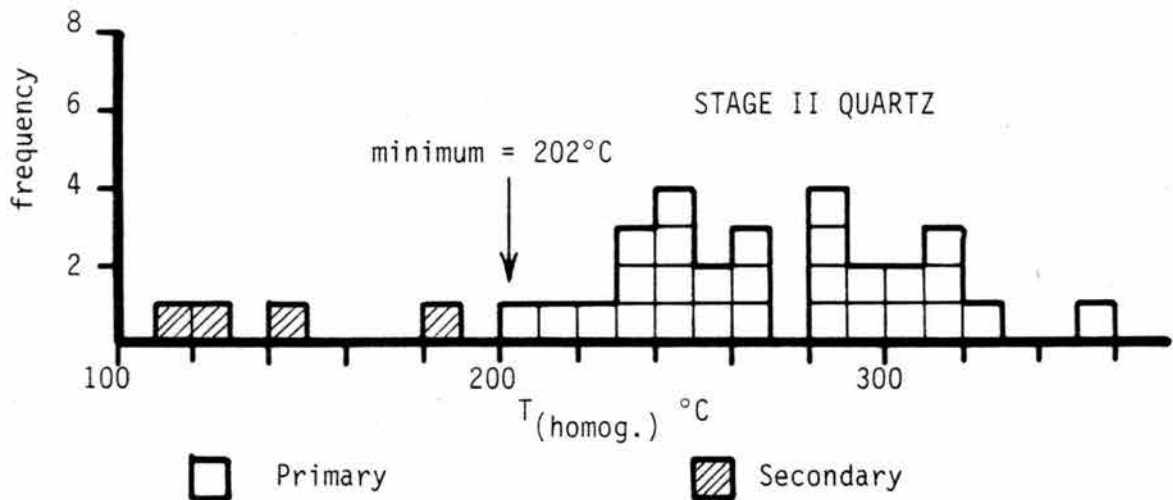
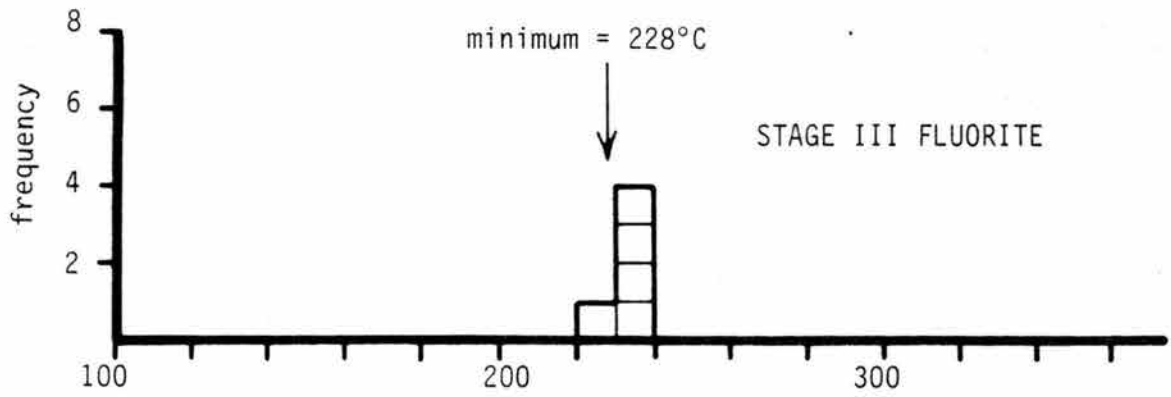
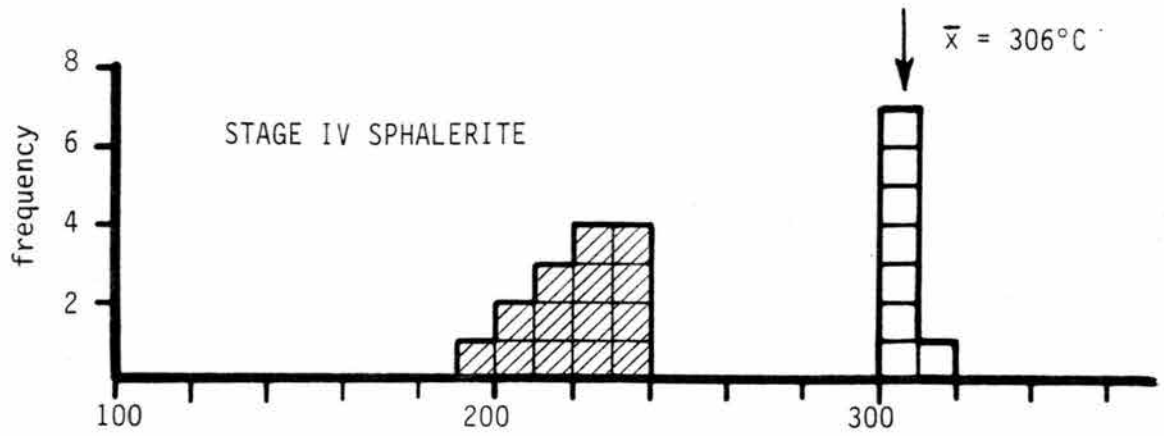


Fig. 55. Fluid inclusion homogenization temperatures.

Pit stibnite-rich jasperoid. Fluid inclusions are quite small, all under 8  $\mu$ m, with most under 5  $\mu$ m. Fluid to vapor ratios range from 20 : 1 to 1 : 50 (visual estimate) (Fig. 56). One vapor-dominated inclusion was analyzed, which homogenized to a vapor at 202° C. At least one inclusion contained a second liquid phase, evidenced by a double meniscus, although in general, inclusions were too small to make this distinction. No daughter crystals were present.

The lowest four  $T_h$  values shown in Figure 55 are considered to be secondary inclusions, or primaries which necked down, resulting in anomalously low  $T_h$ . Otherwise, all inclusions appeared to be isolated primaries that hadn't necked down, or leaked. Based on the presence of widely variable fluid to vapor ratios, and the great spread in  $T_h$  values to greater than 350° C, the fluid is interpreted to have been boiling during quartz deposition. Minimum temperature of formation is therefore 202° C, at the base of the bulk of data.

(b) Fluorite

Purple fluorite from stage III jasperoid is erratically concentrated within and near the Argus and Southwest Pit feeder structures. The sample utilized came from the Southwest Pit ore zone. Masses of fluorite crystals less than 3 mm replace dark grey stage III silver-rich jasperoid, and appears to have been deposited late during stage III mineralization. Fluorite is inclusion-rich and exhibits a wide range in fluid to vapor ratios ranging from over 10 : 1 to vapor-dominant (Fig. 57). Discrimination of more than one fluid phase was impossible due to small inclusion size, generally less than 10  $\mu$ m. They contain no daughter crystals.

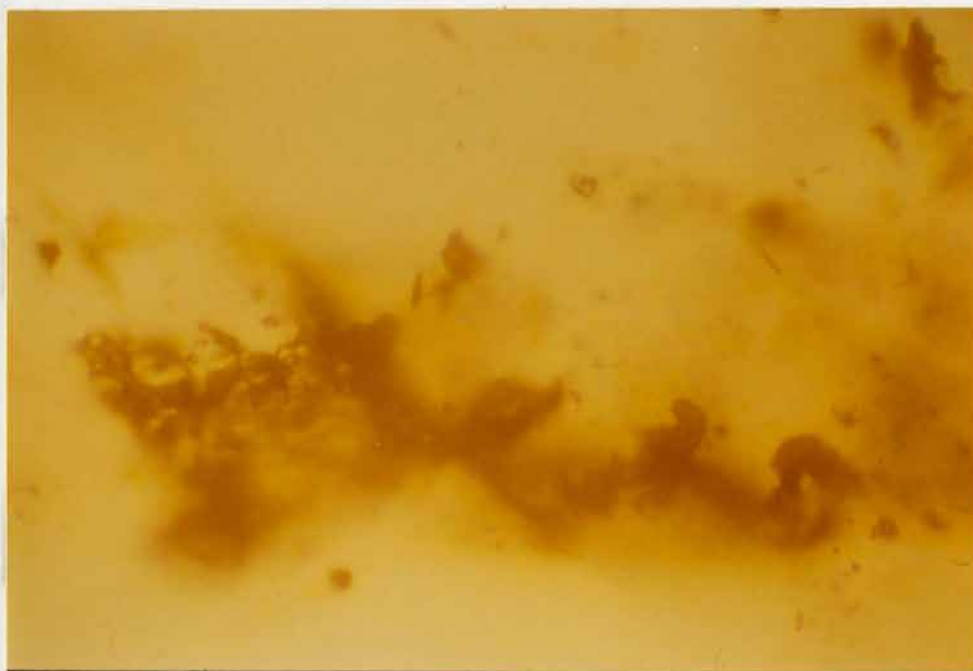


Fig. 56. Fluid inclusions in stage II quartz display a wide range of fluid: vapor ratios. Field of view 0.13 X 0.2 mm.

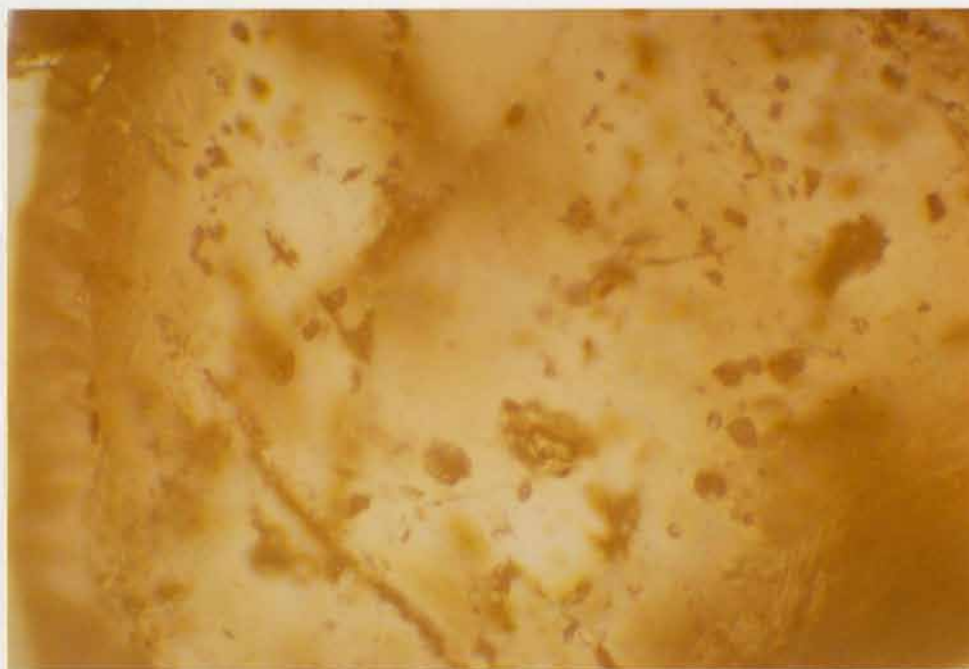


Fig. 57. Fluid inclusions in stage III fluorite with wide range in fluid: vapor ratios. Field of view 0.33 X 0.49 mm.

Fluorite, due to its softness and excellent cleavages is difficult to work with. Only where temperatures could be replicated three times are the numbers considered valid. Growth or cleavage planes localized most inclusions (hundreds in some fields of view). These inclusions began homogenizing at 150° C, however none of them were reproducible due to fluid leaking. They are considered unreliable.

Data furnished to Silver King in 1982 by Homestake Mining Company (generated by a consultant) showed  $T_h$ 's ranging from 139° to over 210° C for fluorite. The report noted that inclusions were located adjacent to cleavage planes, but reported no replications. Based on the present study, these data are not considered reliable or representative of the primary fluid environment.

Fluorite data shown on figure 55 are from completely isolated primary inclusions. Three replications were made on all inclusions; only reproducible data are shown. Five numbers are insufficient to determine, with certainty, the minimum temperature of formation in a system which may have been boiling. However, based on the available data, this temperature is estimated to be approximately 228° C.

Nearly clear, coarse-grained, open space vein fluorite hosted by the Argus fault was collected from the Taylor -350 drift. Limestone wall rocks and breccias cut by the vein are not silicified. Based on drill logs, this level is about 150 feet below the base of silica replacement in the system. No fluid inclusions could be found in this fluorite at magnifications up to 800X. The contrast between this and higher level inclusion-rich purple fluorite in jasperoid is remarkable. Two interpretations are possible. Fluorite was either deposited in two discreet stages from distinct fluids, or, if the two types of fluorite

are contemporaneous, one can infer that the base of silica replacement is related to the base of fluid boiling (or effervescence).

(c) Sphalerite

Coarse-grained (up to 1cm), very low iron, yellow to brownish yellow sphalerite was collected from a late stage open space sphalerite-galena-(Ag-sulfosalt) vein with white calcite gangue (Fig. 58). The sample came from a high-angle NE-trending vein near its intersection with the Argus fault in the Argus Pit. The sample assayed 56 ounces Ag per ton (Lavin, person. comm., 1982).

Figure 55 shows two groups of data. The lower temperature set defines a group of small secondaries contained along a growth plane (Fig. 59), and represent an annealing event that occurred at about 225° C. The set of higher  $T_h$  data is from large primaries up to 500 m (Fig. 60). Many exhibited negative crystal shapes and posed severe internal reflection problems. Fluid to vapor ratios appeared uniform. Several clearly contained a second fluid phase. No daughter crystals were noted. The consistency of data indicates a minimum temperature of formation of 306° C from non-boiling fluids.

#### DEPTH OF FORMATION

Stratigraphic reconstruction, based on thicknesses scaled from Plate 2, and those reported by Drewes (1967) define the range of possible depths of formation. Several assumptions used in this analysis include: Kalamazoo volcanics are comagmatic with porphyritic rhyolites and are pre-mineral, but closely related in time and space with the mineralizing event (evidence as discussed above); younger

Fig. 58. Stage IV  
sphalerite-  
tetrahedrite-  
galena-  
unnamed Ag-Pb-Sb  
sulfosalt-  
calcite vein in  
Argus Pit.  
Sample #26.



Fig. 59. Secondary fluid inclusions in sphalerite (with double meniscus). Field of view 0.13 X 0.2 mm.



Fig. 60. Primary fluid inclusions in sphalerite with double meniscus. Field of view 0.33 X 0.49 mm.

volcanics are believed to be post-mineral, since they lie on an unconformity beneath which Kalamazoo volcanics are only locally preserved; Eocene Stinking Spring Conglomerates were deposited on the lower Ely Limestone [Drewes (1967) states that conglomerates overlie both the Ely and the Arcturus, which implies over 3000 feet pre-deposition offset. Miocene/Pliocene gravity sliding complicates this relationship].

Stratigraphic thicknesses bracket depth of formation with potential minimum and maximum values: Pilot Shale/Joanna Limestone is 500 to 600 feet in the mine area, as scaled from Plate 2; Chainman Shale is 1100 feet according to Drewes (1967). This estimate is consistent with thicknesses scaled off Plate 2, east of the mine where the top of the Chainman is not preserved; only the lower 0 to 1000 feet of the Ely Limestone appears to be preserved beneath Eocene

conglomerates as scaled off Plates 1 and 3 of Drewes (1967) (this relationship is problematical due to Tertiary faulting); Eocene Stinking Spring Conglomerate ranges from 900 to 1200 feet thick where preserved beneath Kalamazoo equivalent volcanics as scaled from plates 1 and 3 of Drewes (1967); Kalamazoo equivalent volcanics are at least 300 feet thick where preserved beneath younger volcanics (Drewes, 1967).

Stratigraphic reconstruction brackets depth of formation of the Taylor silver deposit (base of the Pilot Shale) between 2800 feet and 4200 feet, or,  $3500 \pm 700$  feet.

Fluid inclusion data permit independent depth calculations. Boiling conditions during stages II and III imply hydrostatic load, thereby requiring no pressure corrections. Depth estimates from Haas (1971) range from 2950 to 3280 feet corresponding to an assumed salinity range of 5 to 10 wt % equivalent NaCl at 300°C. This estimate is based on the system  $H_2O - NaCl$ . The presence of other volatiles, including  $CO_2$ , methane, ethane, or propane would induce boiling at even deeper levels (Bodnar and Kuhn, 1982; Kuhn, 1985). These depth estimates agree well with stratigraphic reconstruction ( $3500 \pm 700$  feet).

## CHAPTER V

### GEOCHEMISTRY

#### INTRODUCTION AND PROCEDURES

Trace element geochemistry of the Taylor mine area was studied in detail. Emphasis is split between surface and drill hole samples. Due to budgetary constraints, not all samples could be analyzed for all the elements of potential interest.

In 1982, 189 surface rock chip samples were collected for assay. Plate 3 shows all surface sample locations. Unless otherwise noted, rock chip samples are 3 to 4 pound grab samples. An attempt was made to collect an even distribution of chips over the area sampled without bias for any particular alteration or coloration type. Where bias was intentionally introduced, Appendix III lists sample type. In an area of subdued outcrop, a typical rock chip sample represents a circular area 15 feet to 20 feet in diameter. Where exposures allowed, continuous chip samples were commonly taken perpendicular to bedding or obvious structures. Chips included in the sample came from 2 to 6 inches deep to avoid the bleached surface rind whenever possible. Most surface rock chip samples were taken from weathered outcrop, exposures in old catcuts and prospect pits, and from old prospect dumps. Only a few samples come from open pits developed by recent mining. Surface

samples and analyses thereby largely reflect the exploration characteristics of the district prior to recent development.

Silver King prepped rock chip samples in their Ward lab. Samples were crushed to -0.25 inches; a 0.5 lb split was then pulverized to -100 mesh for assay. Silver King performed  $\frac{1}{2}$  assay ton fire silver assays on all samples. The pulps were then delivered to Bondar-Clegg for trace element analysis by Atomic Absorption (AA).

Thirty-four rock chip samples from the sequence 114 to 178 were inadvertently discarded after silver analysis but prior to trace element analysis. These samples were recollected in November of 1982 from the same outcrops, and assayed for Ag by Bondar-Clegg using AA. The mean of the AA values is 0.122 oz Ag/ton, or 79% of the mean of the fire assays at 0.154 oz Ag/ton. Although this comparison is between different sample collections, the disparity could in part reflect silica-encapsulated Ag missed by Bondar-Clegg's acid dissolution.

A total of 111 samples from six drill holes were selected for trace element analysis. Five core holes and one rotary hole (twinned by a core hole) enabled integration of detailed drill logs, transmitted and reflected light studies with trace element results. Selected holes are widely spaced to obtain a broad distribution of data through the deposit and define zonation patterns. All six holes cut ore.

Silver King's original drill sample pulps were analyzed. Pulps represent 5 foot sample intervals. Cuttings and core splits were originally prepped in Silver King's Ward lab in the same manner as the surface rock chip samples. Due to the length of hole D-10, composites were made for selected intervals. This entailed rolling each pulp using at least 80 corners, then cutting precisely 50 grams out for the

composite. These composites were reassayed for Ag to check validity (Appendix IV).

Bondar-Clegg, Lakewood, Colorado, performed all trace element analyses by AA. Due to recognized inconsistencies in some of the pulps (as prepped by Silver King), all pulps were re-pulverized to -150 mesh prior to trace element analysis. Appendix III lists specific Bondar-Clegg analytic procedures.

Exploration Research Laboratories (now SOREX), Salt Lake City, Utah, analyzed hand samples from 23 jasperoid outcrops for eight vapor phase components by gas chromatography/ mass spectrometry (GCMS). Exploration Research Labs rough-crushed the samples, sieved out the minus 60 plus 200 mesh fraction, and put 1 gm of this material into a 20 cc glass headspace vial crimped at the top with a teflon-lined septum. They heated the bottom of the vial to 375° C for one hour, extracted one cc of headspace gas, and injected the gas into a GCMS system. Exploration Research Labs calibrated analyses with gas standards, and subtracted constants from CO<sub>2</sub> values to account for atmospheric contamination. It is assumed that the majority of volatiles are derived from the break down of fluid inclusions in the rock. Whole rock analysis tests both primary and secondary inclusions and is thus only a qualitative estimate of the primary fluid.

The GEOCHEM software package by Geomicro Systems Services Ltd. facilitated statistical analysis of trace element data. Where analytic limits were surpassed, values were arbitrarily entered as one half the lower detection limit or twice the upper reporting limit.

Table 9 shows thresholds for correlation coefficients at the 95% and 99% confidence levels.

Table 9. Correlation coefficient thresholds at the 95% and 99% confidence levels (From Snedecor and Cochran, 1967). Degrees of freedom = N-2.

Degrees of Freedom	5%	1%	Degrees of Freedom	5%	1%
1	0.997	1.000	24	0.388	0.496
2	0.950	0.990	25	0.381	0.487
3	0.878	0.959	26	0.374	0.478
4	0.811	0.917	27	0.367	0.470
5	0.754	0.874	28	0.361	0.463
6	0.707	0.834	29	0.355	0.456
7	0.666	0.798	30	0.349	0.449
8	0.632	0.765	35	0.325	0.418
9	0.602	0.735	40	0.304	0.393
10	0.576	0.708	45	0.288	0.372
11	0.553	0.684	50	0.273	0.354
12	0.532	0.661	60	0.250	0.325
13	0.514	0.641	70	0.232	0.302
14	0.497	0.623	80	0.217	0.283
15	0.482	0.606	90	0.205	0.267
16	0.468	0.590	100	0.195	0.254
17	0.456	0.575	125	0.174	0.228
18	0.444	0.561	150	0.159	0.208
19	0.433	0.549	200	0.138	0.181
20	0.423	0.537	300	0.113	0.148
21	0.413	0.526	400	0.098	0.128
22	0.404	0.515	500	0.088	0.115
23	0.396	0.505	1000	0.062	0.081

## DRILL HOLE GEOCHEMISTRY

A total of 111 samples from six drill holes (Plate 3) were analyzed for a variety of trace elements including Ag, Au, Sb, As, Cu, Pb, Zn, Hg, Tl, and Ba. See Appendix IV for raw data.

## DISTRIBUTIONS IN DRILL HOLES

Summary statistics and correlation coefficients for the complete drill data set are presented in Tables 10 and 11. Figures 61 through 64 show drill hole histograms with summary drill logs.

All 28 thallium analyses are less than the 0.5 ppm detection limit. Sixteen of 28 mercury assays are greater than the 5 ppm upper reporting limit. Lovering and Heyl (1974) reported mercury values as high as 380 ppm from the district. Thallium and mercury results are accordingly omitted from the summary figures and tables.

Drill hole D-1 (Fig. 61) cut the heart of the ore body near its thickest section, along a low-angle fault. Mineralization is characterized by low Sb and very low As values.

Hole D-9 (Fig. 62) represents some of the better mineralization along the Southwest Pit fault. Higher Sb values may reflect contamination by stage II mineralization. The interval from 65 to 70 contains 10.24 oz Ag/ton with 2200 ppm Sb. Fragments of fine-grained reticulate-textured jasperoid (Fig. 32) contain apparent oxidized stibnite.

Hole D-10 (Fig. 63) is the best hole (in terms of length of intercept) ever drilled on the property. It was apparently drilled

Table 10: Drill data summary statistics.

	N	Mean	Median	St. dev.	Min.	Max	Range
Ag (oz/t)	111	4.59	2.1	5.819	0.04	33.06	33.02
Au (ppm)	0.086	0.154	0.095	0.168	0.005	0.980	0.975
Sb (ppm)	111	353	127	564	1.0	2900	2899
As (ppm)	111	122	18	382	4.0	2000	1996
Cu (ppm)	73	74	64	67	8.0	490	482
Pb (ppm)	73	292	148	433	11	3020	3009
Zn (ppm)	73	787	545	819	35	4560	4525
Ba (ppm)	28	207	200	59	160	500	340
Ag/Au	86	1405	945	1434	132	9447	9315
Ag/Sb	111	1.36	0.66	1.66	0.034	8.1	8.1
Ag/As	111	6.0	2.8	9.5	0.112	62.1	62
Ag/Cu	73	2.68	1.78	3.08	0.297	16.03	15.73
Ag/Pb	73	0.745	0.564	0.726	0.085	4.4	4.315
Ag/Zn	73	0.63	0.15	1.76	0.032	13.3	13.2
Ag/Ba	28	0.659	0.349	0.714	0.047	2.7	2.7
Sb/Au	86	3390	1093	4937	28.3	21,176	21,148
As/Au	86	640	269	1020	22	6250	6228
Cu/Au	73	740	600	684	29	5000	4971
Pb/Au	73	2329	1973	2635	83	20,600	20,517
Zn/Au	73	9548	4974	11,501	76	77,000	76,924
Ba/Au	28	2802	2000	2566	493	10,500	10,007
Sb/As	111	9.5	5.3	12.7	0.06	69.0	69.0
Sb/Cu	73	3.8	2.3	20.8	0.05	22.3	22.3
Sb/Pb	73	1.4	0.7	2.2	0.02	13.3	13.3
Sb/Ba	28	0.29	0.24	0.24	0.01	0.75	0.75
As/Pb	73	0.35	0.13	0.52	0.03	2.5	2.4
As/Ba	28	0.063	0.045	0.054	0.02	0.25	0.23
Pb/Ba	28	0.93	0.72	0.89	0.13	5.1	4.9
Pb/Cu	73	4.7	2.7	5.7	0.6	30.3	290,744
Sb/Zn	73	0.61	0.20	1.4	0.005	10.5	10.5

Table 11: Drill data correlation coefficients.

## (a) Raw data:

	Ag	Au	Sb	As	Cu	Pb	Zn	Ba
Ag	1.000 (111)	0.553 (86)	0.445 (111)	0.500 (111)	0.327 (73)	0.585 (73)	0.154 (73)	-0.296 (28)
Au		1.000 (86)	0.087 (86)	0.642 (86)	0.355 (73)	0.661 (73)	-0.012 (73)	-0.263 (28)
Sb			1.000 (111)	0.048 (111)	0.484 (73)	0.296 (73)	0.743 (73)	-0.192 (28)
As				1.000 (111)	0.055 (73)	0.666 (73)	-0.172 (73)	-0.095 (28)
Cu					1.000 (73)	0.660 (73)	0.527 (73)	-0.191 (28)
Pb						1.000 (73)	0.175 (73)	-0.272 (28)
Zn							1.000 (73)	-0.295 (28)

(b) Log<sub>10</sub> data:

	Ag	Au	Sb	As	Cu	Pb	Zn	Ba
Ag	1.000 (111)	0.761 (86)	0.663 (111)	0.540 (111)	0.699 (73)	0.806 (73)	0.348 (73)	-0.455 (28)
Au		1.000 (86)	0.423 (86)	0.560 (86)	0.557 (73)	0.655 (73)	0.156 (73)	-0.342 (28)
Sb			1.000 (111)	0.560 (111)	0.640 (73)	0.597 (73)	0.447 (73)	-0.396 (28)
As				1.000 (111)	0.185 (73)	0.666 (73)	-0.173 (73)	-0.075 (28)
Cu					1.000 (73)	0.618 (73)	0.623 (73)	-0.176 (28)
Pb						1.000 (73)	0.440 (73)	-0.432 (28)
Zn							1.000 (73)	-0.492 (28)

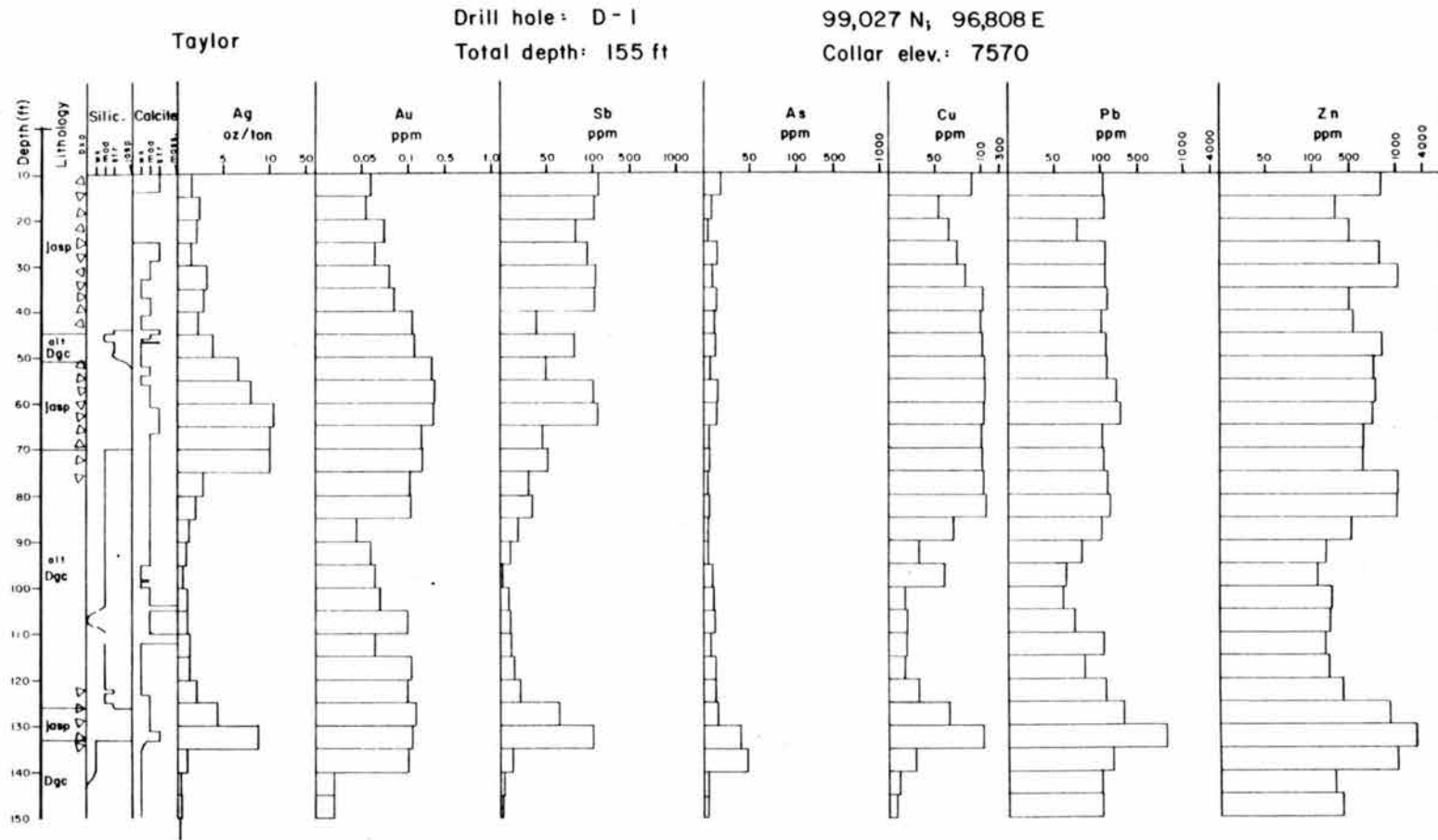


Fig. 61. Drill hole D-1 histogram.

Drill hole: D-9  
 Total depth: 143ft

98,218 N ; 96,288 E  
 Collar elev.: 7461

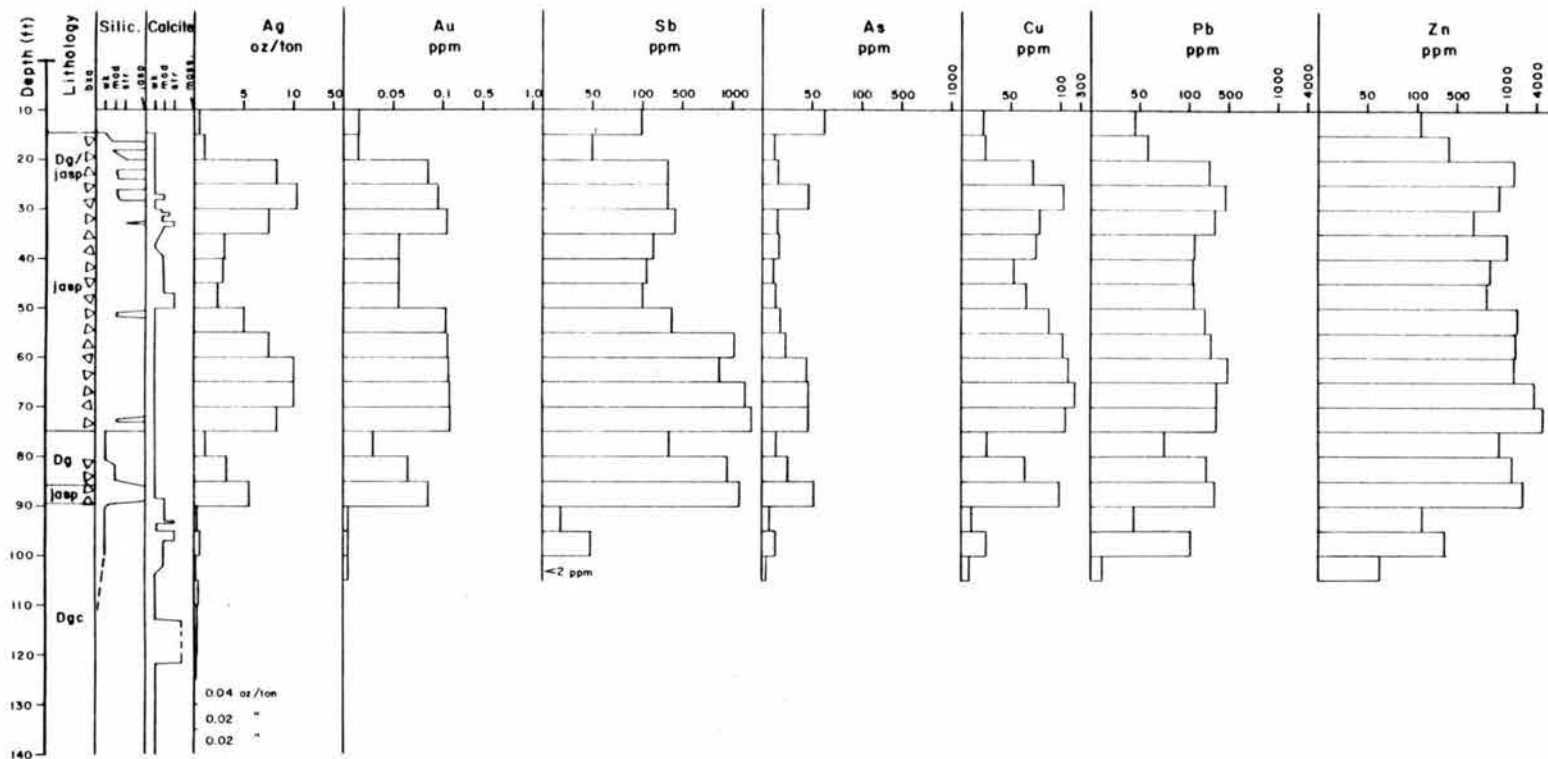


Fig. 62. Drill hole D-9 histogram.

Drill hole: D-10  
Total depth: 262 ft

99,656 N, 97,230 E  
Collar elev.: 7600

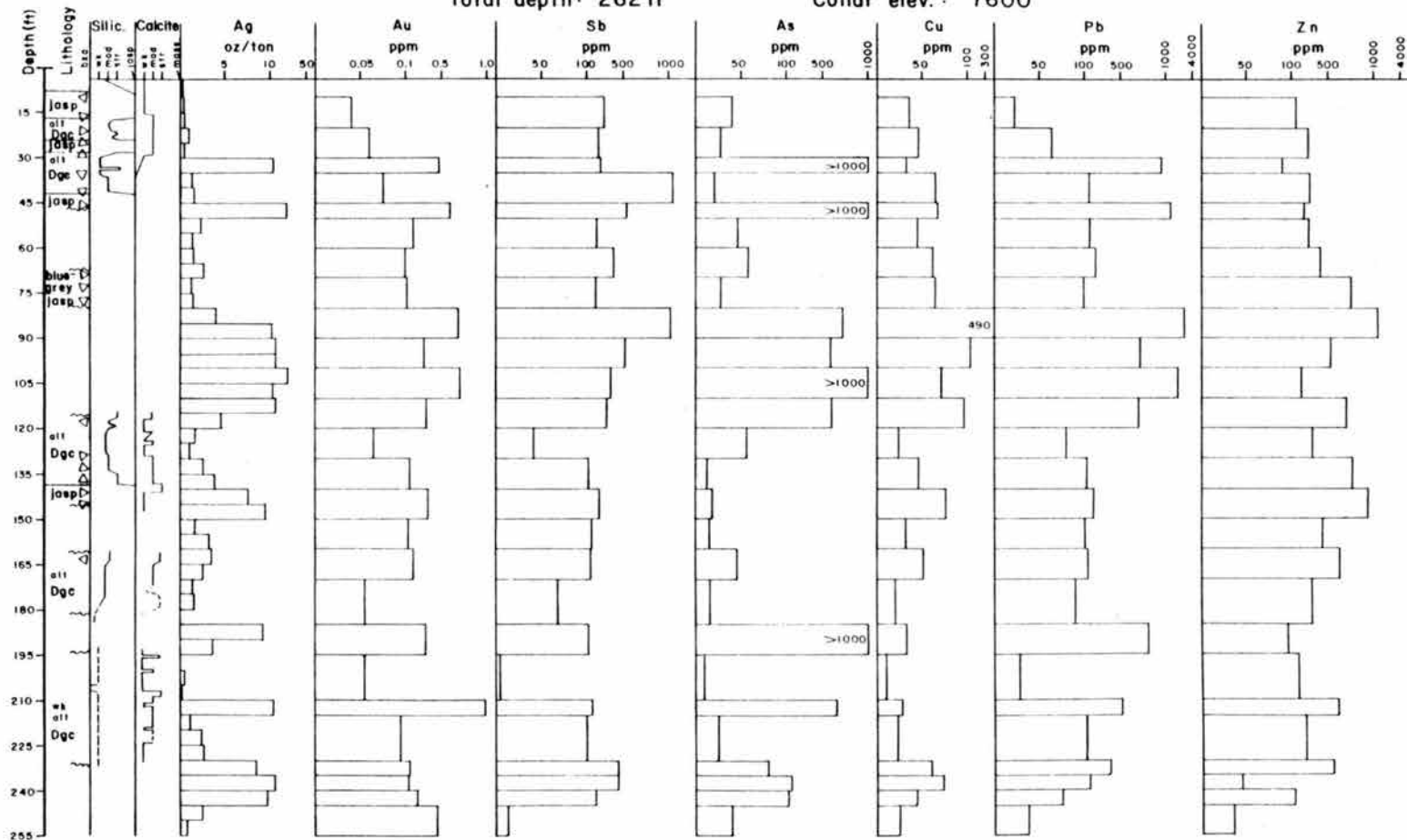


Fig. 63. Drill hole D-10 histogram.

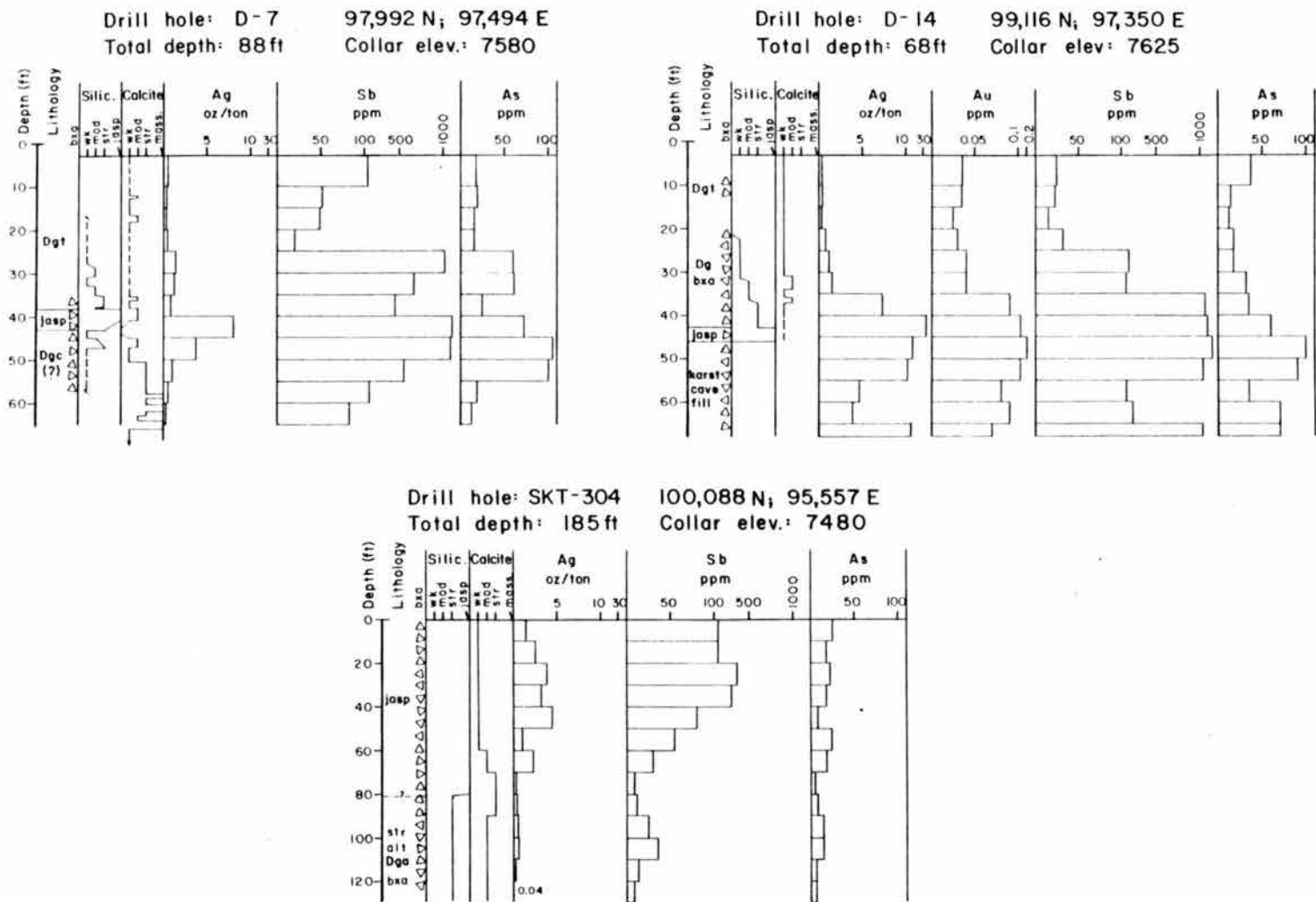


Fig. 64. Drill holes D-7, D-14, and SKT-304 histograms.

directly down the Argus fault. Offset holes indicate that this mineralized zone thins away from the fault. Hole D-10 contains by far the highest Au and As values encountered in all assayed drill samples. The same samples contain moderate levels of Sb, with high Ag and Pb. These intervals may contain both stage I and stage III components.

Holes D-7 and D-14 (Fig. 64) were both drilled near the Argus fault south of D-10. Hole D-14 cut recent karst cave fill containing up to 15 oz Ag/ton. Rotary hole SKT- 304 (Fig. 64) tested the northwest lobe of the ore body, hosted by Guilmette member a limestone breccias.

#### RELATIONSHIP TO SILVER GRADE

Drill data were broken into three classes, based on Ag content. Classes include low-grade, with Ag less than 2 oz/ton, medium-grade, with Ag from 2 to 4.99 oz/ton, and high-grade, containing 5 or more oz Ag/ton. Tables 12 through 16 contain basic statistics for the three populations.

Table 15 compares correlation coefficients in the three groups. Correlations of Ag: Au, Ag: Sb, Ag: Cu, Au: Sb, As: Zn, As: Ba, and Pb: Zn fall off steadily from low-grade to high-grade, while those of Au: Pb, Sb: Zn, and As: Pb rise. Ag correlates poorly with other elements in high-grade rock, probably reflecting irregularly distributed coarse-grained mineralogy and nugget effects, which are insignificant at lower grades. A strong correlation between Au and As in high-grade rock is apparent in drill hole D-10 (Fig. 63), in which higher Au-As values may represent stage I mineralization hosted along the Argus fault.

Table 12: Low grade drill data summary statistics  
(Ag less than 2 oz/t).

	N	Mean	Median	St. dev.	Min.	Max.	Range
Ag (oz/t)	51	0.82	0.81	0.48	0.04	1.8	1.76
Au (ppm)	33	0.068	0.055	0.079	0.005	0.46	0.46
Sb (ppm)	51	147	41	276	1.0	1450	1449
As (ppm)	51	22	15	19	4.0	103	99
Cu (ppm)	27	34	25	23	8	90	82
Pb (ppm)	27	90	80	49	11	238	227
Zn (ppm)	27	384	302	270	35	1110	1075
Ba (ppm)	12	229	200	82	190	500	310
Ag/Au	33	801	617	725	132	3909	3777
Ag/Sb	51	1.33	0.49	1.81	0.034	7.8	7.74
Ag/As	51	1.81	1.49	1.5	0.196	7.1	6.9
Ag/Cu	27	1.21	1.01	0.64	0.3	2.55	2.26
Ag/Pb	27	0.428	0.383	0.266	0.113	1.597	1.48
Ag/Zn	27	0.157	0.08	0.313	0.032	1.73	1.70
Ag/Ba	12	0.171	0.178	0.072	0.047	0.258	0.211
Sb/Au	33	2557	686	4117	28	19,333	19,305
As/Au	33	597	309	788	83	4067	3983
Cu/Au	27	904	582	974	54	5000	4946
Pb/Au	27	2848	1846	3968	83	20,600	20,517
Zn/Au	27	12,135	5727	15,391	76	77,000	76,924
Ba/Au	12	4526	3231	2974	1615	10,500	8885
Sb/As	51	5.73	2.38	10.5	0.25	69.0	68.8
Sb/Cu	27	3.0	1.25	4.9	0.049	22.3	22.3
Sb/Pb	27	1.6	0.43	3.1	0.017	13.3	13.3
Sb/Ba	12	0.14	0.055	0.22	0.006	0.75	0.75
As/Pb	27	0.33	0.18	0.41	0.042	1.82	1.78
As/Ba	12	0.061	0.042	0.057	0.02	0.24	0.22
Pb/Ba	12	0.53	0.55	0.25	0.13	1.19	1.06
Pb/Cu	27	3.6	2.8	3.0	0.6	14.8	14.2
Sb/Zn	27	0.42	0.12	0.95	0.005	4.8	4.8

Table 13: Medium-grade drill data summary statistics  
(Ag ranges from 2.0 to 4.99 oz/t).

	N	Mean	Median	St. dev.	Min.	Max	Range
Ag (oz/t)	28	3.05	2.96	0.86	2.04	4.96	2.92
Au (ppm)	22	0.106	0.095	0.041	0.055	0.190	0.135
Sb (ppm)	28	233	117	368	21	1900	1879
As (ppm)	28	24	15	28	5	150	145
Cu (ppm)	20	74	65	34	22	158	136
Pb (ppm)	20	169	140	67	76	358	282
Zn (ppm)	20	840	775	460	244	2010	1766
Ba (ppm)	10	197	200	17	160	230	70
Ag/Au	22	1101	836	467	530	2010	1481
Ag/Sb	28	1.11	0.70	0.88	0.068	3.4	3.3
Ag/As	28	7.3	6.1	4.5	0.86	19.3	18.5
Ag/Cu	20	1.6	1.4	0.7	0.44	3.2	2.7
Ag/Pb	20	0.62	0.61	0.17	0.33	0.95	0.62
Ag/Zn	20	0.14	0.14	0.06	0.06	0.29	0.23
Ag/Ba	10	0.49	0.48	0.15	0.34	0.78	0.44
Sb/Au	22	2096	1185	2958	210	14,692	14,482
As/Au	22	218	144	183	42	778	736
Cu/Au	20	778	712	382	230	1412	1182
Pb/Au	20	1781	1688	850	721	4323	3602
Zn/Au	20	9179	5882	6465	2568	26,923	24,355
Ba/Au	10	2027	1667	918	1000	4182	3182
Sb/As	28	9.5	7.8	6.9	1.62	35.4	33.8
Sb/Cu	20	2.85	1.57	3.26	0.22	14.9	14.7
Sb/Pb	20	0.97	0.82	0.74	0.13	3.4	3.3
Sb/Ba	10	0.36	0.34	0.18	0.11	0.64	0.53
As/Pb	20	0.11	0.08	0.08	0.03	0.34	0.31
As/Ba	10	0.053	0.045	0.02	0.03	0.09	0.07
Pb/Ba	10	0.89	0.82	0.38	0.36	1.88	0.152
Pb/Cu	20	2.71	2.54	1.35	1.08	5.42	4.34
Sb/Zn	20	0.225	0.164	0.213	0.025	0.952	0.927

Table 14: High-grade drill data summary statistics  
(Ag greater than 5 oz/t).

	N	Mean	Median	St. dev.	Min.	Max	Range
Ag (oz/t)	32	11.95	10.05	6.13	5.49	33.06	27.57
Au (ppm)	31	0.28	0.20	0.21	0.07	0.98	0.91
Sb (ppm)	32	786	407	772	46	2900	2854
As (ppm)	32	367	51	648	6.0	2000	1994
Cu (ppm)	26	116	98	89	28	490	462
Pb (ppm)	26	596	380	612	77	3020	2943
Zn (ppm)	26	1165	695	1153	43	4560	4517
Ba (ppm)	6	178	180	13	160	190	30
Ag/Au	31	2263	1835	1950	376	9447	9071
Ag/Sb	32	1.62	1.08	1.88	0.097	8.095	7.998
Ag/As	32	11.57	6.38	15.12	0.112	62.07	61.95
Ag/Cu	26	5.03	3.39	4.15	0.52	16.03	15.5
Ag/Pb	26	1.17	0.8	1.04	0.085	4.4	4.3
Ag/Zn	26	1.5	0.42	2.73	0.06	13.27	13.21
Ag/Ba	6	1.91	1.82	0.49	1.28	2.71	1.43
Sb/Au	31	5195	1705	6179	132	21,176	21,045
As/Au	31	984	500	1398	22	6250	6228
Cu/Au	26	540	429	383	29	1389	1360
Pb/Au	26	2210	2111	1438	350	5226	4876
Zn/Au	26	7145	2151	8970	191	31,059	30,867
Ba/Au	6	644	500	194	493	1032	539
Sb/As	32	15.5	7.7	16.9	0.058	61.7	61.6
Sb/Cu	26	5.4	4.6	4.7	0.37	18.4	18.0
Sb/Pb	26	1.53	0.45	1.92	0.13	7.6	7.5
Sb/Ba	6	0.45	0.29	0.19	0.27	0.74	0.47
As/Pb	26	0.55	0.12	0.70	0.04	2.5	2.4
As/Ba	6	0.085	0.044	0.076	0.032	0.25	0.22
Pb/Ba	6	1.78	0.97	1.51	0.72	5.06	4.34
Pb/Cu	26	7.34	3.84	8.33	1.12	30.31	29.20
Sb/Zn	26	1.11	0.59	2.01	0.032	10.5	10.5

Table 15: Drill hole correlation coefficients by silver grade.

	Low	Medium	High
Ag: Au	0.540 (33)	0.245 (22)	0.194 (31)
Ag: Sb	0.345 (51)	0.239 (28)	0.073 (32)
Ag: As	0.352 (51)	0.216 (28)	0.330 (32)
Ag: Cu	0.526 (27)	0.166 (20)	-0.216 (26)
Ag: Pb	0.490 (27)	0.610 (20)	0.304 (26)
Ag: Zn	0.364 (27)	0.659 (20)	-0.386 (26)
Ag: Ba	-0.268 (12)	-0.206 (10)	0.168 (6)
Sb: Au	0.015 (33)	-0.251 (22)	-0.334 (31)
As: Au	0.354 (33)	0.055 (22)	0.599 (31)
Cu: Au	0.081 (27)	0.125 (20)	0.092 (26)
Pb: Au	0.019 (27)	0.271 (20)	0.551 (26)
Zn: Au	-0.148 (27)	-0.006 (20)	-0.365 (26)
Ba: Au	-0.019 (12)	-0.644 (10)	0.734 (6)
Sb: As	0.448 (51)	0.832 (28)	-0.249 (32)
Sb: Cu	0.377 (27)	-0.141 (20)	0.413 (26)
Sb: Zn	0.067 (27)	0.521 (20)	0.807 (26)
Sb: Pb	0.213 (27)	0.446 (20)	0.092 (26)
Sb: Ba	-0.110 (12)	0.351 (10)	0.278 (6)
As: Cu	0.075 (27)	-0.340 (20)	-0.198 (26)
As: Pb	0.142 (27)	0.201 (20)	0.579 (26)
As: Zn	0.028 (27)	-0.139 (20)	-0.420 (26)
As: Ba	-0.073 (12)	-0.380 (10)	-0.455 (6)
Cu: Pb	0.403 (27)	0.239 (20)	0.590 (26)
Cu: Zn	0.441 (27)	0.410 (20)	0.403 (26)
Pb: Zn	0.685 (27)	0.591 (20)	-0.063 (26)
Pb: Ba	-0.317 (12)	-0.096 (10)	-0.435 (6)
Zn: Ba			-0.588 (6)

Table 16: Average metal and metal ratios in drill holes by silver grade.

	low grade	medium grade	high grade
Ag (oz/t)	0.82 (51)	3.05 (28)	11.9 (32)
Au (ppm)	0.068 (33)	0.106 (22)	0.28 (31)
Sb (ppm)	147 (51)	233 (28)	786 (32)
As (ppm)	22 (51)	24 (28)	367 (32)
Cu (ppm)	34 (27)	74 (20)	116 (26)
Pb (ppm)	90 (27)	169 (20)	596 (26)
Zn (ppm)	384 (27)	840 (20)	1165 (26)
Ba (ppm)	229 (12)	197 (10)	178 (6)
Ag/Au	801 (33)	1101 (22)	2263 (31)
Ag/Sb	1.33 (51)	1.11 (28)	1.6 (32)
Ag/As	1.8 (51)	7.3 (28)	11.6 (32)
Ag/Cu	1.2 (27)	1.6 (20)	5.0 (26)
Ag/Pb	0.43 (27)	0.62 (20)	1.17 (26)
Ag/Zn	0.16 (27)	0.14 (20)	1.5 (26)
Ag/Ba	0.17 (12)	0.49 (10)	1.9 (6)
Sb/Au	2557 (33)	2095 (22)	5195 (31)
As/Au	597 (33)	218 (22)	984 (31)
Cu/Au	904 (27)	778 (20)	540 (26)
Pb/Au	2848 (27)	1781 (20)	2210 (26)
Zn/Au	12,135 (27)	9180 (20)	7145 (26)
Ba/Au	4526 (12)	2027 (10)	644 (6)
Sb/As	5.7 (51)	9.5 (28)	15.5 (32)
Sb/Cu	3.0 (27)	2.9 (20)	5.4 (26)
Sb/Pb	1.6 (27)	0.97 (20)	1.53 (26)
Sb/Ba	0.14 (12)	0.36 (10)	0.45 (6)
As/Pb	0.33 (27)	0.11 (20)	0.55 (26)
As/Ba	0.06 (12)	0.05 (10)	0.085 (6)
Pb/Ba	0.53 (12)	0.89 (10)	1.78 (6)
Pb/Cu	3.6 (27)	2.7 (20)	7.3 (26)
Sb/Zn	0.42 (27)	0.23 (20)	1.11 (26)

Table 16 compares means of elements and metal ratios. Ag/Au, Ag/As, Ag/Cu, Ag/Pb, Ag/Ba, Sb/As, Sb/Ba, and Pb/Ba ratios rise steadily from low-grade to high-grade rock, while Ag/Sb, Cu/Au, Zn/Au, and Ba/Au ratios fall. The Ag/Au trend predicts that higher-grade silver deposits should contain proportionately less Au.

#### MINOR TRACE ELEMENTS

Table 17 gives trace element contents of five selected drill samples. Samples from hole D-1 approximate the bulk of the ore body. Sample D-9: 60-65 contains visible fluorite (reflecting significant input of late stage III fluids). Sample D-9: 70-75 contains the highest Sb level of all drill samples (probably reflecting contamination by stage II jasperoid). Sample D-10: 210-215 contains the highest Au of all drill samples (probably reflecting contamination by stage I jasperoid).

Sample D-9: 60-65, with visible fluorite, contains the highest Cu, Mo, Ni, and Fe levels, but the lowest Au levels in the five samples tested. On the other hand, the Au-rich sample, D-10: 210-215, contains the highest As, Mn, Bi, Te, Sr, and Rb levels, but the lowest Cu, Zn, Ni, Cr, and F levels. This contrast probably reflects the shift from low-temperature stage I mineralization to the higher-temperature stage III to stage IV main ore stage. The gold-rich stage contains a typical "epithermal" suite while the fluorine-rich stage is enriched in a chalcophile or "mesothermal" suite.

Table 17. Minor trace elements in drill holes.  
(Data furnished by Magmachem Inc.)

Element	D-1 50-55	D-1 125-130	D-9 60-65	D-9 70-75	D-10 210-215
Ag (oz/t)	6.72	4.34	10.05	8.24	11.34
Au (ppm)	0.365	0.190	0.155	0.180	0.980
Sb (ppm)	48	65	870	2900	174
As (ppm)	8	17	44	47	650
Cu (ppm)	131	66	183	158	28
Pb (ppm)	174	358	490	380	515
Zn (ppm)	785	945	1720	4560	605
Hg (ppm)	> 5	> 5	> 5	> 5	> 5
Tl (ppm)	< 0.5	< 0.5	0.5	1.0	0.5
Ba (ppm)	200	190	50	130	50
Mo (ppm)	1	< 1	8	6	6
Ni (ppm)	9	11	20	17	7
Co (ppm)	1	2	2	2	1
Mn (ppm)	84	1300	295	209	1588
Fe (%)	0.20	0.30	1.15	0.95	0.60
Cr (ppm)	110	81	85	42	16
Bi (ppm)	< 1	< 1	< 1	< 1	2600
V (ppm)	26	30	10	9	14
Te (ppm)	2.4	0.2	1.8	2.2	2.6
Li (ppm)	3	5	4	5	3
Be (ppm)	0.5	0.5	0.5	0.5	0.5
U (ppm)	2.0	7.0	2.0	2.0	1.0
W (ppm)	5	5	5	4	4
F (ppm)	215	395	> 20,000	2770	120
Sn (ppm)	< 5	< 5	< 5	< 5	< 5
Sr (ppm)	76	170	71	51	240
Nb (ppm)	5	< 5	< 5	< 5	< 5
Rb (ppm)	< 5	8	< 5	< 5	76
Y (ppm)	< 5	< 5	< 5	< 5	< 5
Ta (ppm)	9	< 3	12	< 3	< 3

## VERTICAL ZONATION

In an effort to document vertical metal zonation, linear regression analysis was used to correlate metal ratios with drill hole elevations. No statistically significant trends occur over the vertical interval tested (375 feet). It is noteworthy, however, that high-grade ores mined in 1966 through the Taylor shaft (-350 foot level, below the zone of silicification) averaged 58 oz Ag/ton, and 4.2% combined Pb, Cu, and Zn (Wise and Banghart, 1970), while higher-grade siliceous ores (Table 14) average 12 oz Ag/ton with only 2000 ppm combined base metals. Thus, where Ag increase by a factor of 5 at depth, base metals increase by a factor of 21.

## SURFACE ROCK CHIP GEOCHEMISTRY

Summary statistics and correlation coefficients for the complete data set are presented in Tables 18 and 19. Figures 65 through 71 illustrate the distribution of Ag, Au, Sb, As, Cu, Pb, and Zn in silicified surface rocks. See Appendix V for raw data.

Figures 72 and 73 show metal distributions along two Brunton and chain traverses across the Taylor deposit. Samples were collected on 50 foot centers as closely as possible. The south traverse (Fig. 72) crosses both the Argus and Southwest Pit faults although dissemination of metals into wall rock is minimal. The north traverse (Fig. 73) crosses the principal bulk-tonnage silver deposit, over what is now the Bishop Pit.

Table 18: Surface data summary statistics.

	N	Mean	Median	St. dev.	Min.	Max	Range
Ag (oz/t)	188	0.967	0.100	2.54	0.005	17.35	17.35
Au (ppm)	150	0.089	0.020	0.186	0.002	1.03	1.03
Sb* (ppm)	155	1439	49	4666	1.0	20,000	19,999
As (ppm)	155	77.5	35	196	1.0	2000	1999
Cu (ppm)	103	138	41	474	2.0	3900	3898
Pb (ppm)	103	189	21	693	4.0	6500	6496
Zn (ppm)	103	362	76	976	4.0	7750	7746
Ba (ppm)	39	931	310	1955	200	11,000	10,800
Ag/Au	149	875	343	1475	0.61	11,899	11,898
Ag/Sb	154	0.88	0.14	2.53	0.0	23.77	23.77
Ag/As	154	1.11	0.11	2.82	0.002	28.12	28.12
Ag/Cu	102	0.42	0.13	0.69	0.002	4.14	4.13
Ag/Pb	102	0.32	0.19	0.33	0.004	1.92	1.92
Ag/Zn	102	0.18	0.08	0.34	0.001	2.85	2.85
Ag/Ba	39	0.295	0.07	0.53	0.0	2.83	2.83
Sb/Au	150	11,116	2200	23,887	50	142,860	142,810
As/Au	149	4048	1400	6420	35	36,000	35,965
Cu/Au	98	4844	1400	13,890	9.7	106,000	106,990
Pb/Au	98	4538	2400	7129	8.0	44,828	44,820
Zn/Au	98	9913	3800	17,539	7.0	138,800	138,793
Ba/Au	34	21,372	4667	36,700	301	158,000	158,699
Sb/As	155	23	2.3	68	0.013	444	444
Sb/Cu	103	166	1.03	572	0.04	4000	4000
Sb/Pb	103	52	1.3	174	0.04	1333	1333
Sb/Ba	39	3.36	0.65	8.2	0.0	39.2	39.2
As/Pb	103	3.5	1.2	9.9	0.014	95.2	95.2
As/Ba	39	0.22	0.13	0.33	0.007	1.91	1.90
Pb/Ba	39	1.01	0.375	1.91	0.002	9.26	9.26
Pb/Cu	103	1.8	1.2	3.2	0.05	31.6	31.5
Sb/Zn	103	24.3	0.69	87.2	0.005	667	667

\* Sb actually reached levels of over 6% in some samples.

Table 19: Surface rock chip correlation coefficients.

(a) Raw data:

	Ag	Au	Sb	As	Cu	Pb	Zn	Ba
Ag	1.000 (188)	0.028 (149)	-0.029 (154)	0.070 (154)	0.784 (102)	0.867 (102)	0.727 (102)	-0.182 (39)
Au		1.000 (150)	0.459 (150)	0.073 (150)	-0.045 (98)	-0.017 (98)	-0.015 (98)	0.265 (39)
Sb			1.000 (155)	0.024 (155)	-0.015 (103)	0.252 (103)	0.219 (103)	0.442 (39)
As				1.000 (155)	0.116 (103)	0.028 (103)	0.042 (103)	0.101 (39)
Cu					1.000 (103)	0.337 (103)	0.535 (103)	-0.118 (39)
Pb						1.000 (103)	0.934 (103)	-0.176 (39)
Zn							1.000 (103)	-0.110 (39)

(b) Log<sub>10</sub> data:

	Ag	Au	Sb	As	Cu	Pb	Zn	Ba
Ag	1.000 (188)	0.343 (149)	0.283 (154)	0.128 (154)	0.637 (102)	0.769 (102)	0.680 (102)	-0.478 (39)
Au		1.000 (150)	0.718 (150)	0.373 (150)	0.350 (98)	0.141 (98)	0.335 (98)	-0.201 (39)
Sb			1.000 (155)	0.407 (155)	0.431 (103)	0.217 (103)	0.442 (103)	-0.119 (39)
As				1.000 (155)	0.324 (103)	0.173 (103)	0.332 (103)	0.342 (39)
Cu					1.000 (103)	0.659 (103)	0.688 (103)	-0.334 (39)
Pb						1.000 (103)	0.763 (103)	-0.551 (39)
Zn							1.000 (103)	-0.278 (39)

Fig. 65. Silver distribution in silicified surface rocks.

EXPLANATION



> 3.00 oz Ag/ton  
1.0 to 2.99 oz Ag/ton  
0.5 to 0.99 oz Ag/ton  
< 0.5 oz Ag/ton

	cover
J	Jasperoid
Mc	Chainman Shale
Mj	Joanna Limestone
MDp	Pilot Shale
Dgt	Guilmette transition beds
Dgc	Guilmette member c
Dgb	Guilmette member b
Dga	Guilmette member a
Ds	Simonson Dolomite

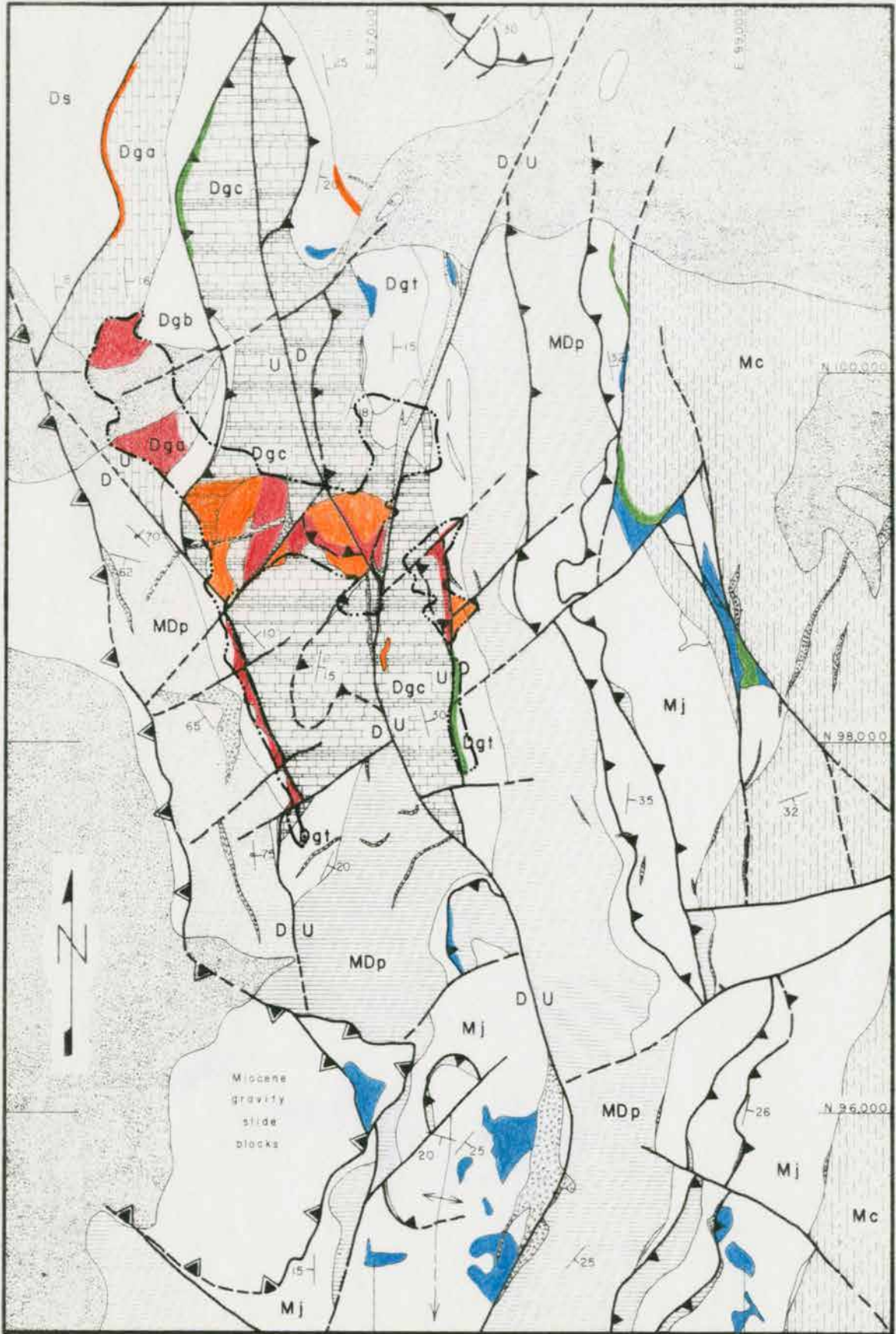


Fig. 66. Gold distribution in silicified surface rocks.

<u>EXPLANATION</u>	
	> 500 ppb Au
	250 to 499 ppb Au
	50 to 249 ppb Au
	< 50 ppb Au
	cover
J	Jasperoid
Mc	Chainman Shale
Mj	Joanna Limestone
MDp	Pilot Shale
Dgt	Guilmette transition beds
Dgc	Guilmette member c
Dgb	Guilmette member b
Dga	Guilmette member a
Ds	Simonson Dolomite

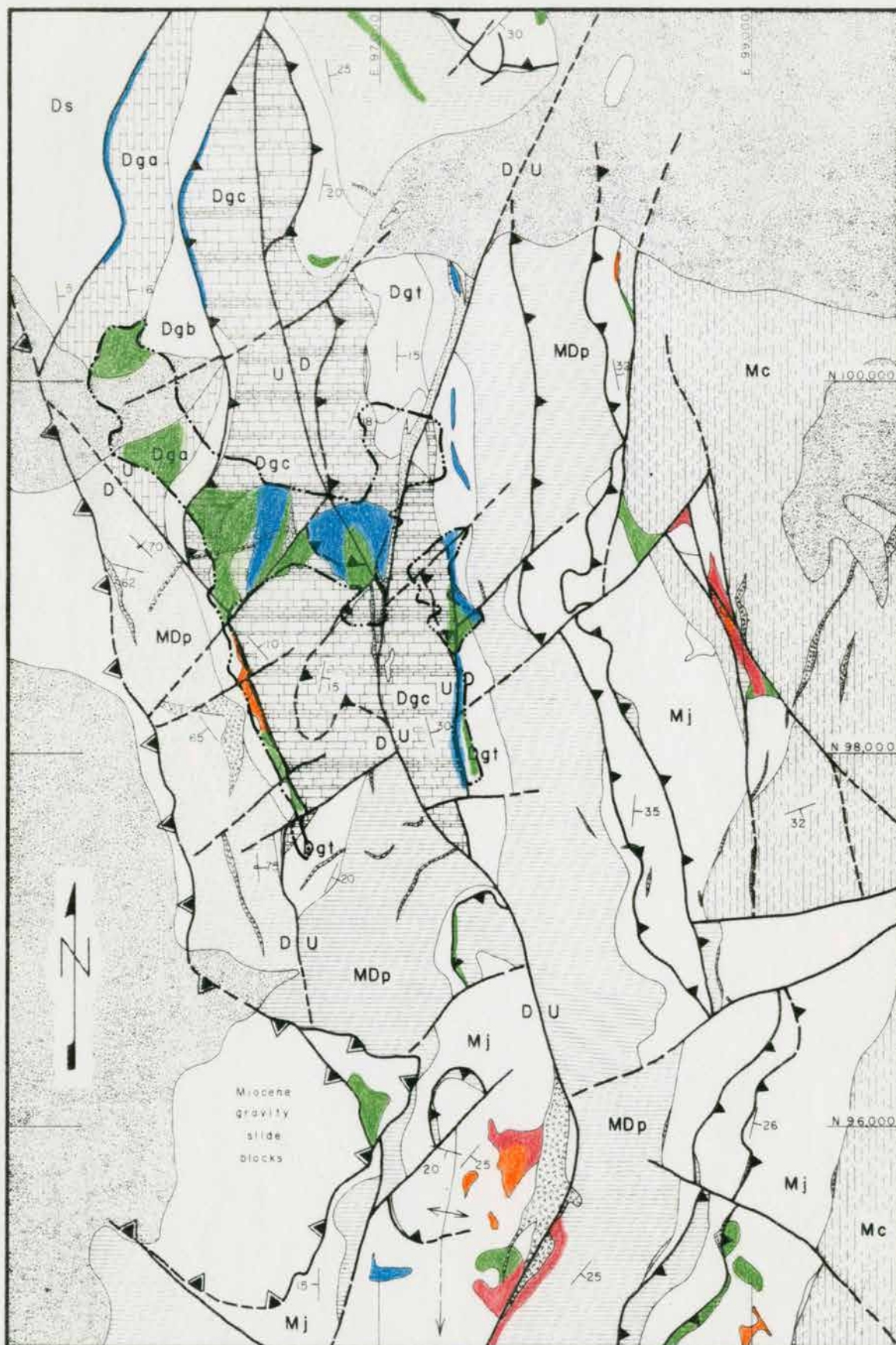


Fig. 67. Antimony distribution in silicified surface rocks.

<u>EXPLANATION</u>	
	<p>&gt; 1% Sb</p> <p>1000 to 10,000 ppm Sb</p> <p>100 to 1000 ppm Sb</p> <p>&lt; 100 ppm Sb</p>
<p>J</p> <p>Mc</p> <p>Mj</p> <p>MDp</p> <p>Dgt</p> <p>Dgc</p> <p>Dgb</p> <p>Dga</p> <p>Ds</p>	<p>cover</p> <p>Jasperoid</p> <p>Chainman Shale</p> <p>Joanna Limestone</p> <p>Pilot Shale</p> <p>Guilmette transition beds</p> <p>Guilmette member c</p> <p>Guilmette member b</p> <p>Guilmette member a</p> <p>Simonson Dolomite</p>

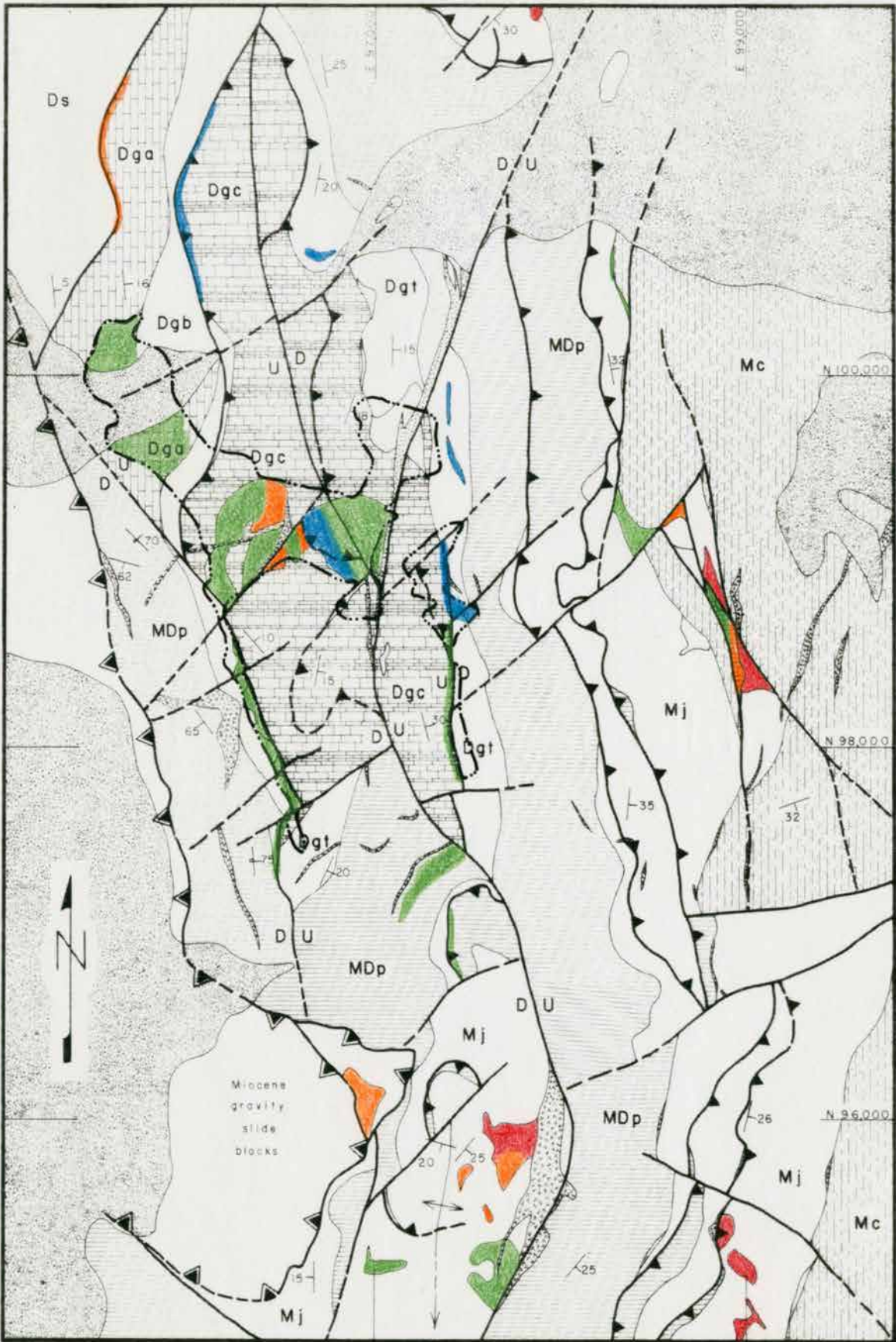


Fig. 68. Arsenic distribution in silicified surface rocks.



EXPLANATION

> 200 ppm As  
100 to 199 ppm As  
50 to 100 ppm As  
< 50 ppm As

	cover
J	Jasperoid
Mc	Chainman Shale
Mj	Joanna Limestone
MDp	Pilot Shale
Dgt	Guilmette transition beds
Dgc	Guilmette member c
Dgb	Guilmette member b
Dga	Guilmette member a
Ds	Simonson Dolomite

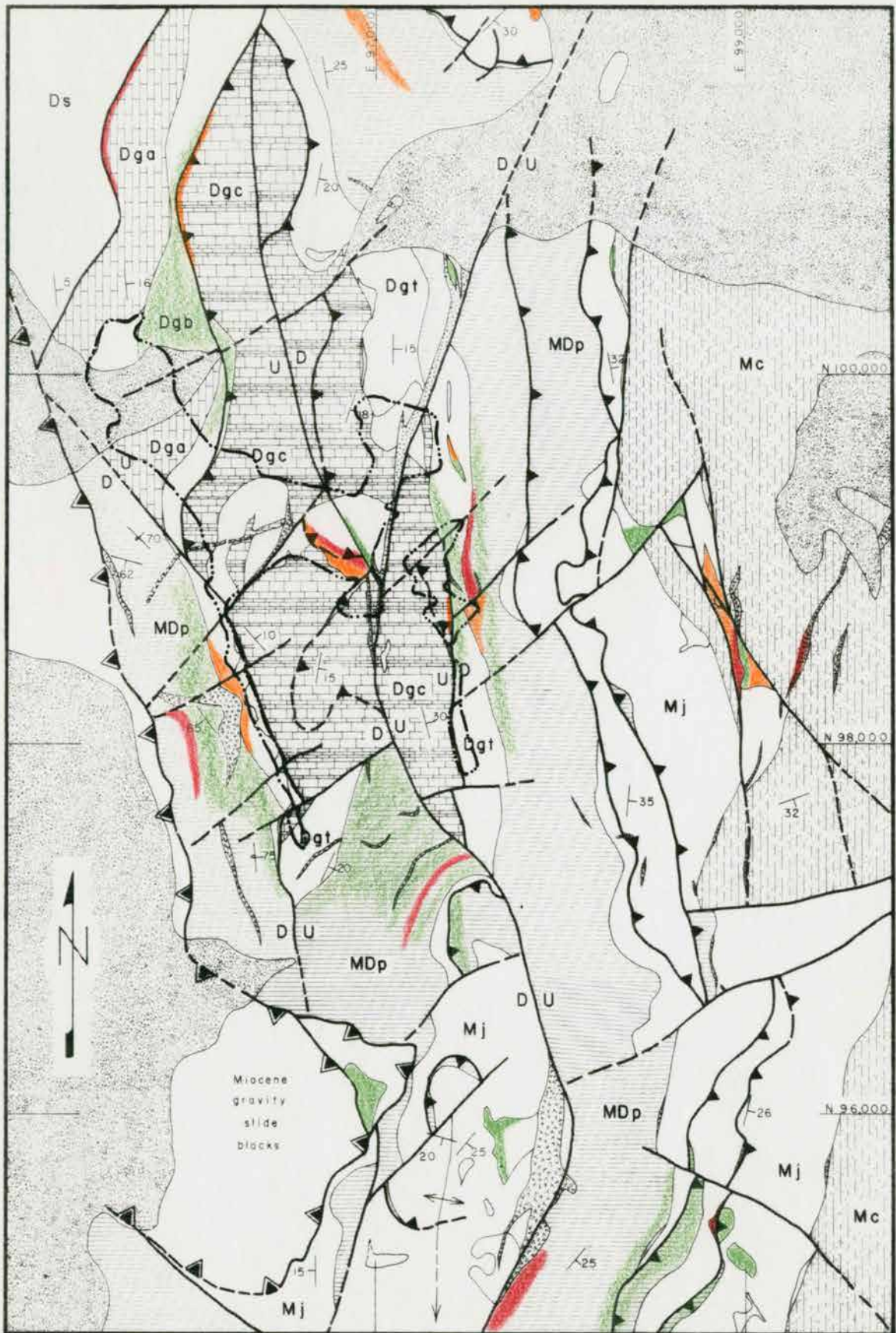


Fig. 69. Copper distribution in silicified surface rocks.

<u>EXPLANATION</u>	
	> 150 ppm Cu
	100 to 149 ppm Cu
	50 to 100 ppm Cu
	< 50 ppm Cu
J	cover
Mc	Jasperoid
Mj	Chainman Shale
MDp	Joanna Limestone
Dgt	Pilot Shale
Dgc	Guilmette transition beds
Dgb	Guilmette member c
Dga	Guilmette member b
Ds	Guilmette member a
	Simonson Dolomite

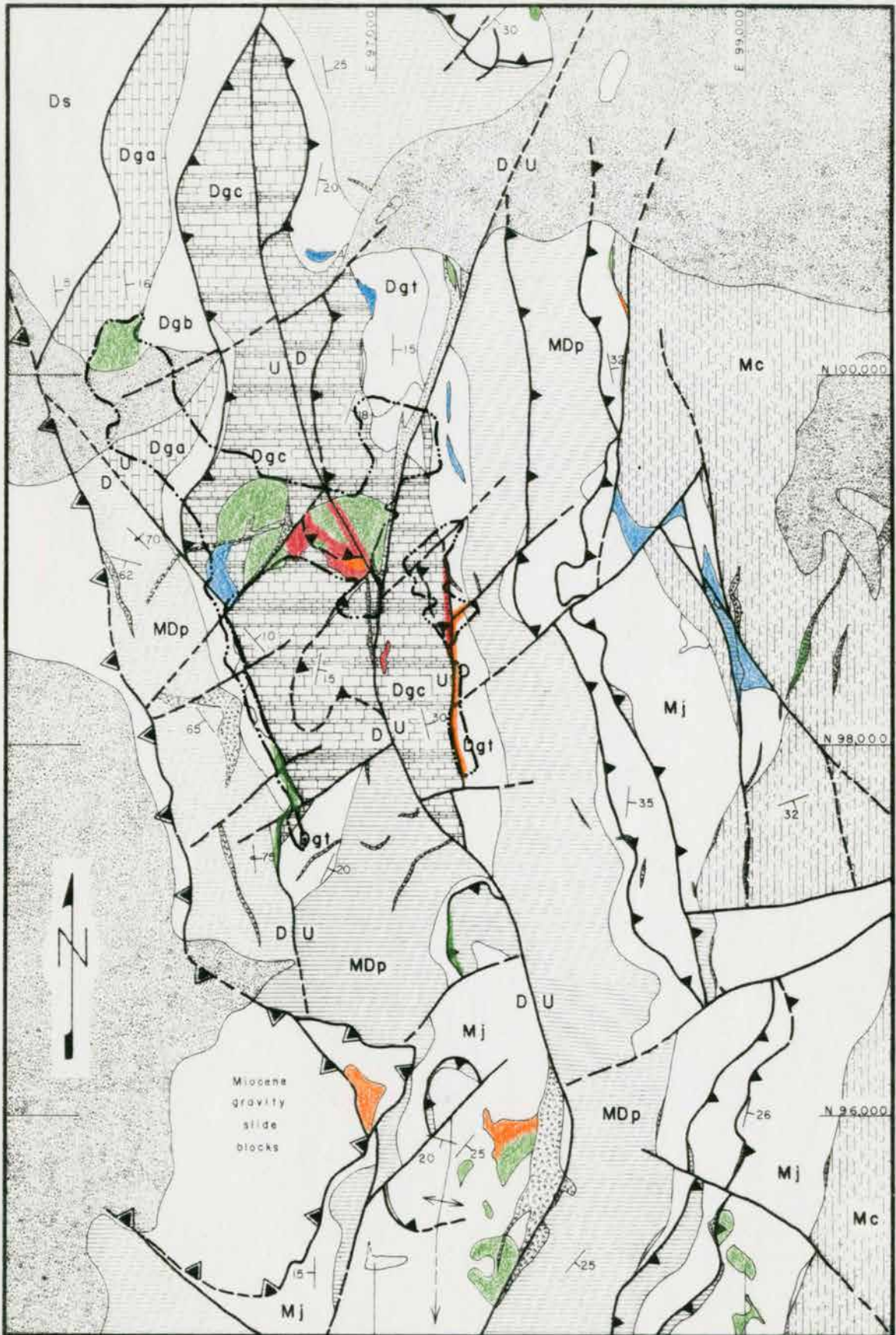


Fig. 70. Lead distribution in silicified surface rocks.

<u>EXPLANATION</u>	
	> 300 ppm Pb
	150 to 299 ppm Pb
	50 to 149 ppm Pb
	< 50 ppm Pb
	cover
J	Jasperoid
Mc	Chainman Shale
Mj	Joanna Limestone
MDp	Pilot Shale
Dgt	Guilmette transition beds
Dgc	Guilmette member c
Dgb	Guilmette member b
Dga	Guilmette member a
Ds	Simonson Dolomite

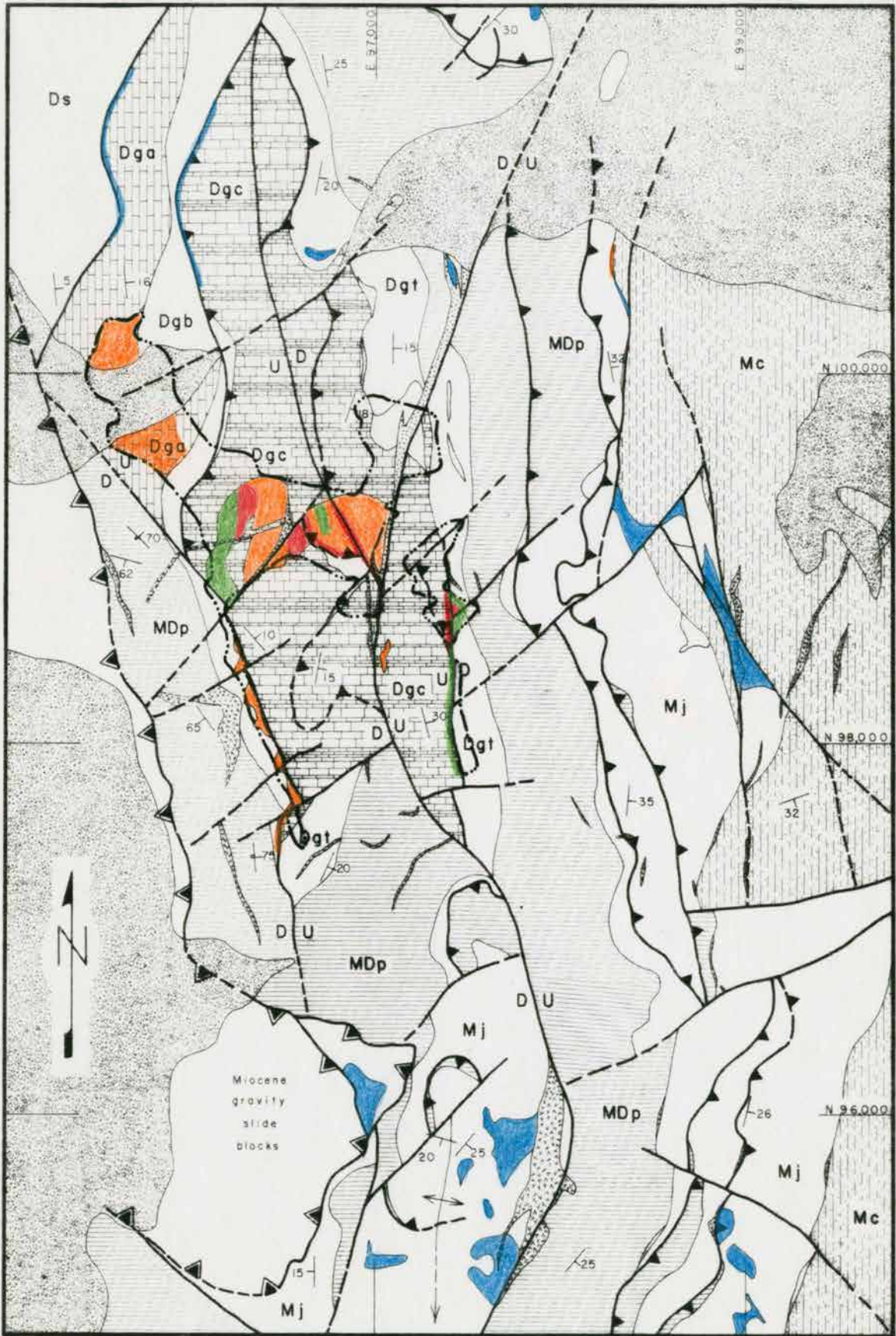
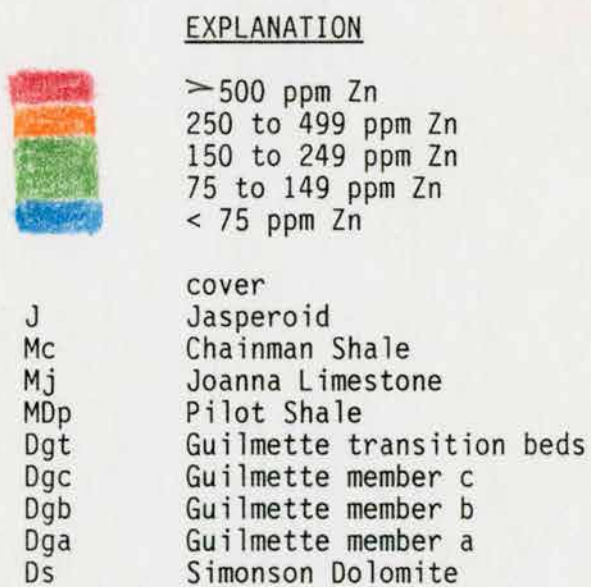


Fig. 71. Zinc distribution in silicified surface rocks.



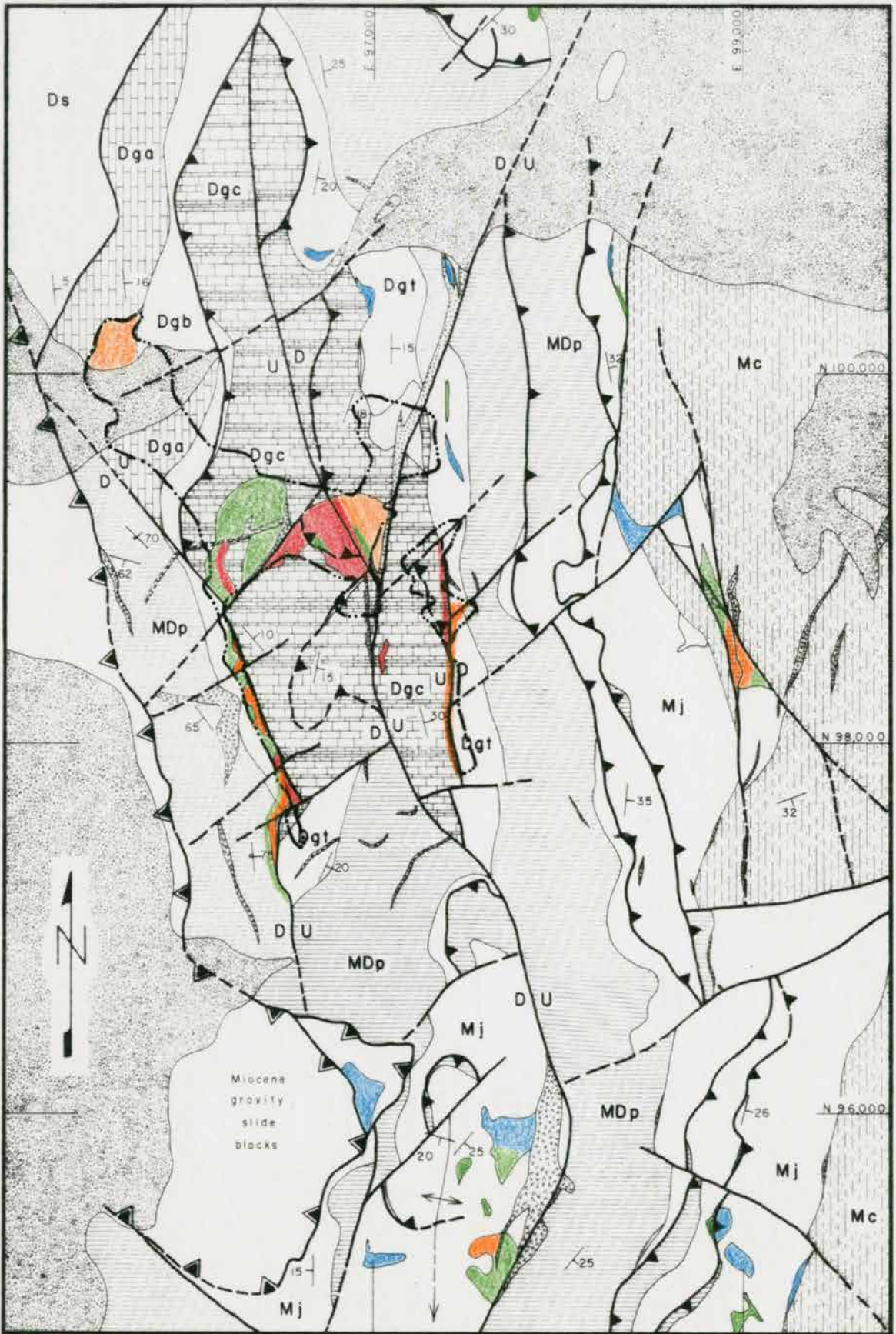


Fig. 72. South rock chip traverse.

EXPLANATION

	cover
J	Jasperoid
Mc	Chainman Shale
Mj	Joanna Limestone
MDp	Pilot Shale
Dgt	Guilmette transition beds
Dgc	Guilmette member c
Dgb	Guilmette member b
Dga	Guilmette member a
Ds	Simonson Dolomite

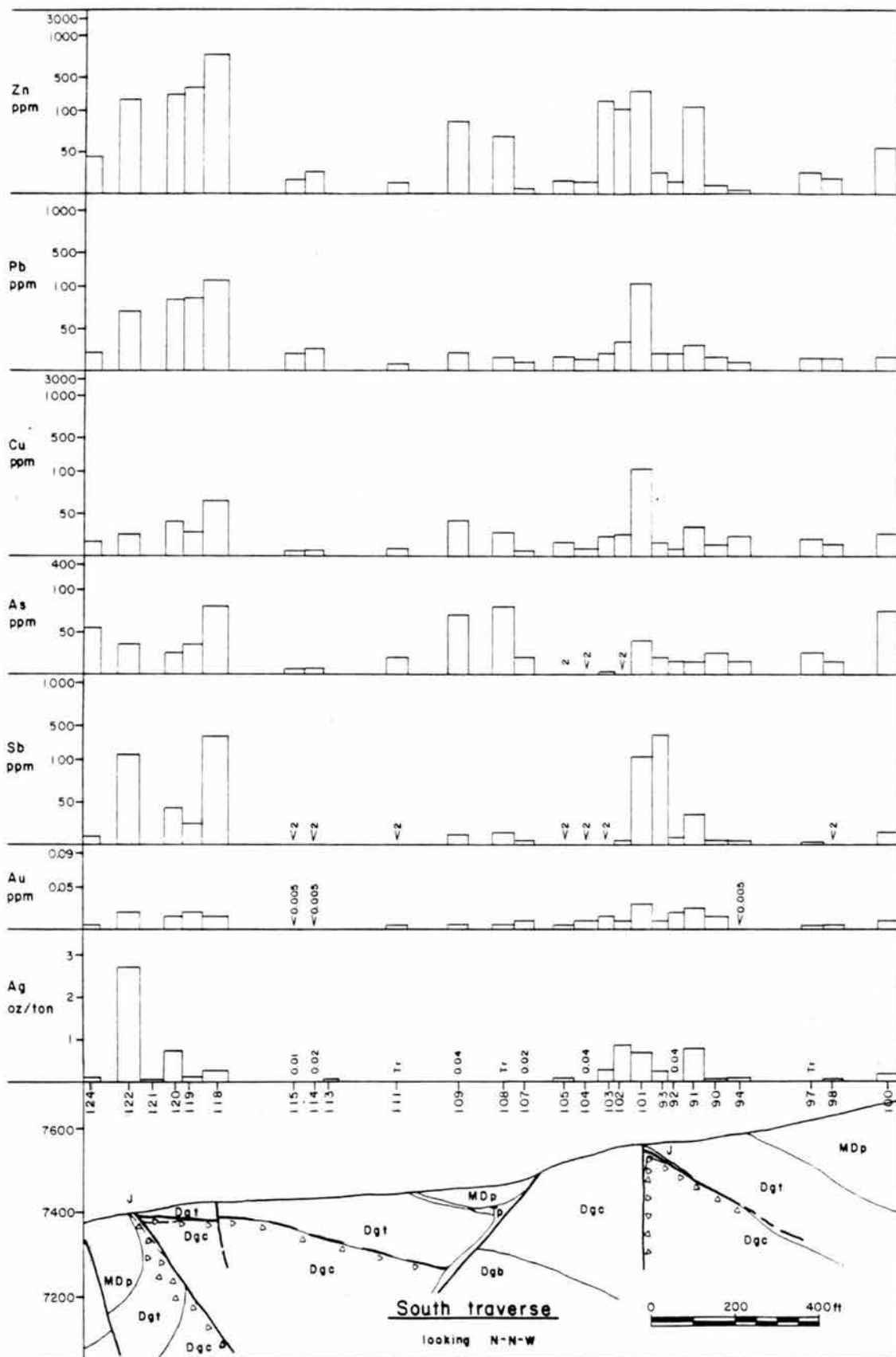
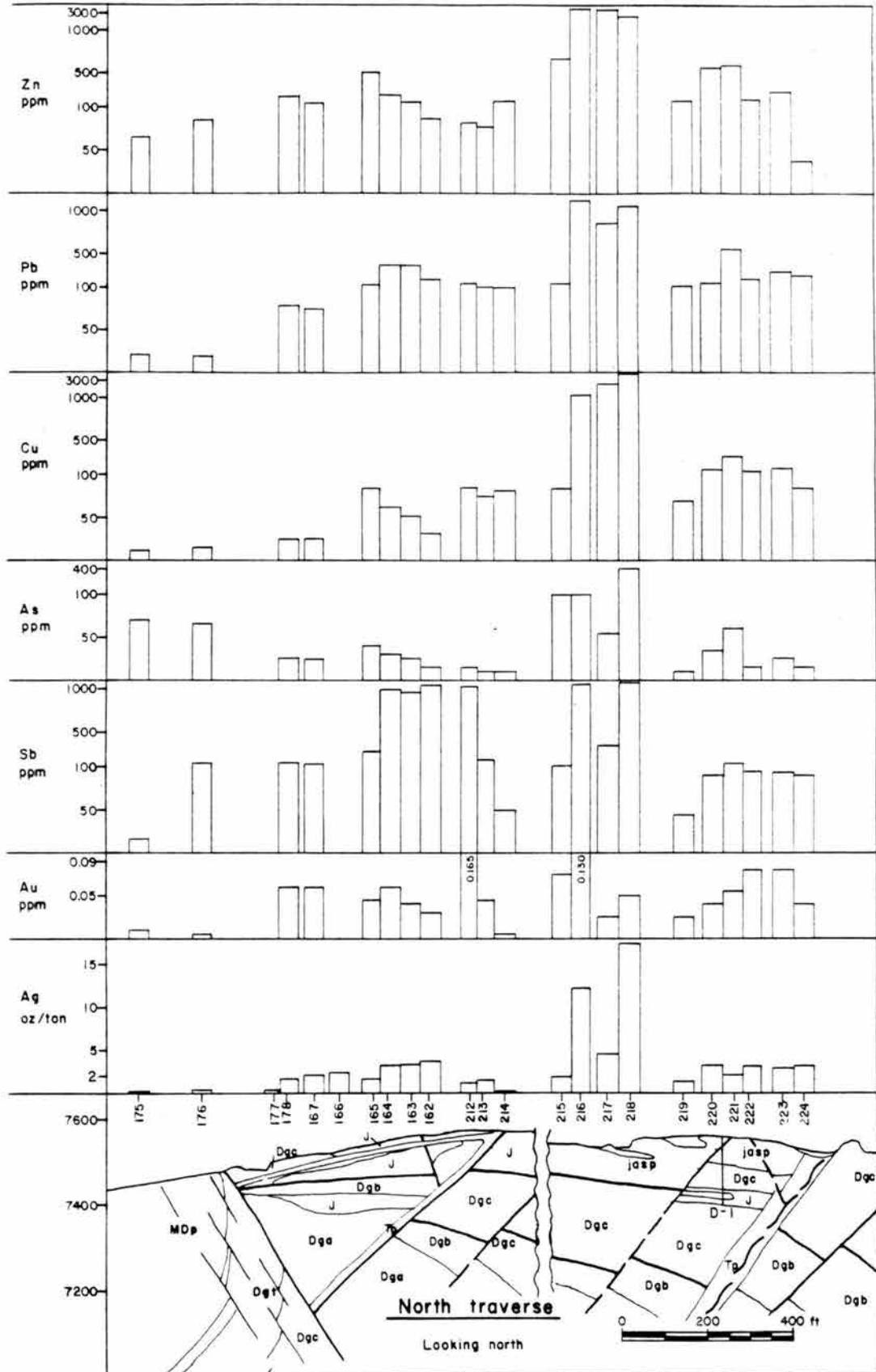


Fig. 73. North rock chip traverse.

EXPLANATION

	cover
J	Jasperoid
Mc	Chainman Shale
Mj	Joanna Limestone
MDp	Pilot Shale
Dgt	Guilmette transition beds
Dgc	Guilmette member c
Dgb	Guilmette member b
Dga	Guilmette member a
Ds	Simonson Dolomite



## LATERAL ZONATION

Lateral zonation is distinct. Lead appears to be the most tightly constrained near the central feeder structures, followed by Cu, Zn, then Ag. Lead, Cu, Zn, and Ag are all strongly enriched within and immediately above the ore body. Gold and Sb define a distinct halo at distances over a half mile outside the ore body. Arsenic shows the most erratic distribution forming highs, notably in the Pilot Shale, with no other metals.

Mercury and thallium are not included in summary figures and tables. Thallium was detected in only 17 of 39 samples, including 8 of 13 Pilot Shale samples (0.5 to 2.5 ppm). Mercury was greater than 5 ppm in 14 of 39 samples. Twelve of the high values occurred within the immediate mine area, indicating the presence of substantial Hg in stage III Ag-rich jasperoids.

## TRACE ELEMENTS BY ROCK TYPE

Rock chip data were broken up by principal rock types including Guilmette Formation, Pilot Shale, barren (stage I) jasperoid, antimony (stage II) jasperoid, and dark grey (stage III) jasperoid. Tables 20 through 24 contain summary statistics for each rock type.

Tables 25 and 26 present means of metals and metal ratios for each rock type. Relatively high Au, Ba, erratic, locally high As, and very high Sb characterize the Pilot shale, barren jasperoid, and antimony jasperoid. These rocks contain relatively low base metals and base metal to Au ratios. Silicified Guilmette and dark grey jasperoid are

Table 20: Pilot Shale summary statistics.

	N	Mean	Median	St. dev.	Min.	Max	Range
Ag (oz/t)	44	0.133	0.050	0.279	0.005	1.87	1.87
Au (ppm)	44	0.054	0.005	0.172	0.002	1.03	1.03
Sb (ppm)	44	83.6	13	254	1.0	1600	1599
As (ppm)	44	119	50	303	7.0	2000	1993
Cu (ppm)	19	26	20	20	10	101	91
Pb (ppm)	19	22	20	9.8	12	53	41
Zn (ppm)	19	80	52	87	19	386	367
Ba (ppm)	13	1386	540	1625	310	5870	5560
Ag/Au	44	556	281	768	2.8	4275	4272
Ag/Sb	44	1.13	0.13	2.25	0.0	9.6	9.6
Ag/As	44	0.11	0.04	0.2	0.002	1.17	1.16
Ag/Cu	19	0.17	0.12	0.17	0.006	0.64	0.63
Ag/Pb	19	0.22	0.09	0.29	0.01	1.21	1.20
Ag/Zn	19	0.07	0.04	0.07	0.003	0.267	0.264
Ag/Ba	13	0.009	0.002	0.015	0.0	0.06	0.06
Sb/Au	44	6142	1200	10,452	67	44,500	44,433
As/Au	43	7955	5333	6935	155	26,000	25,845
Cu/Au	19	4428	4000	2905	9.7	10,200	10,190
Pb/Au	19	4224	3533	3266	13.6	12,500	12,486
Zn/Au	19	11,298	9400	8879	48	38,000	37,952
Ba/Au	8	67,250	46,000	51,113	301	158,000	157,699
Sb/As	44	0.91	0.19	1.47	0.013	5.69	5.68
Sb/Cu	19	9.1	1.0	22.1	0.048	80	80
Sb/Pb	19	7.42	0.81	17.93	0.077	69.6	69.5
Sb/Ba	13	0.45	0.036	0.97	0.0	3.2	3.2
As/Pb	19	8.6	3.3	20.7	1.04	95.2	94.2
As/Ba	13	0.22	0.098	0.27	0.007	0.91	0.90
Pb/Ba	13	0.036	0.044	0.021	0.002	0.081	0.079
Pb/Cu	19	1.1	1.2	0.47	0.41	2.1	1.7
Sb/Zn	19	1.6	0.26	3.2	0.03	13.5	13.4

Table 21: Guilmette Formation summary statistics.

	N	Mean	Median	St. dev.	Min.	Max	Range
Ag (oz/t)	41	1.07	0.18	2.73	0.005	17.02	17.02
Au (ppm)	37	0.029	0.015	0.053	0.002	0.325	0.323
Sb (ppm)	37	172	17	512	1	3050	3049
As (ppm)	37	55	25	144	1	900	899
Cu (ppm)	23	164	25	540	6	2650	2644
Pb (ppm)	23	127	29	260	8	1040	1032
Zn (ppm)	23	386	117	831	4	3470	3466
Ba (ppm)	5	292	210	169	200	630	430
Ag/Au	37	1207	741	1521	34	7132	7098
Ag/Sb	37	1.8	0.4	4.3	0.02	24	24
Ag/As	37	2.1	0.4	4.8	0.01	28.1	28.1
Ag/Cu	23	0.5	0.2	0.6	0.02	2.8	2.8
Ag/Pb	23	0.3	0.2	0.3	0.02	0.9	0.9
Ag/Zn	23	0.15	0.10	0.16	0.01	0.69	0.68
Ag/Ba	5	0.31	0.23	0.21	0.07	0.7	0.6
Sb/Au	37	6844	1400	20,605	50	122,000	121,950
As/Au	37	4067	1667	7757	100	36,000	35,900
Cu/Au	23	7123	1700	21,233	400	106,000	105,600
Pb/Au	23	5647	3300	7496	829	34,600	33,771
Zn/Au	23	15,527	5600	29,000	600	138,800	138,200
Ba/Au	5	6665	8000	2706	3333	9692	6359
Sb/As	37	2.7	1.0	4.1	0.05	19.8	19.7
Sb/Cu	23	2.1	0.57	4.8	0.04	23.3	23.2
Sb/Pb	23	1.4	0.4	4.0	0.04	19.8	19.7
Sb/Ba	5	0.70	0.61	0.48	0.22	1.6	1.4
As/Pb	23	0.6	0.3	0.7	0.03	2.5	2.5
As/Ba	5	0.13	0.12	0.07	0.05	0.25	0.2
Pb/Ba	5	1.4	0.57	1.4	0.38	3.9	3.6
Pb/Cu	23	1.76	1.43	0.98	0.33	3.9	3.5
Sb/Zn	23	0.99	0.23	3.05	0.005	15.2	15.2

Table 22: Barren (stage 1) jasperoid summary statistics.

	N	Mean	Median	St. dev.	Min.	Max	Range
Ag (oz/t)	8	0.68	0.08	1.23	0.005	3.74	3.74
Au (ppm)	7	0.19	0.085	0.33	0.010	1.00	0.99
Sb (ppm)	7	964	440	1310	8	4000	3992
As (ppm)	7	45	25	44	10	135	125
Cu (ppm)	7	44	46	28	5	76	71
Pb (ppm)	7	52	17	67	7	198	191
Zn (ppm)	7	69	27	82	7	257	250
Ba (ppm)	2	215			210	220	10
Ag/Au	7	784	38	1467	3.8	4275	4271
Ag/Sb	7	0.067	0.007	0.083	0.001	0.24	0.24
Ag/As	7	1.94	0.11	3.13	0.007	8.55	8.54
Ag/Cu	7	0.75	0.09	1.4	0.045	4.14	4.09
Ag/Pb	7	0.37	0.46	0.21	0.036	0.65	0.61
Ag/Zn	7	0.42	0.17	0.48	0.011	1.47	1.46
Ag/Ba	2	0.40			0.22	0.58	0.36
Sb/Au	7	14,839	4267	19,500	540	46,667	46,127
As/Au	7	2235	294	4608	35	13,500	13,465
Cu/Au	7	747	844	538	59	1689	1630
Pb/Au	7	1676	200	2247	8	6600	6592
Zn/Au	7	1527	1733	1286	7	3024	3017
Ba/Au	2	6000			4667	7333	2667
Sb/As	7	30	18	29	0.06	93	93
Sb/Cu	7	22	10	20	0.8	53	52
Sb/Pb	7	103	10	193	0.32	571	571
Sb/Ba	2	3.6			0.9	6.4	5.4
As/Pb	7	3.8	3.6	4.1	0.08	12.6	12.5
As/Ba	2	0.06			0.05	0.07	0.02
Pb/Ba	2	0.7			0.5	0.9	0.4
Pb/Cu	7	2.0	1.3	2.2	0.09	6.4	6.3
Sb/Zn	7	45	16	68	0.3	200	200

Table 23: Antimony (stage 2) jasperoid summary statistics.

	N	Mean	Median	St. dev.	Min.	Max	Range
Ag (oz/t)	21	0.4	0.08	0.7	0.005	2.7	2.7
Au (ppm)	19	0.31	0.24	0.29	0.002	1.01	1.01
Sb* (ppm)	19	8177	2100	9126	5	20,000	20,000
As (ppm)	19	58	52	25	20	100	80
Cu (ppm)	19	59	57	39	9	142	133
Pb (ppm)	19	16	13	14	5	70	65
Zn (ppm)	19	117	71	97	12	405	393
Ba (ppm)	4	3145	510	4535	510	11,000	10,490
Ag/Au	19	285	20	1027	0.6	4629	4628
Ag/Sb	19	0.043	0.002	0.13	0.0	0.58	0.58
Ag/As	19	0.23	0.08	0.58	0.004	2.6	2.6
Ag/Cu	19	0.32	0.1	0.75	0.002	3.4	3.4
Ag/Pb	19	0.51	0.23	0.50	0.016	1.9	1.9
Ag/Zn	19	0.08	0.05	0.10	0.001	0.44	0.44
Ag/Ba	4	0.01	0.005	0.007	0.002	0.02	0.02
Sb/Au	19	26,516	10,000	30,548	1005	93,023	92,018
As/Au	19	1132	245	3290	98	15,000	14,902
Cu/Au	19	2970	243	10,859	9.8	49,000	48,990
Pb/Au	19	376	47	916	16	3500	3484
Zn/Au	19	1304	423	2524	77	10,550	10,473
Ba/Au	4	5010	1397	6214	554	15,714	15,160
Sb/As	19	125	40	142	0.17	444	444
Sb/Cu	19	235	49	343	0.05	1333	1333
Sb/Pb	19	799	143	1103	1	4000	3999
Sb/Ba	4	19	1.8	18	0.7	39	38
As/Pb	19	5	4	4	0.5	20	20
As/Ba	4	0.14	0.18	0.08	0.008	0.196	0.188
Pb/Ba	4	0.018	0.01	0.013	0.002	0.033	0.032
Pb/Cu	19	0.6	0.2	0.8	0.05	2.6	2.5
Sb/Zn	19	105	37	175	0.4	667	666

\* Sb actually reaches highs of over 6%.

Table 24: Dark grey (stage 3) jasperoid summary statistics.

	N	Mean	Median	St. dev.	Min.	Max	Range
Ag (oz/t)	25	3.27	2.4	3.95	0.005	17.35	17.35
Au (ppm)	21	0.077	0.06	0.058	0.015	0.255	0.240
Sb (ppm)	21	2307	141	5767	10	20,000	20,000
As (ppm)	21	63	38	80	15	400	385
Cu (ppm)	20	349	84	850	9	3900	3891
Pb (ppm)	20	666	184	1437	13	6500	6487
Zn (ppm)	20	964	276	1797	12	7750	7738
Ba (ppm)	11	229	220	28	200	290	90
Ag/Au	20	1791	1272	2535	1.23	11,899	11,897
Ag/Sb	20	0.37	0.25	0.34	0.0	1.19	1.19
Ag/As	20	2.27	1.46	2.1	0.002	7.27	7.27
Ag/Cu	19	0.65	0.42	0.64	0.003	2.2	2.2
Ag/Pb	19	0.33	0.31	0.22	0.004	0.75	0.75
Ag/Zn	19	0.23	0.12	0.20	0.001	0.65	0.65
Ag/Ba	11	0.74	0.49	0.79	0.12	2.83	2.71
Sb/Au	21	19,674	4073	40,238	380	142,857	142,477
As/Au	21	1281	750	1743	91	8000	7909
Cu/Au	20	6202	1421	16,633	360	78,000	77,640
Pb/Au	20	7724	2985	11,153	143	44,828	44,685
Zn/Au	20	12,368	4600	15,757	240	55,800	55,560
Ba/Au	11	3685	3333	1437	1758	6000	4242
Sb/As	21	30.5	4.8	60.2	0.20	222	222
Sb/Cu	20	23	1.1	67	0.21	299	298
Sb/Pb	20	51	0.8	218	0.42	1000	1000
Sb/Ba	11	3.1	1.1	3.0	0.39	9.2	8.8
As/Pb	20	0.8	0.1	1.5	0.01	5.3	5.2
As/Ba	11	0.35	0.15	0.51	0.05	1.9	1.9
Pb/Ba	11	2.5	1.4	2.9	0.45	9.3	8.8
Pb/Cu	20	3.5	1.8	6.6	0.22	32	31
Sb/Zn	20	6.0	0.46	18.3	0.15	84	84

Table 25: Surface rock chip correlation coefficients by rock type.

	MDP	DG	BJ	SbJ	DJ
Ag: Au	-0.038 (44)	0.947 (37)	-0.249 (7)	-0.129 (19)	-0.018 (20)
Ag: Sb	-0.080 (44)	0.364 (37)	0.063 (7)	-0.139 (19)	-0.061 (20)
Ag: As	0.010 (44)	0.109 (37)	-0.398 (7)	-0.118 (19)	0.790 (20)
Ag: Cu	0.877 (19)	0.856 (23)	-0.007 (7)	-0.109 (19)	0.908 (19)
Ag: Pb	0.749 (19)	0.688 (23)	0.986 (7)	0.937 (19)	0.906 (19)
Ag: Zn	0.785 (19)	0.788 (23)	0.105 (7)	0.392 (19)	0.899 (19)
Ag: Ba	-0.020 (13)	-0.280 (5)	-	0.866 (4)	-0.299 (11)
Au: Sb	0.437 (44)	0.277 (37)	-0.097 (7)	0.475 (19)	0.385 (21)
Au: As	0.141 (44)	0.025 (37)	-0.126 (7)	0.755 (19)	0.003 (21)
Au: Cu	-0.181 (19)	0.155 (23)	0.321 (7)	-0.238 (19)	0.014 (20)
Au: Pb	-0.172 (19)	0.494 (23)	-0.311 (7)	0.029 (19)	0.472 (20)
Au: Zn	-0.002 (19)	0.380 (23)	-0.291 (7)	0.411 (19)	0.467 (20)
Au: Ba	-0.219 (13)	0.487 (5)	-	0.244 (4)	0.473 (11)
Sb: As	0.120 (44)	0.940 (37)	0.248 (7)	0.511 (19)	0.196 (21)
Sb: Cu	-0.129 (19)	0.504 (23)	0.497 (7)	-0.098 (19)	-0.015 (20)
Sb: Pb	-0.027 (19)	0.559 (23)	-0.025 (7)	-0.201 (19)	0.627 (20)
Sb: Zn	0.419 (19)	0.606 (23)	-0.175 (7)	0.393 (19)	0.594 (20)
Sb: Ba	-0.223 (13)	0.312 (5)	-	0.335 (4)	-0.032 (11)
As: Cu	0.283 (19)	0.440 (23)	-0.151 (7)	-0.429 (19)	0.943 (20)
As: Pb	0.002 (19)	0.670 (23)	-0.379 (7)	-0.021 (19)	0.293 (20)
As: Zn	-0.013 (19)	0.673 (23)	-0.304 (7)	0.535 (19)	0.400 (20)
As: Ba	0.099 (13)	0.731 (5)	-	-0.576 (4)	-0.214 (11)
Cu: Pb	0.691 (19)	0.744 (23)	-0.033 (7)	-0.189 (19)	0.237 (20)
Cu: Zn	0.748 (19)	0.889 (23)	0.088 (7)	-0.272 (19)	0.349 (20)
Pb: Zn	0.721 (19)	0.958 (23)	0.072 (7)	0.315 (19)	0.983 (20)
Pb: Ba	-0.318 (13)	0.735 (5)	-	0.372 (4)	-0.170 (11)
Zn: Ba	-0.214 (13)	0.457 (5)	-	0.921 (4)	-0.113 (11)

Table 26: Average metal and metal ratios in surface samples (by rock type).

	Mdp	Dg	BJ	SbJ	DJ
Ag (oz/t)	0.133 (44)	1.07 (41)	0.68 (8)	0.36 (21)	3.27 (25)
Au (ppm)	0.054 (44)	0.029 (37)	0.192 (7)	0.31 (19)	0.077 (21)
Sb (ppm)	83.6 (44)	172 (37)	964 (7)	8177 (19)	2308 (21)
As (ppm)	119 (44)	55 (37)	45 (7)	58 (19)	63 (21)
Cu (ppm)	26 (19)	164 (23)	44 (7)	59 (19)	349 (20)
Pb (ppm)	21.6 (19)	127 (23)	52 (7)	15.5 (19)	666 (20)
Zn (ppm)	79.7 (19)	386 (23)	69 (7)	117 (19)	964 (20)
Ba (ppm)	1386 (13)	292 (5)	215 (2)	3145 (4)	229 (11)
Ag/Au	556 (44)	1207 (37)	784 (7)	285 (19)	1791 (20)
Ag/Sb	1.13 (44)	1.77 (37)	0.07 (7)	0.04 (19)	0.37 (20)
Ag/As	0.11 (44)	2.07 (37)	1.94 (7)	0.23 (19)	2.27 (20)
Ag/Cu	0.17 (19)	0.45 (23)	0.75 (7)	0.32 (19)	0.65 (19)
Ag/Pb	0.22 (19)	0.27 (23)	0.37 (7)	0.51 (19)	0.33 (19)
Ag/Zn	0.07 (19)	0.15 (23)	0.42 (7)	0.078 (19)	0.23 (19)
Ag/Ba	0.009 (13)	0.31 (5)	0.40 (2)	0.01 (4)	0.74 (11)
Sb/Au	6142 (44)	6844 (37)	14,839 (7)	26,516 (19)	19,674 (21)
As/Au	7955 (44)	4067 (37)	2235 (7)	1132 (19)	1281 (21)
Cu/Au	4428 (19)	7123 (23)	747 (7)	2970 (19)	6202 (20)
Pb/Au	4224 (19)	5647 (23)	1676 (7)	376 (19)	7724 (20)
Zn/Au	11,298 (19)	15,527 (23)	1527 (7)	1304 (19)	12,368 (20)
Ba/Au	67,250 (8)	6665 (5)	6000 (2)	5010 (4)	3685 (11)
Sb/As	0.913 (44)	2.69 (37)	29.7 (7)	125 (19)	30.5 (21)
Sb/Cu	9.2 (19)	2.14 (23)	21.8 (7)	235 (19)	23.2 (20)
Sb/Pb	7.42 (19)	1.43 (23)	103 (7)	799 (19)	51.4 (20)
Sb/Ba	0.45 (13)	0.69 (5)	3.6 (2)	19.4 (4)	3.14 (11)
As/Pb	8.61 (19)	0.59 (23)	3.8 (7)	5.16 (19)	0.8 (20)
As/Ba	0.22 (13)	0.13 (5)	0.06 (2)	0.14 (4)	0.35 (11)
Pb/Ba	0.036 (13)	1.38 (5)	0.69 (2)	0.018 (4)	2.5 (11)
Pb/Cu	1.05 (19)	1.76 (23)	2.0 (7)	0.59 (19)	3.47 (20)
Sb/Zn	1.56 (19)	0.99 (23)	45.2 (7)	105 (19)	6.0 (20)

characterized by high Me:Ag ratios, high base metals, low Ba, and of course, high Ag and Ag:Me ratios.

Table 25 shows correlation coefficients. The single most consistent correlation is between Ag and Pb in all rock types. Me:base metal correlations are consistently high in Guilmette and dark grey jasperoids. Antimony:Me and Ba:Me correlations are strongest in antimony jasperoids. Gold, in general, correlates poorly with other elements. A Au:As correlation of 0.755 in antimony jasperoid is predictable in that both elements are enriched in this rock type, however the Au:Ag correlation of 0.947 in silicified Guilmette appears to be highly anomalous relative to poor Au:Ag correlations in all other rock types.

#### VOLATILE PHASES

Exploration Research Laboratories analyzed 23 hand samples from surface jasperoid exposures for contained vapor phases (procedures described earlier in this chapter). Table 27 shows the data. Samples were not analyzed for H<sub>2</sub>O. Methane, ethane, propane, and carbon dioxide data indicate that organic-derived volatiles are much more abundant than CO<sub>2</sub>. The sum of methane + propane + ethane to carbon dioxide ratios average 9.32 to 1. Map distribution is erratic, however silver-rich jasperoids tend to contain less organic volatiles than surrounding stage I and II jasperoids.

The quotient CO<sub>2</sub>/CH<sub>4</sub> yields average values of 40.6 for Ag-rich (+ 1 oz Ag/ton) jasperoids but only 2.7 for Au-rich (+ 150 ppb Au) jasperoids. Eight of twelve jasperoids containing over 1 oz Ag/ton

Table 27. Volatile phase data.

Sample #	jasp type	host rock	Ag (oz/t)	Au (ppm)	CO2 (ppm)	CH4 (ppm)	C2H6 (ppm)	C3H8 (ppm)	H2S (ppm)	CO5 (ppm)	SO2 (ppm)	CS2 (ppm)	(Σ org)/CO2
(stage III dark grey jasperoid)													
18	DJ(?)	Mj	Tr	0.140	1121.3	5	51	143	ND	4.7	ND	11	0.53
29b	DJ(?)	Dgt	Tr	0.050	828.6	530	3905	2838	2.3	ND	ND	0.1	22.76
122	DJ	Dgc	2.7	0.020	715.2	25	1446	767	4.7	ND	ND	1.1	6.72
222	DJ	Dgc	3.18	0.080	438.6	8	147	149	ND	10.1	0.9	18.0	0.88
164	DJ	Dgc	3.2	0.060	506.4	12	200	336	2.9	19.3	ND	15.0	1.51
197	DJ	Dgt	17	0.325	372.8	188	1194	1732	40.5	1.1	ND	3.4	9.10
202	DJ	Dga	3.22	0.065	589.8	19	777	639	0.2	ND	ND	0.6	5.23
212	mixed	Dgc	1.05	0.165	317.7	792	2336	4816	12.1	2.9	ND	1.4	23.69
215	DJ	Dgc	1.96	0.075	475.2	8	149	84	0.3	ND	ND	0.1	0.74
218	DJ	Dgc	17.4	0.050	337.0	14	146	74	0.3	ND	ND	0.1	0.75
221	DJ	Dgc	2.04	0.055	339.4	66	588	1013	22.6	1.4	ND	3.7	4.67
224	BGJ	Dgc	3.16	0.040	1243.0	6	65	127	ND	23.5	ND	31.1	0.55
(stage II antimony jasperoid)													
66	SbJ	Mj	Tr	0.280	348.2	342	4341	1180	14.8	ND	ND	0.1	19.29
69	SbJ	Mj	0.1	0.245	393.4	288	2617	287	3.6	ND	ND	ND	11.17
74	SbJ	Mj	0.22	0.090	564.8	36	1713	807	7.1	ND	ND	0.1	7.77
144	SbJ	Mj	0.58	0.700	508.2	272	1805	811	2.6	ND	ND	Tr	9.56
152	SbJ	Mj	0.1	0.920	342.7	27	100	113	ND	ND	ND	0.5	2.28
154	SbJ	Mj	0.2	1.010	393.4	551	5222	1866	22.5	ND	ND	Tr	25.08
(stage I barren jasperoid)													
150	BJ	Mj	0.1	0.085	1086.7	17	220	530	47.5	13.7	ND	1.2	2.04
162	mixed	Dgc	3.74	0.030	366.6	701	3490	3890	13.1	0.3	ND	1.5	24.85
89	BJ	Mj	0.11	1.000	456.6	145	1750	1665	30.7	ND	ND	0.8	10.52
213	BJ	Dgc	1.36	0.045	449.8	14	148	216	0.3	20.7	0.9	34.3	1.07
(silicified Pilot Shale)													
155	silic.	MDp	0.14	1.030	370.9	438	2187	1725	3.6	ND	ND	Tr	13.95

have  $\text{CO}_2/\text{CH}_4$  greater than 24, while eight of nine jasperoids containing over 150 ppb Au have  $\text{CO}_2/\text{CH}_4$  under 3.2. Hofstra et al. (1987) noted just the opposite relationship at Jerritt Canyon, where the gold-rich event had elevated  $\text{CO}_2/\text{CH}_4$  compared with other events. At Taylor, stratigraphy may impose the principal control on  $\text{CH}_4$ . The Joanna Limestone hosts most of the gold-rich jasperoids, sandwiched between the organic-rich Pilot and Chainman Shale units. Evolution of organic-derived volatiles during hydrothermal activity must have been particularly intense within these stratigraphic horizons.

The Ag-rich jasperoids contain an average 8.1 ppm  $\text{H}_2\text{S}$  and 6.64 ppm COS, while the Au-rich samples contain an average 14.5 ppm  $\text{H}_2\text{S}$  and less than 1 ppm COS. The gold-rich event at Jerritt Canyon likewise contains elevated  $\text{H}_2\text{S}$  (Hofstra et al., 1987). Unlike  $\text{CO}_2/\text{CH}_4$ , which appears to be strongly influenced by stratigraphy,  $\text{H}_2\text{S}$  and COS values may reflect broader P-T-X conditions in the hydrothermal system. The combination of lower  $\text{H}_2\text{S}$  and higher COS suggests that Ag-rich jasperoids were deposited within an oxidized environment relative to Au-rich jasperoids.

## CHAPTER VI

### CONCLUSIONS

#### SUMMARY OF GEOLOGIC HISTORY

Regional and local evidence indicates the following sequence of post Middle Jurassic geologic events took place in the Southern Schell Creek Range and the Taylor district:

- (1) Muscovite-bearing granites intruded the region centered on the Snake Range, between 150 and 161 Ma.
- (2) East-vergent, older-on-younger, bedding plane thrust faults cut the region prior to 110 Ma.
- (3) A gentle, open fold developed in the Taylor mine area during thrust fault movement.
- (4) The fold induced ramping of bedding plane faults within, and east of the mine area, and imbricated susceptible portions of the section, particularly the upper Pilot/lower Joanna.
- (5) Cu-Au-bearing monzonitic plutons intruded the Robinson district from 90 to 110 Ma.
- (6) Rocks beneath the brittle/ductile transition suffered low grade regional metamorphism while overlying rocks were thrust and folded.
- (7) Active tectonism ceased across the region at about 75 Ma, and was superceded by an environment of relaxation (at least in

supercrustal rocks). Compressive tectonism moved eastward into the Laramide belts of Colorado and Wyoming.

- (8) Seventy to seventy-five Ma muscovite-bearing plutons intruded eastern Nevada.
- (9) Magmatism triggered uplift, centered on the Snake Range. This positive region may be the source area for the Paleocene Sheep Pass Formation conglomerates. Tectonism activated northeast-trending high-angle normal (?) faults.
- (10) Renewed peraluminous magmatism between 43 and 48 Ma, centered again on the Snake Range, triggered a major Eocene uplift. This uplift was probably the source area for the Eocene Stinking Spring Conglomerates, shed westward across the Schell Creek and Egan Ranges.
- (11) Low-angle denudational faulting accompanied Eocene uplift of the Snake Range. Denudation was greatest in the Snake Range, but effected the Confusion Range to the east and the Schell Creek Range to the west. Movement on low-angle denudational faults in the Taylor mine area cut out substantial portions of the Guilmette member b, and the Joanna Limestone. High-angle northeast-trending faults acted locally as tear faults during low-angle fault movement. Gravity-driven denudational faults cut down section into massive limestones where they encountered a fold in the Taylor mine area, and severely brecciated the section.
- (12) The west-dipping Taylor normal fault offsets denudational faults.
- (13) Calc-alkaline volcanism is first documented in northeast Nevada at 43 Ma. The arc swept southwestward and was most active in the Southern Schell Creeks around 35 Ma. As many as 45 porphyritic

rhyolite dikes and sills intruded existing structures in the Taylor mine area. The older [Kalamazoo (?)] volcanics unconformably overlay Eocene conglomerates.

- (14) Active tectonism and uplift returned to the region with Oligocene metaluminous magmatism. Several north-trending arches developed in the Snake, Schell Creek, and Egan Ranges. Low-angle faults were reactivated in the Southern Schell Creeks. High-angle reverse faults breached the reactivated south-plunging fold at Taylor. Oligocene volcanics across Eastern Nevada were folded. An inferred compressional tectonic environment related to crustal shortening is most consistent with observed structuring (Moores et al., 1968).
- (15) Silver-bearing jasperoid bodies formed where hydrothermal fluids, focused up active reverse faults, exited laterally into low-angle breccia zones at the top of Guilmette Limestone members a, and c. Rhyolite bodies were extensively argillized; alteration intensity increases toward the mine area.
- (16) Younger (32 to 34 Ma) volcanics unconformably overlay older volcanics and Eocene conglomerates. Folding and high-angle fault movement continued after the mineralizing event. The fold rotated younger volcanics eastward at least 40°. White calcite healed post-mineral fault breccias.
- (17) Latite vitrophyre dikes cross cut the younger volcanics. Two vitrophyre dikes intruded the mine area along the reactivated Taylor fault. These dikes are unaltered and probably related to 20 to 25 Ma regional magmatism.

- (18) North-south-trending high-angle normal faults dissected the region after 17 Ma, when earliest olivine basaltic volcanism is documented.
- (19) Principal uplift on Basin and Range faults took place during late Miocene and Pliocene time and tilted the Southern Schell Creek range about 15° west.
- (20) Basin and Range uplift produced extreme relief and unnaturally steep slopes in eastern Nevada. Gravity slides of major proportion moved slices of Upper Paleozoic and younger rocks into unpredictable positions, often onto the flanks of ranges.

#### SUMMARY OF MINERALIZATION

Pre-mineral intrusion of high potassium, fluorite-bearing porphyritic rhyolites and post-mineral intrusion of latite vitrophyre dikes bracket mineralization of the Taylor district. These rocks have not been reliably dated, however regional data suggest they are approximately 35 Ma and 20 to 25 Ma, respectively. District-wide spatial association between rhyolite intrusives and jasperoids infers that mineralization is genetically related to the 35 Ma rhyolitic magmatism.

Stratigraphic reconstruction suggests that the top of the Guilmette Formation (top of the "transition beds") was 3500 ± 700 feet deep, at the time of silver deposition.

Field relations, petrographic observations, trace element chemistry, and fluid inclusion studies all indicate that mineralization

occurred in four general, but distinct, stages. Later stages successively overlap earlier stages.

Jigsaw to granular quartz textures dominate stage I jasperoids. Granular textures imply grain for grain replacement in which rate of quartz deposition keeps pace with calcite dissolution. Exposures are tenacious, hematite-stained, and normally lack evidence of complex multiple-stage brecciation or silicification. The rock is light grey on fresh surfaces and lacks visible accessory minerals. Stage I jasperoids contain erratic Au up to 1 ppm (average= 190 ppb, with the highest standard deviation of 330 ppb), with low base metal and Ag values (except where contaminated by subsequent stages). With the exception of Au, stage I jasperoids are geochemically and mineralogically dead. Fragments of stage I are common in stage II and are locally important in stage III jasperoids.

Stibnite or its oxidation products distinguish stage II jasperoids. They are dominated by fine- to coarse-grained reticulate quartz textures. Reticulate textures develop when calcite dissolution advances ahead of open space quartz deposition. Contrasting fragment and matrix types, as seen in thin section, document at least three brecciation events during stage II jasperoid deposition. Exposures are strongly brecciated, brown weathering, and contain abundant vugs. Fresh surfaces are medium to dark grey. In addition to stibnite, stage II jasperoid contains late barite, with trace pyrite and sphalerite in vugs. Metal content includes 1 to 3% Sb at the outcrop scale, reaching highs of 18% Sb, erratic Ag up to 2.5 oz/ton, up to 1 ppm Au, locally over 1000 ppm As, locally in excess of 1% Ba, and up to 400 ppm Zn. An average Pb content of 16 ppm is the lowest of all rock types, and

readily distinguishes stage II from Ag-rich stage III jasperoids. Stage II contains the lowest metal: Au and Pb: metal ratios of all rock types. Some or much of the Au probably reflects the presence of Au-rich stage I jasperoid fragments. Stage II quartz was deposited from boiling fluids at minimum 202° C.

Stage III represents the main Ag-bearing jasperoid ore stage. Jasperoid texture is universally hypidiomorphic, comprised of a wide range of quartz grain types from coarse idiomorphic to very fine-grained jigsaw textures. Contrasting fragment types, grain size, and textural distributions imply that stage III jasperoid suffered at least four brecciation events during its deposition in a tectonically active environment. Outcrops weather brown and are highly fractured to brecciated with white calcite matrix. Fresh surfaces are dark grey to near black. Fracture-controlled azurite, malachite and jarosite are rare accessories in exposures of oxidized Ag-rich (high grade) jasperoid. Weathered outcrops of stage III jasperoid contain high Ag, averaging over 3 oz/ton, up to 380 ppm Hg, up to 1% combined base metals (probably reflecting contamination by stage IV), with low As, Ba, and erratic Sb contents. Ag: Au ratios are highly erratic but generally greater than 1000:1. High Ag: metal, base metal: metal, and metal: As ratios characterize stage III. Siliceous ores (based on averages of "medium grade" drill intercepts) that contain approximately 3.1 oz Ag/ton, also average 105 ppb Au, 1100 ppm combined base metals, 250 ppm Sb, 25 ppm As, less than 200 ppm Ba, 50 to 100 ppm Hg (estimated from data reported by Lovering and Heyl (1974)), Ag: Au over 1100:1 (all other rock types average less than 1000:1), and As: Au less than 300:1 (all other rock types average over 1000:1). Stage III

jasperoids were not identified outside the mine area. Extensive silicification bottoms out about 200 feet below the current erosional surface. The base of silicification crosses structure and stratigraphy. Accessory purple fluorite from stage III jasperoid was deposited from minimum 228° C fluids which were probably boiling.

Organic-derived volatiles dominated the [non-water] volatile component of hydrothermal fluids during all jasperoid stages.

Rhyolite bodies across the district were weakly to moderately argillized during jasperoid deposition. Kaolinite with lesser sericite, and local silica flooding, dominate the alteration mineralogy. Sediments adjacent to principal feeder structures were partially silicified. Partial silicification extends up to 75 feet up section and 300 feet on strike from mapped jasperoids in the permeable Guilmette transition beds. Remnant limestone is generally recrystallized at microscopic scale adjacent to silica fronts. Calcite is the only recognized secondary carbonate mineral.

Stage IV open space calcite-sphalerite-tetrahedrite-galena-[Ag-Pb-Sb-sulfosalt]-pyrite-silica veins and breccia fillings comprise the last stage of hypogene ore deposition. Sulfides rim jasperoid fragments followed by white calcite infilling. Veins contain several 10's oz Ag/ton. Stage IV probably contributed a significant percentage of the silver to the Taylor deposit. Jasperoid breccias that contain over 5 oz Ag/ton are often healed by late white calcite, indicative of stage IV mineralization. Azurite is a common accessory in oxidized high-grade jasperoid containing stage IV veins. In addition to high Ag, stage IV veins contain up to 1.5% combined base metals, Sb over 2000 ppm, 200 to 300 ppb Au, and high Hg, with low Ba. Siliceous ores

averaging 12 oz Ag/ton contain a significant stage IV contribution. These ores average 2000 ppm combined base metals, 800 ppm Sb, 280 ppb Au, 180 ppm Ba, high Ag:metal ratios, including Ag:Au of 2300:1, high metal:Ba ratios, and the lowest average Cu:Au ratio (540:1) of all rock types. Silver to metal correlations are poor in higher grade rock resulting from coarser grained, unevenly distributed mineralogies. Stage IV sphalerite was deposited from non-boiling fluids at a minimum temperature of 306° C.

Intense late montmorillonite argillization of rhyolites was confined to the immediate mine area. Calcite, siderite, and trace pyrite are locally associated with late montmorillonite. Carbonatization of some sheared rhyolite bodies occurred within, and adjacent to the Argus and Southwest Pit feeder structures.

#### GENETIC MODEL

Any model of mineral deposition at Taylor must explain the following features:

- (1) Taylor is a prograde system. Minimum temperatures of formation increased from less than 200° C during stage I to over 300° C during stage IV.
- (2) Trace element contents show corresponding shifts from Au dominant in stage I, to Sb-As-Au-Ba dominant in stage II, to Ag-Pb-Zn-Hg dominant in stage III, to Ag-Pb-Sb-Zn dominant in stage IV.
- (3) Stage II jasperoid quartz was deposited from boiling fluids. Stage III fluorite in jasperoid was probably deposited from

boiling fluids, while fluorite below the base of silicification shows no indication of boiling conditions.

- (4) The base of silicification crosses structure and stratigraphy, implying a fundamental depth-related control on wall rock reactions.
- (5) Whole rock vapor phase analyses on jasperoids indicate that organic-derived volatiles occurred at several times greater concentration levels than CO<sub>2</sub> plus all other [non-water] volatile components. Liquid-liquid-vapor fluid inclusions demonstrate that non-water volatiles are sufficiently abundant to form a second liquid phase, and therefore must have dominated the vapor phase.
- (6) Total organic content has not been measured in the stratigraphic section at Taylor, however visual estimates of carbonaceous material indicate that the organic component is greater in the Guilmette transition beds than in underlying Guilmette units, and increases substantially above the Pilot Shale-Guilmette contact.
- (7) Ilchik (1984) and Ilchik et al. (1986) demonstrated that indigenous organic matter in the Pilot Shale was thermally matured [with evolution of volatiles] during gold mineralization at Alligator Ridge.
- (8) Kaolinite-sericite-silica alteration of rhyolites, associated with stages I through III jasperoid deposition, gave way to a Mg-rich montmorillonite- calcite alteration assemblage during stage IV ore deposition. Clay paragenesis implies corresponding shifts from acidic pH and low  $a_{\text{cation}^+}/a_{\text{H}^+}$  ratios to alkaline pH and high  $a_{\text{Mg}^+}/a_{\text{H}^+}$  ratios (Beane, 1984).

- (9) Banded silica-sulfide-calcite veins were deposited below the level of silicification. Buchanan (1981) relates this style of mineral deposition to episodic boiling in epithermal systems.
- (10) Fournier (1985a, 1985b) examined P-T-X controls on calcite and silica solubilities, which are sensitive to several factors. Quartz solubility increases (and calcite solubility decreases) with a drop in volatile content (particularly CO<sub>2</sub>), a shift to alkaline pH, rising salinity (above about 300° C), rising temperature, and increases in pressure (above about 300° C). Fournier (1985a, 1985b), suggests that decompressional boiling would likely cause deposition of calcite and dissolution of quartz by inducing rapid loss of CO<sub>2</sub>, while increasing pH and salinity, and lowering temperature and pressure through adiabatic expansion.
- (11) Therefore, a low-pH buffer is required to maintain calcite solubility and depress silica solubility in a boiling system.

Fig. 74 illustrates a proposed genetic model:

A high-potassium-fluorine magmatic system intruded the Southern Schell Creeks at about 35 Ma. The south-plunging Taylor anticline focussed the magmatic/hydrothermal system into what was to become the Taylor silver district. Early rhyolitic magma invaded the district along high-angle northeast-trending faults, and spread out along the low-angle Taylor normal fault, and bedding plane shears cutting the Pilot Shale and lower and upper Joanna Limestone contacts. Initial porphyry intrusion was dry. Associated metamorphism is evidenced only by local thermal recrystallization of limestone within several feet of dikes and sills.

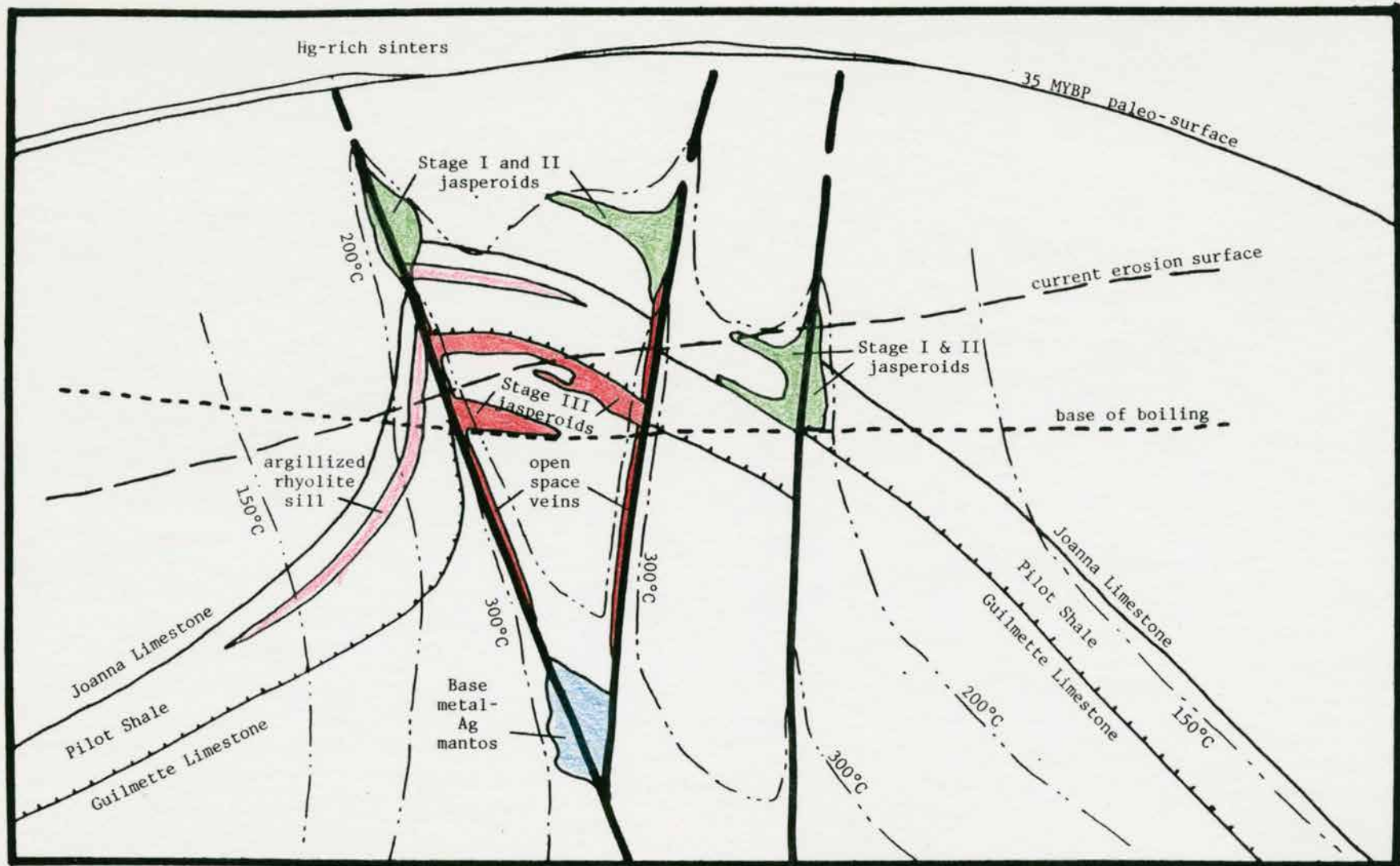


Fig. 74. Schematic cross section illustrating the Taylor silver system at the end of stage IV.

Porphyry intrusion generated a strong regional geothermal gradient centered on the district. Concentric isotherms moved upward and outward as the system heated up through time.

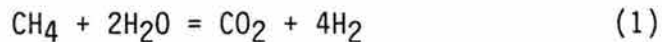
Initial dilute stage I and II hydrothermal fluids deposited Au, Sb, As, and Ba where the 175° C (to be consistent with Radtke's (1981, 1984) model for Carlin) and 200° C isotherms intersected organic-rich, permeable, and reactive stratigraphy, at depths sufficiently shallow to permit organic volatiles,  $\pm$  CO<sub>2</sub>, to boil. It is proposed that metals contained in stage I and II jasperoids were leached from the stratigraphic section, especially the Pilot Shale which contains a great abundance of these elements. Joanna Limestone hosts the most extensive stage I and II deposits, stratigraphically above the Pilot Shale.

Isotherms continued to move up and out.

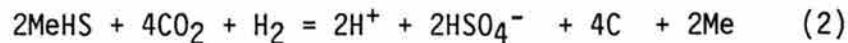
Higher temperature, 228° C, stage III hydrothermal fluids were focused directly into the most structurally complex and tectonically active loci of the district. Silica, Ag, Pb, Zn, and Hg were deposited from effervescing fluids below the Pilot Shale contact. Banded silica-sulfide-calcite veins were deposited at depth, suggesting that episodic boiling reached these levels during tectonic-induced depressuring. The base of silicification, however, marks the depth of steady, long-term boiling. The trace element content of stage III jasperoids reflects a distinct departure from stages I and II, and the Pilot Shale-type suite. Without benefit of salinity data or stable isotopes, specific metal sources cannot be documented. However, it is proposed that stage III jasperoids contain a significant magmatic-derived metal component, essentially the result of upward intrusion and mixing of hot magmatic-

derived fluids into a large meteoric convective cell. Deposition of stages I and II jasperoids continued within lower temperature regions peripheral to the silver deposit on the flanks of the Taylor anticline.

Silicification and deposition of disseminated sulfides took place under boiling conditions. Thermal maturation of indigenous organic matter evolved  $\text{CH}_4$ ,  $\text{C}_2\text{H}_6$ , and  $\text{C}_3\text{H}_8$ . Reactions between organic molecules and water produced  $\text{H}_2$  by the reaction (Fournier, 1985a):



Metals carried in sulfide complexes were precipitated according to the reaction (Fournier, 1985a):



The  $\text{HSO}_4^-$  was partitioned into the vapor phase. Excess  $\text{H}^+$  buffered the solution to acidic pH, thus maintaining calcite solubility and depressing silica solubility. Active tectonism produced rapid shifts in confining pressures, thereby effecting changes in rates of wall rock reaction at the microscopic scale, reflected in the hypidiomorphic and brecciated textures in stage III jasperoids.

Isotherms continued to move up and out.

Ultimately, as the hydrothermal system sustained high temperatures over a sufficient time interval, the indigenous organic material was consumed, and lost its ability to buffer the system. Boiling ceased due to diminished volatile supplies. Solution pH rapidly rose through the loss of  $\text{CO}_2$  and drastic increases in  $a_{\text{cation}^+}/a_{\text{H}^+}$  ratios. Deposition of jasperoid ceased, and was superceded by deposition of open space stage IV sulfide-calcite-(silica) veins and breccia fillings. Kaolinite-dominated alteration gave way to a montmorillonite + carbonate alteration assemblage.

Silver deposition took place in the Guilmette Formation, below the Pilot Shale contact. While it is true that tectonic breccias in the Guilmette focussed hydrothermal fluids, it is noteworthy that silicified Pilot within 30 feet of one of the most intensely mineralized fault intersections in the district [in the Argus Pit] contains fractions of an ounce Ag/ton up to less than 2 oz/ton.

A modified Buchanan (1981) model is proposed to explain the relationship between silver deposition at Taylor and gold mineralization in the Pilot Shale (and equivalent Webb Formation) at Alligator Ridge and Rain. Deposition of metals is related to level of boiling, not necessarily of water, but specifically of organic-derived volatiles. Silver and base metals are deposited below the Pilot Shale contact in a region of gentle effervescence. Base metal content increases below the level of silicification (high-grade ores mined by Silver King in 1966 and 1967 at depth through the Taylor shaft contained 58 oz Ag/ton and 4.2% base metals (Wise and Banghart, 1970), in contrast to higher grade siliceous ores which run 12 oz Ag/ton with only 2000 ppm base metals). Since the Pilot Shale contains more organic material than the Guilmette, it can be reasonably inferred that intensity of boiling sharply increases at the contact. Gold, Sb, As, and Ba are deposited in the region of stronger boiling in the Pilot Shale. Gold grades are highest just above the contact and decrease up section at both Alligator and Rain. Gold deposits at Alligator Ridge and Rain both occur on the flanks of anticlines, and may be zoned away from a thermal center. At each of these deposits (Ilchik, 1984; Klessig, 1984; Knutsen and West, 1984), and at Carlin (Radtke, 1981, 1984), late stage fluids shifted to strongly oxidizing, and

deposited alunite and barite. This shift may have occurred when the indigenous organic material was consumed, and could no longer maintain a low Eh. Partitioning of  $\text{HSO}_4^-$  into the vapor phase simultaneously lowered the pH in regions of condensation in the upper portions of the systems, stabilizing barite, alunite, and jarosite. In contrast to the Guilmette, the Pilot contains a significant indigenous pyrite component, which would also help maintain low Eh.

## REFERENCES CITED

- Anderson, R. Ernest, 1983, Cenozoic structural history of selected areas in the eastern Great Basin, Nevada-Utah: U.S. Geol. Survey Open-File Rept. 83-504, 49 p.
- Armstrong, Richard Lee, 1968, Sevier orogenic belt in Nevada and Utah: Geol. Soc. America Bull., v. 79, p. 429-458.
- Armstrong, Richard Lee, 1972, Low-angle (denudation) faults, hinterland of the Sevier Orogenic Belt, eastern Nevada and western Utah: Geol. Soc. America Bull., v. 83, p. 1729-1754.
- Armstrong, Richard Lee, 1974, Magmatism, orogenic timing, and orogenic diachronism in the cordillera from Mexico to Canada: Nature, v. 247, p. 348-351.
- Bagby, William C., and Berger, Byron R., 1985, Geologic characteristics of sediment-hosted disseminated precious-metal deposits in the western United States: Rev. Econ. Geology, v. 2, p. 169-202.
- Banghart, Roger C., 1966, Taylor mine progress report, with recommendations for 1967: unpub. report, Silver King Mines, Inc., 13 p.
- Bartley, J. M., Fryxell, J. E., Murray, M. E., and Wright, S. D., 1984, Patterns of Tertiary extension in the Great Basin exemplified in the Grant/Quinn Canyon Range, Nevada [abs.]: Geol. Soc. America Abstracts with Programs, v. 16, p. 438.
- Bartley, John M., and Wernicke, Brian P., 1984, The Snake Range decollement interpreted as a major extensional shear zone: Tectonics, v. 3, p. 647-657.
- Beane, Richard E., 1982, Hydrothermal alteration in silicate rocks: southwestern North America, in Titley, Spencer R., ed., Advances in Geology of the Porphyry Copper Deposits, Southwestern North America: Univ. of Arizona Press, Tucson, Arizona, p 117-138.
- Blackwell, D. D., Kelley, Share, and Reese, M., 1984, Fission track evidence on the late Cenozoic deformation of the Ruby Mountains, Nevada [abs.]: Geol. Soc. America Abstracts with Programs, v. 16, p. 446.

- Bodnar, R. J., and Kuehn, C. A., 1982, Effect of dissolved CO<sub>2</sub> on the estimated depths of formation of epithermal gold-silver deposits as calculated from fluid inclusion data: written commun., 49 p.
- Brokaw, A. L., and Shawe, D. R., 1965, Geologic map and sections of the Ely 3 SW Quadrangle, White Pine County, Nevada: U.S. Geol. Survey Misc. Geol. Investigations map, I-449, 1:24000.
- Brokaw, Arnold L., 1967, Geologic map and sections of the Ely Quadrangle, White Pine County, Nevada: U.S. Geol. Survey map, GQ-697, 1:24000.
- Buchanan, L. J., 1981, Precious metal deposits associated with volcanic environments in the southwest, in Dickinson, William R., and Payne, William D., eds., Relations of Tectonics to Ore Deposits in the Southern Cordillera: Arizona Geol. Soc. Digest, v. 14, p. 237-262.
- Cameron, Terry E., and Frost, Eric G., 1981, Regional development of major antiforms and synforms coincident with detachment faulting in California, Arizona, Nevada, and Sonora [abs.]: Geol. Soc. America Abstracts with Programs, v. 13, p. 421, 422.
- Cameron, Terry E., Frost, Eric G., and John, Barbara, 1981, Development of regional arches and basins and their relationship to Mid-Tertiary detachment faulting in the Chemehuevi Mountains, San Bernardino County, California, and Mojave County, Arizona [abs.]: Geol. Soc. America Abstracts with Programs, v. 13, p. 48.
- Compton, R. R., and Todd, V. R., 1983, Late Miocene displacement of cover rocks of the Raft River-Grouse Creek-Albion Mountains core complex, NW Utah [abs.]: Geol. Soc. America Abstracts with Programs, v. 15, p. 403.
- Coney, Peter J., 1974, Structural analysis of the Snake Range decollement: Geol. Soc. America Bull., v. 85, p. 973-978.
- Coney, Peter J., 1980, Cordilleran Metamorphic core complexes: an overview, in Crittenden, M.D.Jr., Coney, P.J., and Davis, G.H., eds., Cordilleran Metamorphic Core Complexes: Geol. Soc. America Memoir 153, p.7-31.
- Coney, Peter J., and Harms, Tekla A., 1984, Cordilleran metamorphic core complexes: Cenozoic extensional relics of Mesozoic compression: Geology, v. 12, p. 550-554.
- Conway, Richard Dean, 1965, Structure and stratigraphy of a portion of the southern Schell Creek Range, White Pine County, Nevada: Unpub. M.S. thesis, Univ. of Washington, 63 p.
- Couch, B. F., and Carpenter, J. A., 1943, Nevada's metal and mineral production (1859-1940 inclusive): Nevada Univ. Bull. 37, Geol. and Mining Series 38, 159 p.

- Dickinson, W. R., 1981, Plate tectonic evolution of the southern cordillera, in Dickinson, W. R., and Payne, W. D., eds. Relations of Tectonics to Ore Deposits in the Southern Cordillera: Arizona geol. Soc. Digest, v. 14, p. 113-136.
- Drewes, Harold, 1962, Stratigraphic and structural controls of mineralization in the Taylor mining district near Ely, Nevada: Geol. Survey Research, Short Papers in Geology, Hydrology, and Topography, Article 1, p. B1-B3.
- Drewes, Harold, 1964, Diverse recurrent movement along segments of a major thrust fault in the Schell Creek range near Ely, Nevada: Geol. Survey Research 1964, U.S. Geol. Survey Prof. Paper 501-B, p. B20-B24.
- Drewes, Harold, 1967, Geology of the Conners Pass Quadrangle, Schell Creek Range, east-central Nevada: U.S. Geol. Survey Prof. Paper 557, 93 p.
- Erickson, Einar C., 1964, New silver ore discoveries in the Taylor mining district, White Pine County, Nevada: unpub. rept., Silver King Mines, Inc., 40 p.
- Foock, Thomas D., 1977, Sheep Pass (Cretaceous? to Eocene) in east-central Nevada--Implications for petroleum exploration [abs.]: Am. Assoc. Petroleum Geologists Bull., v. 61, p. 1378.
- Fournier, Robert O., 1985a, Silica minerals as indicators of conditions during gold deposition, in Tooker, Edwin W., ed., Geologic Characteristics of Sediment- and Volcanic-Hosted Disseminated Gold Deposits- Search for an Occurrence Model: U.S. Geol. Survey Bull. 1646, p. 15-26.
- Fournier, R. O., 1985b, The behavior of silica in hydrothermal solutions, in: Rev. Econ. Geology, v. 2, p. 45-61.
- Fournier, R. O., 1985c, Carbonate transport and deposition in the epithermal environment, in: Rev. Econ. Geology, v. 2, p. 63-72.
- Fryxell, Joan E., 1984, Structural geology of the west-central Grant Range, Nye County, Nevada [abs.]: Geol. Soc. America Abstracts with Programs, v. 16, p. 514.
- Gans, P. B., Clark, D. H., Miller, E. L., Wright, J. E., and Sutter, J. F., 1986, Structural development of the Kern Mts, and N. Snake Range [abs.]: Geol. Soc. America Abstracts with Programs, v. 18, p. 108.
- Gans, P. B., Miller, E. L., McCarthy, J., and Ouldcott, M. L., 1985, Tertiary extensional faulting and evolving ductile-brittle transition zones in the northern Snake Range and vicinity: new insights from seismic data: Geology, v. 13, p. 189-193.

- Gans, Phillip B., 1982, Geometry of Mid-Tertiary extensional faulting, northern Egan Range, east-central Nevada [abs.]: Geol. Soc. America Abstracts with Programs, v. 14, p. 165.
- Glazner, Allen F., and Bartley, John M., 1984, Timing and tectonic setting of Tertiary low-angle normal faulting and associated magmatism in the southwestern United States: Tectonics, v. 3, p. 385-396.
- Greybeal, F. T., 1981, Characteristics of disseminated silver deposits in the western United States, in Dickinson, W. R., and Payne, W. D., eds., Relations of Tectonics to Ore Deposits in the Southern Cordillera: Arizona Geol. Soc. Digest, v. 14, p. 271-282.
- Haas, J. L., Jr., 1971, The effect of salinity on the maximum thermal gradient of a hydrothermal system at hydrostatic pressure: Econ. Geol. v. 66, p. 940-946.
- Hague, Arnold, 1870, Geology of the White Pine district [White Pine County, Nevada]: U.S. Geol. Explor. 40th Parallel (King), v. 3, p. 409-444.
- Havenstrite, Stuart R., 1983, Geology and ore deposits of the Taylor mining district, White Pine County, Nevada, in papers given at the precious-metals symposium, Sparks, Nevada, November 17-19, 1980: Nevada Bur. Mines Geology, Rept. 36, p. 14-26.
- Heck, F. R., Demets, D. C., and Speed, R. C., 1984, Reactivation of Mesozoic thrusts as normal faults, Humbolt Range, north-central Nevada [abs.]: Am. Assoc. Petroleum Geologists Bull., v. 68, p. 938.
- Hill, J. M., 1916, Notes on some mining districts in eastern Nevada: U.S. Geol. Survey Bull. 648, 214 p.
- Hill, R. H., Adrian, B. M., Bagby, W. C., Bailey, E. A., Goldfarb, R. J., and Pickthorn, W. J., 1986, Geochemical data for rock samples collected from selected sediment-hosted disseminated precious-metal deposits in Nevada: U.S. Geol. Survey Open-File Rept. 86-107, 30 p.
- Hofstra, A.H., Landis, G.P., and Rowe, W.A., 1987, Sediment-hosted disseminated gold mineralization at Jerritt Canyon, Nevada. IV. Fluid geochemistry [abs.]: Geol. Soc. America Abstracts with Programs, v. 19, p. 704.
- Hose, Richard K., and Blake, M. C., 1976, Part I: Geology, in Geology and mineral resources of White Pine Co., Nevada, Nevada Bur. Mines Geology Bull. 85, p. 1-35.
- Hose, Richard K., and Whitebread, Donald H., 1983, Tertiary phases of extensional tectonism in the Snake Range, east-central Nevada [abs.]: Geol. Soc. America Abstracts with Programs, v. 15, p. 384.

- Humphrey, F. L., 1960, Geology of the White Pine mining district, White Pine County, Nevada: Nevada Bur. Mines Geology Bull. 57, 119 p.
- Ilchik, Robert Paul, 1984, Hydrothermal maturation of indigenous organic matter at the Alligator Ridge Gold Deposits, Nevada: unpub. M.S. thesis, Univ. California at Berkeley, 48 p.
- Ilchik, Robert Paul, Brimhall, George H., and Schull, H. Walter, 1986, Hydrothermal maturation of indigenous organic matter at the Alligator Ridge gold deposits, Nevada: Econ. Geol., v. 81, p. 113-130.
- Jordan, T. E., Allmendinger, R. W., and Miller, D. M., 1983, Known and inferred Mesozoic deformation, hinterland of the Sevier Belt, northwestern Utah [abs.]: Geol. Soc. America Abstracts with Programs, v. 15, p. 319.
- Kellogg, Harold E., 1959, Stratigraphy and structure of the southern Egan Range, Nevada: unpub. Ph.D. thesis, Columbia Univ., p.
- Kellogg, Harold E., 1963, Paleozoic stratigraphy of the southern Egan Range, Nevada: Geol. Soc. America Bull., v. 74, p. 685-708.
- Kellogg, Harold E., 1964, Cenozoic stratigraphy and structure of the southern Egan Range, Nevada: Geol. Soc. America Bull., v. 75, p. 949-968.
- Klessig, P. J., 1984, History and geology of the Alligator Ridge gold mine, White Pine County, Nevada, in Wilkins, Joe Jr., ed., Gold and Silver Deposits of the Basin and Range Province Western U.S.A.: Arizona Geol. Soc. Digest, v. 15, p. 77-88.
- Knutsen, Gale C., and West, Perry W., 1984, Geology of the Rain disseminated gold deposit, Elko County, Nevada, in Wilkins, Joe Jr., ed., Gold and Silver Deposits of the Basin and Range Province Western U.S.A.: Arizona Geol. Soc. Digest, v. 15, p. 73-76.
- Kuehn, Carl A., 1984, P-T-X characteristics of fluids associated with the Carlin sediment-hosted gold deposit [abs.]: Geol. Soc. America Abstracts with Programs, v.16, p. 566.
- Lawrence, Edmond F., 1963, Antimony deposits of Nevada: Nevada Bur. Mines Geology Bull. 61, 248 p.
- Lee, Donald E., Marvin, Richard F., Stern, T. W., and Peterman, Zell E., 1970, Modification of potassium-argon ages by Tertiary thrusting in the Snake Range, White Pine County, Nevada: U.S. Geol. Survey Prof. Paper 700-D, p. D92-D102.
- Lincoln, F. C., 1923, Mining districts and mineral resources of Nevada: Nevada Newsletter Publishing Co.

- Lovering, T. G., 1972, Jasperoid in the United States-its characteristics, origin, and economic significance: U.S. Geol. Survey Prof. Paper 710, 164 p.
- Lovering, T. G., and Heyl, A. V., 1974, Jasperoid as a guide to mineralization in the Taylor mining district and vicinity near Ely, Nevada: Econ. Geol., v. 69, p. 46-58.
- Lund, Karen, and Beard, L. S., 1986, Structural history of the northern Grant Range, east-central Nevada: overprinting of structural styles [abs.]: Geol. Soc. America Abstracts with Programs, v. 18, p. 392.
- Matti, Jonathan Clarke, 1978, Depositional history of Middle Paleozoic carbonate rocks deposited at an ancient continental margin, central Nevada: unpub. Ph.D. thesis, Stanford Univ., 485 p.
- McDowell, Fred W., and Kulp, J. Lawrence, 1967, Age of intrusion and ore deposition in the Robinson Mining district of Nevada: Econ. Geol., v. 62, p. 905-909.
- Miller, Calvin F., and Bradfish, Larry J., 1980, An inner cordilleran belt of muscovite-bearing plutons: Geology, v. 8, p. 412-416.
- Miller, D. M., 1983, Mesozoic metamorphism and low-angle faults in the hinterland of Nevada linked to Sevier-Belt thrusts [abs.]: Geol. Soc. America Abstracts with Programs, v. 15, p. 644.
- Miller, David M., and Hoggatt-Hillhouse, Wendy C., 1983, Geometry and age of Cenozoic low-angle faults, Pilot Range, Utah and Nevada [abs.]: Geol. Soc. America Abstracts with Programs, v. 15, p. 403.
- Miller, E. L., 1983, Mesozoic vs. Cenozoic ductile deformation in the hinterland of the Sevier Thrust Belt [abs.]: Geol. Soc. America Abstracts with Programs, v. 15, p. 319.
- Miller, E. L., Bol, A. J., Gans, P. B., Miller, M. M., Mortimer, N., and Rowles, L. D., 1982, Structural and stratigraphic relationships between lower and upper plate rocks of the Snake Range decollement, northern Snake Range, east-central Nevada [abs.]: Geol. Soc. America Abstracts with programs, v. 14, p. 216.
- Miller, E. L., Gans, P. B., and Wright, J. E., 1986, Metamorphic history of the east-central Basin and Range Province: tectonic setting and relationship to magmatism [abs.]: Geol. Soc. America Abstracts with Programs, v. 18, p. 158.

- Misch, Peter, 1960, Regional structural reconnaissance in central-northeast Nevada and some adjacent areas: observations and interpretations, in *Geology of east-central Nevada: Intermountain Assoc. Petroleum Geologists, 11th Annual Field Conf., 1960 Guidebook*, p. 17-42.
- Misch, Peter, 1983, Development of tectonic concepts in the Snake Range Belt, central E. Nevada to S. Idaho [abs.]: *Geol. Soc. America Abstracts with Programs*, v. 15, p. 317.
- Moore, E. M., Scott, R. B., and Lumsden, W. W., 1968, Tertiary tectonics of the White Pine-Grant Range region, east-central Nevada, and some regional implications: *Geol. Soc. America Bull.*, v. 79, p. 1703-1726.
- Newman, Gary W., 1978, Eocene structuring in east-central basin and range [abs.]: *Am. Assoc. Petroleum Geologists Bull.*, v. 62, p. 890.
- Osmond, J. C. Jr., 1954, Dolomites in Silurian and Devonian of east-central Nevada: *Am. Assoc. Petroleum Geologists Bull.*, v. 38, p. 1911-1956.
- Radtke, Arthur S.; Rye, Robert O.; and Dickson, Frank W., 1981, Geology and stable isotope studies of the Carlin gold deposit, Nevada: *Econ. Geol.*, v. 75, p. 641-672.
- Radtke, A. S., 1985, Geology of the Carlin gold deposit, Nevada: *U.S. Geol. Survey Prof. Paper 1267*, 124 p.
- Roberts, R. J., 1942, Manganese deposits in the Nevada district, White Pine County, Nevada: *U.S. Geol. Survey Bull.* 931-M, p. 295-318.
- Roberts, Robert J., and Crittenden, M. D., 1973, Orogenic mechanisms, Sevier Orogenic Belt, Nevada and Utah, in Dejong, K.A., and Scholten, R., eds., *Gravity and Tectonics*: New York, John Wiley and Sons, p. 409-428.
- Rehrig, William A., 1986, Processes of regional Tertiary extension in the western Cordillera: Insights from the metamorphic core complexes: *Geol. Soc. America Spec. Paper 208*, p. 97-122.
- Rodgers, David, 1983, Structural evolution of the southern Deep Creek Range, Utah [abs.]: *Geol. Soc. America Abstracts with Programs*, v. 15, p. 319.
- Rodgers, David W., 1986, Thermal history of the Deep Creek Range, Nv-Ut, and implications for cordilleran tectonics [abs.]: *Geol. Soc. America Abstracts with Programs*, v. 18, p. 177.

- Shawe, D. R., Poole, F. G., and Heyl, A. V., 1978, Geologic framework of the cordilleran region traversed by field excursion C-1 in eastern Nevada and western Utah, in Shawe, Daniel R., ed., Guidebook to mineral deposits of the central Great Basin: Nevada Bur. Mines Geology, Rept. 32, p. 3-9.
- Smith, Roscoe M., 1970, Treasure Hill reinterpreted: Econ. Geol., v. 65, p. 538-540.
- Smith, Roscoe M., 1976, Part II: Mineral Resources, in: Geology and mineral resources of White Pine County, Nevada: Nevada Bur. Mines Geology Bull. 85, p. 36-105.
- Snoke, Arthur W., 1983, Problems concerning superimposed Mesozoic and Cenozoic tectonism in the hinterland of the Sevier Orogenic Belt-- a viewpoint from the Ruby Mountains-East Humboldt Range-Wood Hills, Nevada [abs.]: Geol. Soc. America Abstracts with Programs, v. 15, p. 319.
- Snoke, Arthur W., McCall, Rosemary G., and McKee, Edwin H., 1983, Tertiary stratigraphy and structure in the northern East Humboldt Range, Nevada--a clue to Cenozoic regional tectonic patterns [abs.]: Geol. Soc. America Abstracts with Programs, v. 15, p. 403.
- Snoke, A. W., Dallmeyer, R. D., and Fullagar, P. D., 1984, Superimposed Tertiary mylonitization on a Mesozoic metamorphic terrane, Ruby Mountains-East Humboldt Range, Nevada [abs.]: Geol. Soc. America Abstracts with Programs, v. 16, p. 662.
- Speed, R. C., and Sleep, N. H., 1982, Antler orogeny and foreland basin: a model: Geol. Soc. America Bull., v. 93, p. 815-828.
- Spencer, A. C., 1917, The geology and ore deposits of Ely, Nevada: U.S. Geol. Survey Prof. Paper 96, 189 p.
- Stewart, John H., 1980a, Geology of Nevada: Nevada Bur. Mines Geology, Spec. Pub. 4, 136 p.
- Stewart, John H., 1980b, Regional tilt patterns of Late Cenozoic basin-range fault blocks, western United States: Geol. Soc. America Bull., Part 1, v. 91, p. 460-464.
- Stewart, John H., Moore, William J., and Zietz, Isidore, 1977, East-west patterns of Cenozoic igneous rocks, aeromagnetic anomalies, and mineral deposits, Nevada and Utah: Geol. Soc. America Bull., v. 88, p. 67-77.
- Walker, C. Trevor, Dennis, John G., and Lumsden, William W., 1984, Mechanism of low-angle detachment faulting near Ely, Nevada [abs.]: Geol. Soc. America Abstracts with Programs, v. 16, p. 685.

- Whitebread, Donald H., 1966, Snake Range decollement and related structures in the southern Snake Range, eastern Nevada [abs.]: Geol. Soc. America Spec. Paper 101, p. 345-346.
- Whitehill, H. R., 1875, Biennial report of the state mineralogist of Nevada for the years 1873 and 1874: Carson City, Nevada.
- Wilkins, Joe, Jr., 1984, The distribution of gold- and silver-bearing deposits in the Basin and Range Province, Western United States, in: Wilkins, Joe, Jr., editor, Gold and silver deposits of the Basin and Range Province Western U.S.A., Arizona Geol. Soc. Digest, v. XV, p. 1-27.
- Wise, Joseph P., and Banghart, Roger C., 1970, Taylor Mining district progress report January 31, 1970, with recommendations: unpub. rept., Silver King Mines, Inc., 23 p.
- Young, A. R., 1966, Measured section of the Devonian Guilmette Formation, Schell Creek Range, White Pine County, Nevada: unpub. rept., Phillips Petroleum Company.
- Young, J. C., 1960, Structure and stratigraphy in the north-central Schell Creek Range, eastern Nevada: unpub. Ph.D. thesis, Princeton Univ.

## APPENDIX I

## WHOLE ROCK DATA

	Sample #						
	13	19	172 a	172 b	172 c	172 d	172 e
SiO <sub>2</sub>	74.37	74.62	71.19	73.59	71.74	74.27	71.67
Al <sub>2</sub> O <sub>3</sub>	13.06	12.71	16.59	13.01	12.92	12.73	15.15
Fe <sub>2</sub> O <sub>3</sub>	0.29	0.10	0.48	0.23	0.31	0.05	0.77
FeO	0.48	0.48	0.48	0.36	0.24	0.36	0.24
CaO	1.19	0.44	1.87	2.08	2.47	1.71	1.56
MgO	0.52	0.20	2.53	0.50	0.31	0.31	1.73
Na <sub>2</sub> O	1.87	1.19	0.68	0.94	1.00	0.81	1.08
K <sub>2</sub> O	4.83	5.79	2.57	5.01	4.81	4.76	4.07
TiO <sub>2</sub>	0.07	0.05	0.08	0.06	0.06	0.06	0.07
MnO	0.06	0.05	0.01	0.07	0.08	0.05	0.01
P <sub>2</sub> O <sub>5</sub>	0.01	0.01	0.02	0.00	0.01	0.01	0.05
BaO	0.02	0.06	0.01	0.01	0.01	0.01	0.01
Cr <sub>2</sub> O <sub>3</sub>	0.01	0.02	0.01	0.02	0.01	0.02	0.01
ZrO <sub>2</sub>	0.01	0.01	0.01	0.01	0.01	0.01	0.01
CuO	0.00	0.00	0.00	0.00	0.00	0.00	0.01
LOI	1.49	1.14	3.91	2.75	2.90	2.79	2.70
TOTAL	98.30	96.91	100.48	98.68	96.91	98.10	98.17

APPENDIX II

FLUID INCLUSION DATA

QUARTZ

Sample # 69: collected from Antimony Pit jasperoid.

	Th (a) °C	appear °C	Th (b) °C	appear °C	Th (c) °C	appear °C	approx. size	comments
1	122	100	124	99.9	123	99.8	5 $\mu\text{m}$ X 14 $\mu\text{m}$	two phase along growth plane possible secondary
2	110	89.4	110.5	89.7	111	89.1	5 $\mu\text{m}$ X 18 $\mu\text{m}$	two phase along growth plane possible secondary
3	226	142	229	134	229	133.4	3.6 $\mu\text{m}$ X 9 $\mu\text{m}$	fourth trial: Th = 230
4	265	181	265.5	181.3	267	183	3 $\mu\text{m}$ X 11 $\mu\text{m}$	three phase primary
5	185	-	183	125	183	-	3.6 $\mu\text{m}$ X 5 $\mu\text{m}$	primary/secondary ???
6	143.8	61	144	-	-	-	14 $\mu\text{m}$ X 14 $\mu\text{m}$	possibly necked down
7	235	-	234.8	202	236	-	1 $\mu\text{m}$ X 3.5 $\mu\text{m}$	
8	257	-	258	231	258	-	2 $\mu\text{m}$ X 7 $\mu\text{m}$	
9	283	224	287	226	287.3	-	1 $\mu\text{m}$ X 2.9 $\mu\text{m}$	about 5% vapor
10	311	-	310.6	280	310	-	3 $\mu\text{m}$ X 4.3 $\mu\text{m}$	about 5% vapor
11	321	286.5	318.5	-	-	-	18 $\mu\text{m}$ X 15 $\mu\text{m}$	about 15% vapor
12	330	-	329.4	295	327	-	18 $\mu\text{m}$ X 9 $\mu\text{m}$	about 15% vapor
13	GT 350	-	GT 350	-	LT 354	318	10 $\mu\text{m}$ X 22 $\mu\text{m}$	about 20% vapor
14	238.6	195	240.5	-	240.6	-	6 $\mu\text{m}$ X 10 $\mu\text{m}$	about 10% vapor
15	214.5	175	219	174.4	218	-	2 $\mu\text{m}$ X 5 $\mu\text{m}$	
16	233	195.6	232.6	-	-	-	2 $\mu\text{m}$ X 3 $\mu\text{m}$	
17	242	202	243	-	-	-	2 $\mu\text{m}$ X 4 $\mu\text{m}$	
18	246.4	188.2	247.6	191.8	248.4	-	5 $\mu\text{m}$ X 7 $\mu\text{m}$	
19	255.5	-	256.8	-	256.7	-	4 $\mu\text{m}$ X 7 $\mu\text{m}$	
20	LT 204	-	GT 200	-	-	-	?	vapor-dominated; homogenized to a vapor.
21	284	250	283	-	-	-	1.5 $\mu\text{m}$ X 3 $\mu\text{m}$	
22	296	261	295.8	-	-	-	2 $\mu\text{m}$ X 4 $\mu\text{m}$	
23	309	266	306.8	-	-	-	6 $\mu\text{m}$ X 14 $\mu\text{m}$	
24	239	198.5	239.6	197.5	239.9	-	2 $\mu\text{m}$ X 4 $\mu\text{m}$	
25	248.8	-	247.4	144.2	247.3	-	4 $\mu\text{m}$ X 9 $\mu\text{m}$	
26	GE 290	253	291.6	252	292.4	-	3 $\mu\text{m}$ X 4.7 $\mu\text{m}$	
27	LE 261	-	260	120.5	-	-	11 $\mu\text{m}$ X 18 $\mu\text{m}$	

QUARTZ (continued)

	Th (a) °C	appear °C	Th (b) °C	appear °C	Th (c) °C	appear °C	approx. size	comments
28	281	-	283	198.3	-	-	6 $\mu\text{m}$ X 10 $\mu\text{m}$	
29	GE 282	245	283	244	285	-	3 $\mu\text{m}$ X 5 $\mu\text{m}$	
30	311.8	275.5	312.1	275.3	312.4	-	8 $\mu\text{m}$ X 11.5 $\mu\text{m}$	
31	299.6	-	300	-	300.5	236	5 $\mu\text{m}$ X 10 $\mu\text{m}$	
32	GE 265	-	265.8	215	-	-	5 $\mu\text{m}$ X 18 $\mu\text{m}$	

FLUORITE

Sample # 25: collected from the Southwest Pit ore zone

	Th (a) °C	appear °C	Th (b) °C	appear °C	Th (c) °C	appear °C	approx. size	comments
1	239.4	222	239.5	-	239.4	-		all fluorite inclusions are two-phase liquid-dominated primaries less than 20 $\mu\text{m}$ .
2	228.5	214	228	215.4	228	-		
3	234	207	233.5	-	234.3	-		
4	234.5	209	234.2	210	234.3	-		
5	239.1	-	239	-	239	-		

SPHALERITE

Sample # 243: collected from vein in the Argus Pit.

	Th (a) °C	appear °C	Th (b) °C	appear °C	Th (c) °C	appear °C	approx. size	comments
1	GE 225	200	226	201	-	-	10 $\mu\text{m}$ X 18 $\mu\text{m}$	secondary
2	GE 190	142	LE 195	-	-	-	8 $\mu\text{m}$ X 18 $\mu\text{m}$	secondary
3	234	211.6	233.6	211.3	-	-	5 $\mu\text{m}$ X 18 $\mu\text{m}$	secondary
4	201	175	200	-	-	-	4 $\mu\text{m}$ X 11 $\mu\text{m}$	secondary
5	225	-	224.9	-	-	-	3 $\mu\text{m}$ X 7 $\mu\text{m}$	secondary
6	205	186.7	203.7	-	-	-	14 $\mu\text{m}$ X 29 $\mu\text{m}$	secondary
7	305	286	306	286	306	-	35 $\mu\text{m}$ X 76 $\mu\text{m}$	large primary
8	308.8	288.4	309	-	-	-	24 $\mu\text{m}$ X 40 $\mu\text{m}$	large three phase primary

## SPHALERITE (continued)

	Th (a) °C	appear °C	Th (b) °C	appear °C	Th (c) °C	appear °C	approx. size	comments
9	226.7	182	227	182	-	-	4 $\mu\text{m}$ X 6 $\mu\text{m}$	secondary
10	GE 216	183	218	183	GE 216	-	3 $\mu\text{m}$ X 7 $\mu\text{m}$	secondary
11	213	172	212	174.8	211	-	4 $\mu\text{m}$ X 7 $\mu\text{m}$	secondary
12	236	-	237	199	-	-	16 $\mu\text{m}$ X 27 $\mu\text{m}$	secondary
13	215	179	214	-	-	-	8 $\mu\text{m}$ X 36 $\mu\text{m}$	secondary
14	228	195	227	196	-	-	16 $\mu\text{m}$ X 36 $\mu\text{m}$	secondary
15	233.5	210 $\pm$	234	197	-	-	10 $\mu\text{m}$ X 25 $\mu\text{m}$	secondary
16	237 $\pm$	213 $\pm$	238 $\pm$	218	-	-	20 $\mu\text{m}$ X 36 $\mu\text{m}$	secondary
17	316.5	294	317	293.5	-	-	50 $\mu\text{m}$ X 380 $\mu\text{m}$	large primary
18	301	288	301.5	-	301.5	288.4	100 $\mu\text{m}$ X 500 $\mu\text{m}$	large primary
19	GE 300	287	?	287	302	-	100 $\mu\text{m}$ X 200 $\mu\text{m}$	large three phase primary
20	302.5	286	GE 301	287	GT 296	-	60 $\mu\text{m}$ X 110 $\mu\text{m}$	large three phase primary
21	307	296	307.3	296 $\pm$	-	-	30 $\mu\text{m}$ X 65 $\mu\text{m}$	large three phase primary
22	?	287.8	300	287	300.6	287	65 $\mu\text{m}$ X 150 $\mu\text{m}$	large primary

APPENDIX III

BONDAR-CLEGG ANALYTIC PROCEDURES

element	extraction	finish	lower limit	upper limit
Ag	Aqua regia	AA	0.1 ppm	50 ppm
As	Nitric-perchloric	Colourimetric	2 ppm	1000 ppm
Au	Fusion	AA	5 ppb	5000 ppb
B		Emission spec	1 ppm	
Ba		XRF	20 ppm	6000 ppm
Be	Mult acid tot dig	AA	0.5 ppm	
Bi	HNO <sub>3</sub>	AA	1 ppm	
Co	HNO <sub>3</sub> -HCL hot extr	AA	1 ppm	
Cr	HNO <sub>3</sub> -HCL hot extr	AA	2 ppm	
Cu	Aqua regia	AA	1 ppm	
F	Pot Hydroxide fusion	Specific Ion	20 ppm	20,000 ppm
Fe	HNO <sub>3</sub> -HCL hot extr	AA	0.05 %	
Hg	Aqua regia	AA	5 ppb	5000 ppb
La		XRF	5 ppm	
Li	HF-H <sub>2</sub> SO <sub>4</sub> -HCL	AA	1 ppm	
Mn	HNO <sub>3</sub> -HCL hot extr	AA	1 ppm	
Mo	HNO <sub>3</sub> -HCL hot extr	AA	1 ppm	
Nb		XRF	5 ppm	
Ni	HNO <sub>3</sub> -HCL hot extr	AA	1 ppm	
Pb	Aqua regia	AA	2 ppm	
Rb		XRF	5 ppm	
S	LECO induct. furnace	LECO	0.01 %	
Sb		XRF	2 ppm	2000 ppm
Se	multi acid tot dig	Colourimetric	1 ppm	
Sn		XRF	5 ppm	
Sr		XRF	5 ppm	
Ta		XRF	3 ppm	
Te	HBr-Br <sub>2</sub> -MIBK	AA	0.2 ppm	
Th		Neutron activ.	1 ppm	
Ti	Multi acid-MIBK	AA	0.5 ppm	
TiO <sub>2</sub>		XRF	0.01 %	
Tl	spec. technique	AA	0.5 ppm	
U (f1)	HNO <sub>3</sub>	Fluorometric	0.2 ppm	
V	Mult acid tot dig	AA	2 ppm	
W	Carbonate sinter	Colourimetric	2 ppm	
Y		XRF	5 ppm	
Zn	Aqua regia	AA	1 ppm	

APPENDIX IV

DRILL HOLE GEOCHEM DATA

Depth (ft)	Taylor Drill Hole D-1									
	Ag oz/ton	Au ppm	Sb ppm	As ppm	Cu ppm	Pb ppm	Zn ppm	Hg ppm	Tl ppm	Ba ppm
10-15	1.60	0.060	166	18	90	126	835	+ 5.0	- 0.5	220
15-20	2.34	0.055	114	9	53	139	355	+ 5.0	- 0.5	230
20-25	2.10	0.075	82	6	67	76	500	+ 5.0	- 0.5	210
25-30	1.58	0.065	94	14	75	153	830	+ 5.0	- 0.5	210
30-35	3.16	0.080	127	9	83	156	1370	+ 5.0	- 0.5	200
35-40	2.96	0.085	117	13	120	174	500	+ 5.0	- 0.5	190
40-45	2.24	0.145	39	11	100	108	545	3.25	- 0.5	160
45-50	3.90	0.160	80	12	111	163	870	+ 5.0	- 0.5	190
50-55	6.72	0.365	48	8	131	174	785	+ 5.0	- 0.5	180
55-60	7.98	0.385	101	14	136	284	790	+ 5.0	- 0.5	190
60-65	15.04	0.380	140	14	125	317	770	+ 5.0	- 0.5	190
65-70	10.86	0.260	46	6	113	126	665	+ 5.0	- 0.5	160
70-75	10.06	0.260	51	6	116	137	655	+ 5.0	- 0.5	190
75-80	2.82	0.120	30	5	126	182	1200	+ 5.0	- 0.5	200
80-85	2.04	0.125	35	7	158	211	1180	+ 5.0	- 0.5	200
85-90	1.24	0.045	18	6	71	121	520	4.85	- 0.5	200
90-95	1.00	0.060	11	5	34	80	260	3.80	- 0.5	200
95-100	0.68	0.065	3	10	61	64	176	1.55	- 0.5	500
100-105	1.04	0.070	9	11	18	60	310	1.10	- 0.5	210
105-110	1.04	0.100	11	12	20	73	301	2.10	- 0.5	200
110-115	1.34	0.065	12	8	21	120	255	3.50	- 0.5	190

Depth (ft)	Ag oz/ton	Au ppm	Taylor Drill Hole D-1 (continued)							
			Sb ppm	As ppm	Cu ppm	Pb ppm	Zn ppm	Hg ppm	Tl ppm	Ba ppm
115-120	1.34	0.130	15	13	18	84	295	1.80	- 0.5	210
120-125	2.08	0.100	21	13	33	163	430	3.60	- 0.5	200
125-130	4.34	0.190	65	17	66	358	945	+ 5.0	- 0.5	190
130-135	8.84	0.155	101	40	129	810	3110	+ 5.0	- 0.5	160
135-140	1.04	0.105	13	48	29	238	1110	1.50	- 0.5	200
140-145	0.36	0.020	3	5	12	109	347	0.80	- 0.5	200
145-150	0.40	0.020	2	5	8	118	420	0.50	- 0.5	210

Depth (ft)	Ag oz/ton	Au ppm	Taylor Drill Hole D-7							
			Sb ppm	As ppm	Cu ppm	Pb ppm	Zn ppm	Hg ppm	Tl ppm	Ba ppm
3-10	0.49		136	18						
10-15	0.38		51	19						
15-20	0.30		49	16						
20-25	0.43		20	15						
25-30	1.35		1180	60						
30-35	1.21		665	61						
35-40	0.84		453	24						
40-45	8.02		2000	72						
45-50	3.74		1900	150						
50-55	0.99		550	103						
55-60	0.56		156	18						
60-65	0.32		82	12						

Depth (ft)	Taylor Drill Hole D-9									
	Ag oz/ton	Au ppm	Sb ppm	As ppm	Cu ppm	Pb ppm	Zn ppm	Hg ppm	Tl ppm	Ba ppm
10-15	0.61	0.015	98	61	21	47	128			
15-20	0.97	0.015	49	12	23	59	415			
20-25	8.16	0.085	357	16	71	300	1810			
25-30	11.18	0.095	354	47	113	470	915			
30-35	7.68	0.120	407	15	78	366	675			
35-40	3.01	0.055	201	17	76	140	1010			
40-45	2.87	0.055	149	12	52	132	825			
45-50	2.38	0.055	102	13	65	136	800			
50-55	4.96	0.125	394	18	89	270	2010			
55-60	7.49	0.140	1240	23	112	306	1960			
60-65	10.05	0.155	870	44	183	490	1720			
65-70	10.24	0.175	2200	47	243	384	3720			
70-75	8.24	0.180	2900	47	158	380	4560			
75-80	1.18	0.030	379	13	26	76	935			
80-85	3.15	0.065	955	27	64	281	1750			
85-90	5.49	0.085	1800	51	98	376	2640			
90-95	0.26	0.005	19	8	10	44	150			
95-100	0.57	0.005	49	13	25	103	385			
100-105	0.14	0.005	- 2	4	9	11	62			

Depth (ft)	Taylor Drill Hole D-10									
	Ag oz/ton	Au ppm	Sb ppm	As ppm	Cu ppm	Pb ppm	Zn ppm	Hg ppm	Tl ppm	Ba ppm
10-20	0.25	0.080	293	40	37	22	149			
20-30	0.50	0.060	214	28	46	64	287			
30-35	17.81	0.470	246	+ 1000	32	970	90			
35-45	1.25	0.075	1450	21	65	148	302			
45-50	25.78	0.590	535	+ 1000	68	1690	224			
50-60	1.89	0.190	201	47	45	162	290			
60-70	2.02	0.100	395	58	61	212	415			
70-80	1.17	0.110	195	28	64	99	760			
80-90	8.01	0.305	520	590	125	710	515			
90-100	24.22	0.680	1140	720	490	3020	1460			
100-110	17.99	0.700	370	+ 1000	71	1350	197			
110-120	8.87	0.335	314	600	97	695	695			
120-130	1.14	0.065	41	56	23	80	320			
130-140	3.35	0.145	111	12	47	127	775			
140-150	8.74	0.355	237	18	77	208	935			
150-160	1.95	0.135	160	15	31	105	445			
160-170	2.88	0.190	152	46	51	137	625			
170-185	1.02	0.055	68	17	20	90	315			
185-195	6.36	0.320	117	+ 1000	32	810	96			
195-210	0.21	0.055	4	10	10	28	176			
210-215	11.34	0.980	174	650	28	515	605			

Depth (ft)	Ag oz/ton	Au ppm	Taylor Drill Hole D-10 (continued)					Zn ppm	Hg ppm	Tl ppm	Ba ppm
			Sb ppm	As ppm	Cu ppm	Pb ppm					
215-230	2.04	0.095	101	25	22	115	244				
230-235	8.71	0.140	450	80	60	385	555				
235-240	16.93	0.135	452	160	73	154	43				
240-245	1.40	0.220	203	120	44	77	109				
245-255	4.66	0.460	13	40	25	38	35				

Depth (ft)	Ag oz/ton	Au ppm	Taylor Drill Hole D-14					Zn ppm	Hg ppm	Tl ppm	Ba ppm
			Sb ppm	As ppm	Cu ppm	Pb ppm					
3-10	0.25	0.035	24	38							
10-15	0.31	0.035	22	15							
15-20	0.28	0.025	15	13							
20-25	0.81	0.030	31	18							
25-30	1.05	0.040	179	18							
30-35	1.57	0.040	145	32							
35-40	7.25	0.090	1500	35							
40-45	33.06	0.120	1750	60							
45-50	18.61	0.200	2200	100							
50-55	11.39	0.115	1260	90							
55-60	4.69	0.080	156	35							
60-65	3.94	0.090	211	70							
65-68	15.89	0.070	1080	70							

Depth (ft)	Taylor Drill Hole SKT-304									
	Ag oz/ton	Au ppm	Sb ppm	As ppm	Cu ppm	Pb ppm	Zn ppm	Hg ppm	Tl ppm	Ba ppm
0-10	1.34		141	25						
10-20	2.51		139	18						
20-30	3.85		372	22						
30-40	3.18		197	18						
40-50	4.39		80	8						
50-60	1.00		54	23						
60-70	2.16		30	18						
70-80	0.34		9	6						
80-90	0.38		11	8						
90-100	0.51		25	13						
100-110	0.64		36	13						
110-120	0.21		13	7						
120-130	0.04		9	7						

APPENDIX V

SURFACE ROCK CHIP GEOCHEM DATA

## Rock Chip Samples

## TAYLOR PROJECT

J.M. Edwards

Colorado State Univ., 1988

Sample number	North Coord.	East Coord.	Ag oz/t	Au ppm	Sb ppm	As ppm	Cu ppm	Pb ppm	Zn ppm	Lithology	Material sampled	Comments
H 1a,1b	96,906	98,477								Mj	Weathered outcrop	bxa MJ adjacent to fault contact with Mc.
HG 2	95,973	98,535	0.02							TP	Prospect dump	Quartz-eye rhyolite Porphyry.
G 3	95,901	98,902	0.13	0.255	97	46				Sb-jasp	Prospect pit	Dark grey jasp bxa with calcite matrix. Porphyry fragments.
G 4	96,872	98,974	0.05	0.010	14	25				Mc	Weathered outcrop	Silicified (?) Mc silts and shales. Grey to black weathering.
G 5	97,709	98,031	0.05	0.010	5	42				MDp	Prospect dump	Yellow to tan weathering. Apparently unaltered.
HG 6	97,633	98,107	0.01							TP	Prospect pit	Clay-sericite argillization with yellow and orange Fe-ox.
HG 7	97,884	98,616	0.01							TP	Prospect dump	Argillized with some Qtz veining.
G 8	97,780	99,010	0.05							TP	Prospect dump	Dike cuts MJ. Brecciated at contacts. No silicification.
HG 9	98,167	99,188	Tr							TP	Weathered outcrop	
G 10	97,327	99,005	Tr							TP	Prospect dump	Dike intrudes Mc silts.
HG 11	96,259	98,343	0.035	0.020	7	8				MDp	Prospect dump	Silicified MDp. Thinly laminated. Weathers black/tan/orange/red.
G 12a	95,360	98,538	Tr	0.015	18	80				MDp	Weathered outcrop, fl	Silicified, locally bxa. Possible stibiconite.
G 12b	95,393	98,526	0.025							TP	fl in catcut	Brecciated.
H 13	95,227	97,854								TP	Catcut	Relatively fresh porphyry. (See #79)
HG 14	95,086	95,903	0.04	0.010	L 2	14				MDp	Prospect pit and dump	Silicified, moderately Fe stained. Local bxa.
HG 15	98,453	97,037	1.82	0.025	135	44	181	277	595	Sb (?) Jasp	Prospect dump	Jasp bxa in H.W. of prominent North-South fault.

## Rock Chip Samples

## TAYLOR PROJECT

J.M. Edwards

Colorado State Univ., 1988

Sample number	North Coord.	East Coord.	Ag oz/t	Au ppm	Sb ppm	As ppm	Cu ppm	Pb ppm	Zn ppm	Lithology	Material sampled	Comments
HG 16	98,937	97,386	Tr		11	98	42	15	47	Tp	H.W. Argus pit	Locally silicified, strongly pyritized (10-15% py).
G 17	98,805	97,249	0.135	0.020	L 2	4				Alt Dgc	F.W. Argus pit	Shattered, partially silicified Ls. Possible Sb-oxide.
HG 18a	102,307	97,701	Tr	0.140	G 10,000	105	67	20	237	Sb-jasp	Prospect dump	Dark grey jasp replaces "barren" jasp along fault.
HG 19	102,127	96,496	0.07		72	4	21	17	49	Tp	Weathered outcrop	Feldspar phenos argillized. Otherwise fresh.
HG 20		Taylor 350 level	0.41	0.135	21	53	40	79	620	Calcite veining	Rib	Veining along N5E80SE. Contains quartz, calcite, limonite.
HG 21		Taylor 350 level	6.63	0.110	520	58	136	530	960	Karst bxa	Rib	Banded calcite matrix around Ls fragments.
H 22		Taylor 350 level								Qtz veining	Rib	Veining along N48E80SE structure.
H 23	101,426	97,038								MDp	Weathered outcrop	Carbonaceous siltstone. Possibly silicified.
H 24	97,749	96,558								Sb-jasp	Southwest pit	Fluorite bearing jasp.
H 25	98,550	96,250								Sb-jasp	Southwest pit	Fluorite bearing jasp.
H 26	98,754	97,482								CC/Qtz/Sulf. veining	Argus pit	Qtz-calcite-tetrahedrite-sphalerite (?) veining along N50E fault.
H 27		Taylor 130 level								Sulfides (oxidized)	Rib	Oxidized Galena (?), Tetrahedrite. NNE structure.
H 28		Taylor 350 level								Karst bxa	Rib	Qtz-calcite-fluorite banded fragment (?) in Karst breccia.
HG 29a	100,636	96,635	0.10	0.035	54	17	26	29	34	Alt Dgt	Weathered outcrop	Unaltered Ls fragments in a brown weathering altered matrix.
HG 29b	100,644	96,650	Tr	0.050	29	19	47	47	12	Sb-jasp	Weathered outcrop	Dark grey, brown weathering jasp.
HG 30a		east of map	Tr							"barren" jasp	Weathered outcrop	Tenaceous. Weathers light brown, orange to maroon.

## Rock Chip Samples

## TAYLOR PROJECT

J.M. Edwards

Colorado State Univ., 1988

Sample number	North Coord.	East Coord.	Ag oz/t	Au ppm	Sb ppm	As ppm	Cu ppm	Pb ppm	Zn ppm	Lithology	Material sampled	Comments
HG 30b		east of map	Tr							Sb-jasp	Weathered outcrop	Outcrop noticeably more broken up or shattered than 30a. Weathers brown.
HG 31		east of map	Tr							Sb-jasp	Prospect pit	Sb rich dark grey jasp cutting; veining "barren" light grey or tan jasp.
G 32	101,473	98,702	Tr							Mc	Prospect dump	Thinly laminated black, carbonaceous, calcareous silts, shales, ls.
G 33	100,310	99,987	0.025							Mc	Prospect pit	Weakly silicified silts. Trace bright orange Fe-ox.
HG 34	99,031	96,878	4.915							Sb-jasp	Bishop stope	Dark grey jasp. bxa.
HG 35	99,048	96,900	7.37							Sb-jasp	Bishop stope	Dark grey jasp. bxa.
H 36		east of map area								alt Dgc	Prospect dump	Samples show gradation from ls to jasp. Trace Cu-ox.
G 53	99,512	98,328	0.54	0.040	15	41				Mc	Weathered outcrop	Grey to dark grey silicified silts.
G 54	100,467	98,366	0.54	0.255	495	50	142	18	173	Sb-jasp	Prospect pit	Dark grey jasp fragments in breccia with light grey jasp and alt Mj fragments.
G 55	100,641	98,377	0.04	0.265	49	99	64	58	24	blue-grey jasp	Prospect pit and dump	Yellow Fe-ox (jarosite), on fractures.
HG 56	100,517	98,947	0.08							Tp	Weathered outcrop	
G 62	96,156	99,960	0.04							Mc	Weathered outcrop	Thinly laminated black shales.
HG 63	96,288	99,549	0.32							Tp	Weathered outcrop	Propylitized with trace epidote.
HG 64a	95,175	99,323	0.06	0.240	10,000	52	42	11	45	Sb-jasp	Weathered float	Dark grey jasp, weathers medium grey. Stibiconite casts after stibnite.
HG 64b	95,175	99,324	0.10	0.090	4,000	88	76	7	20	"barren" jasp	Weathered float	Medium to light grey. More tenaceous than 64a. Red hematite staining.
G 65	95,089	99,608	0.22							Mc	Prospect dump	Black shale.

## Rock Chip Samples

## TAYLOR PROJECT

J.M. Edwards

Colorado State Univ., 1988

Sample number	North Coord.	East Coord.	Ag oz/t	Au ppm	Sb ppm	As ppm	Cu ppm	Pb ppm	Zn ppm	Lithology	Material sampled	Comments
HG 66	94,892	98,978	Tr	0.280	G 10,000	45	68	11	168	Sb-jasp	Prospect pit	Stibiconite rich, dark grey jasp. Post jasp bxa. Generation of Qtz porphyroblasts.
HG 67	94,843	98,527	0.08	0.045	100	18				alt Mj	Weathered outcrop	Appears to be coarser grained than fresh Mj. Weathers orange to brown.
G 68	95,037	98,780	0.08	0.210	212	82				MDp	Catcut	Silicified siltstone. Red, orange Fe-"rings" where weathered.
G 69	95,448	98,862	0.10	0.245	G 10,000	63	57	7	30	Sb-jasp	Prospect pit and dump	Dark grey, stibnite, stibiconite rich jasp. Some Qtz porphyroblasts.
HG 70	95,393	98,819	0.25		146	960	41	39	83	Tp	Prospect dump	Argillized with trace epidote. Possible silicification along fractures.
HG 71	97,379	97,534	0.06	0.005	182	32				MDp	Catcut	Partially silicified thinly laminated silts.
G 72	97,394	97,546	0.16	0.005	35	9				Dgt	Weathered outcrop	Weakly altered, near fault contact with MDp (#71).
G 73	97,182	97,454	0.04	0.010	151	65				MDp	Catcut	Maroon weathering, thinly laminated, fissile shale. (silicified?)
HG 74	96,925	97,398	0.22	0.090	900	50	59	12	107	Sb-jasp	Weathered outcrop	Fault bxa. Dark grey jasp with stibnite casts.
G 75	95,718	97,522	0.08	0.265	6000	65	76	15	112	Sb-jasp	Prospect dump	Dark grey with stibnite casts. Post jasp bxa with calcite matrix.
HG 76	95,702	97,662	0.19	0.300	92	40				alt Mj	Prospect dump	Qtz porphyroblasts, stibnite casts. Brown, orange, red Fe-ox stain.
G 77	95,714	97,691	0.16	0.095	2600	25	53	9	45	Sb-jasp	Prospect dump	Medium grey, shattered. Probable stibnite casts thoroughly oxidized.
HG 78	95,958	97,678	0.38	0.650	G 10,000	70	132	18	61	Sb-jasp	Prospect pit and dump	Sb rich jasp with strong white to tan to yellow oxide.
HG 79	95,856	97,980	0.10		13	L 2	47	4	17	Tp	Weathered outcrop	Relatively fresh rhyolite porphyry.
HG 80	95,209	98,065	Tr	L 0.005	73	15				MDp	Weathered outcrop	Silicified (?).
H 81	95,657	99,399								Mc	Weathered float	Silicified.

## Rock Chip Samples

## TAYLOR PROJECT

J.M. Edwards

Colorado State Univ., 1988

Sample number	North Coord.	East Coord.	Ag oz/t	Au ppm	Sb ppm	As ppm	Cu ppm	Pb ppm	Zn ppm	Lithology	Material sampled	Comments
G 82	97,275	97,393	0.08	0.540	83	600				MDp	Catcut	Silicified.
HG 83	96,767	97,188	0.04	0.010	11	35				MDp	Catcut	Weakly silicified. Some calcite veined bxa.
HG 84	96,044	96,979	0.09	0.205	2000	50	112	14	54	Sb-jasp	Prospect pit and dump	Well oxidized, medium to dark grey. Possible stibnite casts.
HG 85	95,683	96,812	0.02	L 0.005	5	30	98	5	12	Sb-jasp	Weathered outcrop	Dark grey. Possible stibnite casts.
G 86	95,400	96,974	0.06	0.045	154	20	82	9	51	Mix jasp	Weathered outcrop	Mixed light and dark grey jasp fragments in bxa.
HG 87	95,471	97,617	0.08	0.085	440	25	46	7	257	"barren" jasp	Weathered outcrop	Tenaceous, light grey jasp.
HG 88	95,475	97,617	0.08	0.140	308	25	59	5	47	Sb(?) -jasp	Weathered outcrop	Mixed jasp bxa. This sample a medium to dark grey separate.
HG 89	95,286	97,556	0.11	1.000	540	35	64	8	7	"barren" (?) jasp	Weathered outcrop	Mixed jasp bxa. This sample a light grey separate.
G 90	97,974	97,630	0.05	0.015	4	25	13	16	10	alt Dgt	Catcut	Weak to moderately altered silty sedimentary bxa.
G 91	97,940	97,587	0.78	0.025	35	15	34	30	140	alt Dgt	Catcut	Moderately altered sedimentary bxa.
G 92	97,924	97,541	0.04	0.020	8	15	8	20	14	alt Dgt	Catcut	Moderately altered sedimentary bxa.
G 93	97,915	97,518	0.23	0.010	395	20	17	20	26	alt Dgt	Catcut	Moderately to strongly altered.
G 94	97,904	97,667	0.08	L 0.005	3	15	23	10	4	alt Dgt	Catcut	Weak to moderate alteration.
G 97	97,819	97,817	Tr	0.005	2	25	20	13	26	MDp	Prospect dump	Carbonaceous, calcareous silts.
G 98	97,852	97,883	0.05	0.005	L 2	15	13	13	19	MDp	Prospect dump	Carbonaceous, calcareous silts.
G 100	97,789	98,002	0.18	0.010	14	75	27	17	56	MDp	Prospect dump	Carbonaceous, calcareous silts.

## Rock Chip Samples

## TAYLOR PROJECT

J.M. Edwards

Colorado State Univ., 1988

Sample number	North Coord.	East Coord.	Ag oz/t	Au ppm	Sb ppm	As ppm	Cu ppm	Pb ppm	Zn ppm	Lithology	Material sampled	Comments
G 101	97,698	97,471	0.67	0.030	124	40	120	121	320	alt Dgt	Prospect pit	Strongly altered, partially silicified Ls bxa.
G 102	97,880	97,423	0.82	0.010	3	L 2	25	33	117	Dgc	Weathered outcrop	Apparently unaltered, massive Ls.
G 103	97,872	97,399	0.28	0.015	L 2	2	23	20	214	Dgc	Catcut/ Weathered outcrop	Weakly altered (?) Dgc. Possibly a sedimentary bxa (?).
G 104	97,864	97,345	0.04	0.010	L 2	L 2	9	13	14	Dgc	Weathered outcrop	Unaltered, massive Ls.
G 105	97,835	97,300	0.08	0.005	L 2	L 2	17	17	15	Dgc	Weathered outcrop	Unaltered, massive Ls.
G 107	97,803	97,210	0.02	0.010	4	20	7	10	6	alt Dgc	Catcut	Moderately altered Dgc Ls (in H.W. of prominent N-S fault).
G 108	97,785	97,164	Tr	0.005	13	80	28	16	68	MDp	Catcut	Strongly sheared silts.
G 109	97,702	97,083	0.04	0.005	11	70	42	21	86	MDp	Roadcut	Silts.
G 111	97,732	96,918	Tr	0.005	L 2	20	8	8	12	Dgt	Catcut	Weakly altered (?) Dgt Ls.
G 113	97,670	96,780	0.06							Dgt	Weathered outcrop/ catcut	Weakly altered.
G 114	97,641	96,743	A Tr B 0.0175	L 0.005	L 2	7	7	27	26	alt Dgt	Catcut	Weak to moderate alteration.
G 115	97,657	96,685	A 0.04 B 0.0087	L 0.005	L 2	7	6	20	17	alt Dgt	Catcut	Weak to moderate alteration of patchy outcrops in catcuts.
HG 118	97,504	96,584	A 0.30 B 0.251	0.015	378	80	67	176	765	alt Dgt	Prospect pit	~20% Ls fragments in strongly altered, partially silicified brown to tan weathering matrix.
HG 119	97,451	96,552	A 0.25 B 0.1225	0.020	24	35	28	86	366	alt Dgt	Prospect pit	Strongly altered, partially silicified, brown to tan weathering.
G 120	97,406	96,449	A 0.31 B 0.729	0.015	43	25	41	84	288	alt Dgt	Prospect pit	Strongly altered, brown weathering, red Fe-ox.
G 121	97,383	96,491	0.06							Dgt	Catcut	Patchy, well weathered outcrops of alt Ls.

## Rock Chip Samples

## TAYLOR PROJECT

J.M. Edwards

Colorado State Univ., 1988

Sample number	North Coord.	East Coord.	Ag oz/t	Au ppm	Sb ppm	As ppm	Cu ppm	Pb ppm	Zn ppm	Lithology	Material sampled	Comments
HG 122	97,342	96,453	A 2.70 B	0.020	159	35	27	70	211	Sb-jasp	Prospect pit	Fault bxa consisting of dark grey jasp fragments in white calcite matrix.
HG 124	97,283	96,380	A 0.04 B 0.1021	0.005	9	55	17	22	43	MDp	Roadcut	Carbonaceous siltstones.
H 125	98,354	97,309								Dgc	Weathered outcrop	Massive Dgc sedimentary rip-up breccia.
H 126	98,054	97,609								Dgt	Catcut	Dgt silty limestone rip-up breccia.
HG 127	99,009	97,869	A Tr B 0.0146	L 0.005	L 2	7				MDp	Prospect dump	Dark grey carbonaceous, weakly calcareous. Possibly partially silicified.
G 128	99,457	97,922	A 0.04 B 0.0292	L 0.005	7	30				MDp	Prospect pit	Carbonaceous, weakly (locally) calcareous, thinly laminated silts, shales. Silicified (?)
HG 129	99,480	97,440	A 0.04 B 0.035	0.015	10	38	9	22	49	Sb-jasp	Catcut	Weathers dark grey with maroon-brown staining.
HG 130	99,490	97,438	A Tr B 0.0262	0.010	8	135	10	25	27	"barren" jasp	Catcut	Weathers light grey with rust-orange staining.
HG 131	99,559	97,433	A 0.06 B 0.0058	L 0.005	6	L 2	2	13	34	Glass porph	Catcut	Black glass matrix, partially altered green.
HG 133	Taylor 350	Shaft level	0.04							Sheared Ls	Rib	Grab from shear in Dgb dipping 25° NNE. Strong mobilized organic carbon.
HG 134	Taylor 350	Shaft level	16.54							Calcite	Rib	Banded dark/white calcite matrix in Karst bxa.
HG 135	Taylor 350	Shaft level	0.78							Karst bxa	Rib	Banded calcite matrix with Ls fragments.
HG 136	Taylor 350	Shaft level	0.08							Plumose calcite	Rib	"Plumose" calcite as matrix with upper Dgb quartzite fragments.
HG 137	Taylor 350	Shaft level	1.42							Clay fault gouge	Rib	Orange, clay rich fault gouge.
H 138	Taylor 350	Shaft level								dk calcite	Rib	Dark grey to black calcite.
G 139	99,863	97,390	A Tr B 0.035	0.025	23	30	9	19	133	Sb-jasp	Prospect dump	Dark grey to black on fresh surfaces.

## Rock Chip Samples

## TAYLOR PROJECT

J.M. Edwards

Colorado State Univ., 1988

Sample number	North Coord.	East Coord.	Ag oz/t	Au ppm	Sb ppm	As ppm	Cu ppm	Pb ppm	Zn ppm	Lithology	Material sampled	Comments
HG 140	99,865	97,433	A 0.08 B 0.0437	0.030	11	45				alt Dgc	Prospect dump	Strongly altered, partially silicified ls. Weathers brown to tan.
G 141	99,853	97,534	A Tr B 0.0233	L 0.005	3	50				MDp	Catcut	Carbonaceous, calcareous silts. Minor calcite veining.
HG 142	98,397	98,986	A 0.12 B 0.0175	0.165	1600	300	20	23	254	MDp	Sb-pit	Sheared/shattered siltstones.
HG 143	98,424	99,035	1.90							Stibnite	Sb-pit	Selective grab of stibnite.
HG 144	98,417	99,015	A 0.58 B 0.496	0.700	G 10,000	90	32	17	405	Sb-jasp	Sb-pit	30 ft. grab coarse stibnite rich jasp.
HG 145	98,418	99,085	A Tr B 0.0204	0.020	272	46	8	14	40	Mc	Sb-pit	Organic detrital, silty, carbonaceous ls. Some interbedded silts.
HG 146	98,444	99,271	A 0.04 B 0.0146	L 0.005	94	38				Mc	Catcut	Carbonaceous silts. Minor silty ls.
HG 147	99,144	99,757	0.14							Tp	Weathered outcrop	Possibly more basic phase, such as diabase.
G 148	99,255	99,861	Tr							Mc	Weathered outcrop, fl	Thinly laminated black shale.
HG 149	100,172	99,828	0.04							Mc	Weathered outcrop	Maroon, orange weathering, Quartzite, yellow jarosite on fresh surfaces.
HG 150	99,321	98,319	A 0.10 B 0.035	0.085	168	10	5	17	9	"barren" jasp	Weathered outcrop	Light grey to white jasp, weathers orange, maroon.
HG 151	99,263	98,318	A 0.10 B 0.0379	0.065	271	55	10	13	24	Sb-jasp	Weathered outcrop	Medium grey with some stibnite casts.
HG 152	99,238	98,602	A 0.12 B 0.0729	0.920	2100	90	9	23	71	mixed (?) jasp	Weathered outcrop	Stibnite casts.
HG 153	99,063	98,487	A Tr B 0.0117	0.005	26	35				Mc	Prospect dump	Silicified thinly laminated shale. Locally bxa, weathers maroon and medium grey.
HG 154	98,906	98,800	A 0.18 B 0.236	1.010	G 10,000	100	15	16	228	Sb-jasp	Weathered outcrop	Medium to dark grey fresh surfaces. Brown weathering. Stibnite casts.
HG 155	98,819	98,818	A 0.14 B 0.0846	1.030	660	160	10	14	49	MDp (?)	Weathered outcrop	Silicified, MDp silt.

## Taylor Project

J.M. Edwards  
CSU, 1988

Sample number	Hg ppm	Tl ppm	Ba ppm
HG 142b	3.950	2.0	500
HG 144b	G 5.00	1.5	11,000
HG 145b	0.900	L 0.5	340
HG 154b	G 5.00	2.0	560
HG 155b	4.400	0.5	310

## Rock Chip Samples

## TAYLOR PROJECT

J.M. Edwards

Colorado State Univ., 1989

Sample number	North Coord.	East Coord.	Ag oz/t	Au ppm	Sb ppm	As ppm	Cu ppm	Pb ppm	Zn ppm	Lithology	Material sampled	Comments
HG 156	98,452	99,302	A Tr B 0.0117		123	200	65	32	60	Tp	Roadcut	
G 157	98,129	99,353	Tr							Mc	Roadcut	Tan weathering carbonaceous silts. Local calcite veining.
G 158	98,060	99,375	A Tr B 0.0117	0.015	80	10				Mc	Roadcut	Grey to dark grey silicified shales, silts.
HG 159	97,709	99,105	A Tr B 0.0176	0.015	38	5				Mc	Weathered outcrop	Silicified (?) laminated shales, silts.
HG 160	97,015	98,497	A Tr B 0.0233	L 0.005	25	L 2				Mc	Weathered outcrop	Silicified (?), tan to red to grey weathering shales, silts.
HG 161	98,691	97,346	5.50							Dgc and jasp bxa	Argus pit	Largely in F.W. of low angle mineralized bxa. Some jasp-calcite, bxa included.
HG 162	99,222	96,362	A 3.74	0.030	1400	15	31	198	87	"barren" jasp	Weathered outcrop	Light grey to white weathering.
G 163	99,200	96,326	A 3.31	0.040	970	25	52	366	176	mixed (?) jasp	Weathered outcrop	Mixed light grey and dark grey jasp.
HG 164	99,192	96,269	A 3.20	0.060	990	30	62	351	232	Sb-jasp	Weathered outcrop	Medium to dark grey on fresh surfaces. Weathers brown.
G 165	99,187	96,237	A 1.70	0.045	288	40	84	122	505	Sb-jasp	Weathered outcrop	Medium to dark grey. Brown weathering.
G 166	99,161	96,161	2.40							Sb-jasp	Catcut	Dark grey.
HG 167	99,157	96,104	A 2.06	0.060	122	25	25	75	137	alt Dgc (?)	Catcut	Partially silicified, local strong calcite veining.
HG 168	99,276	95,866	A 0.26 B 0.184	0.020	15	30				alt Dgb (?)	Roadcut	Strongly altered, partially silicified. Tan to brown weathering.
G 169	99,219	95,778	A 0.12 B 0.035	0.045	6	70				MDp	Recent mine cut	Sheared calcareous siltstones.
HG 174	99,120	95,682	A 0.28 B 0.0233	L 0.005	11	35				MDp	Recent mine cut	Carbonaceous, weakly calcareous tan weathering siltstone.
HG 175	99,086	95,700	A 0.10 B 0.0525	0.010	16	70	12	20	64	MDp	Recent mine cut	Moderate to strong calcite veining.

Taylor Project

J.M. Edwards  
CSU, 1988

Sample number	Hg ppm	Tl ppm	Ba ppm
HG 162b	2.550	0.5	220
G 163b	G 5.00	1.0	200
HG 164b	G 5.00	2.0	200
G 165b	0.195	L 0.5	270
HG 167b	1.100	L 0.5	200
HG 175b	0.305	L 0.5	440

## Rock Chip Samples

## TAYLOR PROJECT

J.M. Edwards

Colorado State Univ., 1988

Sample number	North Coord.	East Coord.	Ag oz/t	Au ppm	Sb ppm	As ppm	Cu ppm	Pb ppm	Zn ppm	Lithology	Material sampled	Comments
G 176	99,107	95,845	A 0.22 B 0.0496	0.005	126	65	14	19	85	MDp	Recent mine cut	Silts with some Ls interbeds. Moderate calcite veining.
HG 177	99,133	96,013	0.18							alt Dgc (?)	Recent catcut	Strongly altered.
G 178	99,146	96,038	A 1.66 B 1.283	0.060	136	25	25	79	214	alt Dgc (?)	Weathered outcrop	Strongly altered. Partially silicified.
G 180	99,899	96,662	1.15	0.035	75	30				alt Dgc	Prospect dump	Altered, partially silicified (dark grey jasp).
HG 181	102,200	97,020	0.31	0.055	8	100				MDp	Prospect pit	Silicified, folded silts.
HG 182	101,659	97,279	0.17	0.005	5	10				MDp	Weathered outcrop	Carbonaceous silts with pyrite. Possibly partially silicified.
H 183	100,510	97,392								Tp	Weathered outcrop	Relatively fresh porphyry.
G 184	100,556	97,498	0.19	0.015	12	60	58	13	66	Sb-jasp	Weathered outcrop	Medium to dark grey on fresh surfaces.
HG 185	101,097	96,873	2.08	0.010	3	30				alt Dgt	Prospect pit	Altered, partially silicified Ls.
H 186	97,413	95,967								Dg ss	Weathered outcrop	Sandstone at base of Dg slide block.
HG 187	97,618	95,972	0.14	0.075	15	250				MDp	Prospect pit	Silicified and sheared silts.
H 188	96,525	96,253								Dg ss	Weathered outcrop	Dg quartzite bxa.
HG 189	96,578	96,587	0.14	L 0.005	13	10				MDp	Weathered outcrop	Brecciated, silicified silts.
G 190	97,017	96,425	0.19	0.010	L 2	30				MDp	Catcut	Carbonaceous, possibly weakly silicified silts.
HG 191	98,160	96,056	0.28	0.005	L 2	30				MDp	Recent mine cut	Carbonaceous, weakly calcite veined silts.
G 192	98,180	96,107	0.15	0.015	L 2	75				MDp	Recent mine cut	Carbonaceous, weakly calcite veined silts.



## Rock Chip Samples

## TAYLOR PROJECT

J.M. Edwards

Colorado State Univ., 1988

Sample number	North Coord.	East Coord.	Ag oz/t	Au ppm	Sb ppm	As ppm	Cu ppm	Pb ppm	Zn ppm	Lithology	Material sampled	Comments
HG 193	98,180	96,172	0.23	0.010	L 2	35				MDp	Recent mine cut	Silts with interbedded altered Ls. Moderate calcite veining.
HG 194	98,269	96,194	0.21	0.005	17	100				alt Dgt	SW pit	Carbonaceous siltstone with interbedded altered Ls.
HG 195	97,954	96,359	0.22	0.010	4	25				Dgt	SW pit	Carbonaceous, altered (?) Ls.
H 196	98,215	96,278								Marble Tp bxa	SW pit	Breccia composed of marble and Tp fragments.
HG 197	98,392	96,283	17.02	0.325	970	60				alt Dgt	SW pit	Partially silicified, carbonaceous Ls.
G 198	98,822	95,188	0.14	0.010	6	25				Mc	Recent catcut	Crushed, sheared, Fe-ox stained shales, silts.
H 199	100,352	94,193								Volcanic agglomerate	Weathered outcrop	White tuffaceous agglomerate.
H 200	100,349	94,080								Moderately welded tuff	Weathered outcrop	Pink, moderately welded tuff.
HG 201	100,120	95,523	4.04	0.060	285	25	74	184	276	Sb-jasp	Weathered outcrop	Dark grey on fresh surfaces, brown weathering.
HG 202	100,250	95,612	3.22	0.065	112	25	98	194	410	Sb-jasp	Prospect pit and dump	Dark grey jasp bxa, brown weathering.
G 203	99,084	95,390	0.18							Mc	Recent mine cut	Strongly sheared, maroon weathering, shales, silts.
HG 204	99,015	95,310	Tr	0.015	6	15				Mc	Recent mine cut	Quartzite.
G 205	98,994	95,257	0.16	0.005	L 2	10				Mc	Recent mine cut	Crushed silts with olive green and brown oxides.
G 206	98,968	95,574	0.19	0.005	4	95				MDp	Recent mine cut	Siltstone. Weak to locally strong calcite veining.
HG 207	100,128	96,058	0.18	0.010	11	60				alt (?) Dgb	Catcut	Mottled-brown-tan weathering. Moderate to strong calcite veining.
G 208	100,509	95,767	0.13	L 0.005	9	60				alt Dgb	Catcut	Altered Ls with some platy silt beds. Moderate calcite veining.

## Rock Chip Samples

## TAYLOR PROJECT

J.M. Edwards

Colorado State Univ., 1988

Sample number	North Coord.	East Coord.	Ag oz/t	Au ppm	Sb ppm	As ppm	Cu ppm	Pb ppm	Zn ppm	Lithology	Material sampled	Comments
G 209	101,192	96,042	0.54	0.025	78	140				alt Dgc	Prospect dump	Altered Ls bxa with calcite trace Cu-ox.
HG 210	101,578	95,631	2.42	0.025	3050	900				Silicified Dga	Prospect dump	Selective grab off dump of silicified Ls with Cu-ox.
HG 211	99,640	95,714	4.32	0.085	100	25				alt Dga	Weathered outcrop	Altered, partially silicified Ls.
HG 212	99,247	96,454	1.05	0.165	1240	15	86	169	82	"mixed"(?) jasp	Weathered outcrop	Brown weathering with red Fe-ox.
HG 213	99,249	96,483	1.36	0.045	192	10	76	102	78	"barren" jasp	Weathered outcrop	Light grey, red Fe-ox on weathered surfaces.
G 214	99,268	96,531	0.16	0.005	49	10	81	101	184	Tp	Catcut	Crushed, argillized. White to greenish.
HG 215	99,025	96,425	1.96	0.075	107	100	83	146	680	Sb-jasp	Prospect pit	Bxa composed of dark grey jasp fragments in a calcite matrix.
G 216	99,023	96,472	12.22	0.130	1650	100	1170	2130	3610	Sb-jasp	Old mine cut	Dark grey jasp bxa. Local calcite matrix. Yellow and rust Fe-ox.
G 217	99,015	96,532	4.50	0.025	350	55	2650	865	3470	alt Dgc	Old mine cut	Altered, partially silicified Ls. Trace Cu-ox.
HG 218	99,027	96,588	17.35	0.050	1930	400	3900	1580	2790	Sb-jasp	Old mine cut	Dark grey jasp bxa with calcite matrix. Cu-ox staining.
G 219	99,012	96,711	1.36	0.025	44	10	69	113	190	alt Dgc	Weathered outcrop	Weak alteration. Massive Ls. Minor calcite veining.
G 220	99,027	96,779	3.12	0.040	90	35	163	158	585	Sb-jasp	Weathered outcrop	Brown weathering.
HG 221	99,001	96,829	2.04	0.055	224	60	302	535	600	Sb-jasp	Weathered outcrop	Brown weathering.
HG 222	99,047	96,864	3.18	0.080	141	15	131	195	198	Sb-jasp	Weathered outcrop	Brown weathering.
G 223	99,040	96,943	2.86	0.080	134	26	189	285	292	Sb-jasp	Weathered outcrop	Brown weathering.
HG 224	99,039	96,994	3.16	0.040	107	15	84	238	38	blue-grey jasp	Weathered outcrop	Blue-grey weathering. Yellow Fe-ox coatings.

Taylor Project

J.M. Edwards  
CSU, 1988

Sample number	Hg ppm	Tl ppm	Ba ppm
HG 212	1.050	L 0.5	290
HG 213	G 5.000	L 0.5	210
G 214	0.200	L 0.5	280
HG 215	3.500	L 0.5	220
G 216	G 5.000	L 0.5	230
G 217	G 5.000	L 0.5	220
HG 218	G 5.000	5.5	210
G 219	4.150	L 0.5	200
G 220	G 5.000	L 0.5	230
HG 221	G 5.000	L 0.5	250
HG 222	G 5.000	L 0.5	220
G 223	G 5.000	L 0.5	200
HG 224	0.850	L 0.5	210

## Rock Chip Samples

## TAYLOR PROJECT

J.M. Edwards

Colorado State Univ., 1988

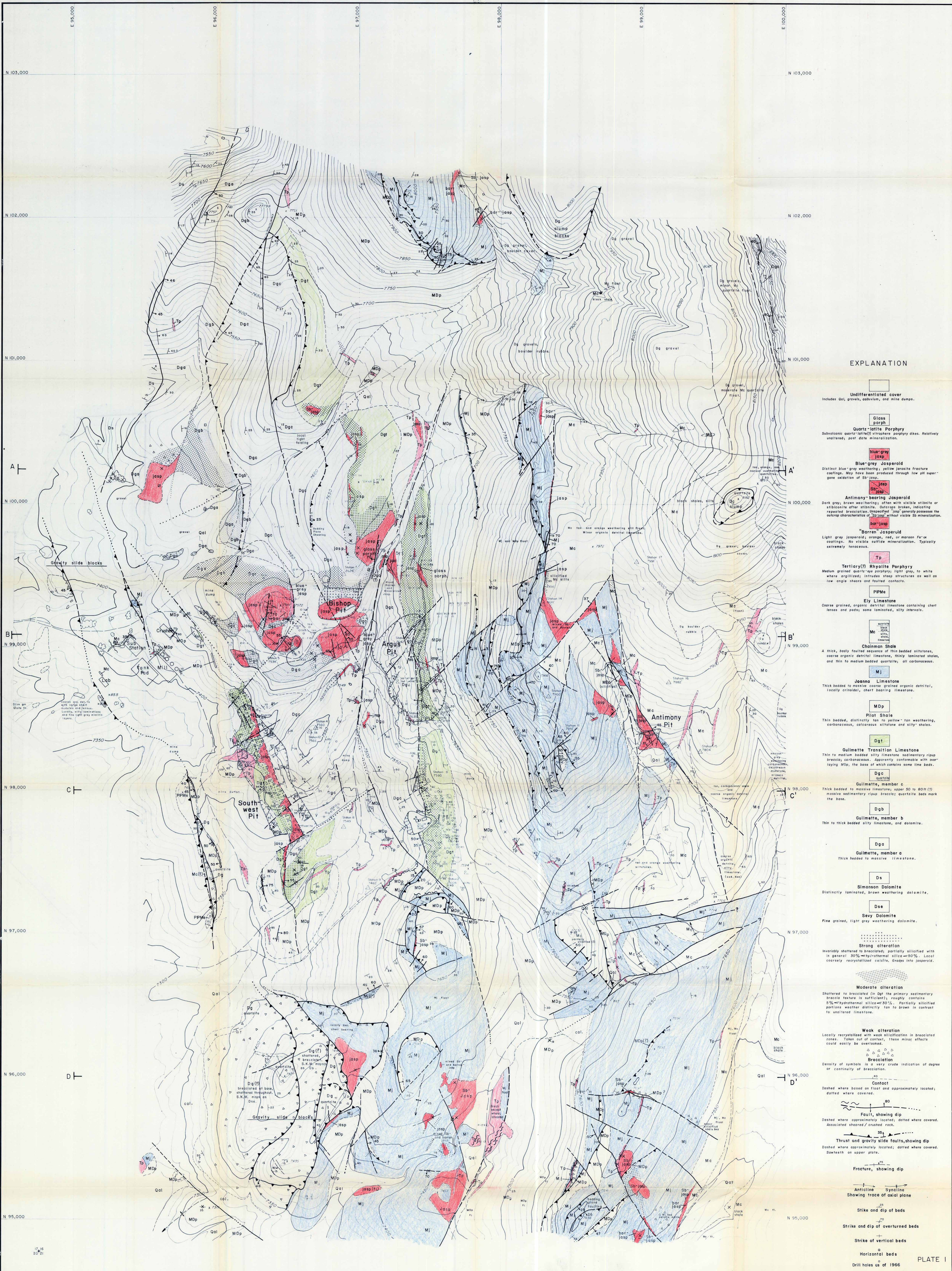
Sample number	North Coord.	East Coord.	Ag oz/t	Au ppm	Sb ppm	As ppm	Cu ppm	Pb ppm	Zn ppm	Lithology	Material sampled	Comments
HG 225	99,410	96,511	1.40	0.035	99	30	89	297	77	blue-grey jasp	Catcut	Blue-grey weathering, with yellow Fe-ox coatings.
HG 226	99,610	97,112	0.16	L 0.005	7	L 2	17	13	36	glass porph	Recent catcut	Black to dark green porphyry. Glass matrix.
HG 227	98,702	97,434	3.63	0.100	461	160	850	730	2650	lam. clay Karst	Argus pit	Tan/orange/red laminated clay, Karst infilling.
HG 228	98,797	97,513	0.16	0.005	67	G 1000	51	21	52	MDp	Argus pit	Crushed, sooty, carbonaceous siltstones along N50E structure.
HG 229	98,785	97,518	0.39	0.015	16	90	25	19	50	MDp	Argus pit	Crushed, oxidized (tan) siltstones in the same fault zone as #228.
HG 230	98,668	97,531	0.18	0.005	L 2	40	21	12	32	MDp	Argus pit	Black, carbonaceous silts. Weak to moderate calcite veining.
HG 231	98,693	97,526	1.87	0.015	31	55	101	53	386	MDp	Argus pit	Oxidized, yellow-tan silts. Weak to moderate calcite veining.
G 232	98,375	99,078	0.2799	0.215	G 10,000	100	26	5	234	Sb-jasp	Sb-pit	30 ft. chipgrab in stibnite rich jasp.
G 233	98,754	98,841	0.0787	0.365	367	90	15	17	139	Sb-jasp	Weathered outcrop	Brown weathering with stibnite casts.
G 234	99,673	97,649	0.0146	0.005	84	60				MDp	Catcut	Typical tan weathering silts.
G 235	98,650	97,467	1.341	0.065	235	65	515	1040	2490	Dgt bxa	Argus pit	Carbonaceous, brecciated Ls. Calcite matrix.
G 236	98,687	97,496	0.0408	0.005	38	25	20	24	47	MDp	Argus pit	Carbonaceous, sheared (bedding plane) silts.
G 237	98,712	97,512	0.0146	L 0.005	89	35	13	17	27	MDp	Argus pit	Carbonaceous, locally sheared silts.
G 238	98,736	97,529	0.0379	L 0.005	14	25	12	20	33	MDp	Argus pit	Carbonaceous, locally sheared silts.
G 239	98,771	97,552	0.146	0.005	46	130	20	42	62	MDp	Argus pit	Carbonaceous, sheared silts.
G 240	98,659	97,633	0.0321	L 0.005	20	50	20	25	76	MDp	Argus pit	Surface oxidized silts.

## Taylor Project

J.M. Edwards  
CSU, 1988

Sample number	Hg ppm	Tl ppm	Ba ppm
HG 227	G 5.000	L 0.5	450
HG 228	1.400	2.5	2200
HG 229	0.550	L 0.5	690
HG 230	0.350	L 0.5	5870
HG 231	0.850	L 0.5	1120
G 232	4.150	3.0	510
G 233	3.350	0.5	510
G 235	G 5.000	1.0	630
G 236	0.250	0.5	540
G 237	0.650	1.0	4000
G 238	0.265	0.5	530
G 239	0.900	1.0	520
G 240	0.450	1.0	510





**EXPLANATION**

- Undifferentiated cover**  
Includes Qal, gravel, cobble, and mine dumps.
- Glass Porphyry**  
Subvolcanic quartz-latte(?) vitrophyre porphyry dikes. Relatively unaltered, post date mineralization.
- Blue-grey Jasperoid**  
Distinct blue-grey weathering, yellow jarosite fracture coatings. May have been produced through low pH supergene oxidation of Sb-jasp.
- Antimony-bearing Jasperoid**  
Dark grey, brown weathering, often with visible stibnite or silibastite after stibnite. Outcrop broken, indicating repeated brecciation. Generally possesses the outcrop characteristics of Sb-jasp without visible Sb mineralization.
- Barren Jasperoid**  
Light grey jasperoid, orange, red, or brown fine-scale coatings. No visible sulfide mineralization. Typically extremely tenacious.
- Tertiary(?) Rhyolite Porphyry**  
Medium grained quartz-rye porphyry, light grey, to white where oxidized; intrudes steep structures as well as low angle shores and faulted contacts.
- Ely Limestone**  
Coarse grained, organic skeletal limestones containing chert lenses and pods; some laminated, silty intervals.
- Chimney Shale**  
A thick, body faulted sequence of thin bedded siltstones, coarse organic detrital limestone, thinly laminated shales, and thin to medium bedded quartzite, all carbonaceous.
- Joanna Limestone**  
Thick bedded to massive coarse grained organic detrital, locally crinoidal, chert bearing limestone.
- Pilot Shale**  
Thin bedded, distinctly lap to yellow-ton weathering, carbonaceous, calcareous siltstone and silty shales.
- Gulmette Transition Limestone**  
Thin to medium bedded silty limestone sedimentary ripple breccias, carbonaceous. Apparently continuous with overlying MDb, the base of which contains some lime beds.
- Gulmette, member a**  
Thick bedded to massive limestone upper 50 to 80 ft (?) massive sedimentary ripple breccias quartzite beds mark the base.
- Gulmette, member b**  
Thin to thick bedded silty limestone, and dolomite.
- Gulmette, member c**  
Thick bedded to massive limestone.
- Simmons Dolomite**  
Distinctly laminated, brown weathering dolomite.
- Sey Dolomite**  
Fine grained, light grey weathering dolomite.
- Strong alteration**  
Invariably shattered to brecciated; partially silicified with in general 30% hydrothermal silica=30%. Locally coarsely recrystallized calcite. Grades into jasperoid.
- Moderate alteration**  
Shattered to brecciated (in Dgt the primary sedimentary breccia texture is sufficient); roughly contains 5% hydrothermal silica=30%. Partially silicified portions weather distinctly tan to brown in contrast to unaltered limestone.
- Weak alteration**  
Locally recrystallized with weak silicification in brecciated zones. Taken out of context, these mineral effects could easily be overlooked.
- Brecciation**  
Density of symbols is a very crude indication of degree or continuity of brecciation.
- Contact**  
Dashed where based on float and approximately located; dotted where covered.
- Fault, showing dip**  
Dashed where approximately located; dotted where covered. Associated sheared/crushed rock.
- Thrust and gravity slide faults, showing dip**  
Dashed where approximately located; dotted where covered. Sawteeth on upper plate.
- Fracture, showing dip**
- Anticline Syncline**  
Showing trace of axial plane
- Strike and dip of beds**
- Strike and dip of overturned beds**
- Strike of vertical beds**
- Horizontal beds**

**PLATE I**

**1:2400 GEOLOGIC MAP**

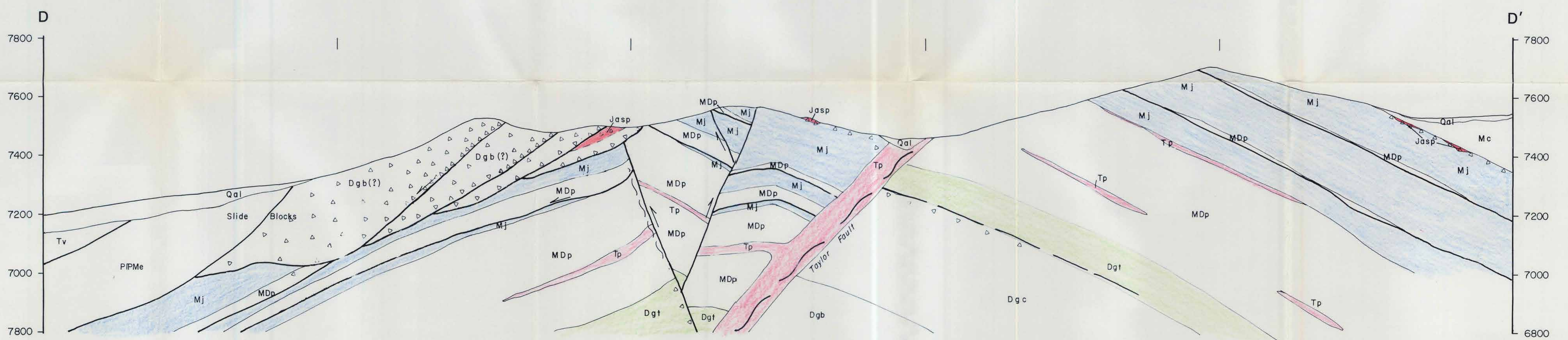
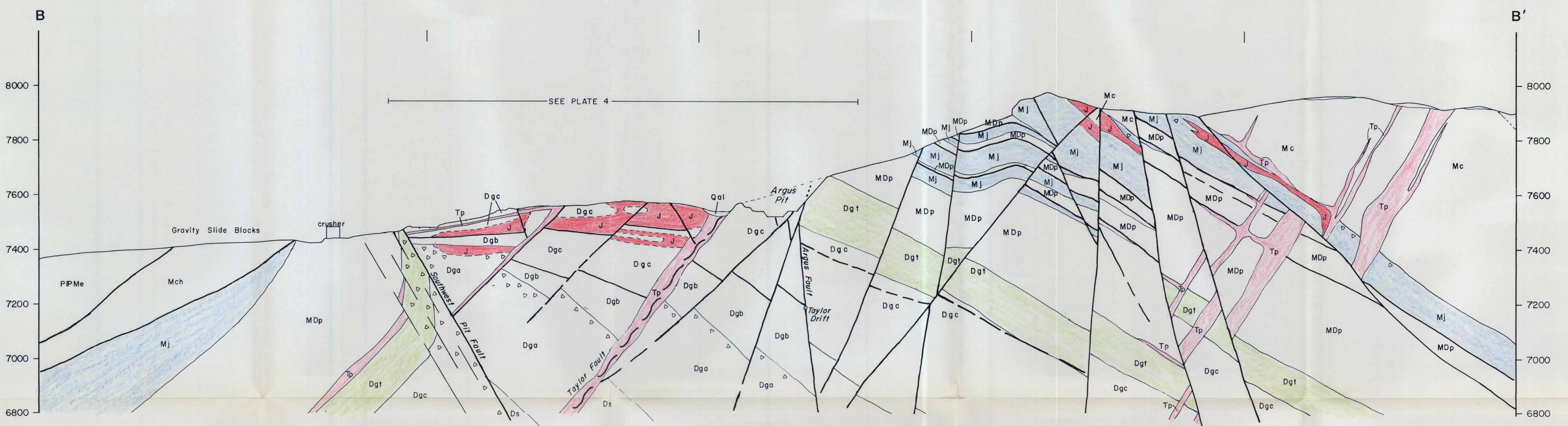
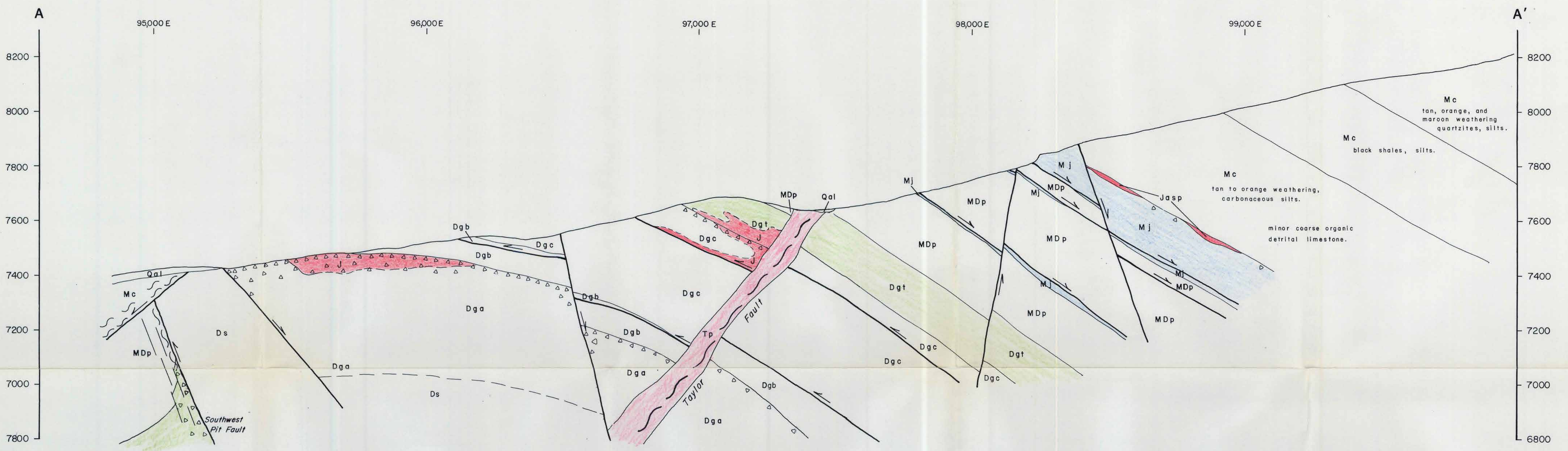
**TAYLOR MINE AREA**

WHITE PINE COUNTY, NEVADA

J. M. EDWARDS  
Colorado State University, 1988

CONTOUR INTERVAL 10'

Topography Compiled by Photogrammetric Methods - INTERMOUNTAIN AERIAL SURVEYS - SIX LINE CITY, UTAH - JULY 1967 - 0548



EXPLANATION  
See Plate 1

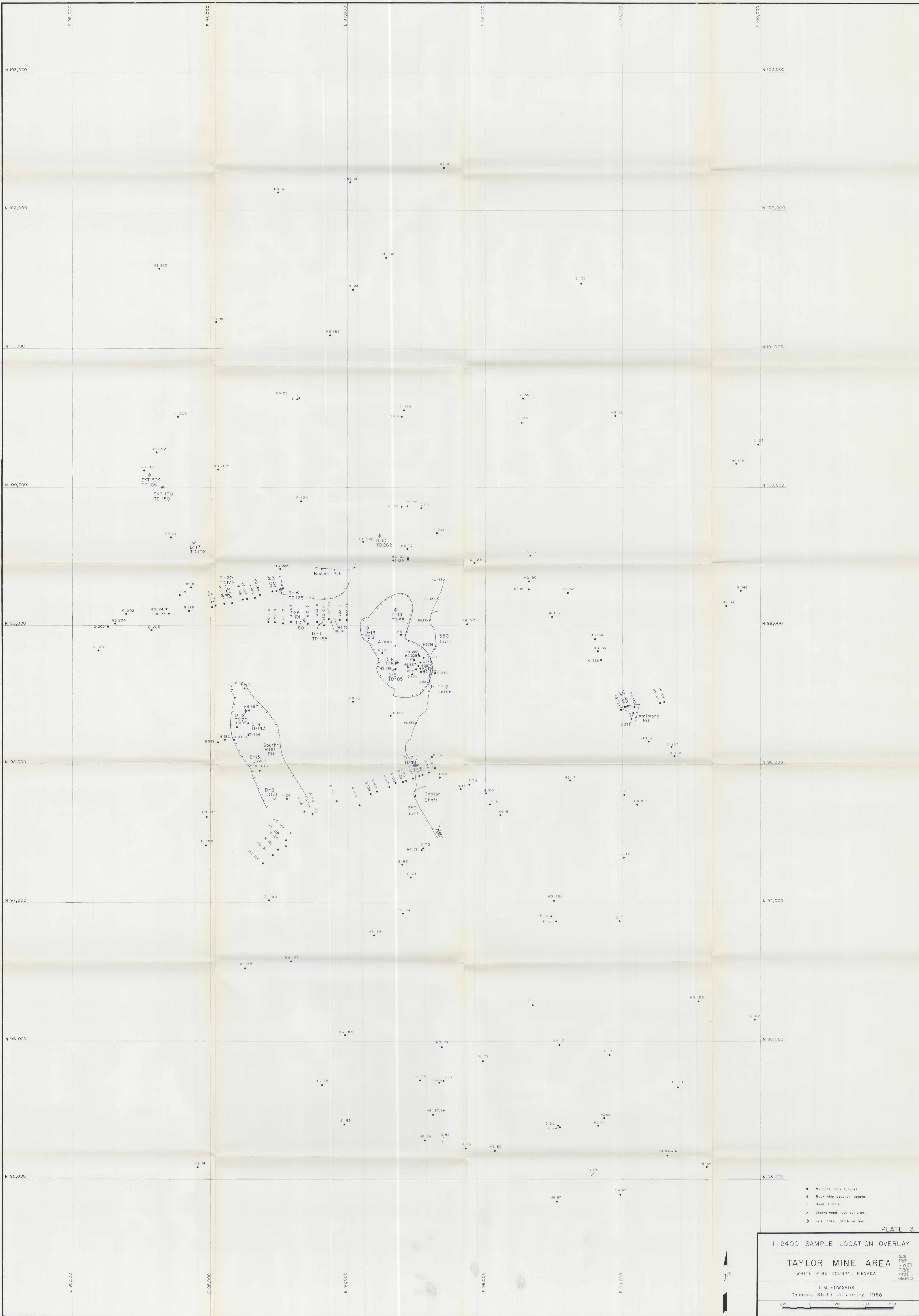
PLATE 2

1:2400 GEOLOGIC CROSS SECTIONS  
 GE 138  
 JNS4  
 E38  
 1988  
 plate 2

TAYLOR SILVER MINE  
 White Pine County, Nevada

J. M. EDWARDS  
 Colorado State University, 1988

0 200 400 600 ft



- Surface rock samples.
- Rock chip geochron sample.
- H Hand sample.
- X Underground rock samples.
- ⊕ Drill hole, depth in feet.

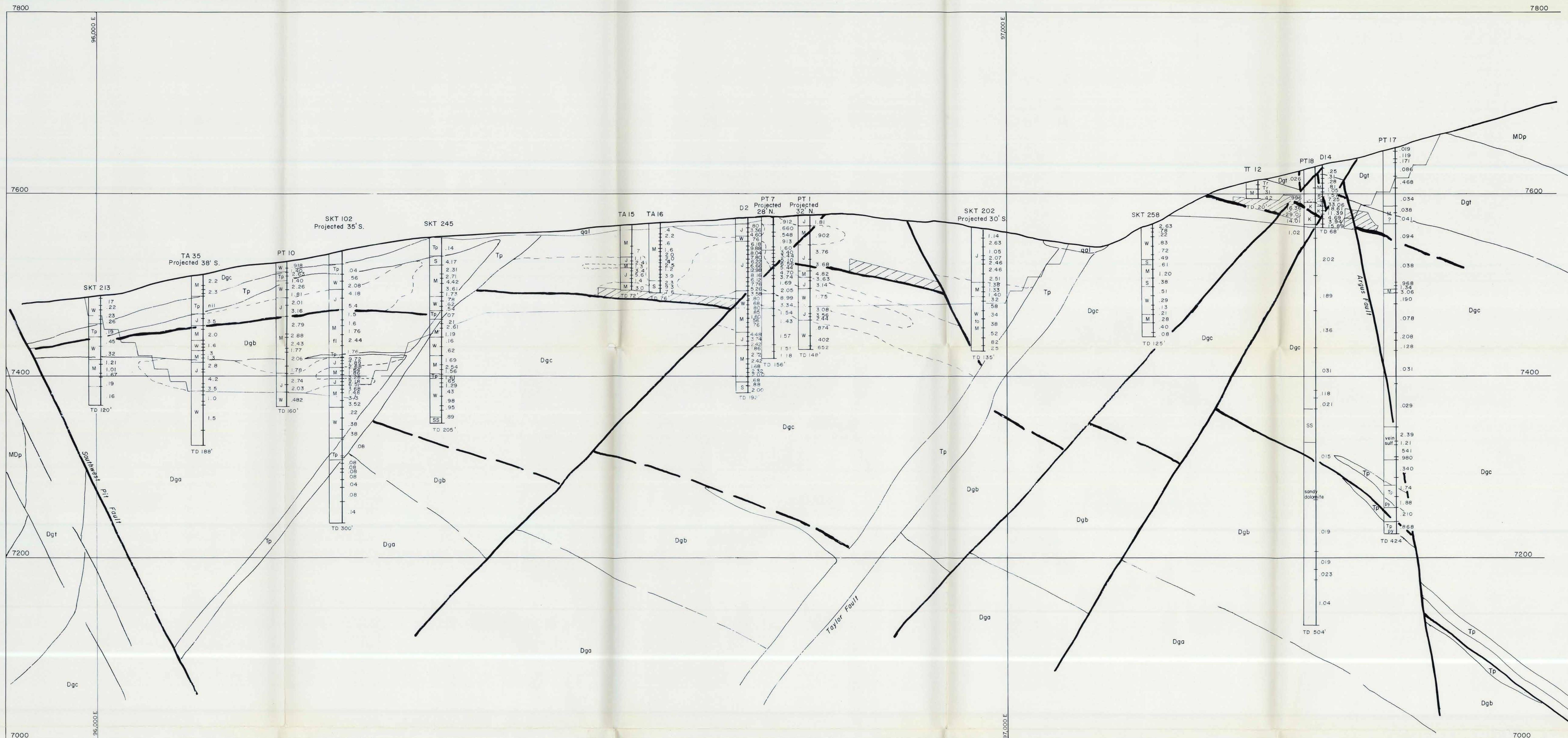
PLATE 3

1:2400 SAMPLE LOCATION OVERLAY

**TAYLOR MINE AREA**  
 WHITE PINE COUNTY, NEVADA

J. M. EDWARDS  
 Colorado State University, 1988





**EXPLANATION**

(See Plate 1 for explanation of rock units)

- Ultimate pit limits
- Old stope
- Drill Hole**
- W** 1.00 to 1.99 oz Ag/ton
- M** 2.00 to 4.99 oz Ag/ton
- S** 5.00 or more oz Ag/ton
- J** Jasperite
- SS** Sandstone
- K** Karst cave fill
- N** Nil to 0.99 oz Ag/ton

**PLATE 4**

CROSS SECTION 99,100 NORTH  
 TAYLOR SILVER MINE  
 White Pine County, Nevada

J.M. EDWARDS  
 Colorado State University, 1988



QE  
 138  
 .w54  
 E38  
 1988  
 plate 4